**Delft University of Technology**

| | |
|---|---|
| Specialization: | Transport Engineering and Logistics |
| Report number: | 2017.TEL.8017 |
| Title: | **Crane fatigue assessment using Multibody Dynamics and Finite Element Method** |
| Author: | C.J. Tawjoeram |

| | |
|---|---|
| Title (in Dutch) | Beoordeling van hijskraan metaalvermoeiing door het gebruik van een Multibody Dynamica en Eindige Elementen Methode |
| Assignment: | Masters thesis |
| Confidential: | No |
| Chair graduation committee (university): | Dr. ir. D.L. Schott |
| Supervisor (university): | Dr. ir. X. Jiang |
| External committee member (TU Delft): | Dr. ir. J.H. den Besten |
| Supervisor (company): | M. Holleman (Maja Stuwadoors BV, Amsterdam) |

Date:                        18 November, 2017

# Preface

This research started within the COHESION-Tracing Condition Status research group. It continued in the context of my master thesis as the final assignment of my master mechanical engineering with a specialization in Transport Engineering and Logistics at the Delft University of Technology. The objective of this research was to quantify the dynamic load influence during operation on the fatigue damage for cranes by using MultiBody Dynamics software ADAMS and Finite element software ANSYS. The results were compared with the fatigue design according to the crane standards which is a static design method. Here the influence of the dynamics is taken into account with safety factors in the calculations. In cooperation with the Maja Stuwadoors BV, one aged 25t floating grab crane was used as study case.

First I would like to thank from the section of Transport Engineering and Logistics from the TU Delft, the members of the COHESION research group for their contribution and support. Not to forget Dineke Heersma from our section.
Dr.ir. Dingena Schott for her comments and suggestions during the research phase. My thesis supervisor from the TU Delft, Dr. ir. Xiaoli Jiang, I am very great full for her help to accomplish this assignment. I learned allot from her critical comments and feedback, her support and guidance from the start of my literature assignment, during COHESION to this graduation assignment. And not to forget Ir. Wouter van den Bos for his suggestions and coaching in the structural fatigue assessment of cranes.

From the Maja Stuwadoors BV, I would like to thank Marco Holleman for giving me the opportunity to perform my research for the 25t Cornelis Tromp floating lemniscate crane. I would also like to thank the maintenance department and the crane operators  for their sharing their knowledge about the operational and mechanical characteristics of the crane and stevedoring field. And least but not least all office employees who I worked with during 11 months.

Also thanks to the ADAMS specialist, Ir. Chris Verheul from Sayfield International. Words cannot describe how grateful I am for his help, support, guidance and the time he took to help me with ADAMS .This cooperation resulted in an ADAMS crane model. Also the support with ANSYS from Infinite Simulation Systems B.V.

Finally I want to thank my wife Cherise, my son Joël, family-in-law, aunt Henna and family members who kept supporting and motivating me during this very challenging and intensive last phase of my masters mechanical engineering study.

Clive Tawjoeram
Amsterdam, November 2017

# English Summary

Crane fatigue is a common problem in practice. Although crane standards have been used for decades to prevent it, fatigue still occurs due to the dynamic characteristic of the crane loading. In general, standards make use of a static design method to do fatigue calculations, where loads are multiplied using safety, amplification and risk factors. It is a simple and practical approach, but can be too conservative and result in over dimensioned or under dimensioned structures or neglecting certain dynamic effects. Therefore this problem requires to be studied from a different point of view to perform fatigue assessments.

In order to find a solution to this problem Multibody dynamics and a finite element method is used to quantify the dynamic load influence during operation on the fatigue damage for one crane type. On the basis of this idea the following research question is formulated: "*How much is the contribution of the dynamic effects during the operational life on the structural fatigue damage using a multibody dynamics and finite element simulation method compared to a conventional fatigue assessment using a crane standard?*" To answer this question a literature review is performed. This reveals that a multibody dynamics-finite element method is commonly used technique. However up to the moment , a different method where crane motion analysis is performed in ADAMS only and service loading is subsequently used in ANSYS for stress analysis has not been identified. Also no ADAMS model for the lemniscate transshipment crane has been identified and that is why in this research an aged 25t floating lemniscate crane is used as a study case to apply the method.

The aim of this research is to compare a dynamic simulation method and a static method to perform a fatigue assessment for a crane. In order to determine the fatigue damage first the number of transshipment moves is determined using a cycle time analysis. A dynamic representation of bodies and contacts is developed using Multibody dynamics software Msc ADAMS for the crane. One working cycle is simulated according to a transshipment method used by the crane owner and loading is exported to a finite element beam model developed using ANSYS APDL to determine the stress spectrum for one specific tubular weld detail. Due to the complexity of the stress spectrum, a Rainflow counting method using JRain is applied to transform this spectrum into a set of representative stress reversals to calculate the stress ranges. This allows to determine the fatigue damage using the formula of Haibach and Miner's accumulative damage rule. Subsequently a fatigue assessment is performed using the NEN2018/2019 crane standard.

The proposed method to perform a crane fatigue assessment using multibody dynamics and finite element method is proven to be feasible and can thus also be applied to a wide range of transport systems in fatigue design methodology. The contribution of the dynamic effects during the operational life using a multibody dynamics and finite element simulation method is in average about 47%-82% higher compared to the NEN2018/2019 crane standard for the tubular welded joint of the crane which is used as a study case in this research. The longitudinal fatigue crack found in reality during the moment that this research was conducted show similarities with past found cracks and thus reveals that this tubular joint is a fatigue critical hotspot.

For both fatigue assessment methods in this study, the dominant influential parameters which determine the outcome are:
1. the difference in loading encountered in both methods
2. the difference in the value of the characteristic fatigue strength
3. the difference in number of cycles encountered by the crane component

The use of multibody dynamics simulation software ADAMS in the fatigue assessment allows to directly visualize the dynamic loading characteristics of the crane for the simulated load cycle. It provides insight in the dynamic effects which occur during operation and allows to understand when these dynamic load influences occur. Although much higher load values were calculated with ADAMS for the lateral and longitudinal loads compared with the crane standard, it is concluded that in terms of structural safety the use of MBD and FEM is advantageous. However a main disadvantage is that the method requires a large amount of effort to simulate a working cycle close to reality. Finally the added value of the method is, that it can be used as a tool during the design phase of new crane designs, whereby improvements can directly be made for critical points that are under- or over-dimensioned.

In order to increase the accuracy of the service loads, it is recommended to incorporate flexibility for cable mechanism and joints connecting the various structural components in the current fully rigid ADAMS crane model. To extend the simulation possibilities to study the influence of the dynamic load effects for other transshipment configurations the use of control theory to develop control systems for the various mechanism will lower the amount time required for cycle-time programming. It is highly recommended to use a combination of beam for global modeling and plate elements to model present cracks at the complex tubular welded joints in the FEM model and use methods like fracture mechanics or strain life method to obtain direct results.

# List of abbreviations

MBD = MultiBody Dynamics

FEM = Finite Element Method

NEN = Nederlands Normalisatie Instituut

SN = Stress-life method

ADAMS = Automatic Dynamic Analysis of Mechanical Systems

FEA = Finite Element Analysis

CAD = Computer Aided Design

CT = Cornelis Tromp

APDL = Parametric Design Language

CoG = Centre of gravity

CoM= centre of mass

DOF = Degrees of freedom

CoR = Centre of rotation

SFORCE = Single component force in Msc Adams

CW = clockwise rotation

CCW = counterclockwise rotation

IL = individual load

LS = load set

# List of figures

# List of tables

# Table of contents

# 1   Introduction

Cranes fulfill an important role in society. Their application can be found in many fields, for example at construction sites, container and bulk terminals and the offshore industry. There are many dynamic effects induced to the structure during the acceleration and braking phase during operation. Horizontal, vertical and rotational movements, like hoisting & slewing, have the tendency in resisting a change in motion during that phase. Both the structural crane weight and the hoisting weight result in inertia and centrifugal forces when accelerating or braking. But also the effect of the hoisting load itself, when it's picked up and dropped. For floating cranes the latter introduces an extra pendulum effect. All these dynamic influences that occur during operation, result that cranes are in general vulnerable to structural fatigue.

It is a phenomenon which is characterized by repeated cyclic loading and unloading in time where the occurring stresses are lower than the yield strength. Final failure occurs when reduced structural cross section becomes insufficient to transmit the load. Fatigue failure or fatigue damage is usually demonstrated in the presence of developed cracks which can be noticed on time and sometimes not. Due to the large number of cycles experienced in a cranes lifetime, fatigue can suddenly occur. When this occurs, it could lead to fatal accidents, large financial consequences, a large impact on machine, humans, the environment and the services we are used to enjoy.

## 1.1   Problem

In practice there are a number of crane standards available which are widely used in engineering to perform fatigue calculations. For example the NEN2019, FEM1.001, Eurocode3, EN13001, Lloyds code for lifting appliances and the state of the art DNVGL-RP-C203. The fatigue assessment method used in all of them are based on the same conventional static design principle. All loads identified are considered as static and multiplied with chosen safety- , amplification or risk factors to take the dynamic effects into account. For example the hoisting weight is multiplied using a load factor, larger than the value of one, to take the dynamic effects during the hoisting movement into account. These choices are however based on experience. Therefore a high risk is present to forget or neglect certain dynamic effects or choosing to high or too low values for the factors. This can result in two major problems:

1. too conservative results, where the design loads are much higher than the real loads resulting that certain points in the structure are over dimensioned.

2. less conservative results, where the design loads are under estimated resulting that certain points in the structure can be under dimensioned.

By contrast, on-situ measurement can be used to perform a fatigue assessment. It is accurate, but too expensive and a large amount of time is required for monitoring and tracing structural degradation for cranes. The basis of this problem is due to the large geometric structural size and the large number of welded joints present where fatigue cracks usually start.

## 1.2   Importance

Fatigue reliability is very important for cranes. According to an article published by Smith and Forbes (2015), the most fatigue critical component of the crane is the boom structure. Their study revealed that in 95% of the cases this component is the most vulnerable to a fatigue failure. In the past such a boom failure occurred for quay cranes of the lemniscate type in the Netherlands, seen in Figure 1. Unfortunately this boom failure resulted in a fatal accident during the transport of containers from ship to shore.  The top welded joint on the upper arm (top boom) failed and the front part of the structure fell down crushing the cabin with the operator at a height of 40m above ground (Figeeforum, 2012).
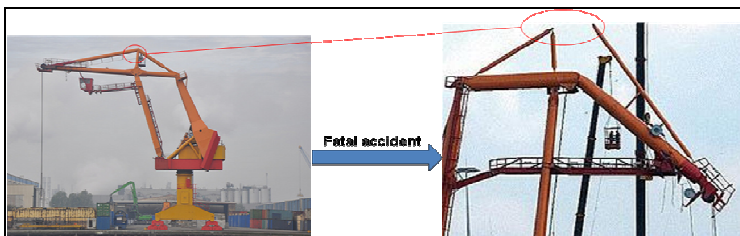


**Figure 1: Fatal accident transshipment crane  (Figeeforum, 2012)**

It was also reported that fatigue cracks were found during inspection at a similar transshipment crane seen in Figure 2.
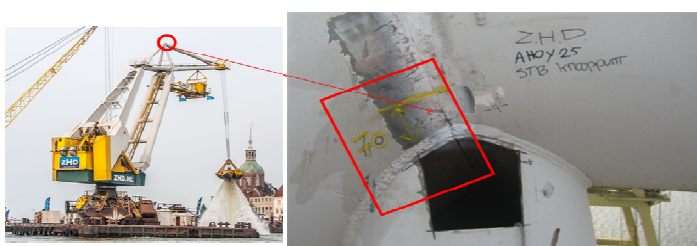


**Figure 2: Weld crack at top boom transshipment crane of lemniscate type (Maja Stuwadoors BV, 2016)**

However the first case was not a fatigue related failure, the second case shows that fatigue failure still occurs. The examples above demonstrate the impact of this problem. It is therefore of great importance to study, utilize and explore other state of the art fatigue design alternatives for example the use of multibody dynamics simulation.

### 1.3   Research question

The previous section described the consequences which a failure can have if it occurs. On the basis of the identified problems and the past accidents, there is a need to assess and utilize crane fatigue design from a different point of view. Therefore the main research question is: "*How much is the contribution of the dynamic effects during the operational life on the structural fatigue damage using a multibody dynamics and finite element simulation method compared to a conventional fatigue assessment using a crane standard?*"

Additional sub research questions are:
1. Which key parameters are required to sufficiently formulate an accurate dynamic representation to simulate the operational profile for a crane?
2. What is the state of the art crane standard?
3. Which multibody dynamics software is widely used by the crane industry and offers the most advantage possibility to visualize and understand calculated loads?
4. How to incorporate the proposed simulation method to determine the fatigue damage for one typical crane?
5. What are the improvements of the simulation method compared to the conventional method for the crane to which the method is applied?

### 1.4   Research objective

This research aims to quantify the dynamic load influence during operation on the fatigue damage for one crane type. This will be done by developing a computational model based on the dynamic representation of contacts and bodies to virtually simulate the crane motions and loading. The calculated loads will be used in a finite element structural model to calculate stresses and predict the accumulated damage.

## 1.5    Research boundary

In this study one crane type is used only. This is a aged 25t floating transshipment crane of the lemniscate type, which is in operation for 21 years now and made available to use as study case by the Maja Stuwadoors BV, seen in Figure 3.



**Figure 3: Study case-Cornelis Tromp 25t floating lemniscate crane (Maja Stuwadoors BV, 2016)**

In order to understand the dynamic load influence during operation of this crane,  a multibody dynamics model will be developed using ADAMS simulation tool. A literature review conducted by Tawjoeram (2015), shows that up to the moment of writing, no ADAMS model for this transshipment crane type has been identified.  The structural response of this dynamic loading will be analyzed with a finite element simulation model created in ANSYS. The fatigue assessment, will mainly focus only the top tubular welded joint on the upper arm structure of the crane. The main reasons are as follows:

1.  it is impossible to assess the complete crane structure
2.  the boom structure is identified as the most fatigue critical component of the total crane structure
3.  because the general service life expectancy for cranes is about 20 to 25 years according to Wiethorn et al., (2015), the crane may be in a state of fatigue failure due to the current 21 years of the use
4.  the company is concerned about the structural integrity of this joint
5.  the impact and large financial consequences if this joint fails due to fatigue

Other dynamic conditions like corrosion, loads due to wind and varying temperature changes are left out of the scope of this research.

An illustration for the research boundary is seen in the following Figure 4.

**Figure 4: Research boundary (Maja Stuwadoors BV, 2016)**


## 1.6   Research method


In general the research approach will be executed as seen in the following Figure 5. The first step will be to identify and setup the crane operational profile with all demanded input parameters. Then the first fatigue assessment will be done using the dynamic method, followed by a fatigue assessment using the static method and the results and findings of both methods will be compared and discussed.
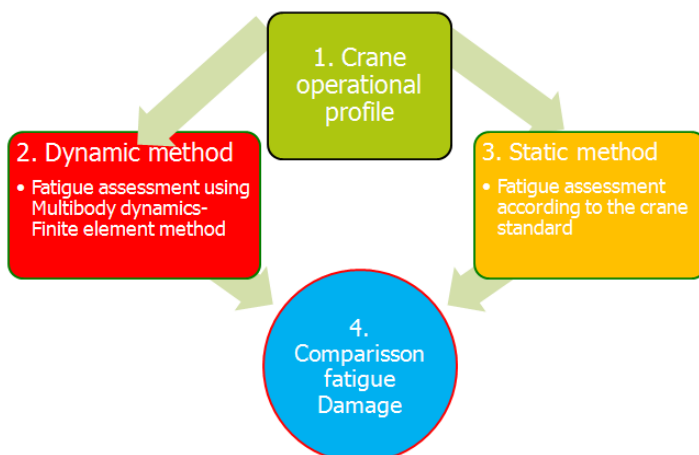


**Figure 5: General research approach**

In more detail, the research method which will be used to quantify the dynamic load influence during operation on the fatigue damage for the chosen crane can be seen in Figure 6. At the first step, all necessary crane geometric, operational and structural parameters will be identified and gathered using the available sources. Geometric parameter information will be used in the development of a part of the 3D CAD model. For the multibody dynamics modeling in Msc ADAMS/view software, the CAD model is imported and inverse dynamics will be used to simulate a load cycle and compute dynamic forces. The latter are used in a transient structural analysis using ANSYS mechanical APDL software to obtain the stress spectrum for the tubular weld. Subsequently the fatigue analysis will be conducted using, the Rainflow counting method, SN-curves and Miner's rule to calculate accumulated damage at the weld of interest. The results will be compared with the fatigue design calculations according to the chosen crane standard, illustrated with the blue arrows.
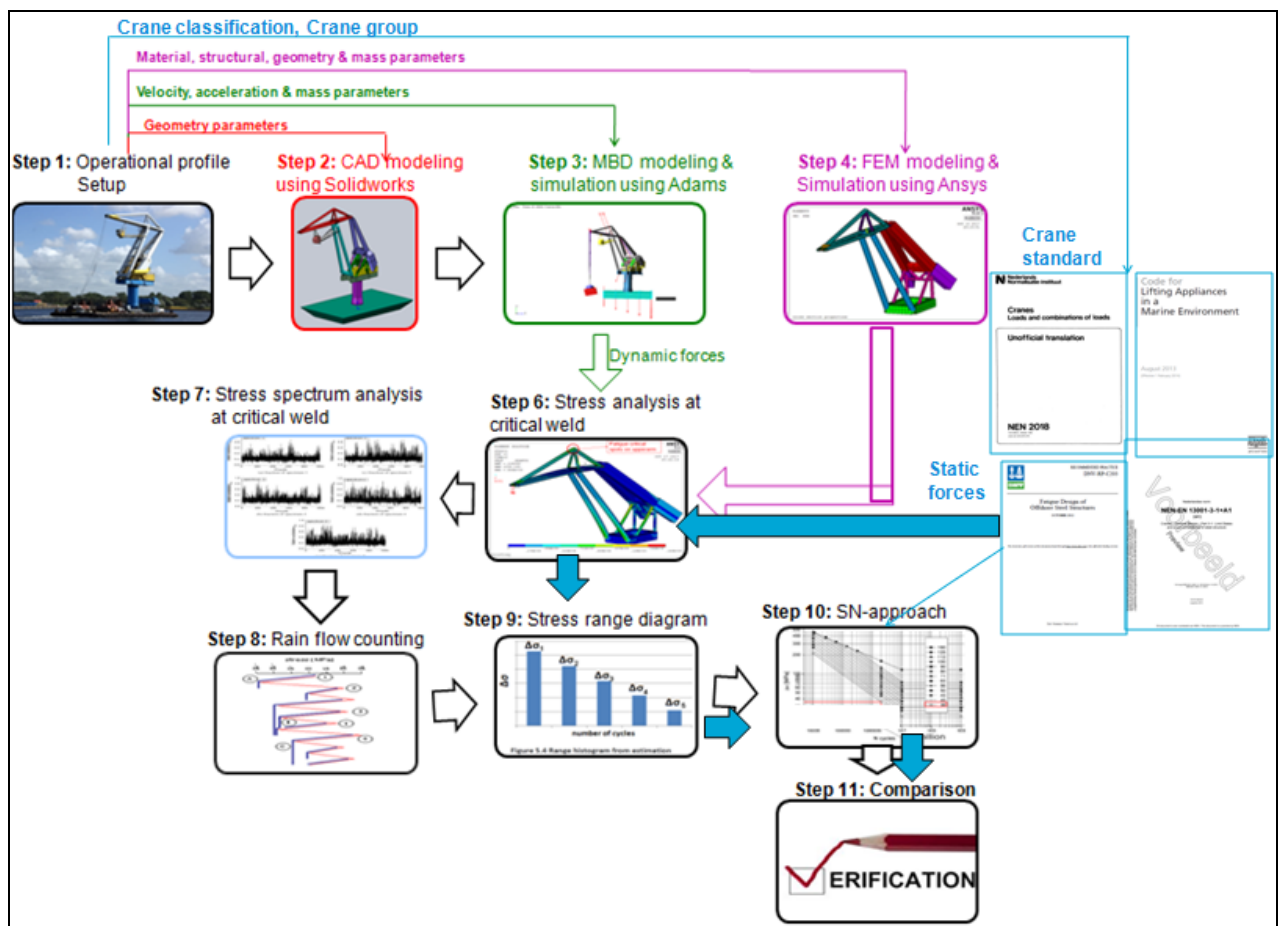


**Figure 6: Research method**

## 1.7   Structure of the thesis

Based on the research method discussed previously, this research will be structured as follows. In Chapter 2 an overview of the different crane designs is provided, a discussion about how this crane works, the necessary parameters are defined, a cycle time analysis is performed and the number of cycles is determined. Then in chapter 3 the development of the multibody dynamics model using ADAMS is described. In this chapter a working cycle is simulated and the dynamic loads are calculated. These load results are used in a ANSYS FEM model to obtain the stress-time spectrum at the welded joint of interest. At the end of this chapter the fatigue damage results of the dynamic loads are presented. Then a fatigue calculation will be performed in chapter 4 according to the NEN 2018/2019 crane standard. The final results from both fatigue assessment methods will be compared and discussed in detailed in chapter 5. The research finalizes with a conclusion and provides recommendations in chapter 6 for further future research on this topic. The scientific paper is presented in Appendix A. All calculation details and additional information about the multibody dynamics modeling and simulation is found in Appendix B. In Appendix C details about the fatigue calculations according to the used crane standard is found.  The batch script written to perform the finite element analysis in ANSYS is described in Appendix D.

## 2    Crane operational profile

This chapter discusses the service profile for the lemniscate crane which will be used as a study case. In the first section a brief overview about the mechanical principles of the crane is provided. Then insight is given in how the crane typically is used. On the basis of this operational profile the occurring dynamic effects are identified which are induced to the structure during the operation. The chapter finalizes with a summary of all key parameters required to sufficiently formulate an accurate dynamic representation to simulate the service condition for the crane.

### 2.1    The lemniscate crane

The lemniscate crane or level-luffing crane considered in Figure 7 is one of the many transshipment crane type designs. It is typically used in bulk solid material and piece good transport in bulk terminals, ship to shore and ship to ship handling. The crane can be mounted on the quay and used as a quay crane or on a pontoon making it flexible to use. The latter makes it possible to be used for the transportation of material between two floating structures or from a floating structure to the quay.
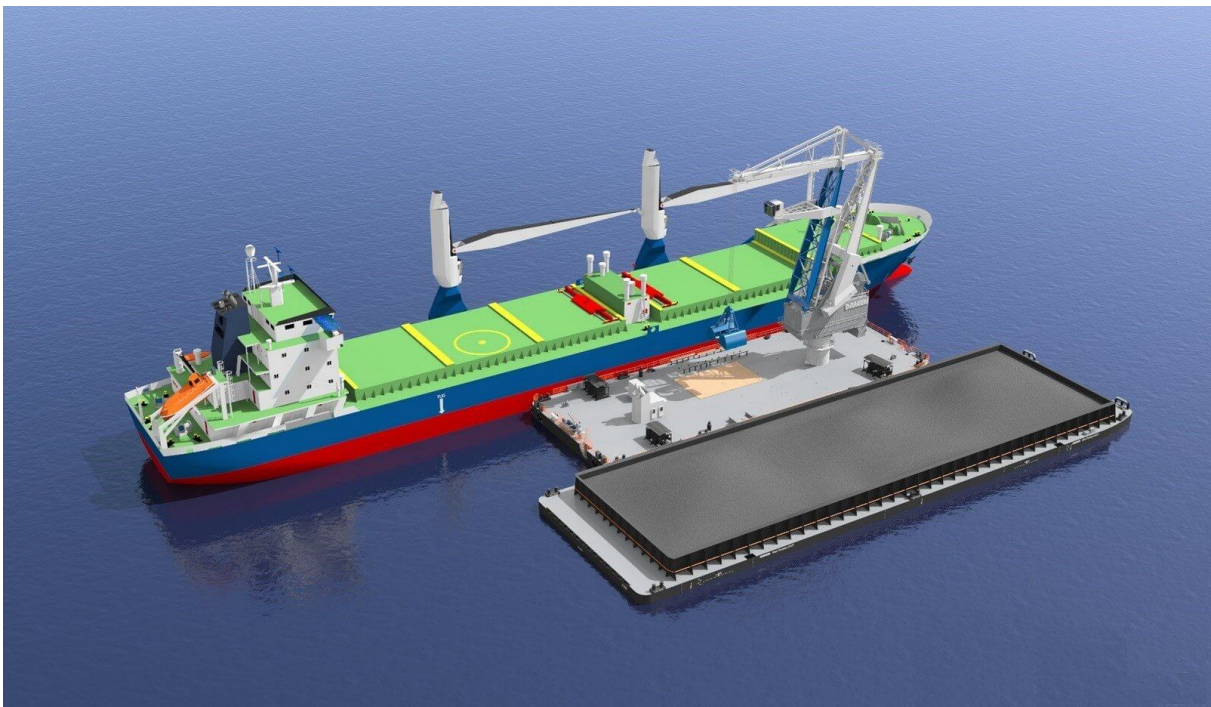


**Figure 7: A transshipment process (Floatingtransshipment.com, 2016)**

According to Kaenders (2005) and Kaenders (2007) the development of this crane goes back to the 1930's in Eberswalde, Germany were they were first produced by the German crane

manufacturer ARDELT. Its mechanism is based on the four-bar linkage and the lemniscate of Bernoulli (Schipper, 1992). The former is applied in a wide range of machinery such as forklift trucks, wheel loaders, bicycles, level luffing balance crane and the double boom level luffing crane seen in Figure 8.



**Figure 8: Applications of the four-bar linkage mechanism (Kaenders, 2007)**

Figure 9 shows the application of the four bar mechanism for the lemniscate crane as the moving booms, hinged to the ground.
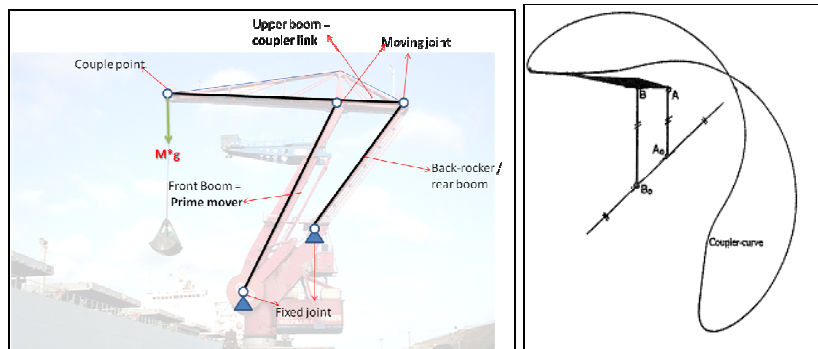


**Figure 9: Four-bar linkage applied to the lemniscate crane (Nieuwenhuis, 2006)**

The main structure of the crane consists of the upper arm, rear arm, front arm, tower, machine floor and a balancing system seen in Figure 10. Typically it is attached to a barge or pontoon via the foot.
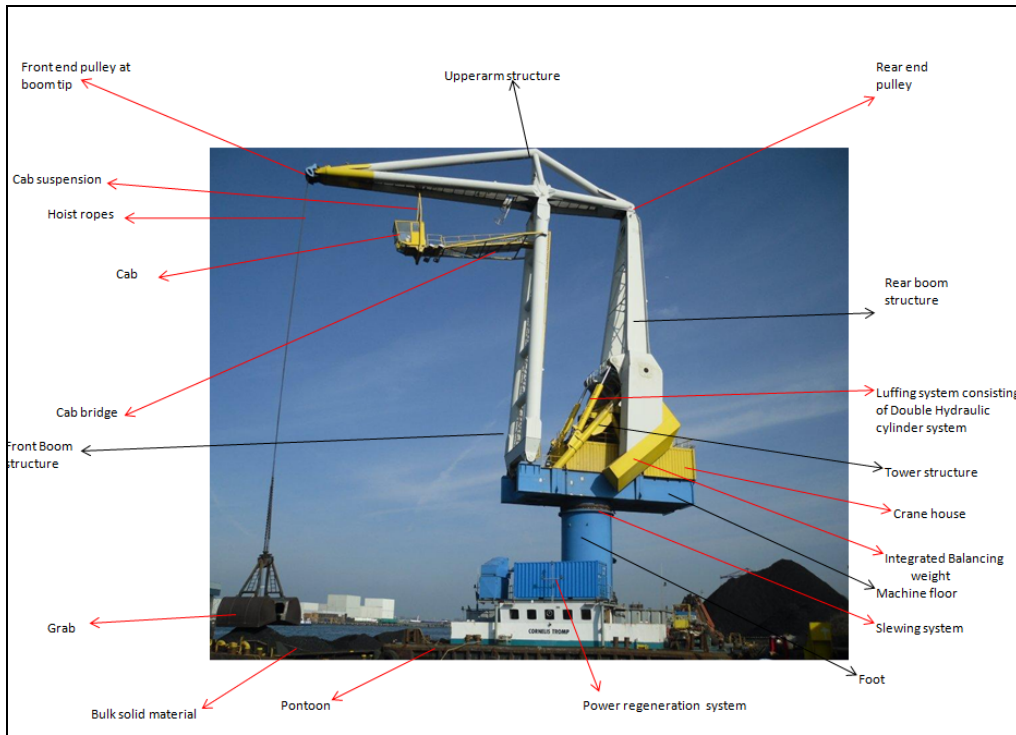
**Figure 10: Components of a floating lemniscate crane (Maja Stuwadoors BV, 2016)**

The upper arm structure is the top part of the crane hinged to both the front and rear boom. Its design is based upon the lever principle. The structure is mainly loaded on in plane-, out of the plane bending and torsion. In the past a number of different arm designs have been constructed shown in Figure 11.



**Figure 11: Upper arm structure designs ( McDermoth, 2005)**

The crane is operated from the cabin, where the operator has an overview on the load. The total cabin structure is hinged at the upper arm or between the upper and front arm seen in Figure 12.

**Figure 12: Cabin structure designs ( McDermoth, 2005)**

The balancing system is a very crucial part of the crane, because it must ensure optimal equilibrium conditions for both the boom mechanism and the whole crane for every possible working condition. The principles of this system are based upon the minimum total potential energy principle and briefly discussed in a publication by the engineering company IV-Groep (2006). Figure 13 shows two types of balancing which are widely used today. One type is integrated in the rear arm, shown on the left and the second one constructed as a mechanism shown on the right.  Both designs make a counter movement when the crane is luffing.



**Figure 13: Balancing system designs ( McDermoth, 2005)**

The hoisting system consists of winding drums, pulleys, rollers and wire ropes seen in Figure 14. For all the lemniscate cranes in operation the hoist and closing cables make a loop starting from the grab or hook, to the front end of the upper arm, looping via rollers to prevent sag to the pulleys on the rear end of the upper arm. Then they bend to the rear arm

to the turn pulleys on the rear arm and the tower, continuing to the main winch where the cables are wrapped.
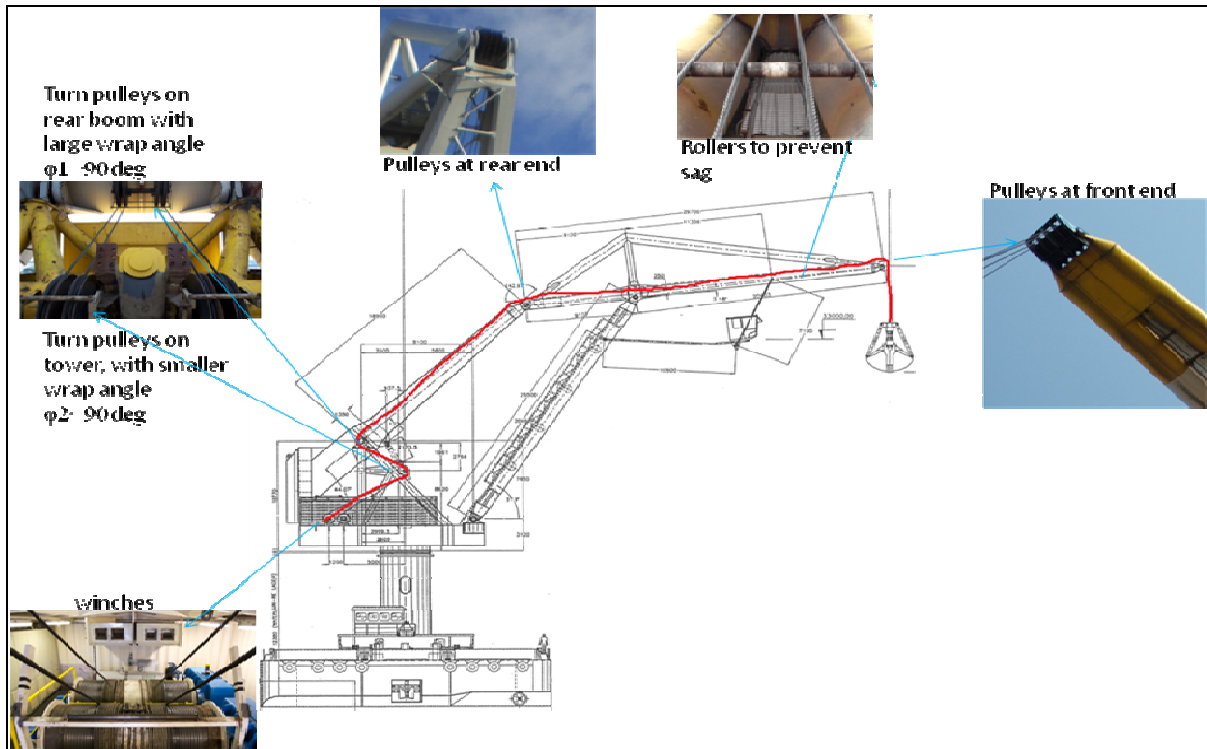


**Figure 14: Hoisting system design (Maja Stuwadoors BV, 2016)**

The luffing system of the crane is designed to displace the load along a horizontal path for a long desired range without hoisting. According to Nieuwenhuis (2006) this displacement is determined by the choice of the arm lengths ($B_0$ -B and $A_o$ -A) and the hinge locations (A, B, $A_o$ and $B_0$) seen in Figure 15. These parameters are varied such that a horizontal load displacement along a straight horizontal line is created at the tip of the top boom. Ideally this is not perfectly a straight line, however for practical purposes this doesn't matter.
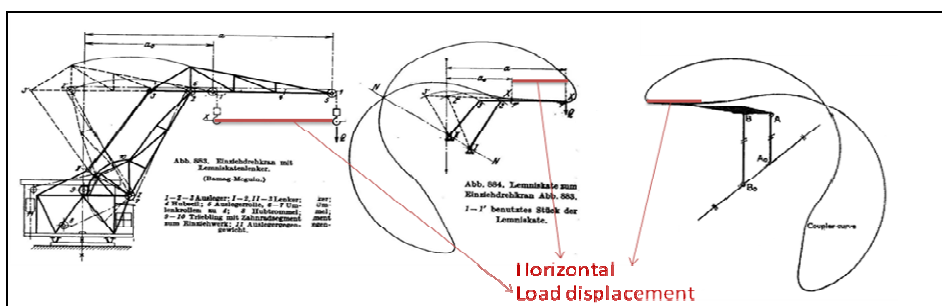


**Figure 15: Horizontal load path (Kaenders, 2007)**

The luffing system could be design in such a way that the rear or front arm is driven. This could be a crankshaft transmission, a linear driving transmission or a pin and rack gear system. Figure 16 shows the types of luffing systems applied today for these cranes. It is

desired to have a maximum load capacity over the entire reach, but depends mainly on the balancing mechanism and arm geometries.
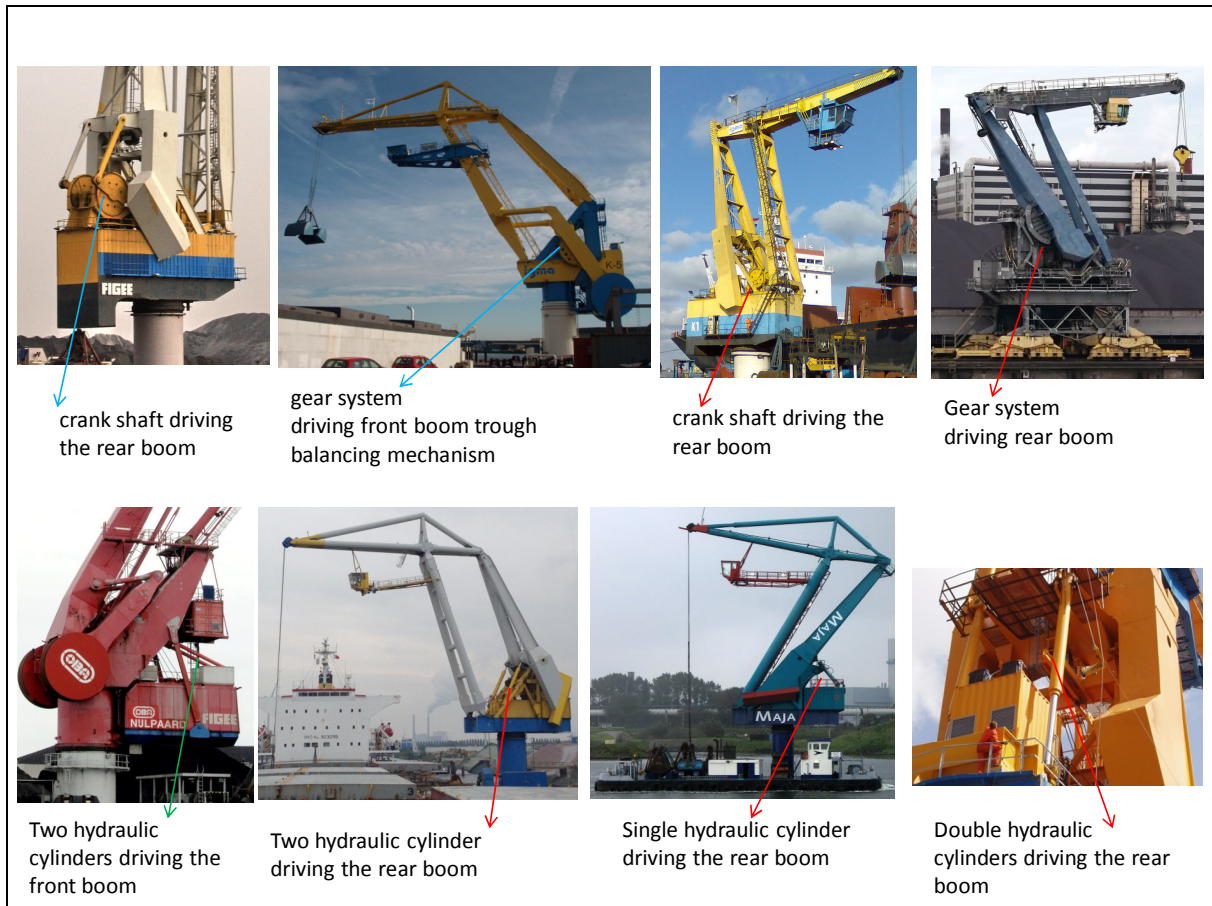


**Figure 16: Luffing system designs ( McDermoth, 2005)**

The slewing system ensures rotational motion of the crane. The system is mounted between the foot of the pontoon and integrated into the machine floor of the crane. Figure 17 shows the various components of this system.
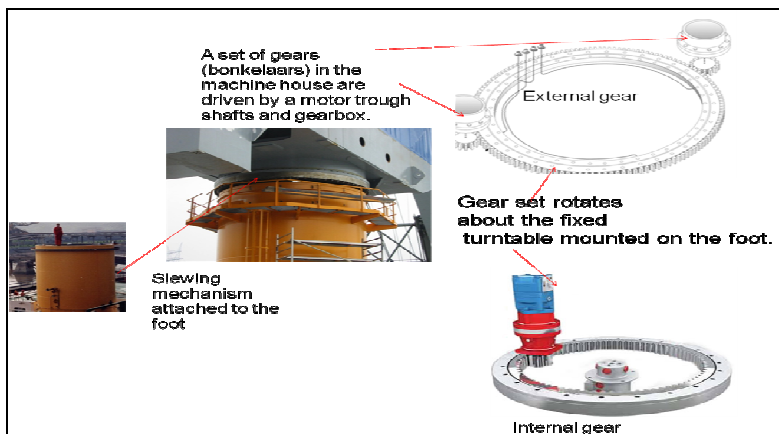


**Figure 17: Slewing system design ("slewing drives", 2016)**

This ends the discussion about the mechanical principles of the lemniscate crane. In the next section its service condition is discussed.

## 2.2   Dynamic load effects during operation

This section discusses the typical crane use and identifies the dynamic effects which occur during the operation.

The crane encounters different movements during the transport of a load from location A to B. These are closing and opening of the grab, hoisting and lowering of grab, luffing in and luffing out and slewing from loading to unloading position. In operation, typically the following movements occur during a working cycle, starting at the moment of loading up to the moment the next loading will start. This sequence of ten movements is illustrated in Figure 18.
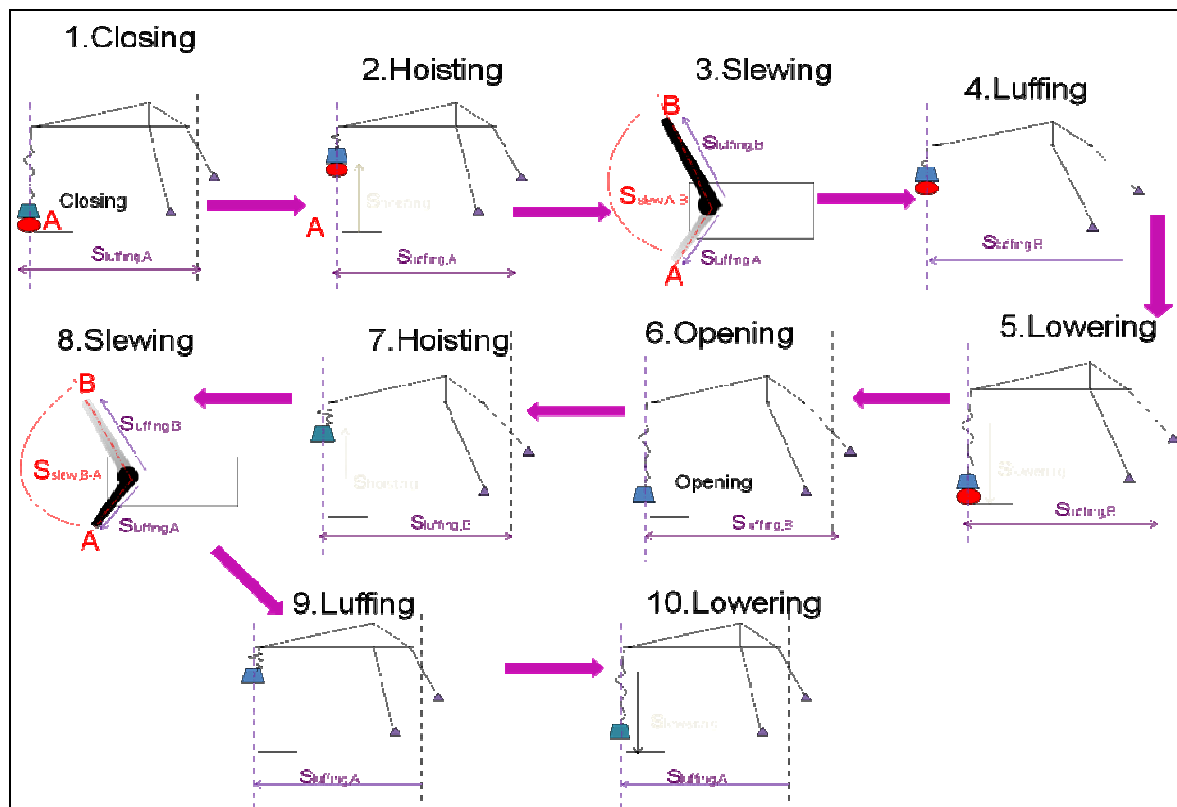


**Figure 18: Typical movement sequence of the lemniscate crane**

Each movement is divided into a acceleration, cruising and decelerating phase. During the accelerating and braking phase of the vertical, horizontal and rotational motion, dynamic forces are introduced into the crane structure as a result of the resistance in a change of motion of both crane and hoisting weight.

The dynamic load effects accompanying rotational motion include inertia torque, centrifugal force and load pendulum action. When slewing acceleration motion occurs, centrifugal force causes the grab to move to an increased radius and inertia will cause the load to lag behind for both acceleration and braking phase as seen in Figure 19. The lagging of the load also occurs during luffing dynamic motion. A simplified representation of this phenomenon is seen in Figure 20.
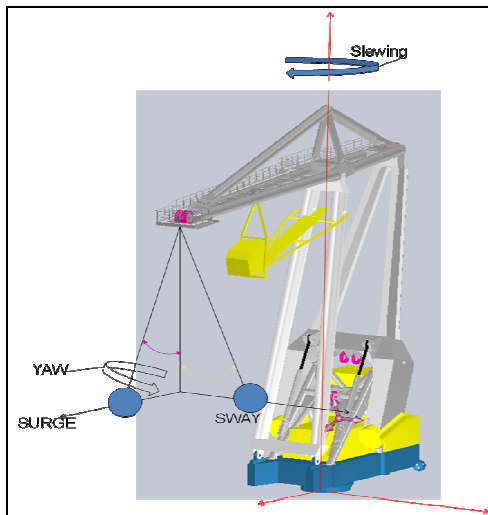


**Figure 19: Rotational dynamic effects during slewing**
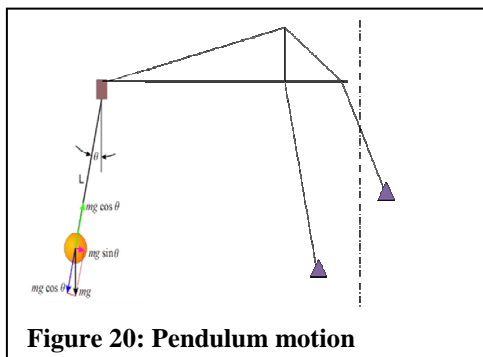


**Figure 20: Pendulum motion**

Other dynamic load effects introduced during operation is when the hoisting weight is being picked up and when dropped. A study on the influence about the latter was conducted by Vermeer et al., (2013). They conducted a research about the maximum load occurrences during the unloading phase for 40t bulk cranes. In this research the influence of the film cohesion, payload and operational control of the crane were evaluated from measurement data which revealed a substantial increased payload of more than 30% on top of the nominal crane load, seen in Figure 21.
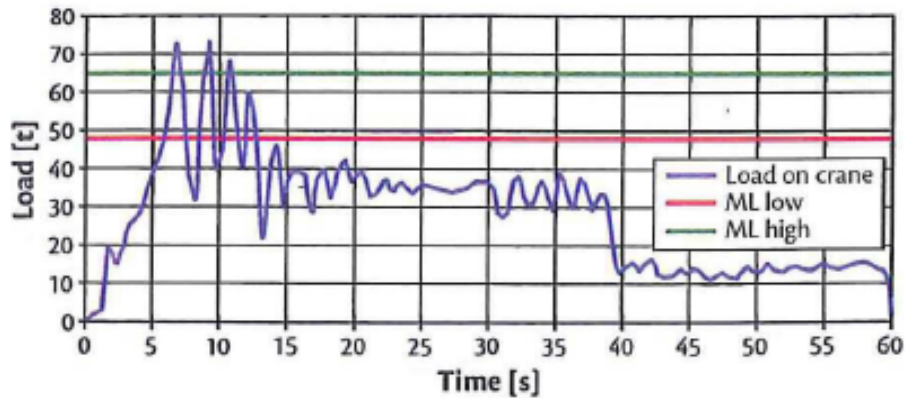
**Figure 21: Maximum load occurrences with payload of approx. 52t (Vermeer et al., 2013)**

The crane used for this research is 99% of the time used for grab duties, according to Holleman (2017). For each material being grabbed specific grabs like the clamshell, scissor or peel grab are used with their own characteristics, see Figure 22 and Figure 23. A frequent occurring situation is the handling of scrap metal where a peel grab is used, see Figure 24. According to a grab manufacturer Verstegen (2017) the dynamic loads on the crane can increase up to 1.2 or 1.3 higher than the sum of the dead weight of the scrap and the grab together. During the grab process the material gets waved into each other. This requires the crane to pull out the material. Most of the time this pulling out occurs vertically and occasionally under an angle. Although pulling from an angle (slanting rope pull) is not permitted according the NEN2018 crane standard. However in practice it cannot be prevented, occasionally this pulling still occurs with large dynamic effects transmitted to the structure.



**Figure 22: Clamshell grab handling**

**Figure 23: Scissor grab handling**



Large grabbing capacity        Theoretical volume        Practical volume
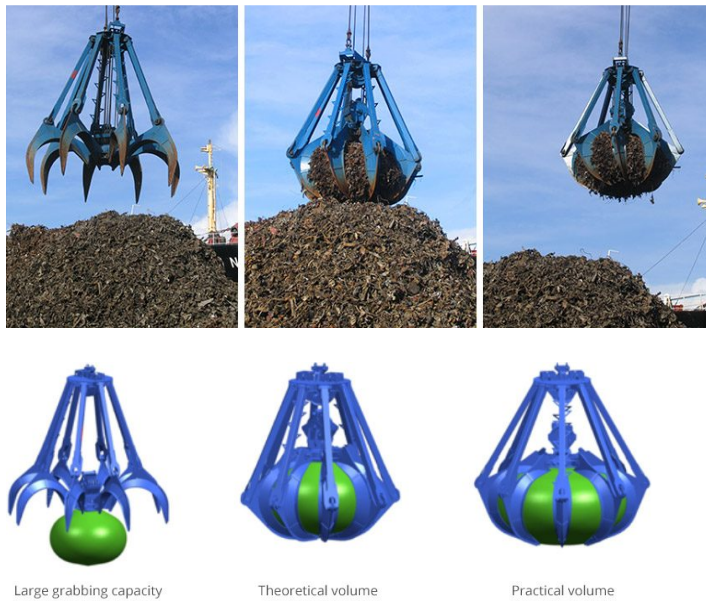
**Figure 24: Peel grab handling (Verstegen, 2017)**

The last dynamic load effect discussed is the pontoon motion which occurs when the crane is loaded and unloaded at different reaches relative to the center of rotation. This causes the total floating structure to undergo a roll, pitch and heave motion shown in Figure 25. According to Nieuwenhuis, G. (2006) a practical roll angle value for a full grab at maximum flight is about 2 degrees.
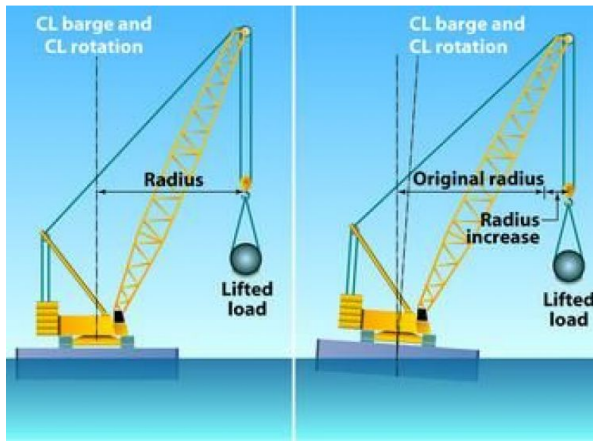
**Figure 25: Barge crane motion (Krabbendam, 2016)**

An occasional loading situation which can occur in practice is that the remaining material is located at a larger reach than the upper arm reach of the crane (Holleman, 2017). This requires the crane driver to simultaneously allow luffing and slewing movements by constantly accelerating and braking within a minimum of time. With these movements the crane operator uses the dynamic effects of the centrifugal and inertia force to move the grab to an increased radius, illustrated with Figure 26.
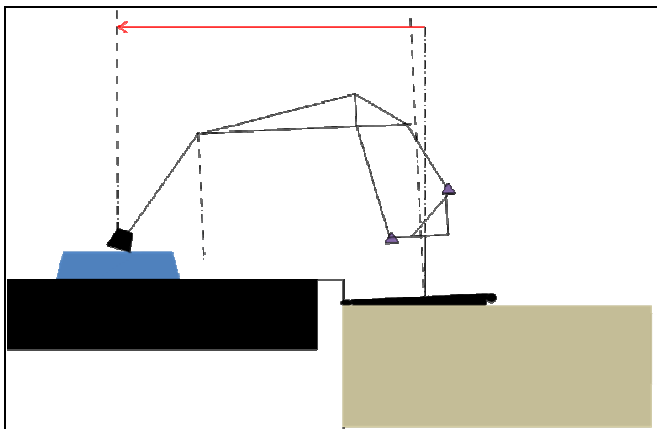


**Figure 26: Occasional loading condition (Holleman, 2017)**

This section discussed the dynamic load effects which occur when the lemniscate crane is in operation.

### 2.3   Operational profile

This section discusses the operational profile for the crane. For the crane used in this study, experts within the Maja Stuwadoors BV and available literature are consulted.

First the geometric specification is required to develop a 3D model using Solidworks. Within the Maja Stuwadoors BV, a CAD model of the upper structure was already available to use. Mass parameters are required and according to the crane book of the 25t Cornelis Tromp described by Jansen (1996), the mass of the slewing upper structure is 367t and for the total floating structure is 1413 tons, seen in the following Table 1.

| Name of part | Mass [ton] | Mass [ton] |
|---|---|---|
| Front arm | | 29 |
| Upper arm | | 38 |
| Rear arm | | 48 |
| Counterweight at rear arm | | 95 |
| Tower | | 32 |
| Machine floor | | 81 |
| Crane house | | 8 |
| Sokkel | | 3 |
| Counterweight at machine floor | | 42 |
| Hoisting equipment(cable,winches,motors,pulleys) | 10 | |
| Slewing equipment (motors,brakes,gearbox,gears, shafts) | 3.3 | |
| Luffing equipment (hydr cylinders, hydr oil, tank, pumps) | 10 | |
| Electrical equipment | 2.1 | |
| Total equipment on crane | 26.9 | |
| Cabin and support structure | 10 | |
| **Total slewing part crane** | | **376** |
| Foot | 20 | |
| Pontoon | 980 | |
| **Total mass under slewing part crane** | **1000** | |
| **Mass total floating crane (pontoon + crane)** | | **1412.9** |

**Table 1: Crane component masses (Jansen, 1996)**

The main operational parameter required is the total time for a working cycle, known as the cycle time. This is the total time needed for the crane to execute the sequence of all the motions together during a duty, starting at the moment of loading up to the moment the next loading will start. The following Table 2 presents a summary of the crane specifications found in the crane book written by Jansen (1996).

| Load reach (both grab and hook load) | 12m (min) | 39.993m (max) |
|---|---|---|
| luffing speed | 1m/s | |
| Hoisting capacity | 25t (incl. grab weight) | |
| | 25t (incl. hook weight) | |
| Hoisting speed | 130m/min (empty grab) | 120m/min(full grab) |
| Max. hoisting height | 30m above water level | 15m below water level |
| Slewing reach | 360deg | |
| Slewing speed | 1.5 rpm (unloaded) = 9 deg/s | |
| | 1 rpm (loaded) = 6 deg/s | |
| **General pontoon specification** | | |
| Length (m) | 40 | |
| Width (m) | 24 | |
| Height (m) | 4 | |
| Draft (m) | 2.5 | |

**Table 2: General crane operational specifications (Jansen, 1996)**

The cycle time depends on a large number of factors for this crane type. The discussion of all these factors is not part of the assignment. However the most important ones for this study are addressed.

One factor are the stages which occur during the total time the crane spends transporting material from A to B. In this process the material volume decreases at location A and increases at location B, see Figure 27. Van Vianen (2015) classified this phenomenon into a free digging stage, an intermediate stage and a cleaning stage. The first stage is the free digging stage. During this stage material is grabbed from the upper part of the hatch. This stage accounts for 40% of the total unloading time where 50% of the transshipment load is displaced from A to B, see Figure 28. Because material volume is sufficient at A, it can be grabbed within a minimum time and dropped at minimum time at B which has sufficient space. This stage has the smallest cycle time due to the fast handling sequences and the largest dynamic effects during the acceleration and braking phase. The second stage is the intermediate stage. During this stage material that is stored at the lower part of the hatch is grabbed. The grab has to be lowered further into the hatch increasing the time spent during this movement. This stage accounts for 33% of the total unloading time where 35% of the transshipment load is displaced from A to B, see Figure 28. The last stage is the cleaning stage. At this stage available machinery is brought into the hatch to move the remaining material volume to the mid where the material can be grabbed at location A. This stage accounts for 27% of the total unloading time where 15% of the transshipment load is displaced from A to B, see Figure 28 and Figure 22. The cycle time during this stage is the highest.
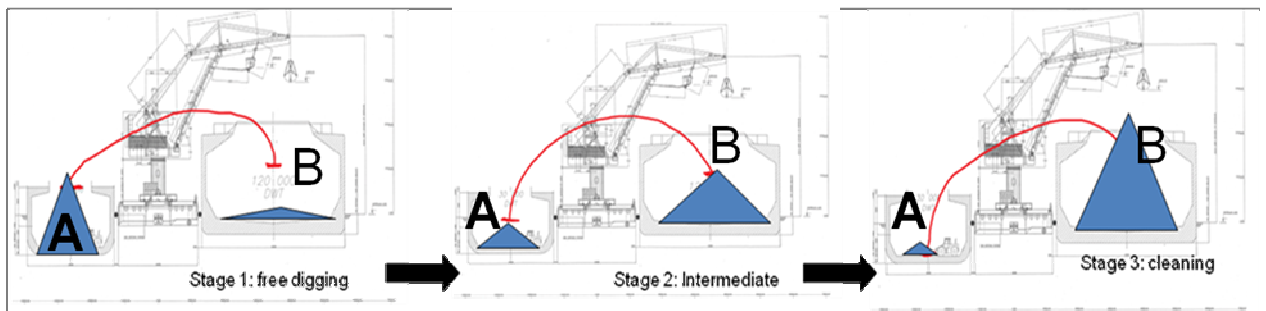
**Figure 27: Transshipment stages (a)**

| | Free dig-<br>ging stage | Intermidi-<br>ate stage | Trimming<br>stage |
|---|---|---|---|
| percentage<br>of the load | 50 % | 35 % | 15 % |
| percentage<br>of the un-<br>loading time | 40 % | 33 % | 27 % |

**Figure 28: Transshipment stages (b) (Verschoof, 1999)**

The second factor influencing the cycle time is the variety in hoisting heights encountered. This is related to the ship geometry being handled. The larger the hoisting height, the longer it takes to hoist or lower the grab, see Figure 29.
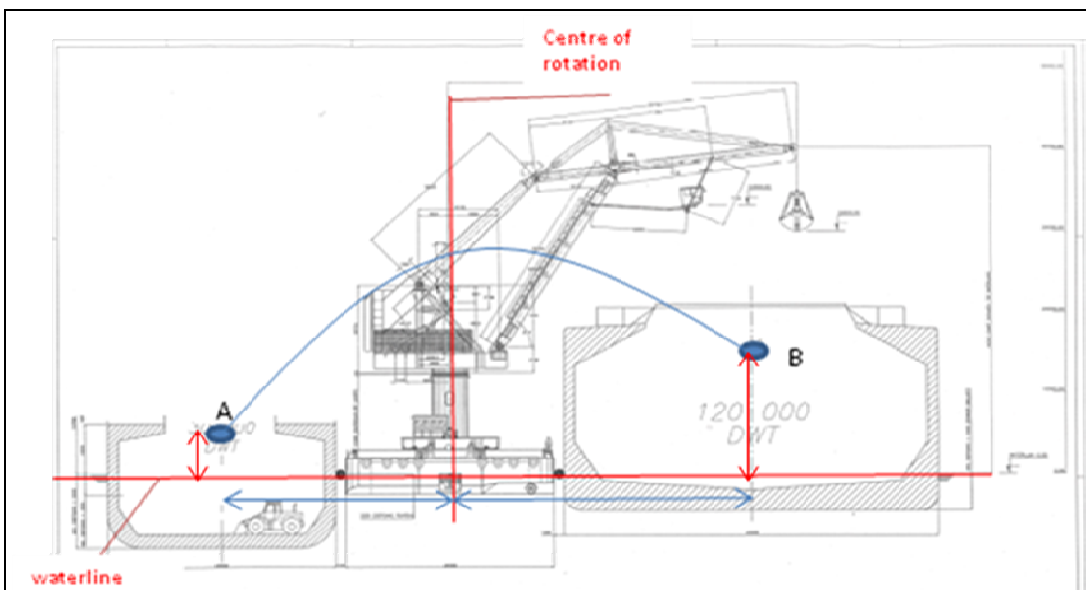


**Figure 29: Variable hoisting & lowering displacement (Croese engineering, 1996)**

A sample of the operational data from 2016 seen in Figure 30, provided by Holleman (2017), revealed that the Cornelis tromp crane was in 72% of the time in operation and 28% out of operation. In the time spent out of operation, the crane was under maintenance or sailing. Pulle (2017) provided the total number of operational hours up to the moment of writing which is 52263 hours.
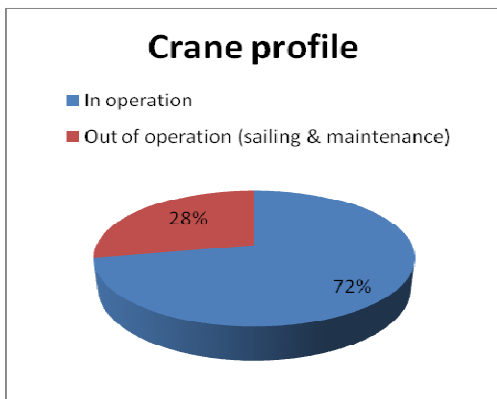
**Figure 30: Crane profile of the CT (Holleman, 2017)**

During the time in operation the crane is shifted from one position A to the other B in order to remain an optimal transshipment process, seen in Figure 31. An interview with Starrenburg (2017) revealed that 1% of the total operational time of the crane is spent in shifting which is about 523 hours. This results in the total effective operational hours of 51740 up to the moment of writing.
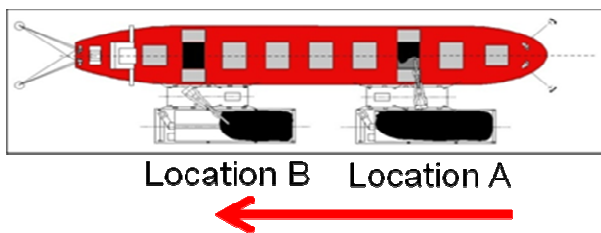


**Figure 31: Shifting process during transshipment (Starrenburg,2017)**

Starrenburg (2017) shows that to achieve optimal transshipment conditions, 98% of the time slewing occurs between 90 and 120 degrees, seen in Figure 32. In very view times a slewing reach of 180 degrees is required.
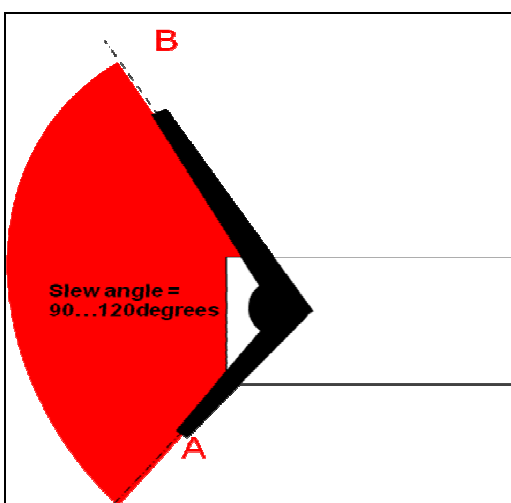


**Figure 32: Optimal slewing reach (Starrenburg, 2017)**

The luffing reach of the crane is designed to allow a horizontal movement from minimum to maximum reach. According to Holleman (2017), a typical luffing movement during operation is the horizontal displacement from an intermediate flight of about 20m to a maximum flight of 40m. This movement requires a minimum amount of time in the total working cycle of the crane.

The transshipment method during operation of the crane has been discussed in this section and the mass and operational parameters have been specified according to the crane book. These will be used in the next section to calculate the number of transshipment moves.

### 2.4   Cycle-time analysis & number of transshipment moves

In this section the number of transshipment moves for the past twenty one years is calculated using a cycle time analysis. The number of moves is one of the main influential parameters required to perform the fatigue assessment.

First a representative transshipment configuration is specified on the basis of the previous discussed crane operational profile. This is illustrated in Figure 33 and the following sequence of motions is assumed:

1. crane starts hoisting a fully loaded grab of 25t at an intermediate flight of 20m at location A. The load is hoisted from rest to a maximum speed of 2m/s.
2. crane rotates 120° CCW with 25t at 20m flight from rest to 1rpm.
3. crane starts luffing out from 20m to 40m flight with 25t. This luffing movement occurs from 0m/s to 1m/s.
4. crane lowers the 25t load at 40m flight from rest to a maximum speed of 2m/s.
5. crane is then unloaded at location B. The remaining hoisting weight is the empty grab with a dead weight of 9t according to (Maja stuwadoors BV, 2017). It must be noticed that this value depends on the chosen grab and is not a fixed value, however for the calculation this value is chosen.
6. crane starts hoisting the 9t at 40m flight from rest to 2.1m/s.
7. crane slews 120° CW back with 9t at 40m from rest to 1.5rpm.
8. crane is luffing in from 40m to 20m flight with 9t from 0m/s to 1m/s
9. crane lowers 9t at 20m flight from rest to 2.1m/s.
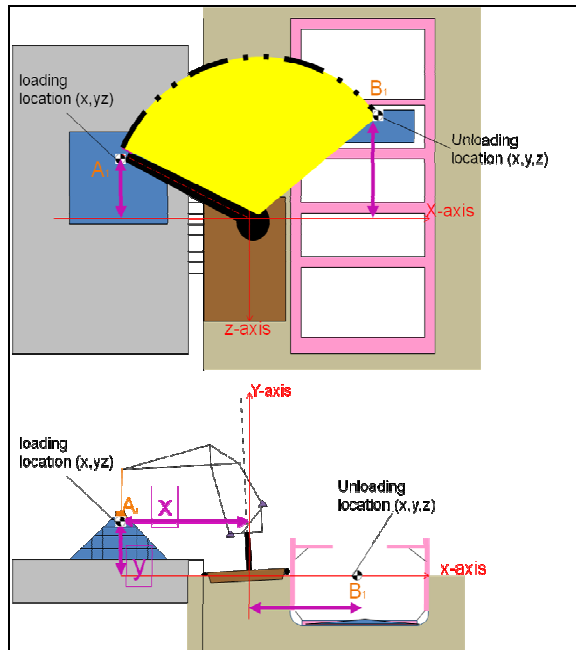
**Figure 33: Representative crane service profile**

The second step is to determine the required time for all the sequence of movements for a complete working cycle. This is presented in a cycle time diagram which is based on kinematical calculations. The following example demonstrates this calculation for the hoisting movement, seen in Table 3:

1. Hoisting displacement value is chosen based on personal observation during the transshipment of scrap metal from a barge to a sea ship at HKS scrap metal Amsterdam (personal communication, February 24, 2017) and a technical drawing from Croese Engineering (1996) provided by Maja Stuwadoors BV (2017).

2. Hoisting, luffing and slewing velocities are derived from the crane book by (Jansen, 1996) as discussed previously

3. Acceleration & braking times are chosen based on the observations mentioned at point 1, an interview with an experienced crane operator (Vorthoren, 2017), the book from Verschoof (1999), who presents an extensive methodology on the design and maintenance of cranes and a research conducted within the section of transport engineering and logistics by Steuten (1993). He performed a conceptual study for the hydraulic system of a 36t lemniscate crane and the influence of different possible cycle time configurations during a working cycle.

| Motion | Hoisting & lowering full grab | | Hoisting & lowering empty grab | |
|---|---|---|---|---|
| Total displacement (m) | 15 | | 15 | |
| velocity(m/min) | 120 | | 130 | |
| acceleration time (s) | 4 | | 4 | |
| deceleration time (s) | 4 | | 4 | |
| Acceleration(m/s^2) | 0.5 | | 0.54 | |
| deceleration(m/s^2) | 0.5 | | 0.54 | |
| velocity | 2 | | 2.16 | |
| **time-displacement** | **t(s)** | **S(m)** | **t(s)** | **S(m)** |
| accelerating | 4.0 | 4.0 | 4.0 | 4.3 |
| cruising | 3.5 | 7.0 | 2.9 | 6.3 |
| braking | 4.0 | 4.0 | 4.0 | 4.3 |
| **TOTAL** | **11.5** | 15.0 | **10.9** | 15.0 |

**Table 3: Cycle time example calculation- Hoisting kinematics**

This time-displacement calculation is done for all sequences of motions for slewing and luffing found in Appendix B in Table 40 and Table 41. Subsequently all individual times are added together resulting in a total cycle time of 118.2s for one load cycle seen in Figure 34. This value was found reasonable and was in accordance with Holleman (2017). A spread sheet was developed to determine this total cycle time and can be found in Appendix B in Table 42.
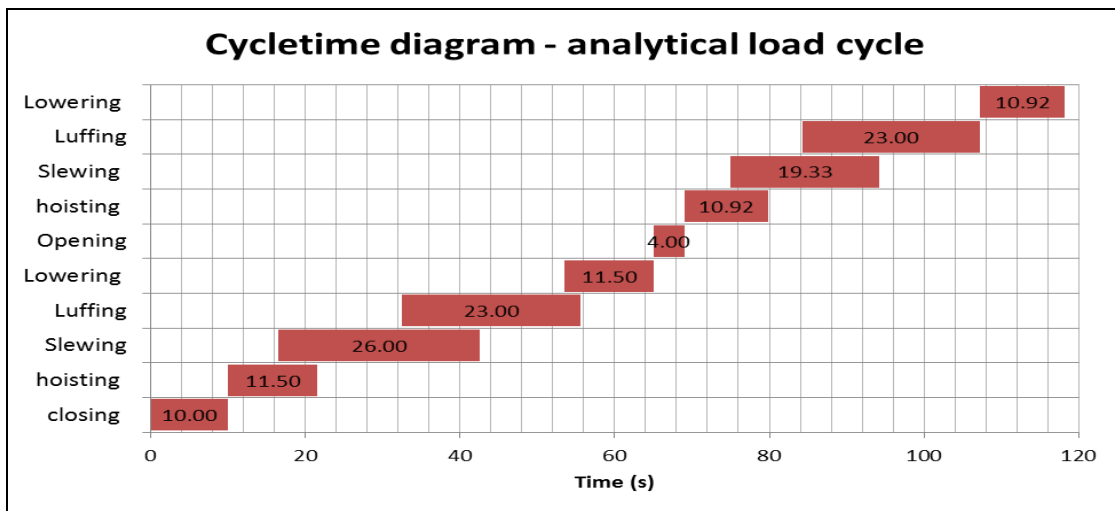


**Figure 34: Cycle time diagram for a free digging stage working cycle**

The last step is to calculate the number of transshipment moves. For this calculation the total operational hours, the time spent for shifting and the effective operational time which was determined in the previous section are used. In order to take the increase in cycle time which occurs during the different transshipment stages into account and also other cycle

time influencing factors where more time is required, the following reasonable assumptions are made for scrap handling:

1. average duration of one move during free digging stage is 118.2s which is about 2min.
2. average duration of one move during free intermediate digging stage is about 2.3min.
3. average duration of one move during free cleaning stage is about 3min.

Taking the average number of effective moves for the three stages is calculated to be 25 transshipment moves per hour. This value is multiplied with the effective hours spent for transshipment and results in 1.31 million transshipment moves up to the moment of writing. The complete calculation of the number of moves is shown in the following Table 4

| 1 | total operational hours up to the moment (Pulle, 2017) | 52263 | hrs |
|---|---|---|---|
| 2 | Assumption % of shifting for total operational time (Starrenburg, 2017) | 1 | |
| 3 | assumption duration of one move during free digging stage | 2,0 | min |
| 4 | assumption duration of one move during intermediate digging stage | 2,3 | min |
| 5 | assumption duration of one move during cleaning stage | 3,0 | min |
| 6 | Average total time spent shifting | 523 | hrs |
| 7 | Average effective time spent for transshipment | 51740 | hrs |
| 8 | Average number of moves per hour during free digging stage | 30 | |
| 9 | Average number of moves per hour during intermediate stage | 26 | |
| 10 | Average number of moves per hour during cleaning stage | 20 | |
| 11 | Average number of moves | 25,36 | |
| | | | |
| | **Total average number of moves up to the moment** | **1,31E+06** | |

Table 4: Number of transshipment moves up to present

In this chapter the mechanical principles, the dynamic load effects which occur when in operation, the transshipment method used during operation and the current average 1.31 million moves have been calculated for the crane used in this research. The latter will be used in the fatigue calculations.

In the next chapter the fatigue assessment according to the dynamic simulation method is discussed.

## 3    Fatigue assessment using MultiBody Dynamics and the Finite Element Method

Multibody system dynamics studies the behavior and influence of complex mechanisms subjected to external forces and movements. A crane is a MultiBody system containing multiple rigid and flexible bodies connected by joints to each other to limit their relative motion and undergoes large rigid body motion. One of the many available Multibody dynamics simulation software packages according to a survey of Lu (2015) is ADAMS (Automatic Dynamic Analysis of Mechanical Systems). ADAMS allows to develop mathematical realistic virtual prototypes and simulate the motion of the mechanical systems being studied. The underlying theory used in ADAMS is based on the principles of Euler-Lagrange equations. ADAMS solves these equations using solvers which use predicted states to advance in time, with any resulting forces being back-calculated (McConville, 2015).

Past researches demonstrated the use of ADAMS to study the dynamic loading characteristics of lifting and hoisting equipment. Ying and Wenyuan (2013) developed a ADAMS model for a dragline to investigate it's dynamic loading and ANSYS to study its effect on the structural strength of its front end. Lu et al., (2013) performed a research on a joint simulation of a trolley vehicle-frame structure coupled vibration using ADAMS and ANSYS for a 40 feet container crane. Cai et al., (2014) showed the use of a coupled/ joint FEM and MBD simulation to obtain stress-time spectra for fatigue assessment for a crawler crane. Wu (2014) performed a dynamic strength calculation on the Reel Fulcrum movement characteristic of bridge crane lifting mechanism. He (2014) demonstrated the use of a rigid-flexible methodology for offshore crane design using ADAMS and ANSYS. Wardeh and Frimpong (2016) developed an ADAMS model of a rope shovel used in the mining industry to simulate its working cycle and study shovel performance. Rupar et al., (2016) developed an model in ADAMS for a loader crane used for timber and waste transport to study its loading influence on fatigue. Qiang et al., (2015) developed an container crane ADAMS model to study the influence of a seismic wave excitation on the overturning of the complete structure. Si et al., (2016) studied the dynamic response of a flexible boom hoisting system of a level luffing dock crane using ADAMS and ANSYS. Zhang et al., (2010) performed a study about the application of combining Ansys and ADAMS in structural engineering. In the research they analyzed the data exchange from Ansys to ADAMS and vice-versa for a cable -stayed space truss where the structural displacement and stress characteristics were in good agreements with the expected results.

Most of these studies use ANSYS to develop a flexible model which are subsequently imported in ADAMS, because of its poor meshing possibilities.  The final result is that within

ADAMS a direct visual representation is provided of the stresses occurring in time for the simulated working cycle. Although this is the most common method used in the literature, however up to the moment writing, a different method where crane motion analysis is performed in ADAMS only and service loading is subsequently used in ANSYS for stress analysis has not been identified. This chapter will demonstrate the use of the latter mentioned method.

This chapter starts with the development of the simulation model for the lemniscate crane. Then the transshipment method used during operation which was described in the previous chapter is simulated. A force analyses is subsequently performed for the calculated loads from ADAMS for the upper arm. The generated service load history will be used as load input for FEM model developed using ANSYS to calculate the stress-time history for the critical tubular welded joint.  Using Rainflow counting method, the stress ranges are then calculated to determine the accumulated fatigue damage from the past 21 years.

### 3.1    Multibody dynamics modeling and simulation

A rigid body model is developed in ADAMS seen in Figure 36. This was done by importing the 3D Solidworks CAD model into ADAMS. For each component, mass and mass of inertia properties were assigned according to the crane specifications from Table 1. Mass of inertia properties for the components were calculated using Solidworks and the use of tables for simplified homogenous rigid bodies seen in Table 43, Table 44 and Table 45 in Appendix B. Next each component was connected to each other using joints. The choices made for the complete model were demanded to both satisfy crane specification and the Gruebler expression (McConville, 2015): $m = 6*\left(n_{bodies}-1\right)-n_{constraints}$ . The main results of this modeling phase can be seen in Table 5 and details of the choices made can be found in Table 46 in Appendix B.

| # of rigid bodies in ADAMS model ( $n_{bodies}$ ) | 18 | | |
|---|---|---|---|
| # of DOF removed with chosen ADAMS joints ( $n_{constraints}$ ) | | 108 | |
| DOF for each rigid body | 6 | | |
| total # of DOF rigid bodies | | 108 | |
| DOF for the ADAMS crane model (m) | | 0 | Criterion: number of DOF must be equal to zero and there must be no redundant constraints |

**Table 5: Kinematic constraints ADAMS crane model**

The hoisting mechanism was modeled using the ADAMS cable module. ADAMS provides two methods to model cables (Mscsoftware, 2014):

1. Simplified method(coupler mode):
   a. neglects cable mass and inertia
   b. computes only cable span tension and forces on pulleys
2. Discretized method(guide mode), see Figure 35:
   a. flexibility based on the Euler Bernoulli beam theory
      i. longitudinal stiffness (Sforce  superposed to translational joint)
      ii. torsional stiffness (one rotational Sforce superposed to cylindrical joint)
      iii. bending stiffness (one Sforce superposed to two revolute joints)
   b. computes cable vibration and pulley forces
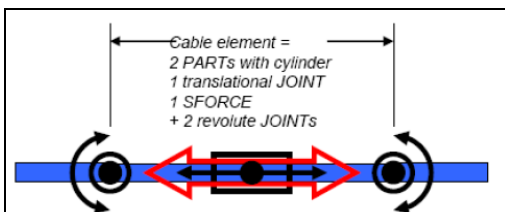


**Figure 35: ADAMS cable element topology (Mscsoftware, 2014)**

Based upon experience the simplified method was used because the simulation model showed stable simulation behaviour and less computational effort was required. ADAMS only calculates the cable tension and the forces on the pulleys in the model. The method neglects cable mass and inertia effects. Input parameters can be found in Appendix B in Table 47 and Table 48.
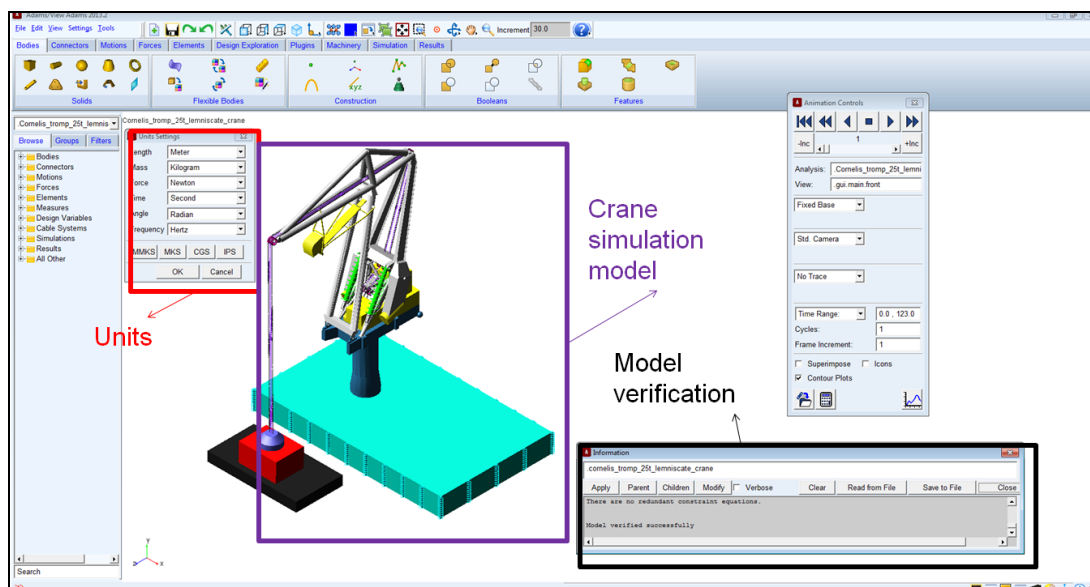


**Figure 36: Overview ADAMS crane simulation model in starting position**

The motions as described in Table 6 were then added using step functions as described in McConville (2015) and Sohoni, (1995). These functions allow a sequence of events to be executed based on the operational profile and the cycle time calculation from the from previous chapter. A sheet showing the details on time durations for the different motions in ADAMS can be found in Table 49 in Appendix B.

|   | *Action* | *Expression* |
|---|----------|--------------|
| 1 | Hoisting | step(time,1,0,12.5,-15) |
| 2 | Slewing | step(time,7.5,0,33.5,-120d) |
| 3 | Luffing | step(time,23.5,0,54.5,64d) |
| 4 | Lowering | step(time,52.5,0,64,15) |
| 5 | Opening | step(time,64,0,68,-1) |
| 6 | Hoisting | step(time,68,0,78.9,-15) |
| 7 | Slewing | step(time,73.9,0,93.3,120d) |
| 8 | Luffing | step(time,83.3,0,114.3,-64d) |
| 9 | Lowering | step(time,114.3,0,125,15) |

**Table 6: ADAMS driving functions**

Then the loads were added to the model, seen in Figure 37. The picking up of the 25t load and the dropping of the load was modeled using the method from Verheul (2017).  This method uses a contact representation based on a 3D spring-damper model. The contact model acts as a magnetic clamp, to assure a constant contact between the hoisting mass and the grab. A step function is combined with the 3D spring damper model to simulate the picking up and dropping of the load. The pontoon motion was modeled using a spring damper model adapted from Song et al., (2017) who established a dynamic model for a goods ship using ADAMS. This method simulates the dynamic roll motion of the pontoon.
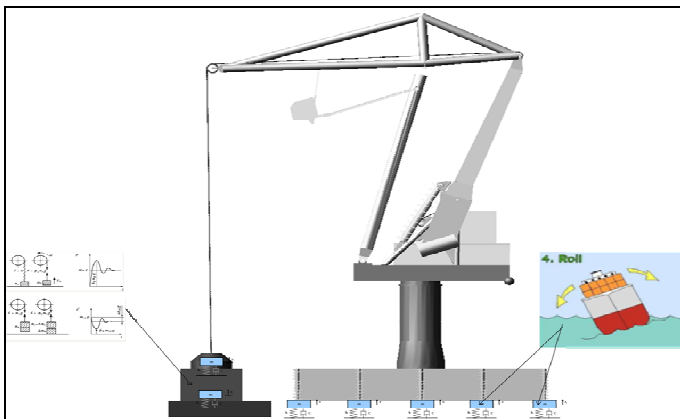


**Figure 37: Modeling of load hoisting & pontoon motion in ADAMS**

The next chapter discusses the verification of the developed model.

## 3.2   Model verification

In the previous paragraph the development of the model was discussed. The next step is to verify if the model mimics the previously discussed transshipment method used in operation from section 2.4.

Figure 38 shows the simulated working cycle diagram in ADAMS. The cycle starts at t=0s and ends at t=125s.
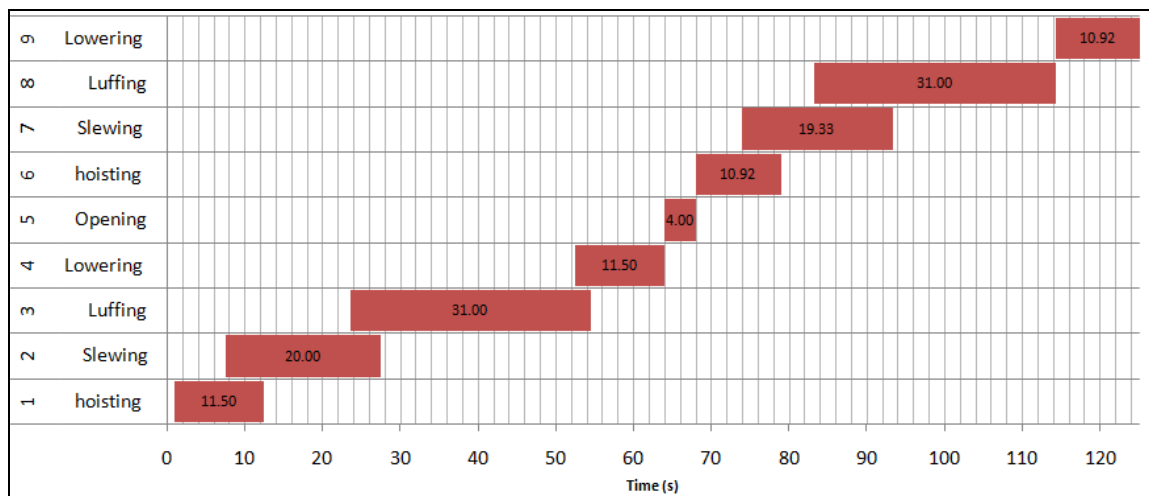


**Figure 38: ADAMS simulated cycle-time diagram based on the free digging stage**

| Total cycle time | 125.18  s |
|---|---|
| Number of cycles per hour | 28.8 |

According to Table 7 the ADAMS model shows an acceptable cycle time deviation of 5.5% with the analytical calculation from  Figure 34. The main reason for this deviation is that the chosen numerical solver required extra time which was about 5s in order to show a stable dynamic simulation for the entire working cycle , due to the large number of contacts present in the model.

|  |  | *Average cycle time [s]* | *Deviation* |
|---|---|---|---|
| **Theoretical model** | Analytical load cycle | 118.18 | 5.59% |
| **ADAMS model** | Simulated load cycle | 125.18 | |

**Table 7: Deviation cycle time ADAMS simulation & analytical calculation**

The next verification step is to compare the measured model speeds in ADAMS with the crane specification. Figure 39 shows the hoisting of the grab with load from 0 to 2m/s along a vertical displacement of 15m. The values were found acceptable and are in accordance with the crane specification.
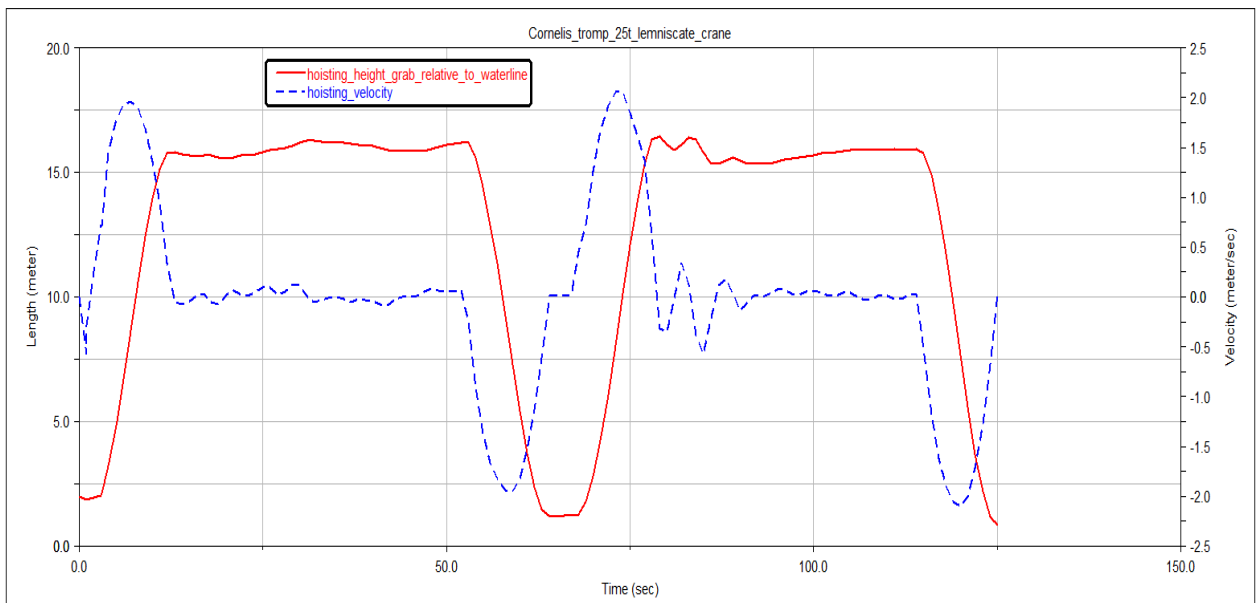
**Figure 39: ADAMS input hoisting signal and measured grab displacement**

Figure 40 shows a slewing angular velocity between 0.104 - 0.157rad/s, which depends on the flight at which the crane rotates. These values are acceptable.
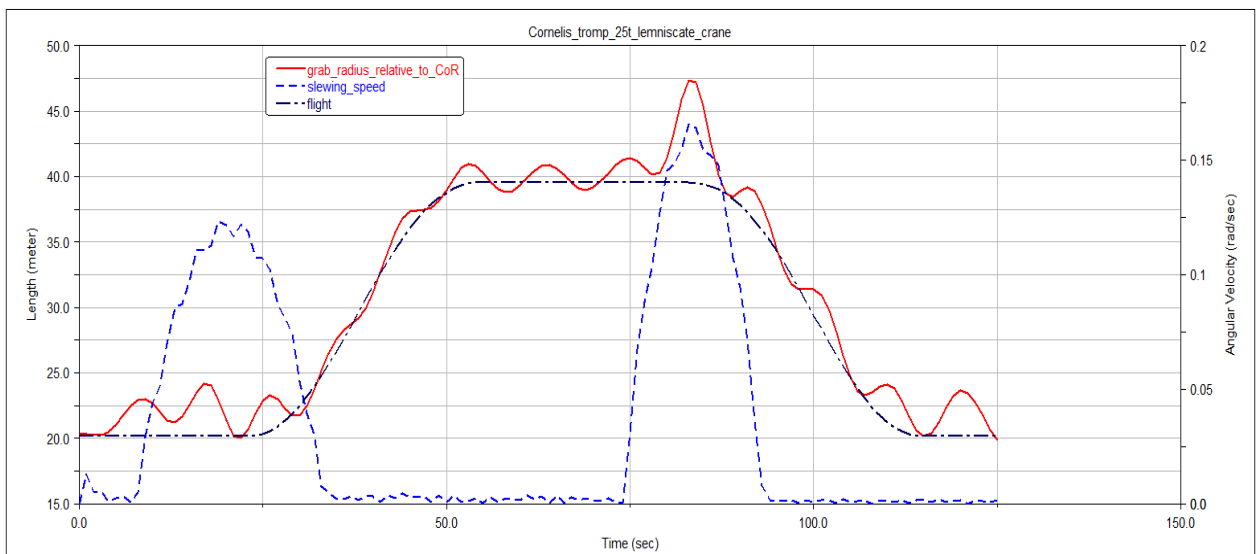


**Figure 40: ADAMS input slewing signal and measured grab motion**

Figure 41 shows a measured luffing speed of 1m/s, which is in accordance with the specification.

Crane fatigue assessment using Multibody Dynamics and Finite Element Method
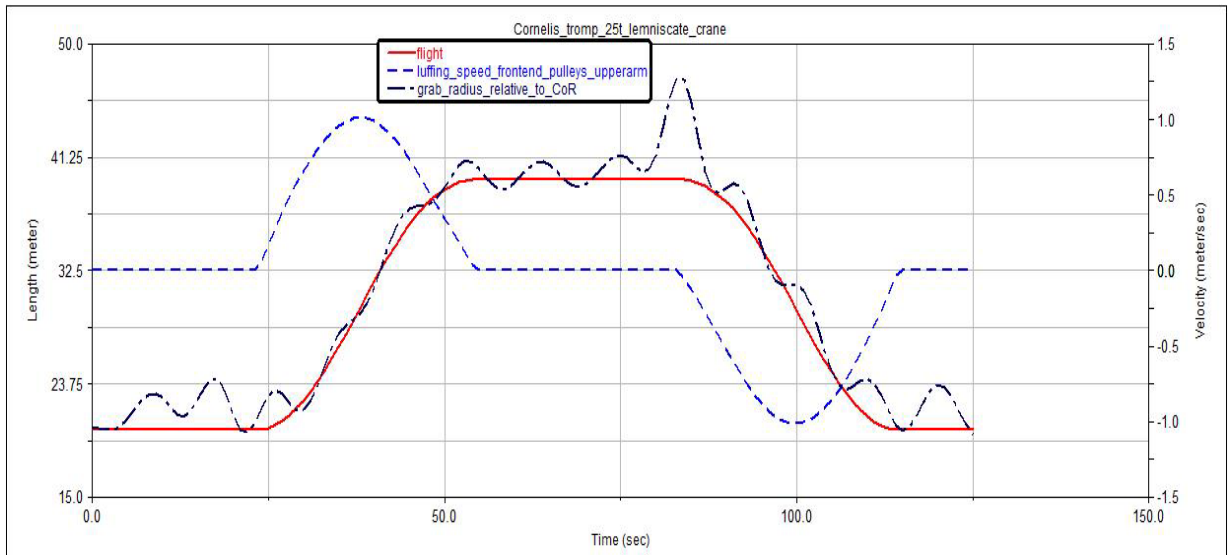
**Figure 41: : ADAMS input luffing signal and measured grab motion**

Figure 42 shows the measurement parameters for the pontoon motion with 5 lines: red line is the roll angle, dotted blue is the pitch angle, dotted magenta is the flight, dark blue is the loading curve and green is the sweeping of the grab to a greater radius during slewing. For this model a value about 1.5 degrees was measured, which differs about 25% with the roll angle of 2 degrees described by Nieuwenhuis (2006) which is chosen as a reference value.
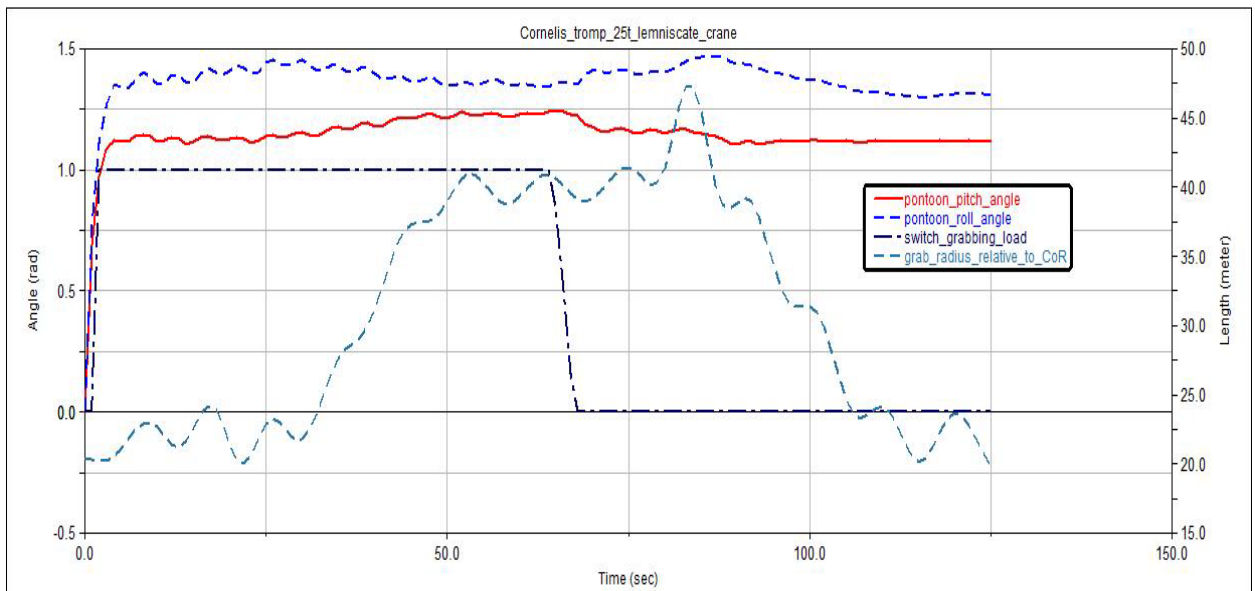


**Figure 42: ADAMS measured pontoon motion when the crane is loaded and unloaded**

The last verification step is to measure the mass distribution of the model. Figure 43 shows that total mass of the upper slewing structure matches total mass prescribed in the crane specification of 376 tons in Table 1.

```
Aggregate mass for objects:
  .Cornelis_tromp_lemniscate_crane.ground
  .Cornelis_tromp_lemniscate_crane.ballastbak_L
  .Cornelis_tromp_lemniscate_crane.ballastbak_R
  .Cornelis_tromp_lemniscate_crane.sokkel
  .Cornelis_tromp_lemniscate_crane.machine_floor
  .Cornelis_tromp_lemniscate_crane.front_arm
  .Cornelis_tromp_lemniscate_crane.crane_house
  .Cornelis_tromp_lemniscate_crane.Tower
  .Cornelis_tromp_lemniscate_crane.upper_arm
  .Cornelis_tromp_lemniscate_crane.rear_arm
  .Cornelis_tromp_lemniscate_crane.counterweight_L_at_machinefloor
  .Cornelis_tromp_lemniscate_crane.counterweight_R_at_machinefloor
 The aggregate mass in the global reference frame is:
  Mass          : 3.76E+005 kg
  Center of Mass Location : 0.0, 20.6081463217, -1.9959888787 (meter, meter, meter)
```

**Figure 43: : Mass verification ADAMS model – slewing upper structure**

Table 8 and Figure 44 show a difference of 8.7% for the CoG in the height of the crane between the hand calculation and the ADAMS model.
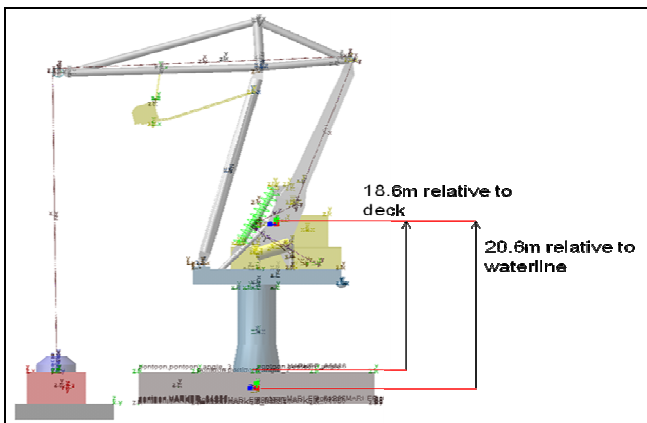


**Figure 44: Illustration mass distribution ADAMS model**

|  | Hand calculation | ADAMS | Deviation |
|---|---|---|---|
| CoG relative to waterline (m) | 18.8 | 20.6 | 8.73% |

**Table 8: Mass distribution ADAMS model**

The total mass of the ADAMS model is 1455t, seen in Figure 45. This is a difference of 2.88% with the real mass of the total floating structure which is 1413t (see Table 1). This value is found to be acceptable.

```
Aggregate mass for objects:
The aggregate mass in the global reference frame is:
  Mass          : 1.4551780953E+006 kg
  Center of Mass Location     : 0.1302314918, 6.6207790666, 5.039118937 (meter, meter, meter)
```

**Figure 45: Mass verification ADAMS model – complete crane pontoon**

The payload for the fully loaded ADAMS crane model is equal to 25t, seen in Figure 46 and an unloaded crane is loaded equal to the dead weight of 9t which is equal to one a grab used in the operation of the chosen crane (Maja Stuwadoors BV, 2016).

```
Aggregate mass for objects:
  .Cornelis_tromp_25t_lemniscate_crane.GRAB
  .Cornelis_tromp_25t_lemniscate_crane.load
The aggregate mass in the global reference frame is:
  Mass              : 2.5E+004 kg
  Center of Mass    :
     Location       : 0.0, 0.72, 19.6667101766 (meter, meter, meter)
     Orientation    : 3.1415926526, 4.9308217183E-003, 3.1415926546 (rad)
```

**Figure 46: ADAMS model loaded with 25 tons inc. grab weight**

Figure 47 shows the moment in time during the simulation when the crane picks up the load at t=2s, starts hoisting and lowers the load and releases it at t=67s. The hoisting mechanism curve describes the shortening of the cable length when declining and an extension of the cables when it shows an upwards trend.
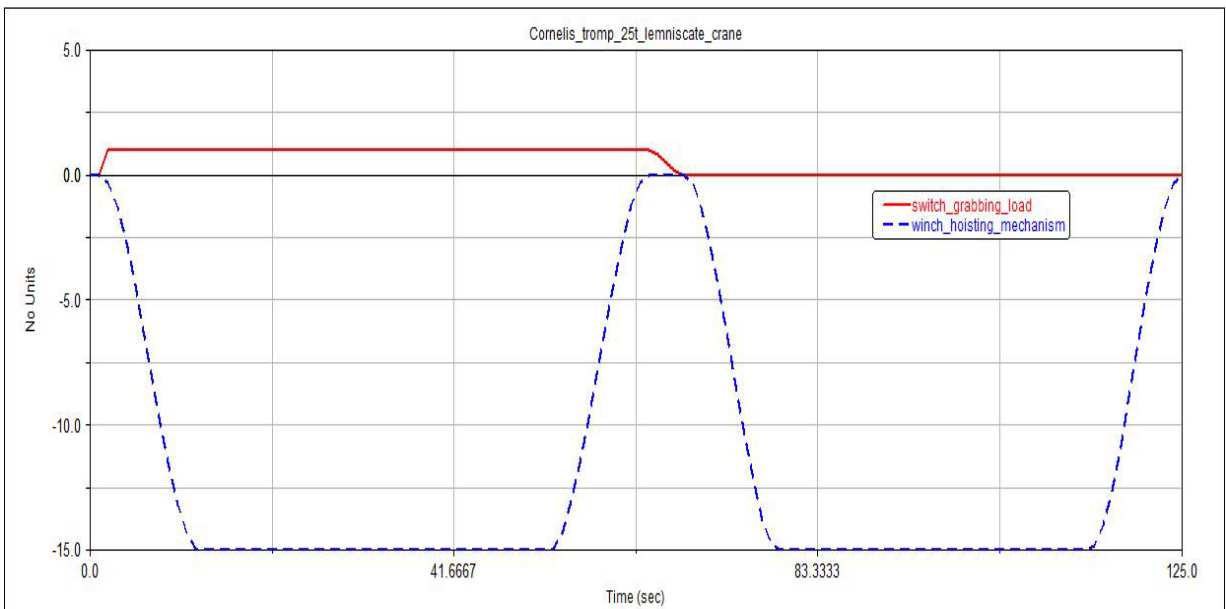


**Figure 47: ADAMS loading switch sequence input signal & cable length measurement**

The cycle time, crane motions and mass distributions of the ADAMS model have been verified with the defined operational profile and the crane specification. All values were found acceptable.

The next paragraph discusses the service load results of the simulation acting on the upper arm structure.

### 3.3    ADAMS load results and analysis

This paragraph will discuss the calculated ADAMS loads on the upper arm structure only at the locations illustrated with the purple colored names in Figure 48 at eight locations for this component. These are the loads at the:

1. Four pulleys at frontend of the boom
2. Support joint of the cabin suspension
3. Left joint upper arm-front arm
4. Right joint upper arm-front arm
5. Rear joint upper arm-rear arm

The calculated loads for each location (represented by a marker in ADAMS) are in the local coordinate system of that marker. For example at the tip, transverse forces are in the local y-axis, lateral forces in the local z-axis and longitudinal forces in the local x-axis.
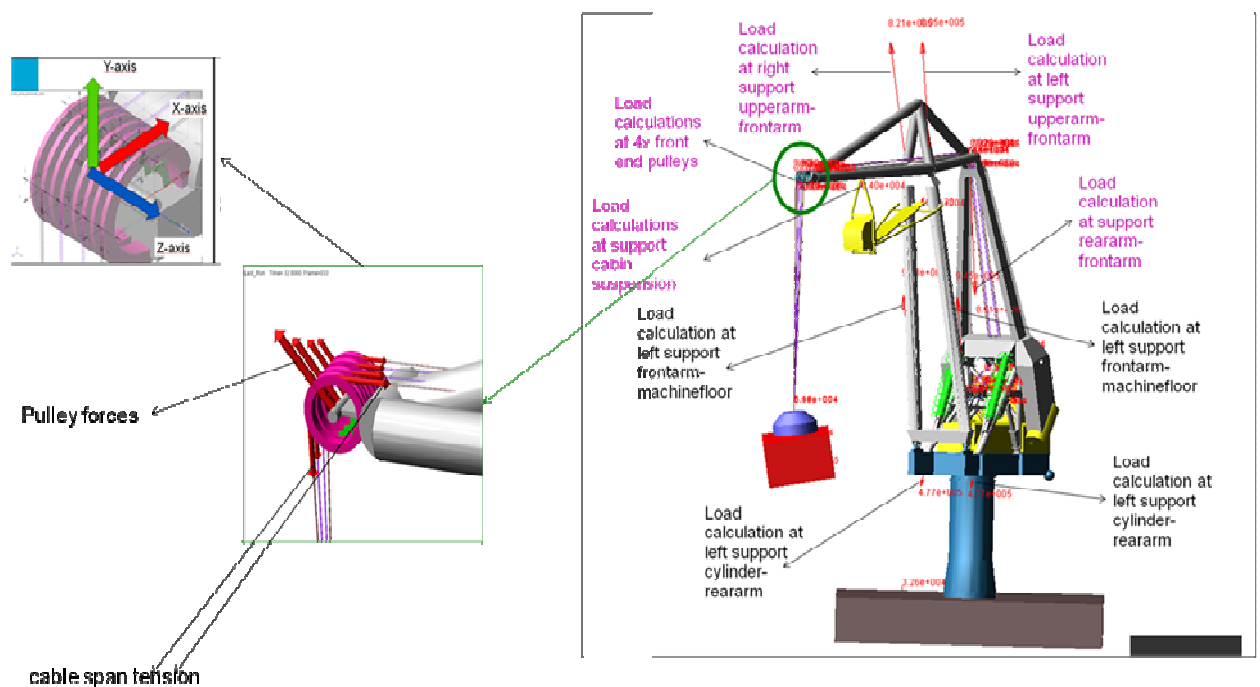


**Figure 48: ADAMS dynamic load calculation during transshipment cycle simulation**

The following graphs in Figure 49 and Figure 50 shows that the loads are transmitted from the moment of loading at t=2s from the hoisting weight via the cables to the pulleys. From the graphs it is concluded that the load is directly transmitted from the grab to the upper arm frontend pulley support, because the cables are modeled as a number of mass less rigid cylinders connected via rigid joints to each other in ADAMS. This proofs that indeed no cable stiffness effect is taken into account within this model using the simplified approach for the cable modeling described with Figure 35.
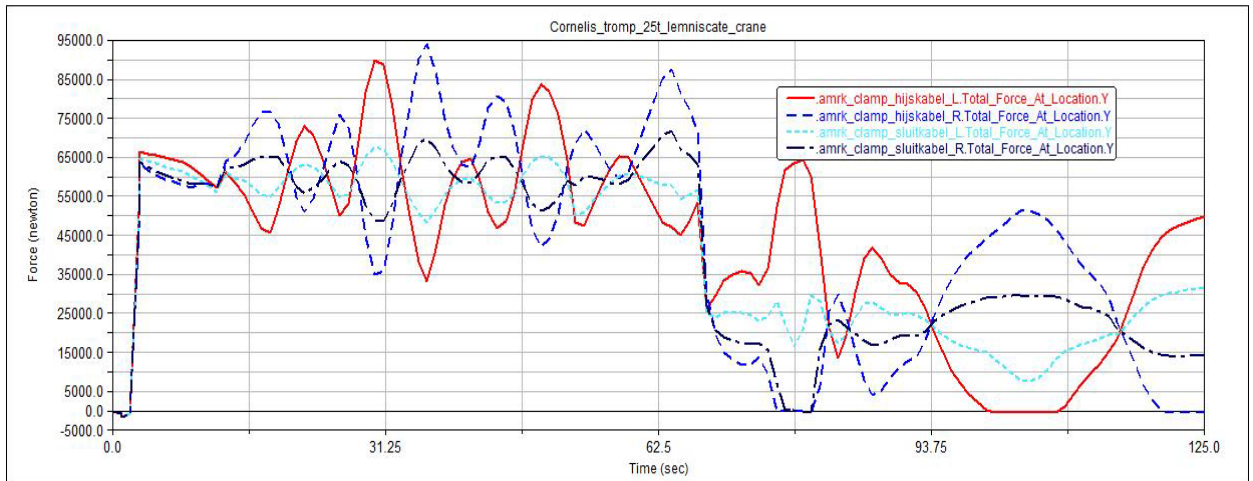
**Figure 49: Load transmitted from grab to cable**
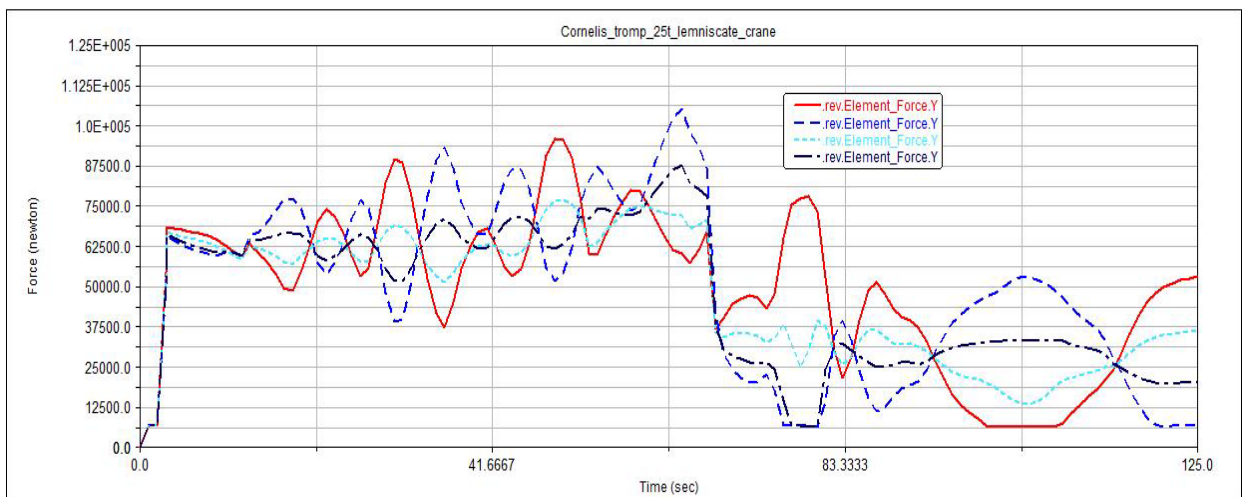


**Figure 50: Load transmitted from cable to frontend pulleys upper arm**

The following Figure 51 show the dynamic character of the vertical loads at the front end pulleys on the upper arm tip.
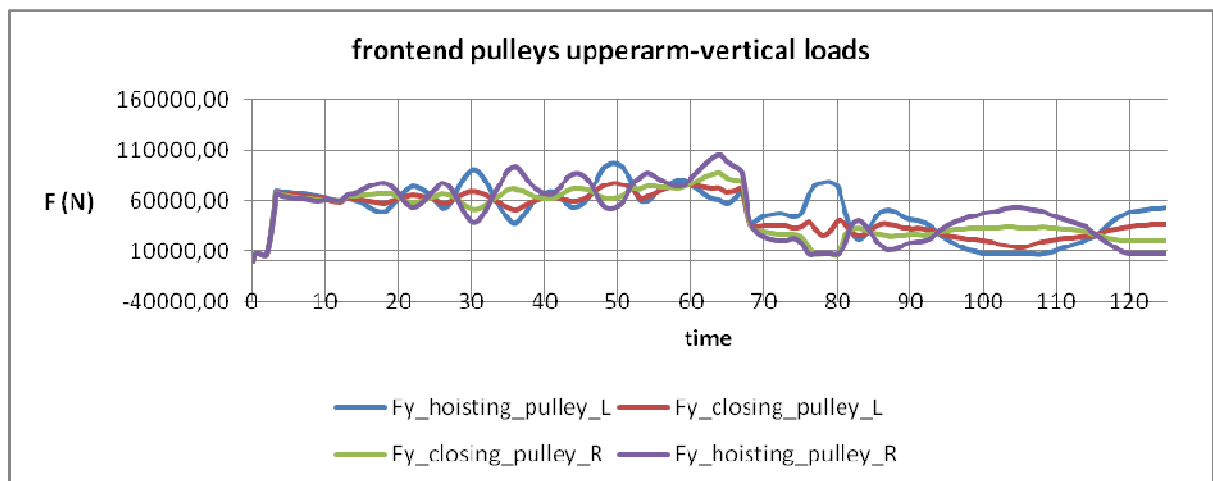


**Figure 51: ADAMS dynamic loads -frontend pulleys upper arm- local y direction**

Due to the load fluctuation, the following Figure 52 shows an example of the summation

$$F = \sum_{i=4}^{j=3} F_{ij}$$

$i = 1,2,3,4$ of the four frontend pulley vertical loads into a single readable load curve, for

$j = x, y, z$

i=1,2,3,4 and j=y.
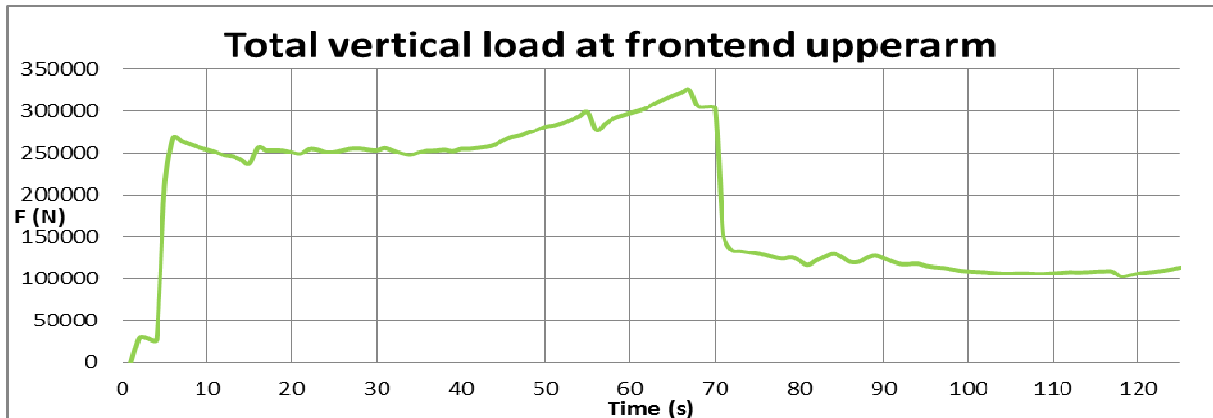


**Figure 52: total vertical dynamic load at front end pulleys**

Figure 53 and Table 9 show the total longitudinal, transverse and lateral loads acting at the frontend pulleys. The following is concluded:

1. the longitudinal curve shows a maximum peak force with magnitude of 245kN at t=30s (during the acceleration phase of luffing-out with full grab)
2. the vertical load curve shows a maximum force with magnitude of 325kN at t=64s (moment when the grab is opened at maximum flight)
3. the lateral load curve shows a maximum force with magnitude of 271kN at t=4s (during the acceleration phase of hoisting a full grab).
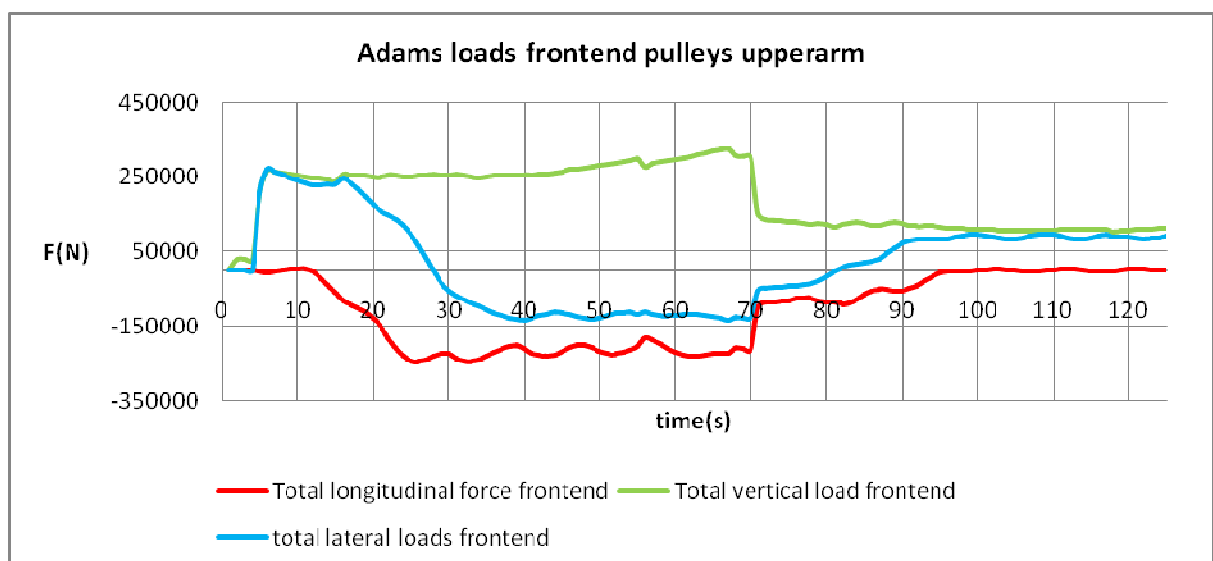


**Figure 53:  ADAMS loads at frontend pulleys upper arm**

| | Total longitudinal force frontend | Total vertical load frontend | total lateral loads frontend |
|---|---|---|---|
| Fmax (kN) | 244,6 | 325,2 | 271,3 |
| Fmin (kN) | 4,5 | 27,2 | 133,9 |

**Table 9: ADAMS maximum loads at frontend pulley-upper arm**

Calculation results obtained from ADAMS for the dynamic longitudinal and lateral forces acting at the front end pulleys on the upper arm can be found in Appendix B in Figure 116, Figure 117 and Table 50 provides an example of the calculated total longitudinal, vertical and lateral load data.

Figure 54, Figure 55 and Table 10 shows the dynamic loads occurring at the rear end pulleys on the upper arm:

1. the longitudinal curve shows a maximum force with magnitude of 318kN at t=25s which occurs during the acceleration phase of luffing out and during the braking phase of slewing CCW with a full grab

2. the vertical load curve shows a maximum force with magnitude of 278kN at t=3s, which occurs during moment of pulling up of the full grab

3. the lateral load curve shows a maximum force with magnitude of 336kN at t=8s which occurs during the braking phase of hoisting and the starting phase of slewing CCW with full grab.
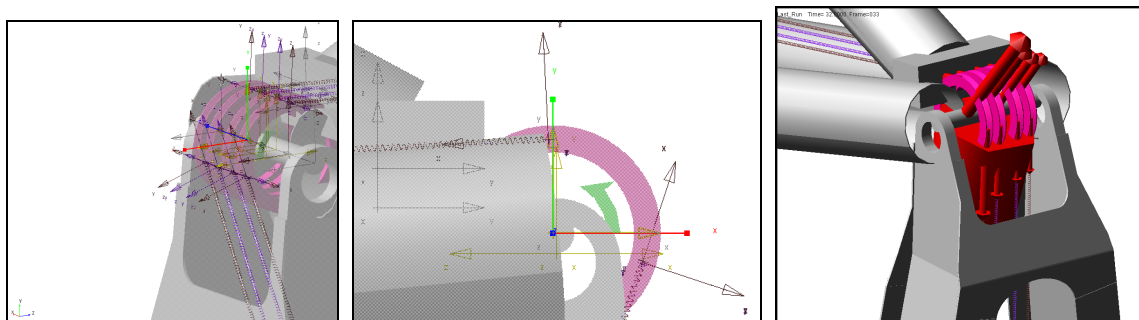


**Figure 54: ADAMS dynamic load illustration at rearend pulleys of upper arm**
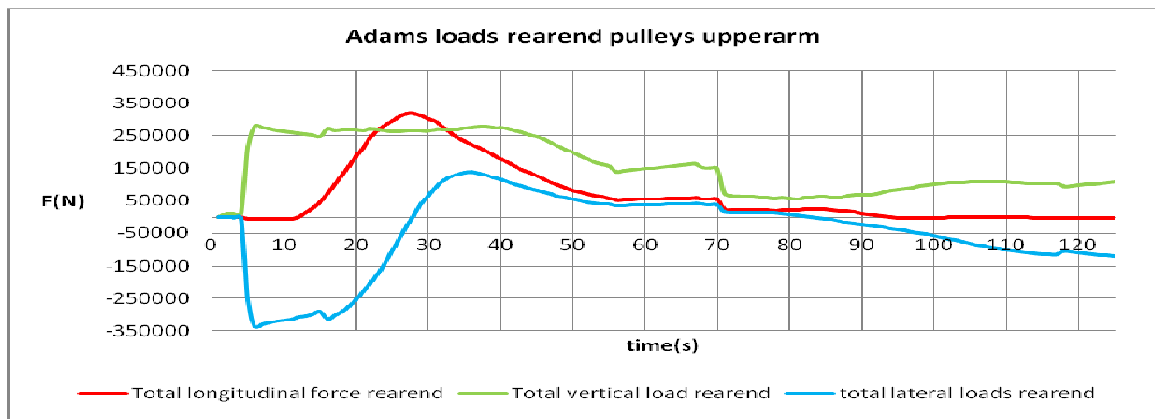
**Figure 55: ADAMS loads at rear-end upper arm**

|            | Total longitudinal force rear-end | Total vertical load rear-end | total lateral loads rearend |
|------------|-----------------------------------|------------------------------|------------------------------|
| Fmax (kN)  | 318,0                             | 278,5                        | 336,5                        |
| Fmin (kN)  | 5,7                               | 9,8                          | 138,2                        |

**Table 10: ADAMS maximum loads at rearend pulley-upper arm**

Detailed calculations of these dynamic loads at the rear end pulleys are provided in Appendix B in Figure 120, Figure 121, Figure 122, Figure 123, Figure 124 and Figure 125.

Figure 57 and Table 11 show the loads occurring at the cabin support on the upper arm. The load curve doesn't show allot of dynamic interaction compared to the loads at the frontend and rear end pulleys. The lateral (z-component) and longitudinal forces (x-component) show some dynamic effect compared to the vertical (y-component) load due to the slewing and luffing motion during operation. The following is concluded:

1.  the vertical force shows a steady state value about 8t, but shows a impact load at t=68s which is at the end of the unloading phase and is transmitted to this suspension point.
2.  the maximum longitudinal force at the joint is 17,4kN (at t=80s) and occurs during the acceleration phase of slewing CW at max flight which is the influence of the centrifugal load of the suspended structure.
3.  the lateral maximum load is 17.5kN (at t=90s) and also occurs during the acceleration phase of slewing with maximum flight which is the influence of the inertia of the structure.
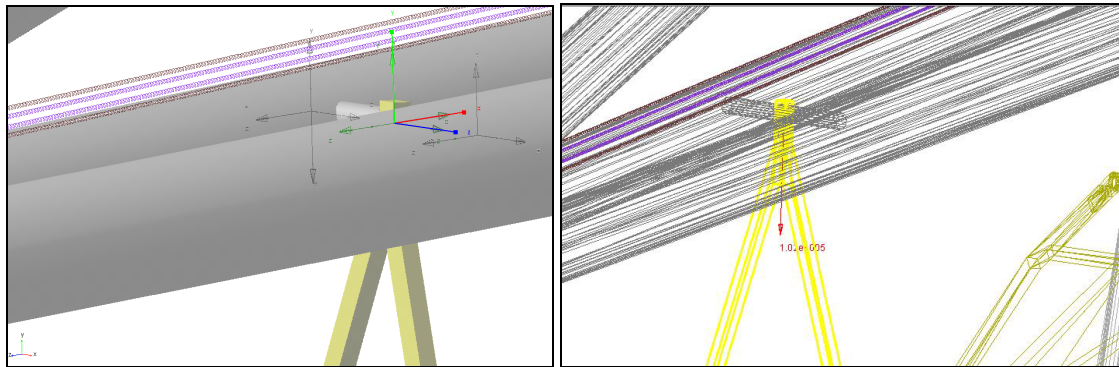
**Figure 56: ADAMS dynamic load illustration at joint cabin suspension and upper arm**

The loads calculated by ADAMS in Figure 57 can be found in Appendix B in Table 51.
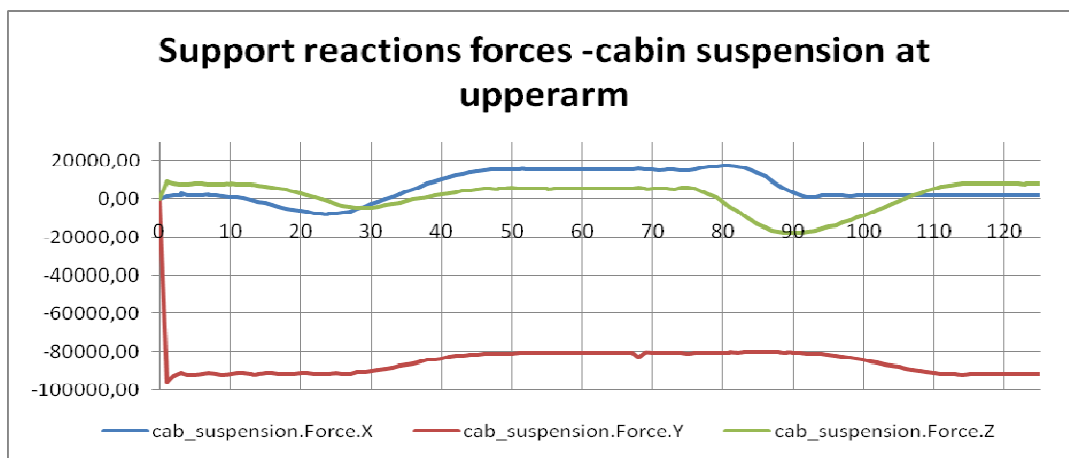


**Figure 57: ADAMS loads at cabin support on upper arm**

|            | Fx   | Fy   | Fz   |
|------------|------|------|------|
| **Fmax (kN)** | 17,4 | 95,4 | 17,5 |
| **Fmin (kN)** | 8,0  | 80,3 | 9,1  |

**Table 11: ADAMS maximum loads at cabin support on upper arm**

Figure 58 show the loads occurring at supports between the upper arm and the front arm and the upper arm and the rear arm. The simulation shows that the longitudinal reaction forces at the support

1. between upper arm and rear arm:
   a) increase to a maximum value during the braking phase of slewing CCW, extreme value of 0.6MN at t=23s
   b) decrease during the braking phase of hoisting between t=67s and t=70s
   c) increase between t=75 and t=83s which is during the acceleration phase of slewing CW and braking phase of hoisting
   d) decreases from a value of 0.8MN at the starting phase of luffing-in movement at t=84s to a minimum value
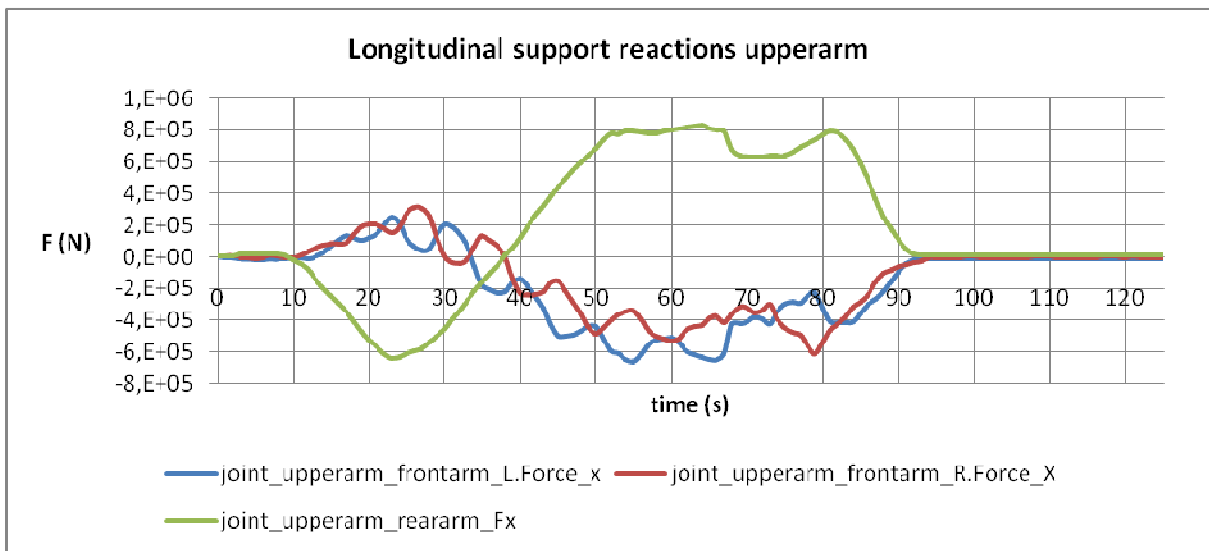
**Figure 58: Upper arm support reaction forces-longitudinal component**

Figure 59 show that the vertical reaction forces in the upper arm supports increase to a maximum value between the moments of loading to the moment of unloading. This is in accordance with the expected behaviour. At the rear arm supports the force has an average max value of 0.8MN and a minimum average value of 0.56MN. At the rear arm support the force has an average max value of 1MN and a minimum average value of 0.5MN.
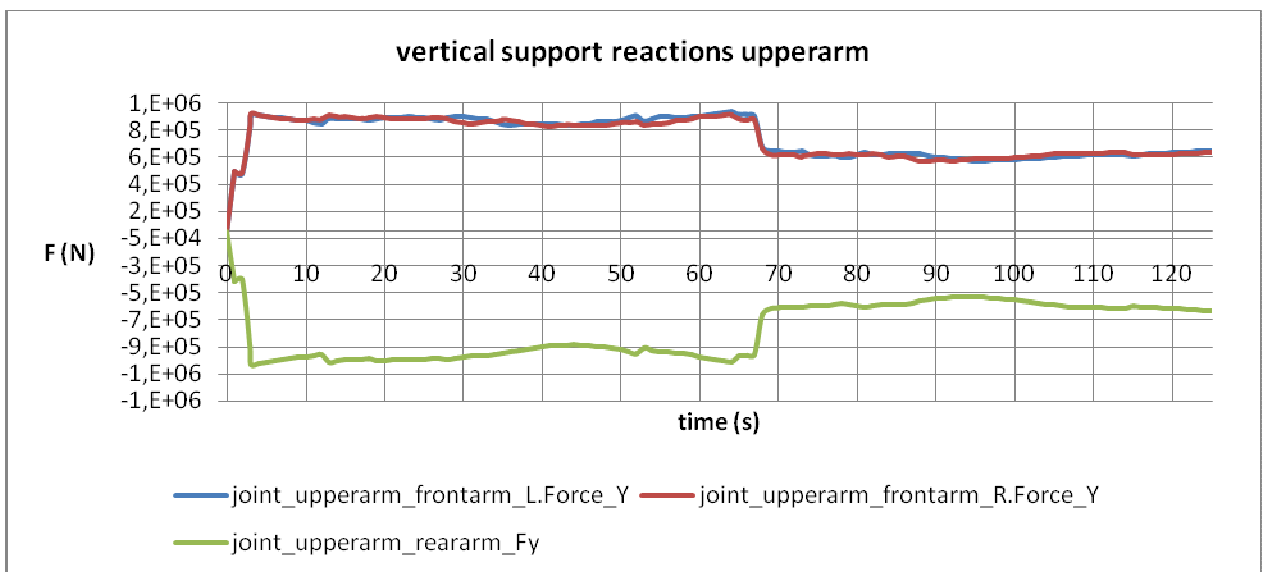


**Figure 59: Upper arm support reaction forces-vertical component**

Figure 60 shows that the lateral reaction force curves decrease to a minimum value which is about zero and intersect at:

1. the simultaneous ending of slewing and starting of luffing motion
2. during the start of breaking phase of luffing motion only.

The value of the lateral force occurring at the rear arm support fluctuates between 0.2MN and 0.6MN and at the front arm support between 0.2MN and 0.5MN.
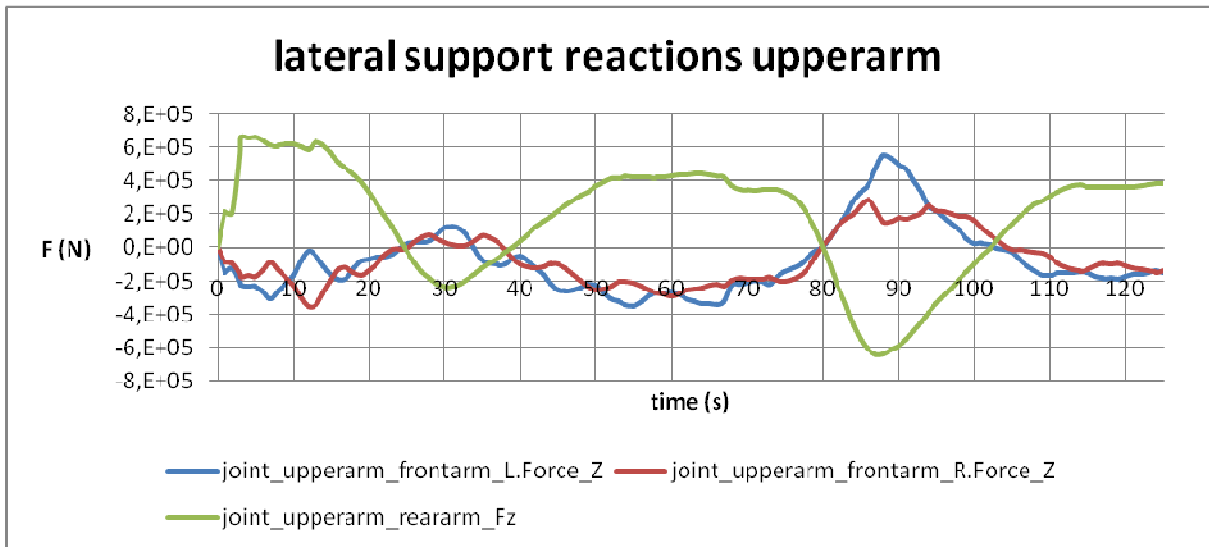
**Figure 60: Upper arm support reaction forces-lateral component**

Figure 61 shows the influence when the flight increases. During transshipment the radius with the center of rotation of the grab increases when slewing motion occurs due to the centrifugal forces. The figure shows how the support reaction forces increase to their maximum value as a cause of this effect.
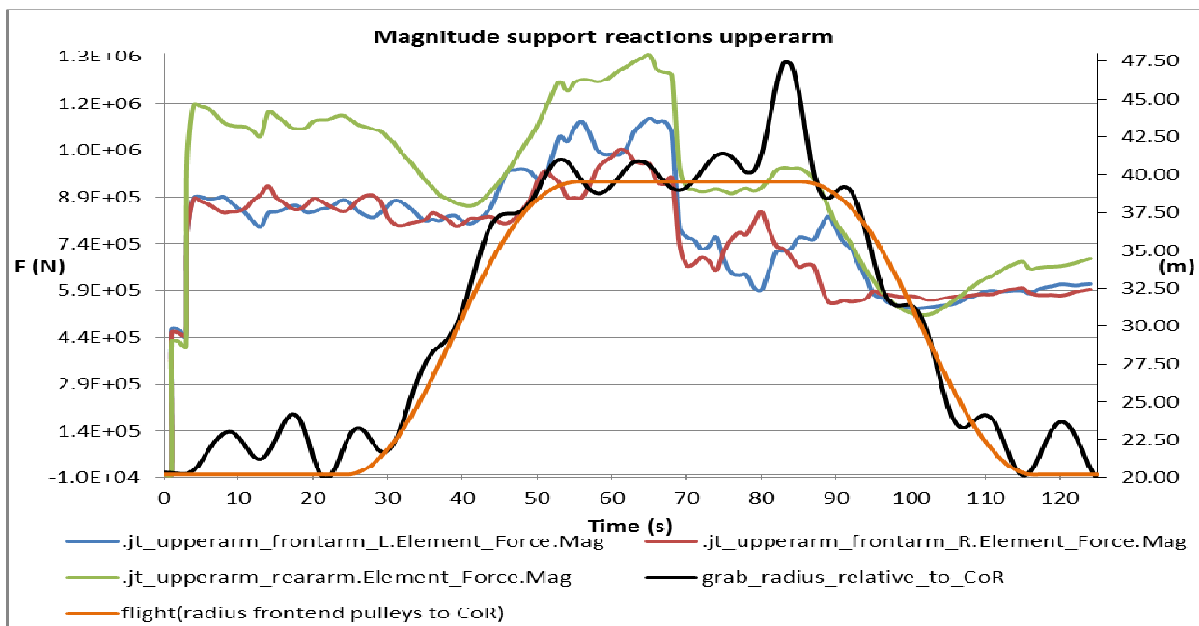


**Figure 61: Resultant support reaction forces upper arm with remaining crane**

In many crane fatigue design calculations using standards, the nominal hoisting weight is multiplied with a chosen load factor to take the dynamic effects for hoisting motion into account. A practical approach used according to the Design with Finite Elements lecture from Van den Bos, (2017) is the use of the following equation: $\varphi_i = \dfrac{F_{max}}{W_{load}}$ , see Figure 62. This factor is determined using the maximum hoisting force component calculated in Table 9

which was 325,2kN and divided with the nominal hoisting weight of 25 tons. This results in a ADAMS load factor of 1.3. This will be compared with the load factor from the standard in the next chapter where a fatigue assessment is performed according to the crane rules.
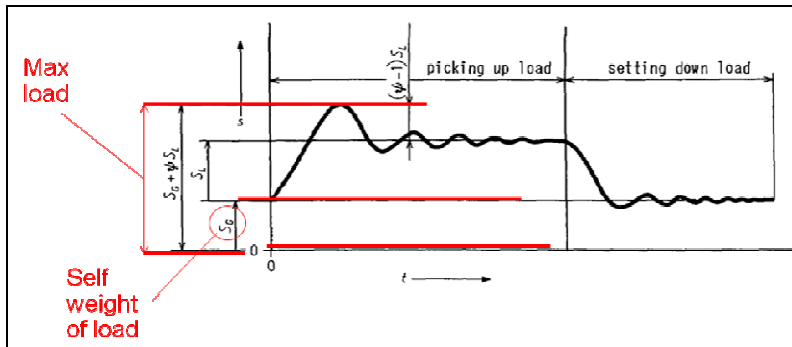


**Figure 62: Load factor calculation using ADAMS loads & NEN2018 methodology (NEN2018)**

An illustration for this calculation is seen in Figure 63

$$\varphi_{adams,load,factor} = \frac{F_{during,hoisting}}{F_{before,hoisting}} = \frac{325181}{250000} = 1.3$$ . This factor will be compared with the load

factor according to the crane standard and briefly discussed in chapter 5.
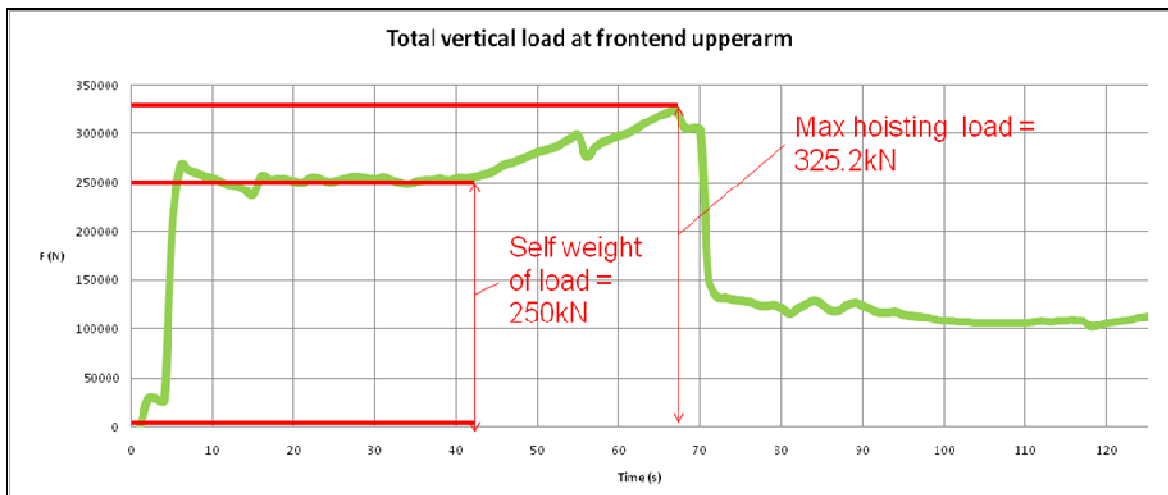


**Figure 63: ADAMS load factor calculation**

All the loads acting on the upper arm structure have been analyzed and in general it is concluded from all the previous graphs discussed in this section, that the largest dynamic effects occur when the crane is operating at max reach of 40m. Next the force time history for the simulated work cycle calculated by ADAMS for the rigid body model is exported and as FEA loads to use as load input for a FEM structural model according to ANYS (2011) and Zhang et al., (2010). The FEM model development is described in the following section.

### 3.4   FEM model setup

A model of the main crane structure is built in ANSYS mechanical APDL software. In order to simulate tension, compression, torsion and bending behaviour of the structure as a result of the dynamic ADAMS loads, beam elements are used in accordance with Nelson and Wang (2004). These elements obey the Timoshenko beam theory, where the beam stresses are linear over the thickness. This offers the advantage to calculate the stresses at the extreme fibers of the beam using the theory of strength of materials. The beam elements used here are illustrated with Figure 64.



**Figure 64: Ansys element choice**
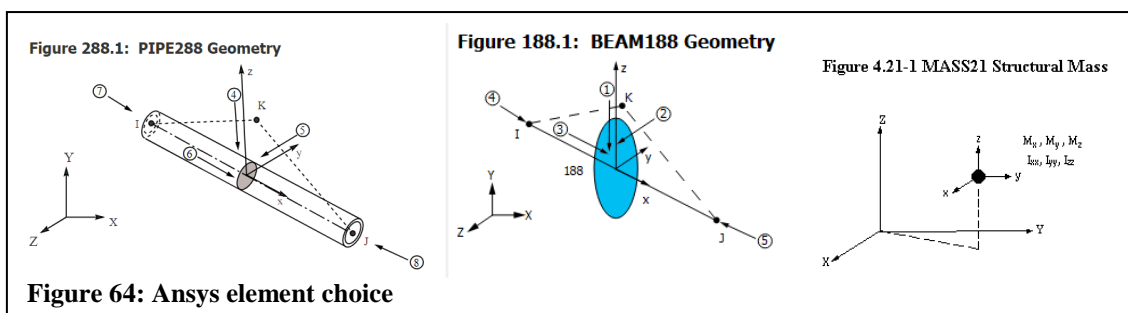
For the modeling, pipe288 elements are used for the tubular members of the upper arm, seen in Figure 65. This is a beam element which is suited to analyze slender to moderately thick pipe structures. Beam188 elements are used for the remaining structure (front arm, rear arm, tower, pulley shafts and machine floor). Mass21 are used to model structural masses for crane house, ladders, cables, and other mechanical components.
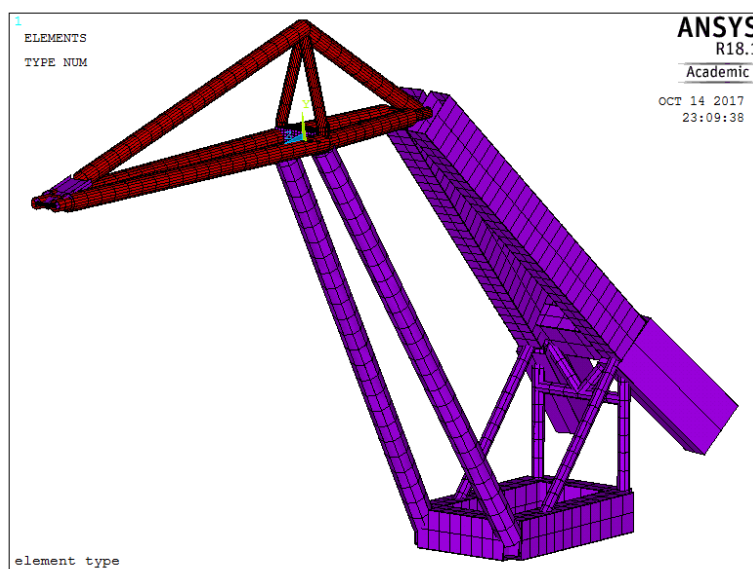


**Figure 65: Element types used in FEM model**

The material is assumed to be linear elastic material behaviour with Young's modulus (E=2.1 GPa), poissons ratio ($\upsilon = 0.3$) and steel density ($\rho = 7850 kg / m^3$) multiplied with factors to take different material weights into account, see Figure 66.
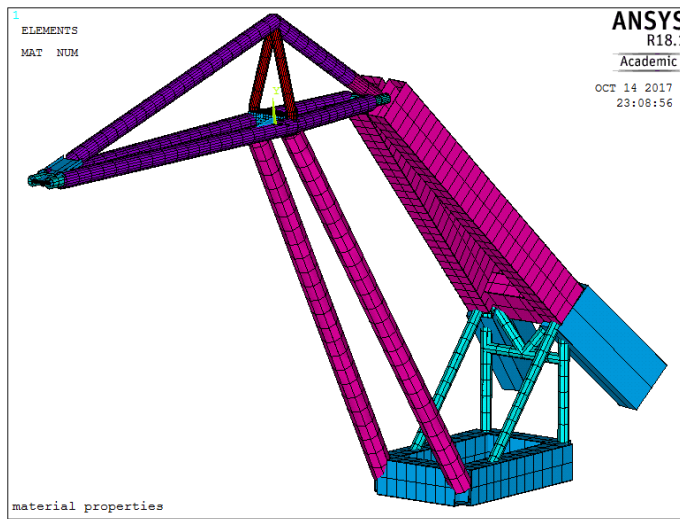


**Figure 66: Material properties used in FEM model**

The boundary conditions Ux,Uy and Uz are applied at the machine floor shown in Figure 67.
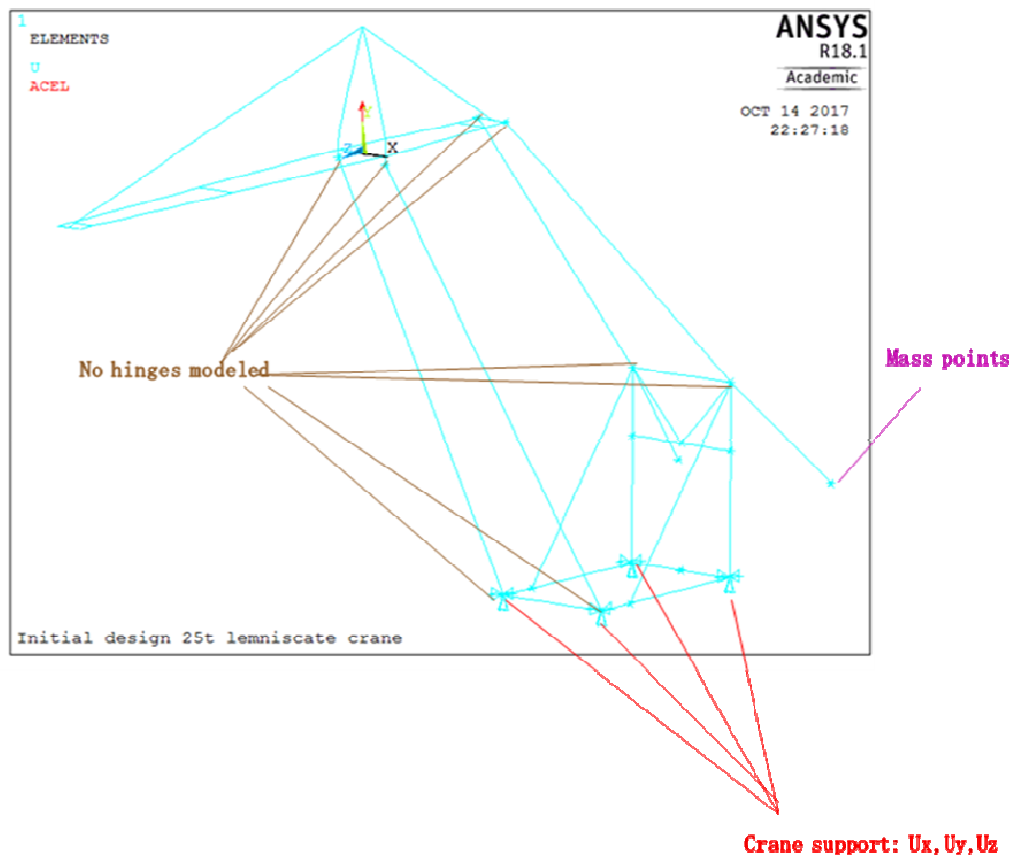


**Figure 67: FEM crane skeleton model without beam cross sections shown**

Various cross sectional properties were assigned to the model in accordance with the crane specification, seen in Figure 68.
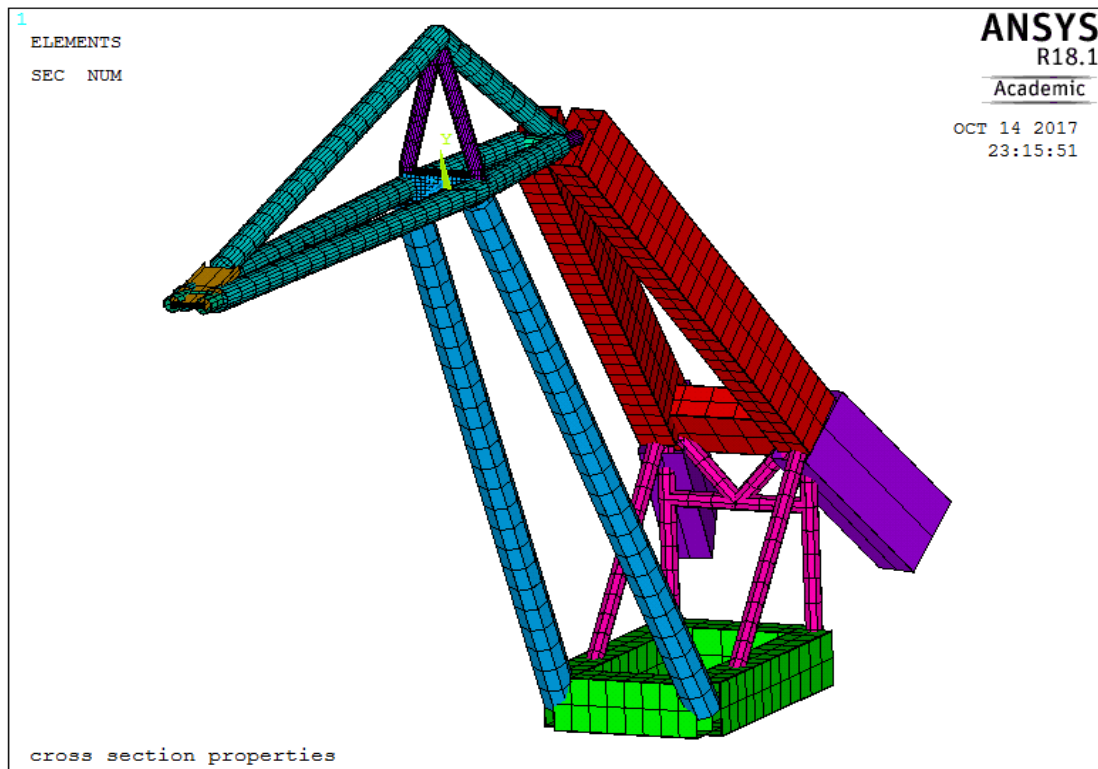
**Figure 68: Crane FEM model with shown beam cross section**

The following step is to perform a verification of the stiffness behavior of the model using elemental loads of the same magnitude in three directions. These loads (inertia forces) simulate gravity effect which act on all the elements of the total model instead of using nodal forces which act only on a single element. This method provides a practical solution to analyze the stiffness of the model according to ANSYS, (2017).

First the upper arm structure is analyzed only by disregarding the remaining structure to which it is attached. Gravity loads are applied in the x, y and z direction seen in Figure 69.
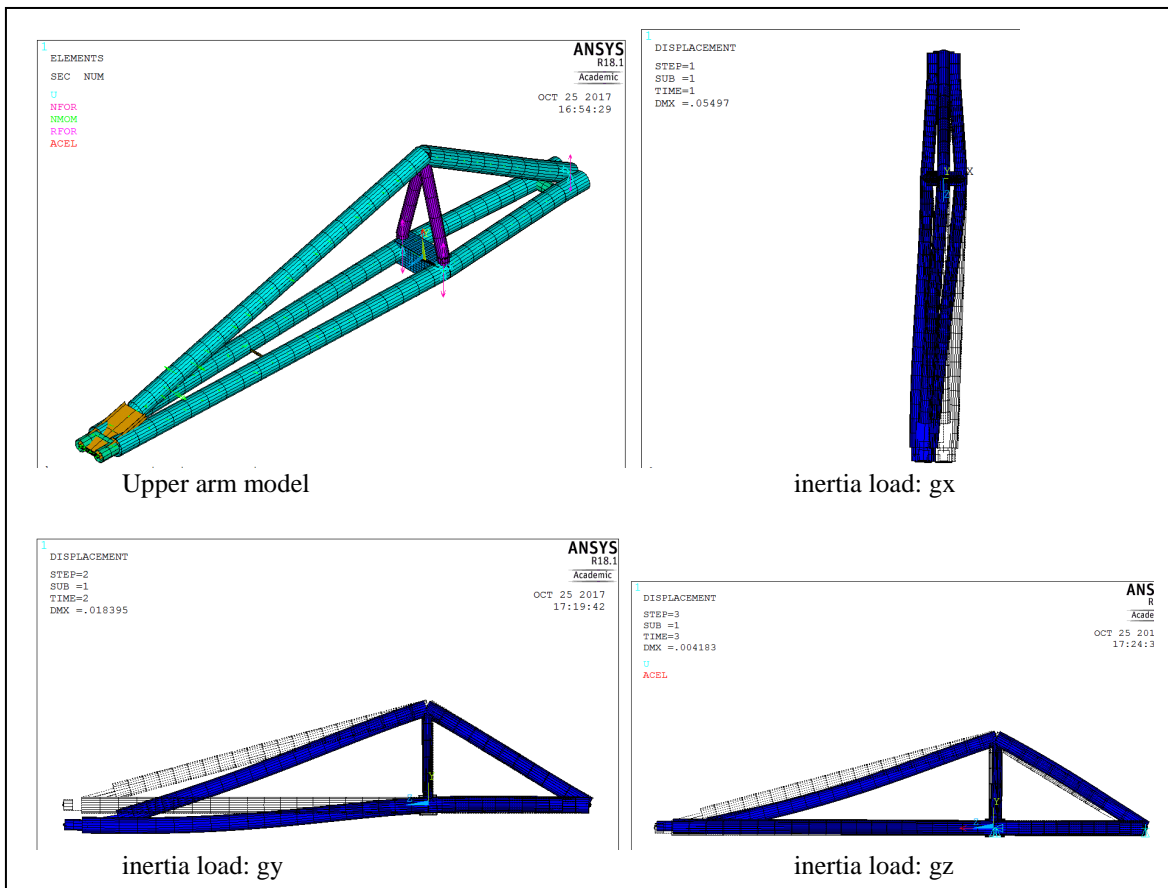
Figure 69: Inertia loads added to upper arm FEM model

Figure 70 shows that its structural mass is 40.5 tons which is 5% larger compared to the real total mass of 38t which was specified in Table 1.
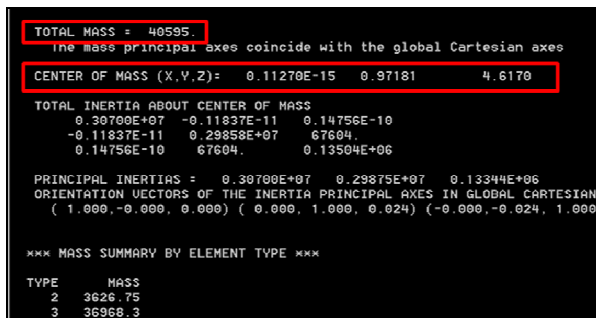


Figure 70: Mass structural FEM model- Upper arm only

The deviation of the CoM seen in Table 12 between the analytical calculation and the structural simulation model is about 2% and is found to be acceptable.

| | Total mass [tons] | CoM x [m] | CoM y [m] | CoM z [m] |
|---|---|---|---|---|
| Real upper arm | 38,886 | 0 | | 4,709 |
| ANSYS upper arm | 40,959 | 0 | 0,97181 | 4,617 |
| Deviation | 5% | | | 2% |

Table 12: verification COG ANSYS upper arm with analytical calculation

Then stiffness behaviour for the complete structural model is analyzed using the same previous applied method. Figure 71 shows that total structural mass is 415 tons which is 9.4% larger compared to the real total mass of 376t which was specified in Table 1.



**Figure 71: Mass structural FEM model- slewing part of crane**

Table 13 shows that the CoM of the structural model in the vertical y-direction is about 25% higher and in the horizontal z-direction 8.9% lower than the real crane slewing structure. These values are found reasonable.

| | Total mass [tons] | CoM x [m] | CoM y [m] | CoM z [m] |
|---|---|---|---|---|
| Real slewing structure | 376 | 0 | -9,748 | -17,94 |
| ANSYS slewing crane structure | 415 | 0 | -12,926 | -16,342 |
| Deviation | 9,4% | | 24,6% | 8,9% |

**Table 13: verification COG real crane with ANSYS crane model**

The FEM model is built and in the following step is to import the FEA loads exported by ADAMS to the structural model to perform a stress analysis. This is discussed in the following section.

## 3.5   Stress spectrum analysis

This chapter focuses on the stress time spectrum which is calculated using ANSYS. ADAMS generates a loads file for the simulated working cycle and contains all action, inertia and reaction forces. Within ANSYS APDL all forces from ADAMS are defined as nodal loads. These are added to the eight locations (predefined nodes in the FEM model) which were identified in section 3.3 with Figure 48. These nodes serve as a data exchange "interface" where all load information from ADAMS is imported into ANSYS. This is illustrated in Figure 72. The ADAMS inertia loads are defined as element loads in ANSYS and thus applied to all elements as described in the previous section. All simulation loads were solved using a transient simulation, because ADAMS loading varies in direction and magnitude as a function of time. Details about the ADAMS loads file and this load transfer process can be found in Appendix B in Figure 126, Figure 127 and Figure 128 .
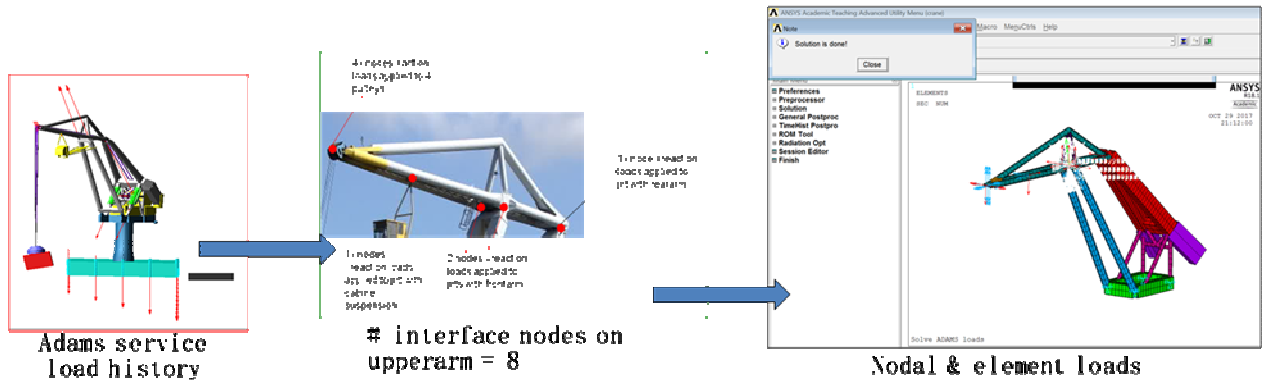
**Figure 72: Load transfer from ADAMS to Ansys**

Figure 73 illustrates the deflection pattern at the frontend of the upper arm. This plot is in accordance with the vertical load fluctuation at the front end pulleys from Figure 52 in section 3.3 and verifies that the ADAMS FEA loads are added to the FEM model. At the moment of loading at t=2s the deflection is about 0.045m and at the moment when the crane is unloaded at maximum reach at t=64s the deflection decreases instantaneous to a value of 0.015m.
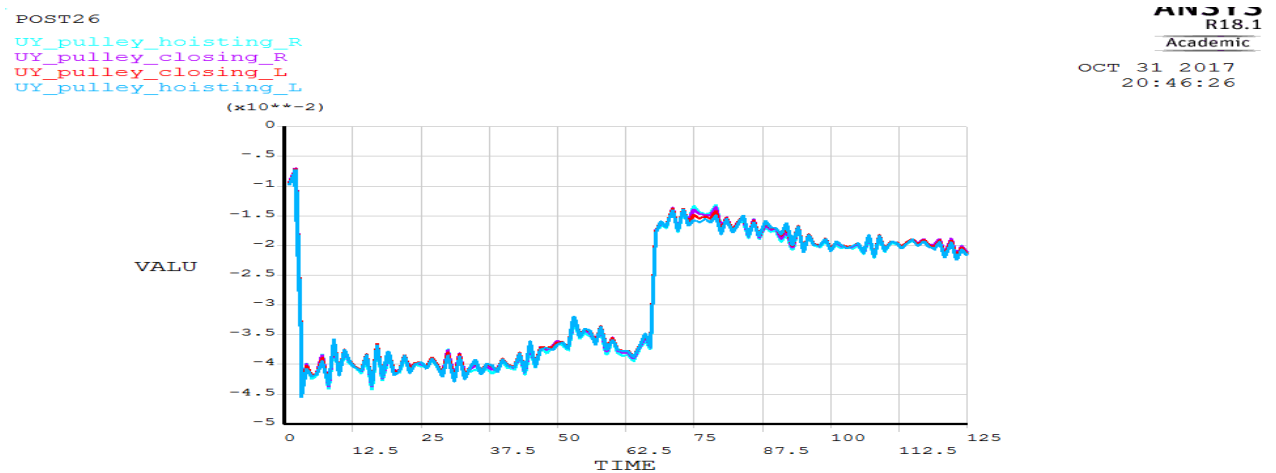


**Figure 73: Dynamic vertical deflection at tip upper arm**

Because of the geometric complexity of the tubular weld at the top point of the upper arm structure it is necessary to make an approach which allows to determine the beam stresses at the extreme fibers at this location. This approach makes use of the nominal stress method which makes it possible to quantify the fatigue damage. The nominal stress excludes macro-geometric effects, concentrated load effects and the stress raising effects of weld geometric singularities. The developed beam model suits well to apply this method for stress analysis at the weld detail of interest, illustrated with Figure 74 and Figure 75 .

Crane fatigue assessment using Multibody Dynamics and Finite Element Method
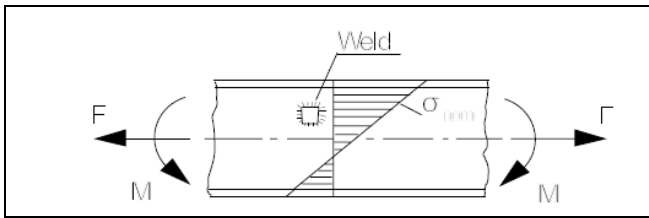
**Figure 74: Nominal stress in a beam (Hobbacher, 2016)**
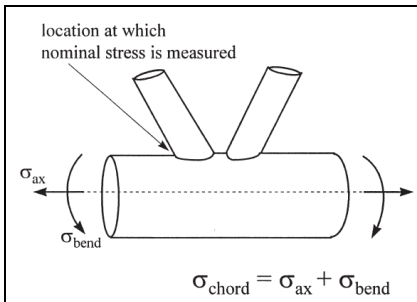


**Figure 75: Nominal stress calculation at tubular weld detail (Spyros et. al, 2000)**

At the nodal top point of the upper arm the axial stress $\sigma_{axial} = F/A$ , in plane bending stress

$\sigma_{bend,y} = \dfrac{M_y * c}{I_z}$ and out of plane bending stress components $\sigma_{bend,z} = \dfrac{M_z * c}{I_y}$ is calculated,

illustrated with Figure 76.
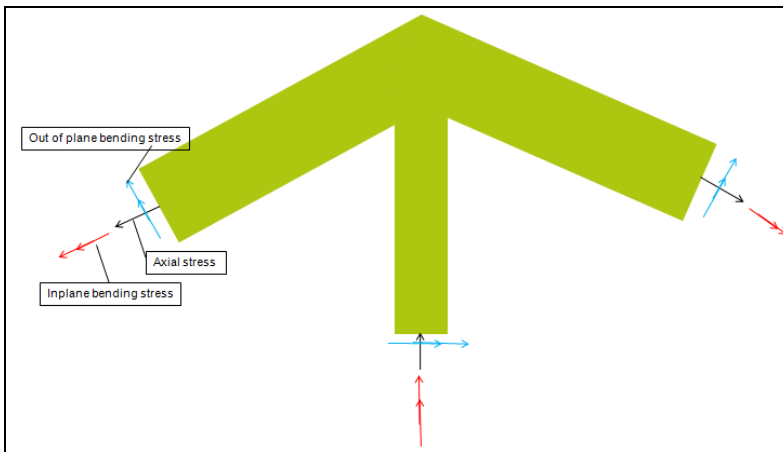


**Figure 76:  Beam model stress components used in fatigue calculation**

In order to establish the nominal stress calculation Figure 80 is used to illustrate the approach. At the real structure the complicated tubular weld is formed by the welding of four pipe members together seen in Figure 77.
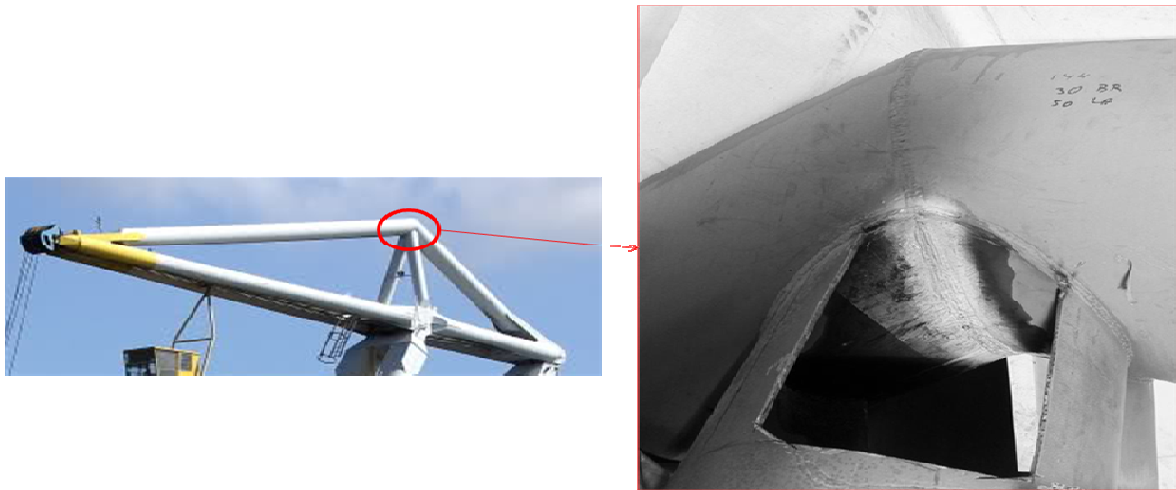
**Figure 77: Geometric construction of tubular joint (Maja Stuwadoors BV, 2016)**

These were modeled as four pipe elements in the FEM model intersecting at the node which is the joint of interest. Each pipe element consists of a cross sectional thickness. At this section four points are defined at the outer circumference to be the extreme fibers where the elastic beam stress will be calculated. Each individual element at the node intersection consists of four points. In order to make the calculation verifiable each member is assigned a name; the forestay, backstay and left and right pylon. The four points are defined at each beam element are point 1 (top), point 2 (bottom), point 3(right) and point 4 (left), seen in Figure 78.
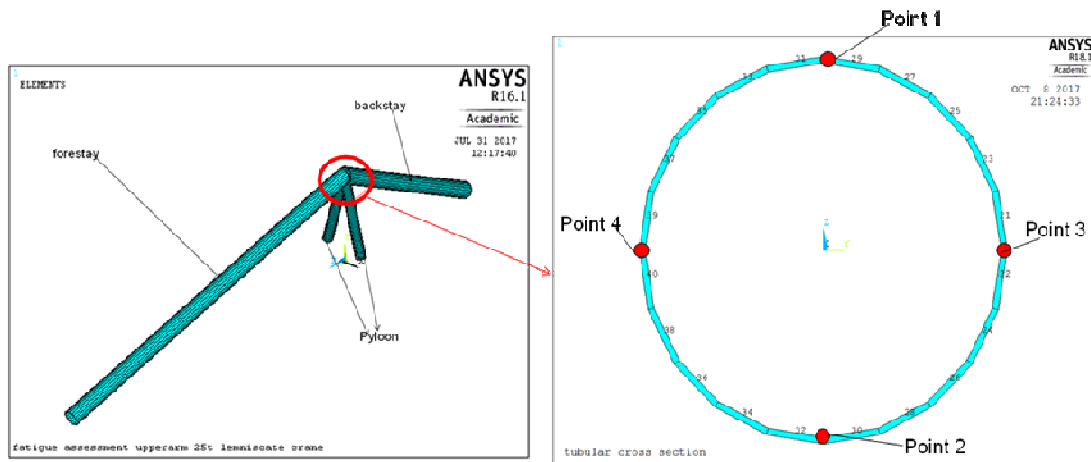


**Figure 78: Beam element extreme fiber points to calculate nominal stress**

On the bases of the orientation of the beam elements in the FEM model, each cross sectional point is projected back on to the real structure, see Figure 79.
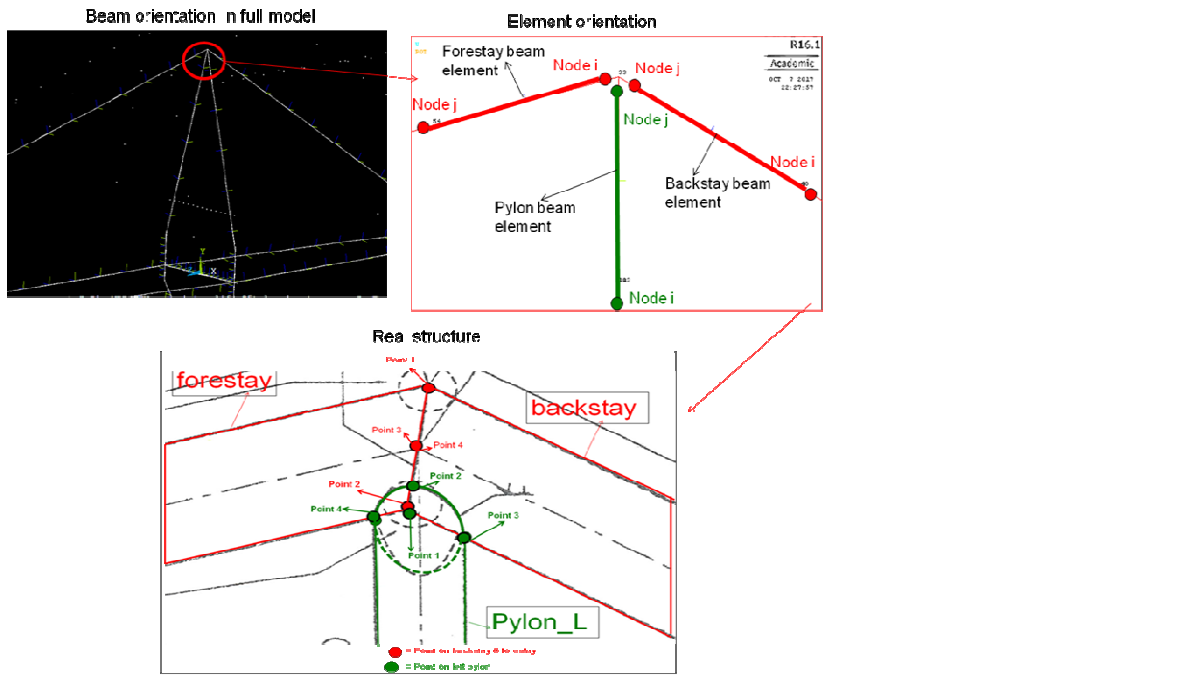
**Figure 79: Projection extreme fiber on element to real structure**

At the node of each of the four individual beam element, three stress components are calculated. Each stress component is then combined to determine the nominal stress at each of the four points for each beam, seen in Figure 80. This results in calculating the nominal stress for each point for each time step.
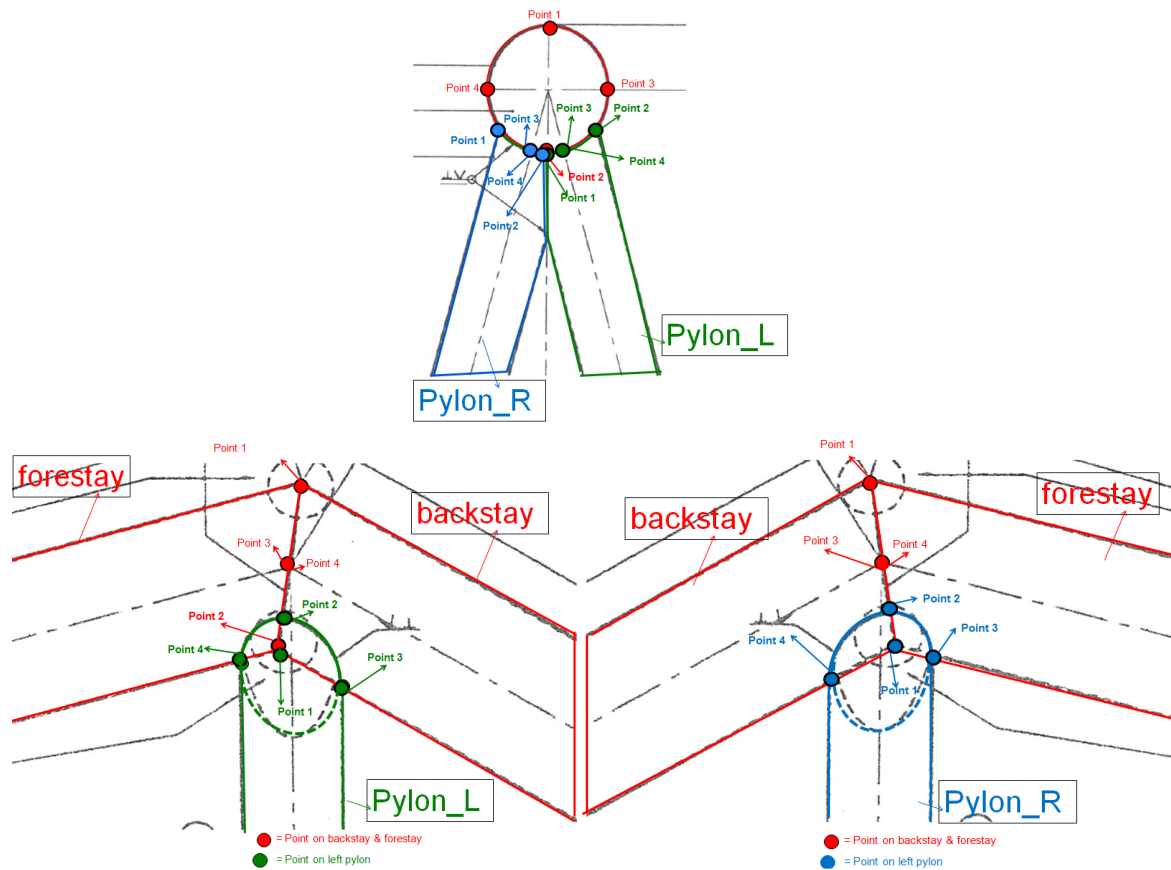




**Figure 80: Reference points for nominal stress calculation at weld of interest**

The Adams loads analysis from section 3.3 shows how the load constantly changes in direction and magnitude as a function of time. This loading results in dynamic stresses induced to the structure which could lead to a fatigue failure. The types of dynamic stresses illustrated in Figure 81 are:

1. cyclic repeated and reversed stresses which are pure alternating stresses
2. fluctuating stresses which could be a
   a. compressive stress with compressive mean
   b. unidirectional or one direction compressive stress
   c. partially reversed with compressive mean
   d. partially reversed with tensile mean
   e. unidirectional or one direction tensile stress
   f. tensile stress with tensile mean
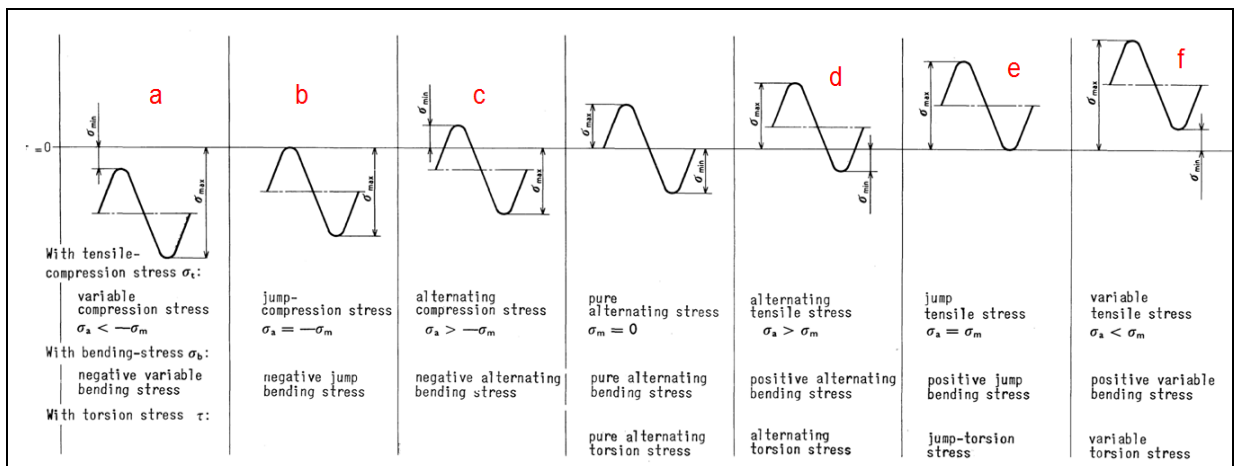


**Figure 81: Classification of different types of changes in stress directions (Netherlands Standards Institution, 1984)**

Figure 82 and Table 52 show the stress spectrum at the forestay weld interface. The stress levels in this cross sectional area are as follows:

1. point 1: Tensile stress with tensile mean
2. point 2: Compressive stress with compressive mean
3. point 3: Tensile stress with tensile mean
4. point 4: Tensile stress with tensile mean

Crane fatigue assessment using Multibody Dynamics and Finite Element Method

In general the stress plots at this weld interface show a large increase when the crane is loaded at t=2s and a decrease is at t=64s. However it is noticed that there is a large stress fluctuation at point 3 and 4, at t=84s when luffing-in with a empty grab starts. This starting phase occurs when the crane was at that moment slewing CW. During this starting moment the dynamic effect of both centrifugal and inertia forces is induced into the structure resulting in this large instantaneous stress fluctuation.
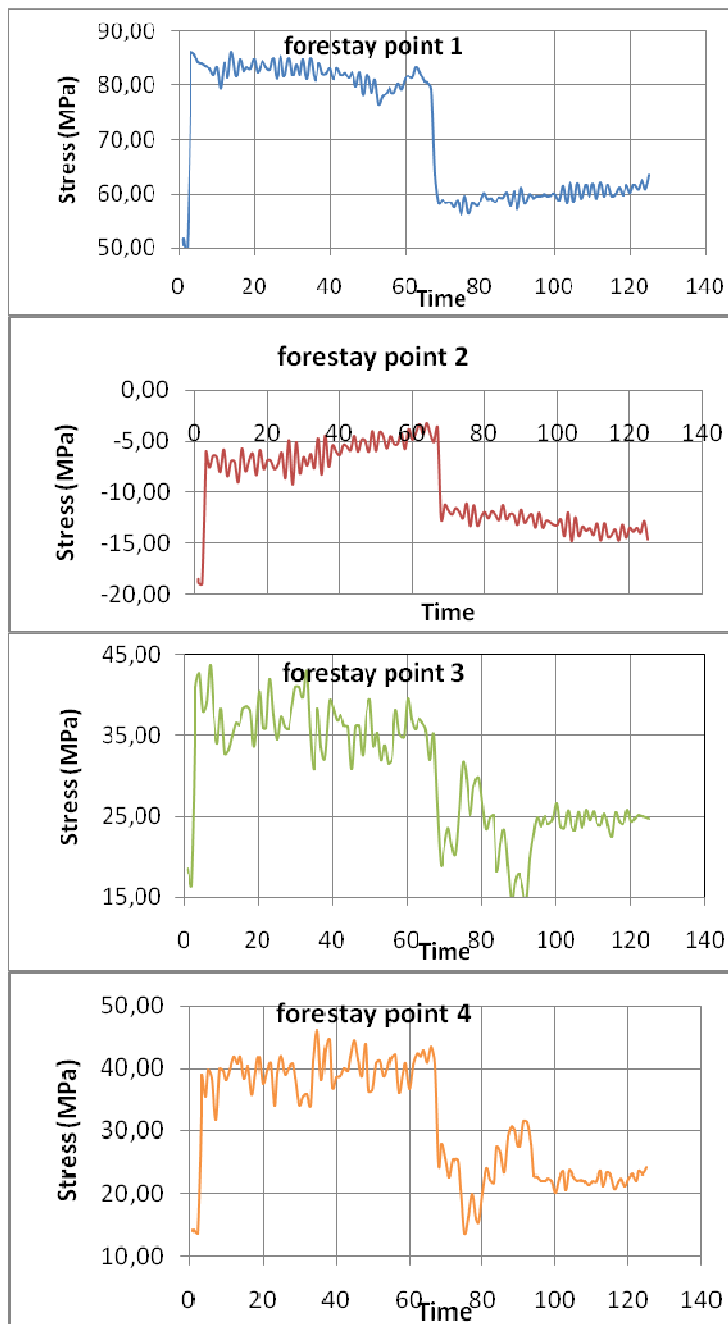


**Figure 82: Simulated stress spectrum-weld interface forestay**

Crane fatigue assessment using Multibody Dynamics and Finite Element Method

Figure 83 and Table 53 show the stress spectrum for the four cross sectional points at the backstay weld interface. The stress levels in this cross sectional area:

1. point 1: Tensile stress with tensile mean
2. point 2: Partially Reversed with tensile mean and partially reversed with compressive mean
3. point 3: Tensile stress with tensile mean
4. point 4: Tensile stress with tensile mean
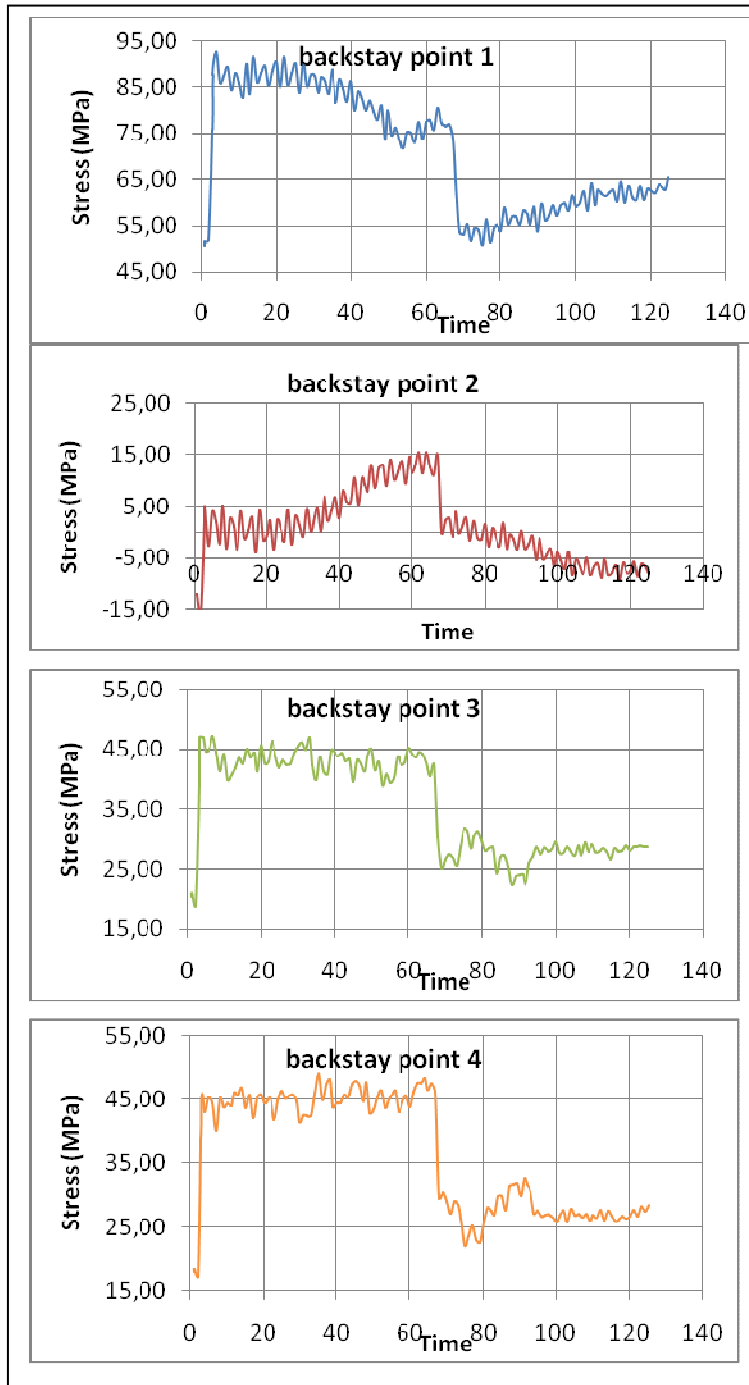


**Figure 83: Simulated stress spectrum-weld interface backstay**

Figure 84 and Table 54 show the stress spectrum for the four cross sectional points at the left pylon weld interface which is a compressive stress with compressive mean stress level over the entire cross sectional area. From the stress plots it is concluded that in general the largest stress fluctuations at point 1, 2,3 and 4 occur between t=10-64s when the crane is performing slewing CCW, luffing out and lowering the full grab for unloading. It is concluded that this structural member encounters the most stress fluctuations.
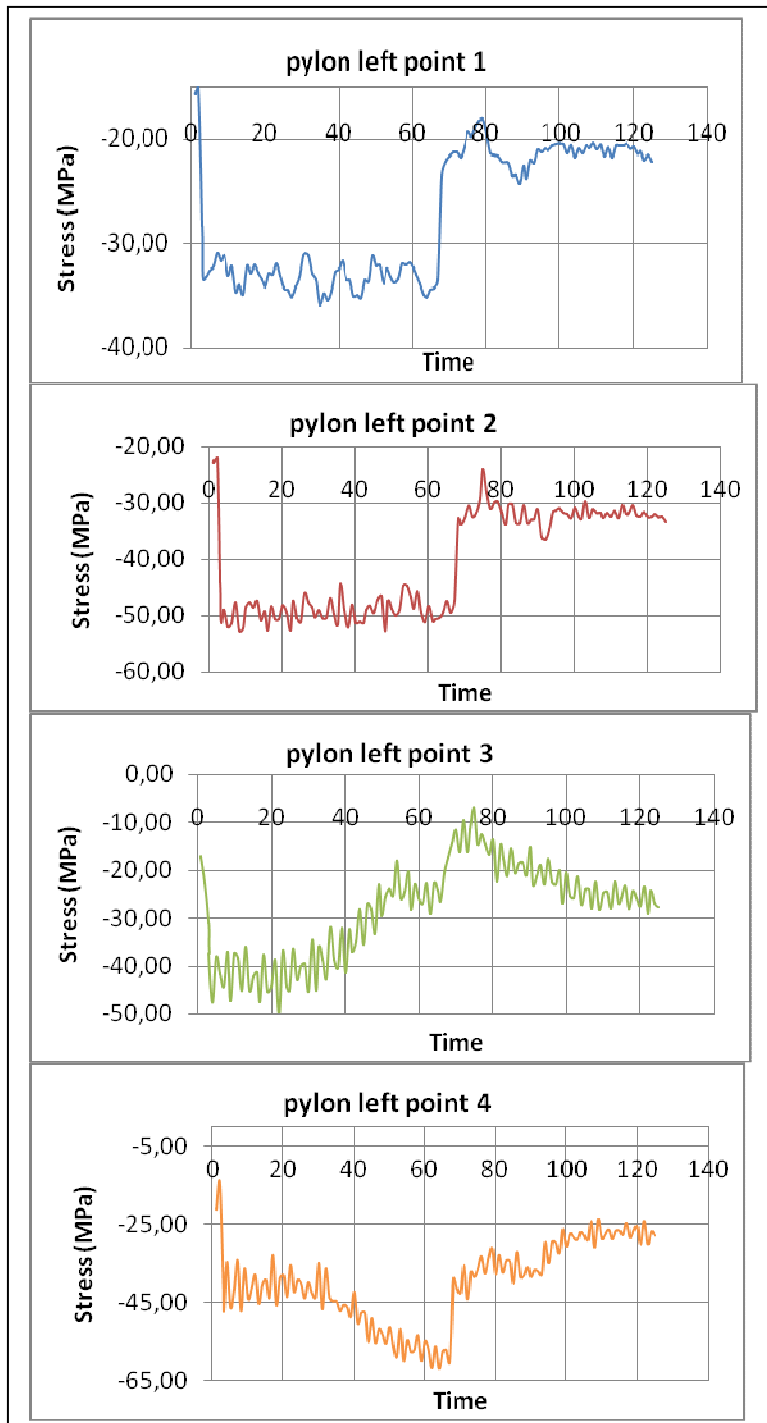


**Figure 84: Simulated stress spectrum-weld interface left Pylon**

Figure 85 and Table 55 show the stress spectrum for the four cross sectional points at the right pylon weld interface which is a compressive stress with compressive mean stress level over the entire cross sectional area.
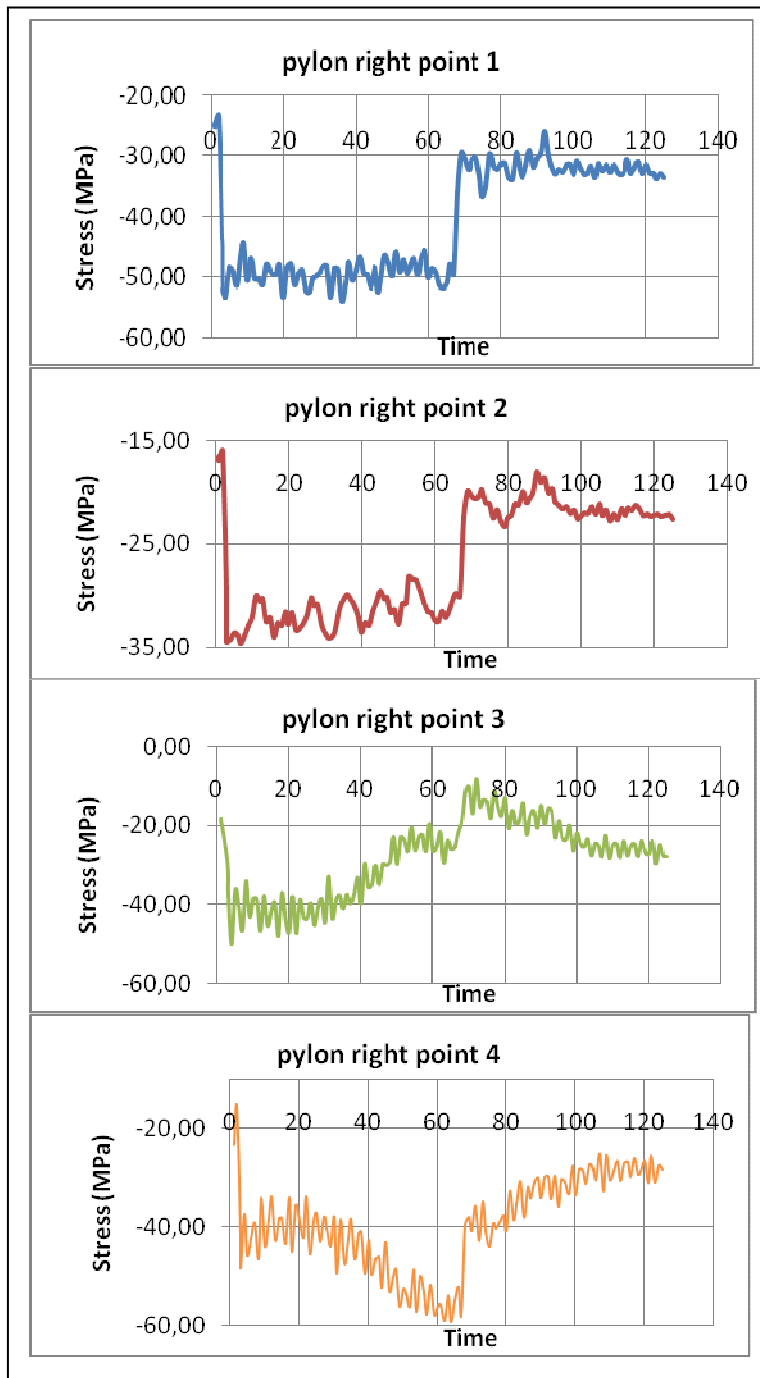


**Figure 85: Simulated stress spectrum-weld interface right Pylon**

The stress history plots of the fatigue induced loading for all structural members at the weld interface have been presented. These representations show the influence of the dynamics load effects during operation.  In the next section the fatigue damage is determined as a result of these dynamic calculated stresses.

### 3.6   Fatigue results based on dynamic simulation method

This paragraph discusses the fatigue calculation for the tubular welded joint detail which was illustrated with Figure 77 . Due to the large number of stress reversals and the irregular sequence of the stress cycles, a Rainflow counting algorithm is performed. This allows to reduce the stress spectrum into a set of representative stress reversals. This counting will be performed using J-Rain from Jesmond Engineering (2013), which is a free available Rainflow Counting Software.

A variable amplitude stress history analytical calculation, see Figure 86, was used as example to verify the output of the software. The output of JRain gave an exact match for the number of cycles for each stress range seen in Table 14. Based on this verification it is assumed that the software will provide a reliable stress range count for the stress history data from the previous section.
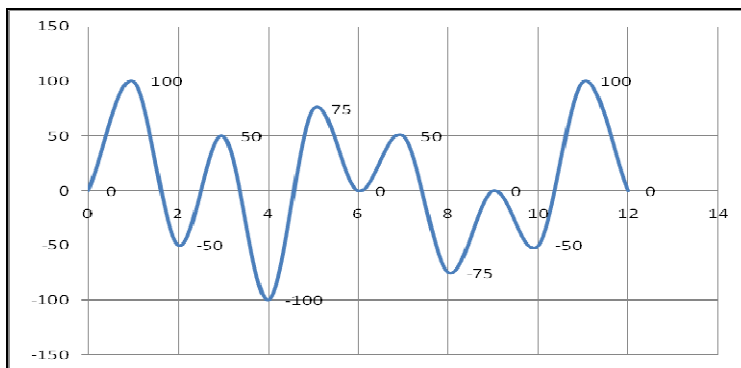


**Figure 86: Variable amplitude stress history analytical calculation to verify JRain software output**

| Max | Min | Cycles |
|---|---|---|
| 0 | -50 | 1 |
| 50 | -50 | 1 |
| 50 | 0 | 1 |
| 75 | -75 | 1 |
| 100 | 0 | 1 |
| 100 | -100 | 1 |

**Table 14: JRain output results for the analytical calculation example**

For each cross sectional point for each individual structural member a stress range table is created. The following stress range tables show the largest stress range values which occurred only once during the acceleration phase of picking up the hoisting weight during the entire transshipment move. These can be seen in all the stress plots from the previous section.

|          | largest stress range (MPa) |
|----------|----------------------------|
| point 1  | 37.08                      |
| point 2  | 15.79                      |
| point 3  | 29.46                      |
| point 4  | 32.38                      |

**Table 15: Largest occurring stress range during picking up of hoisting load at Forestay**

|          | largest stress range (MPa) |
|----------|----------------------------|
| point 1  | 42                         |
| point 2  | 31                         |
| point 3  | 28                         |
| point 4  | 32                         |

**Table 16: Largest occurring stress range during picking up of hoisting load at backstay**

|          | largest stress range (MPa) |
|----------|----------------------------|
| point 1  | 21                         |
| point 2  | 31                         |
| point 3  | 43                         |
| point 4  | 47                         |

**Table 17: Largest occurring stress range during picking up of hoisting load at left pylon**

|          | largest stress range (MPa) |
|----------|----------------------------|
| point 1  | 31                         |
| point 2  | 19                         |
| point 3  | 42                         |
| point 4  | 44                         |

**Table 18: Largest occurring stress range during picking up of hoisting load at right pylon**

All detailed calculations for the 16 stress history tables can be found in Appendix B.

For the fatigue damage calculation the formula of Haibach will be used, reported by Karssen, (2014): $\Delta\sigma_{range}^{m} * \overline{n} = \Delta\sigma_{allow}^{m} * 2 * 10^{6}$.

This formula calculates the fatigue life $\overline{n}$, at which a welded joint with a certain fatigue resistance $\Delta\sigma_{allow}$ will show fatigue cracks at two million cycles assuming a constant nominal stress range $\Delta\sigma_{i}$. The two million cycles is known as a reference life for the chosen weld class with a probability of survival of 97.7% reported by Fricke, (2007) in a research of Nyström & Tomaz (2015). Hobbacher, (2016) states this value as the characteristic fatigue strength or the FAT-class for de SN curve of each weld.

Combining the formula of Haibach and Palmgren-Miners- rule $D = \sum \dfrac{n_{occuring}}{n_{allowable}}$, results in the fatigue damage equation:

$$\Delta\sigma_{range}^m * \overline{n} = \Delta\sigma_{allow}^m * 2*10^6$$

$$\Delta\sigma_{range}^m * n = \Delta\sigma_{FAT}^m * N$$

$$D = \sum \left( \frac{\Delta\sigma_{range}}{\Delta\sigma_{FAT}} \right)^m * \frac{n*\tilde{n}}{N}$$

$$m = 3$$

$$n = current\_transshipment\_moves = 1.31e6$$

$$\tilde{n} = number\_of\_counted\_cycles$$

$$N = 2*10^6$$

$$Failure : D \geq 1$$

Due to the large amount and different types of welded joints in the structure, a weld atlas is used. This atlas is based on the nominal stress approach and contains a Wohler curve or SN-curve (stress-life curve) for each weld configuration, seen in Figure 87. These curves are based on experimental material fatigue life measurements in terms of the stress amplitude and the number of cycles to fatigue failure (weld fatigue strength).
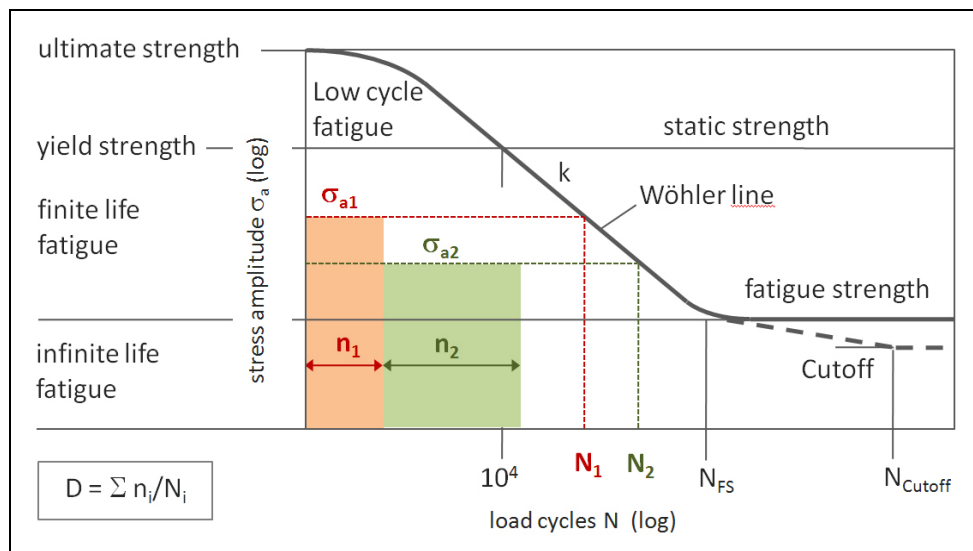


**Figure 87: SN-curve or Woler curve (Cae-sim-sol.com, 2016)**

The allowable stress range or FAT class for the weld is chosen using the SN curve for steel from the weld atlas according to (Hobbacher, 2016) seen in Figure 88.
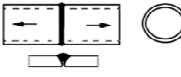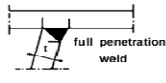
| 216 | | Transverse butt welds welded from one side without backing bar, full penetration | | | Misalignment <10% of plate thickness. |
| | | Root checked by appropriate NDT<br>No NDT | 36 | 28<br>12 | |
| 232 | | Transverse butt weld splice in circular hollow section, welded from one side, full penetration, potential failure from root . | | | Welded in flat position.<br>Axial misalignment < 5% of wall thickness |
| | | root inspected by NDT<br>no NDT | 36 | 28<br>12 | |
| **No.** | **Structural Detail** | **Description**<br>**(St.= steel; Al.= aluminium)** | **FAT**<br>**St.** | **FAT**<br>**Al.** | **Requirements and Remarks** |
| 514 | full penetration weld | Trapezoidal stiffener to deck plate, full penetration butt weld, calculated on basis of stiffener thickness, out of plane bending | 71 | 25 | |

**Figure 88: FAT class for the weld configuration at the top point of the upper arm**

FAT36 is chosen because the tubes are welded together from one side only with a transverse but weld, seen Figure 89.: $\Delta\sigma_{FAT} = 36 MPa$ at N=2e6 cycles.
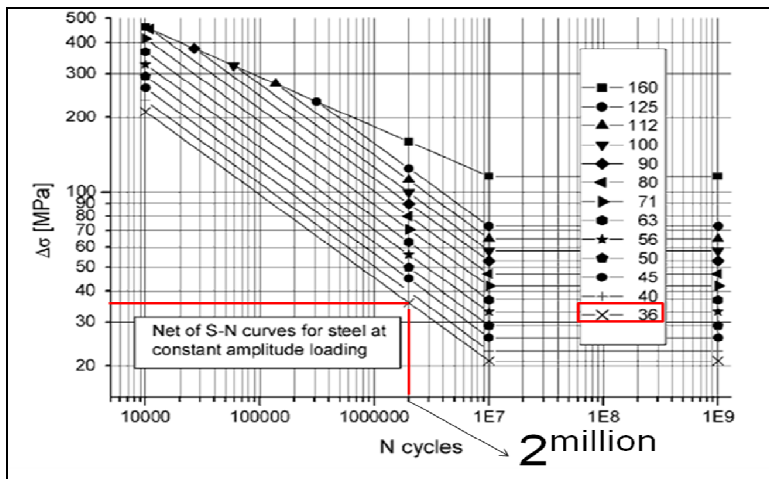


**Figure 89: SN curve for chosen FAT class: Number of cycles to fracture**

## 3.6.1 Example calculation of fatigue damage

An example calculation of the contribution of each stress range to the total fatigue damage for point 1 at the tubular welded joint interface of the forestay member is illustrated here.

All stress components are calculated for 125s. The following Table 19 shows the values calculated using ANSYS only as an illustration for 6s, where:

1. fs_axialstress = stress component due to axial load
2. fs_SByT_i = Bending stress on the element +Y side of the beam
3. fs_SBzT_i = Bending stress on the element +Z side of the beam

|  | Pa | | |
| --- | --- | --- | --- |
| TIME | fs_axialstress | fs_SByT_i | fs_SBzT_i |
| 1,00 | 1,60E+07 | 2,11E+06 | 3,45E+07 |
| 1,01 | 1,64E+07 | 2,16E+06 | 3,53E+07 |
| 2,00 | 1,51E+07 | 1,46E+06 | 3,41E+07 |
| 3,00 | 3,38E+07 | 6,19E+05 | 4,15E+07 |
| 3,12 | 4,01E+07 | 9,81E+05 | 4,60E+07 |
| 4,00 | 3,91E+07 | 3,60E+06 | 4,66E+07 |
| 5,00 | 3,89E+07 | -9,08E+05 | 4,54E+07 |
| 6,00 | 3,87E+07 | 4,12E+05 | 4,52E+07 |

Table 19: Example of calculated stress history components at node-i of forestay beam element

Then Table 20 illustrates the combination of the calculated components from the previous table to determine the nominal stress values. The output of this calculation depends on the beam orientation of the forestay element for example the nominal stress at t=1.00s for point 1 and point 3 is calculated as follows:

$$\sigma_{point\_1} = fs\_axialstress + fs\_SBzT\_i$$
$$\sigma_{point\_1} = 1.60e07 + 3.45e7 = 50.52e6 Pa$$
$$\sigma_{point\_3} = fs\_axialstress + fs\_SByT\_i$$
$$\sigma_{point\_3} = 1.60e07 + 2.11e6 = 18.11e6 Pa$$

|  | MPa | | |
| --- | --- | --- | --- |
| TIME | point 1 | point 2 | point 3 | point 4 |
| 1,00 | 50,52 | -18,51 | 18,11 | 13,90 |
| 1,01 | 51,62 | -18,92 | 18,51 | 14,20 |
| 2,00 | 49,16 | -19,02 | 16,52 | 13,61 |
| 3,00 | 75,30 | -7,78 | 34,38 | 33,14 |
| 3,12 | 86,09 | -5,99 | 41,03 | 39,07 |
| 4,00 | 85,71 | -7,58 | 42,67 | 35,46 |
| 5,00 | 84,31 | -6,46 | 38,02 | 39,84 |
| 6,00 | 83,95 | -6,54 | 39,12 | 38,30 |

Table 20: Example of calculated nominal stress history at node-i of the forestay beam element

This nominal stress history which was illustrated in the previous section in Figure 82 and in the following Figure 90 for the total simulated working cycle of 125s is then used as input in JRain.
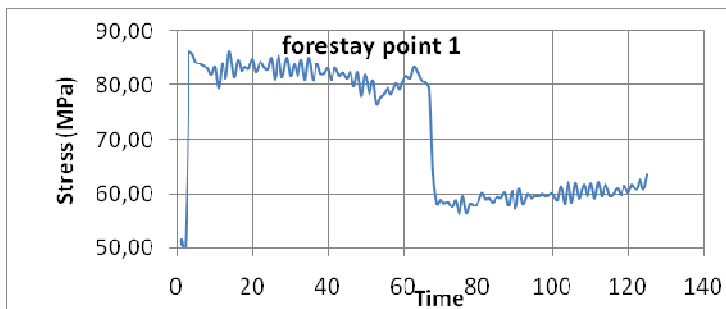


Figure 90: Stress history at top point 1 of forestay beam element

Crane fatigue assessment using Multibody Dynamics and Finite Element Method

The calculated nominal stress history of the other points for the forestay, backstay and pylons can be found in Appendix B in Table 52, Table 53, Table 54 and Table 55. Input file containing nominal stresses for the example of 6s for Jrain, see Figure 91.
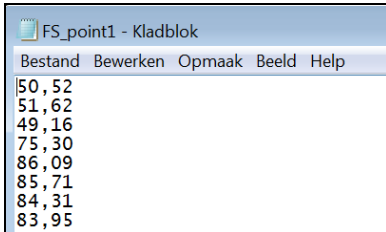


**Figure 91: Illustration input file of nominal stresses for JRain**

The Rainflow counting method is performed using JRain software resulting in the following output illustrated with Figure 92 and Table 21.
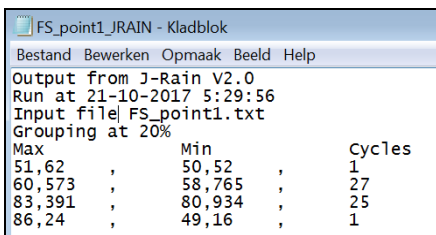


**Figure 92: Illustration output file of nominal stresses in JRain**

| block # | Max (Mpa) | Min (Mpa) | counted cycles |
|--------:|----------:|----------:|---------------:|
| 1 | 51,62 | 50,52 | 1 |
| 2 | 60,573 | 58,765 | 1 |
| 3 | 83,391 | 80,934 | 1 |
| 4 | 86,24 | 49,16 | 1 |

**Table 21: Reduced stress spectrum into stress ranges in JRain**

Then the stress range $\Delta\sigma = \sigma_{max} - \sigma_{min}$, the actual number of cycles and the accumulated fatigue damage is determined. This is shown in Table 22.

| | Stress range histogram FS point 1 | | | | | |
|--------:|----------:|----------:|---------|------------------|-----------------------|--------|
| block # | Max (Mpa) | Min (Mpa) | counted cycles | Stress range (Mpa) | current total # cycles | Damage |
| 1 | 51,62 | 50,52 | 1 | 1,1 | 1,31E+06 | 0,0000 |
| 2 | 60,573 | 58,765 | 1 | 1,808 | 1,31E+06 | 0,0001 |
| 3 | 83,391 | 80,934 | 1 | 2,457 | 1,31E+06 | 0,0002 |
| 4 | 86,24 | 49,16 | 1 | 37,08 | 1,31E+06 | 0,7170 |
| **Total damage** | | | | | | **0,7173** |

**Table 22: Accumulated fatigue damage calculation for point 1 at the forestay beam element**

The Rainflow counting algorithm is applied for all 16 point at the beam elements. These calculations and tables can be found in Appendix B in Table 56, Table 57, Table 58 and Table 59. The resulted of all the fatigue contributions of the 16 points is seen in the following Table 23.

|         | forestay | backstay | pylon left | pylon right |
|---------|----------|----------|------------|-------------|
| point 1 | 0,717    | 1,104    | 0,129      | 0,421       |
| point 2 | 0,059    | 0,491    | 0,424      | 0,092       |
| point 3 | 0,428    | 0,327    | 1,299      | 1,171       |
| point 4 | 0,595    | 0,472    | 1,644      | 1,348       |

**Table 23: Fatigue damage results at 16 points of tubular welded joint of upper arm structure**

Because of the fact that the weld interface of the forestay and backstay members are the same, and thus all points of these members coincide, the final damages of both are calculated as one average value, seen in Table 24.

|         | average damage at forestay/backstay | pylon left | pylon right |
|---------|-------------------------------------|------------|-------------|
| point 1 | 0.91                                | 0.129      | 0.421       |
| point 2 | 0.27                                | 0.424      | 0.092       |
| point 3 | 0.38                                | 1.299      | 1.171       |
| point 4 | 0.53                                | 1.644      | 1.348       |

**Table 24: Fatigue damage at weld interface points based on dynamic method**

In the next chapter a fatigue assessment is performed using the conventional method according to the crane standards.

## 4    Fatigue assessment according to a crane standard

This chapter discusses the fatigue calculation procedure according to a chosen crane standard.

Currently there are a number of crane standards which could be used to perform a fatigue assessment. These are the NEN2063, NEN2019/FEM1.001, DIN15018, NEN-EN13001, Eurocode 3, the Lloyds crane code and the state of the art DNVGL-RP-C203 issued in may 2016. However this standard is the latest, it reports that a fatigue check may be based on the allowable stresses method used in the NEN2019/FEm1.001 or the limit state method used in the EN13001.

Mel (2009) performed a research about the consequences of the EN13001 on the design of STS cranes. He reported that the main difference between the NEN2019/FEM1.001 and the EN13001/NEN2063 the use of the mean stress is. In the former the use of the mean stress has an influence on the stress ratio which determines the allowable stress and in the EN13001 the mean stress has no influence. In his study he compared the fatigue calculation methods and its influence for only one specific K50 welded detail and stress spectrum. This was performed according to the NEN2018/FEM1.001, NEN2063 and EN13001 standard.  The results revealed that the difference in fatigue damage between the NEN2018 and the EN13001 was about 0.9%. He also reported that the results mainly depend on the chosen safety, amplification and risk factors and weld detail.

For the fatigue assessment in this research, the NEN 2018 (Netherlands Standards Institution, 1983) and NEN2019 (Netherlands Standards Institution, 1984) crane standard for the aged 25t lemniscate crane will be used, illustrated in Figure 93. However this crane standard is not valid anymore the main reason to use it is that the crane was designed using this standard according to the crane book (Jansen, 1996) and according to the latest DNV code the NEN2019 which is the same as the FEM1.001 may be used to perform a fatigue calculation.
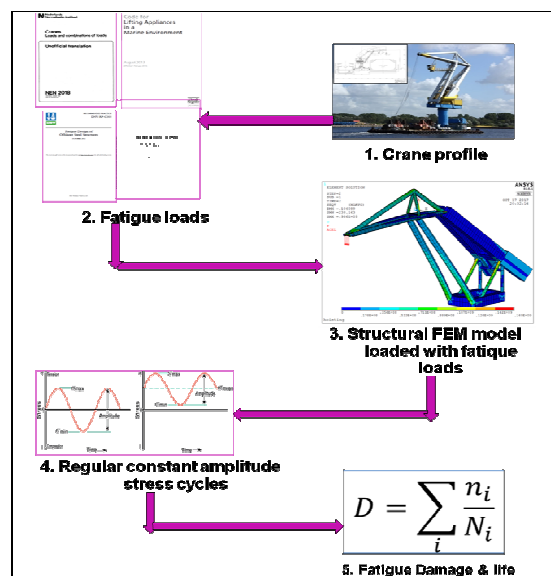


**Figure 93: crane standard fatigue calculation procedure**

### 4.1  Fatigue loads according to NEN crane standard

The NEN2018 and NEN2019 crane standard is an allowable stress method. This standard calculates an allowable fatigue stress for each direction and is based on the crane classification, calculated stress ratio, material yield stress and the weld class.

The 25t lemniscate crane was designed according to the NEN2018 and NEN2019 standards for crane group 5 (Jansen, 1996). Based on this information the following choices are made using the standard.

Figure 94 classifies the crane as regularly used but due to shifting, is interrupted during transshipment; Class of utilization = B.

Table 1 -- Classes of utilization

| class of utili- zation | number of expected load cycles during the effective period of use | | remarks |
|---|---|---|---|
| | over | to...incl. | |
| A | - | 2 x $10^5$ | irregular use with long periods of rest |
| B | 2 x $10^5$ | 6,3 x $10^5$ | regular use in interrupted operation |
| C | 6,3 x $10^5$ | 2 x $10^6$ | regular use in continuous operation |
| D | 2 x $10^6$ | - | full, continuous operation |

**Figure 94: Crane classification NEN2018**

The information in Figure 94 clearly shows that the crane was initially designed for 630000 load cycles. However up to the moment of writing the current number of load cycles is estimated to be 1.31million cycles. This shows that the crane could be in a state of fatigue failure and therefore requires a fatigue reliability investigation.

Figure 95 shows a load spectrum of 3, which assumes that due to grab duty maximum loads are always transmitted into the crane when lifting a full grab.

```
Table 2 -- Design-load spectra
```

| | load spectrum | | remarks |
|---|---|---|---|
| 0 | very light | p = 0 | Crane by exception loaded with the working load, and as a rule with very light loads. |
| 1 | light | p = 1/3 | Crane sometimes loaded with the working load, and as a rule with loads of about 1/3 of the working load. |
| 2 | moderate | p = 2/3 | Crane repeatedly loaded with the working load, and as a rule with loads between 1/3 and 2/3 of the working load. |
| 3 | heavy | p = 1 | Crane frequently loaded with the working load. |

**Figure 95: Load spectrum NEN2018**

These choices explain the design result for crane group 5 shown in Figure 96 and Figure 97 according to the NEN standard.

```
Table 3 -- Crane groups
```

| design-load spectrum | class of utilization | | | |
|---|---|---|---|---|
| | A | B | C | D |
| | crane group | | | |
| 0 | 1 | 2 | 3 | 4 |
| 1 | 2 | 3 | 4 | 5 |
| 2 | 3 | 4 | 5 | 6 |
| 3 | 4 | 5 | 6 | 6 |

**Figure 96: Crane group NEN2018**

| type of crane | | further description of the operation [1] | crane group (see 3.2.4) | hoisting class (see 4.4.2) |
|---|---|---|---|---|
| nr. | name | | | |
| 16 | harbour cranes (slewing cranes, portal cranes) floating cranes | grab or magnet operation | 5 , 6 | b , c |

**Figure 97: Classification of crane type to a crane group NEN2018**

The following Figure 98 and Figure 99 illustrate the choice of the hoisting class and the load factor. Assuming a very slack crane during hoisting at maximum flight, a good controlled hoisting system taking cable flexibility into account.

```
Table 13 -- Hoisting classes
```

| character of the crane system incl. hoisting cable [1] | Course of the accelerations during the hoisting movement [2] | | |
|---|---|---|---|
| | even | uneven | very uneven (bumpy) |
| relatively slack | a | a | b |
| normal | a | b | b |
| relatively stiff | b | b | c |

**Figure 98: hoisting class NEN2018**

Crane fatigue assessment using Multibody Dynamics and Finite Element Method

The crane hoisting speed is 2m/s, with hoisting class b, result in a load factor of 1.6.
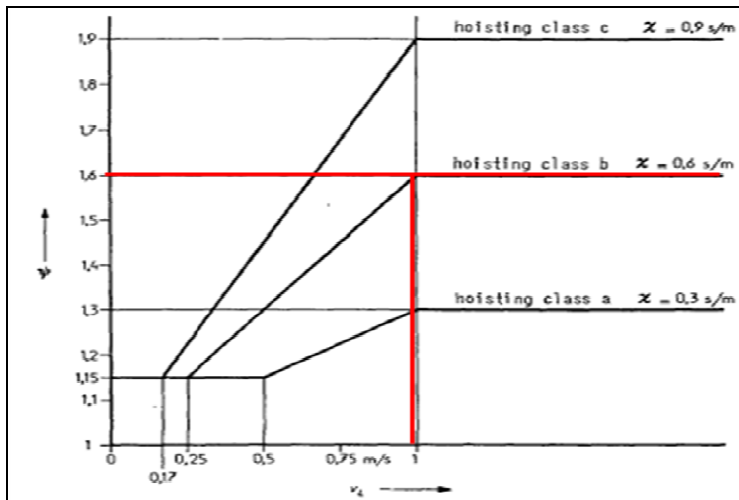


**Figure 99: load factor according to NEN2018**

Table 25 shows the calculated values for each identified individual load.

| Gravity | 9.81 m/s^2 |
|---|---|
| Vertical load exerted on boom due to hoisting load: $F_{y,hoist,dynamic} = m * g * \varphi$ | $F_{y,hoist,dynamic} = 392.4kN$ |
| Horizontal lateral load exerted on the boom(inertia force), due to slewing: $F_{z,inertia,luffing} = 2 * m_{hoist} * a_{normal,luffing}$ | $F_{x,\tan gential,slew} = 52.05kN$ |
| horizontal longitudinal load exerted on the boom(centrifugal force), due to slewing: $F_{z,centrifugal,slew} = 2 * m_{hoist} * a_{normal,slew}$ | $F_{z,centrifugal,slew} = 49kN$ |
| horizontal longitudinal load exerted on the boom due to luffing | $F_{z,inertia,luffing} = 12.5kN$ |

**Table 25: Individual loads according to NEN2018**

The details of the calculations of the individual loads can be found in Appendix C

The following step is to define load sets. These are loads of different type as a result from the crane function (hoisting, slewing and luffing events) and constraints, that act on the crane structure at the same time. These sets simulate the operational conditions of the crane e.a. hoisting the load at maximum flight when slewing CW. In total there are 3 crane configurations: minimum flight, intermediate flight and maximum flight. In this calculation only the maximum flight configuration is taken into account, because it results in the maximum loading of the structure compared to intermediate position. This was demonstrated in section 3.3. Maximum loading at minimum flight is almost never encountered in practice for the crane used in this research according to Holleman (2017) and

is thus neglected in this calculation. For crane slewing two rotations are encountered: CW slewing and CCW slewing. For luffing we encounter luffing in and luffing out. In total 15 load sets are identified and shown in the following Table 26.

| | load sets = combination of individual loads | | | | | | |
|---|---|---|---|---|---|---|---|
| | **IL1** | **IL2** | **IL3** | **IL4** | **IL5** | **IL6** | **Load set Description** |
| | **gravity** | **hoisting load** | **slewing inertia load** | **centrifugal load** | **luffing inertia load** | **pontoon motion** | |
| LS 1 | 1 | | | | | | gravity only |
| LS 2 | 1 | 1 | | | | 1 | gravity+hoisting |
| LS 3 | 1 | | 1 | | | | gravity+slewing CW |
| LS 4 | 1 | | | 1 | | | gravity+slewing CW |
| LS 5 | 1 | | | | 1 | | gravity+luffing in |
| LS 6 | 1 | 1 | 1 | | | 1 | hoisting+slewing CW |
| LS 7 | 1 | 1 | 1 | 1 | | 1 | hoisting+slewing CW |
| LS 8 | 1 | 1 | -1 | | | 1 | hoisting+slewing CCW |
| LS 9 | 1 | 1 | -1 | 1 | | 1 | hoisting+slewing CCW |
| LS 10 | 1 | 1 | | | 1 | 1 | hoisting+luffing in |
| LS 11 | 1 | 1 | 1 | | 1 | 1 | hoisting+slewing CW+luffing in |
| LS 12 | 1 | 1 | 1 | 1 | 1 | 1 | hoisting+slewing CW+luffing in |
| LS 13 | 1 | 1 | | | -1 | 1 | hoisting+luffing out |
| LS 14 | 1 | 1 | -1 | | -1 | 1 | hoisting+slewing CCW+luffing out |
| LS 15 | 1 | 1 | -1 | 1 | -1 | 1 | hoisting+slewing CCW+luffing out |
| | | | | | | | |
| **Total =** | **15** | | | | | | |

**Table 26: Load sets identified for 25t lemniscate crane**

A group factor of M=1.15 is chosen seen Figure 100: Group factor and only applied to the gravitational load: g*= M x g=11.2815 m/s^2. This load is considered as taking the dynamic effect of the pontoon motion on the total floating structure into consideration when the hoisting load is lifted and released. This result in one extra individual load; pontoon motion.



**Figure 100: Group factor NEN2018**

For the fatigue assessment the NEN2018 requires only a calculation according to load combination 1 as seen in Figure 101. This is the situation where the crane is in operation without wind. These don't have a considerable influence on fatigue.

Table 26 — Load combinations for the calculation of the metal structure

| individual loads | | | load combinations | | | | |
|---|---|---|---|---|---|---|---|
| reference | description | symbol | 1 | 2a | 2b | 2c | 2d |
| 4.2 | weight of the own mass | $S_G$ | M | M | 1 | 1 | 1 | 1 |
| 4.3 | weight of the hoisting load | $S_L$ | M.$\phi$ | M.$\phi$ | | 1 | 1 | |
| 4.3 | weight of the parts belonging to the crane to lift the effective load | $S_{Lo}$ | | | (1) | | | |
| 4.4 en 4.5 | inertia forces | | | | | | | |
| 4.4.2 | inertia forces from the hoist movement | $S_{ML}$ | 1) | 1) | | | | |
| 4.5.1 | other inertia forces except centrifugal forces | $S_M$ | | | | | | |
| 4.5.1.1 | crane travelling | $S_{KR}$ | M | M | | | | |
| 4.5.1.2 | crab travelling | $S_{KA}$ | M | M | | | | |
| 4.5.1.3 | slewing | $S_Z$ | M | M | | | | |
| 4.5.1.4 | luffing movements | $S_T$ | M | M | | | | |
| 4.5.2 | centrifugal forces | $S_C$ | M | M | | | | |
| 4.5.3 | slanting rope pull | $S_{SR}$ | M | M | | | | |
| 4.5 | operation effects | $S_B$ | | | | | | |
| 4.5.4 | friction- and rolling resistance | $S_F$ | M | M | | | | (M) |
| 4.5.5 | travelling askew | $S_{SA}$ | M | M | | | | |
| 4.5.6 | buffer action | $S_{BU}$ | | | | 1 | | |
| 4.5.7 | tilting of a travelling crab with a guided load | $S_{KK}$ | | | | | 1 | |
| 4.6 | weather influences | | | | | | | |
| 4.6.2 | wind | $S_W$ | | 1 | | | | 1 |
| | storm | $S_S$ | | | 1 | | | 1 |
| 4.6.3 | snow | $S_N$ | | 1 | | | | |
| 4.6.4 | temperature | $S_{TE}$ | 1 | 1 | 1 | 1 | 1 | 1 |
| 4.7 | loads from cabins and accesses | $S_{KT}$ | | (1) | | | | |
| 4.8 | loads during the assembly | $S_{MO}$ | | | | | | 1 |
| 4.9 | loads resulting from the character of operation | | 2) | 2) | | | | |
| 4.10 | other loads | $S_{OV}$ | | | | | | |

1) These inertia forces are taken into account by the load factor $\phi$, see 4.4.
2) These loads are taken into account by the group factor M, see 4.9.

**Figure 101: Load combinations NEN2018**

Each individual load is applied in six loading steps as FEM loads to the same FEM model built in ANSYS this is illustrated in Figure 102.
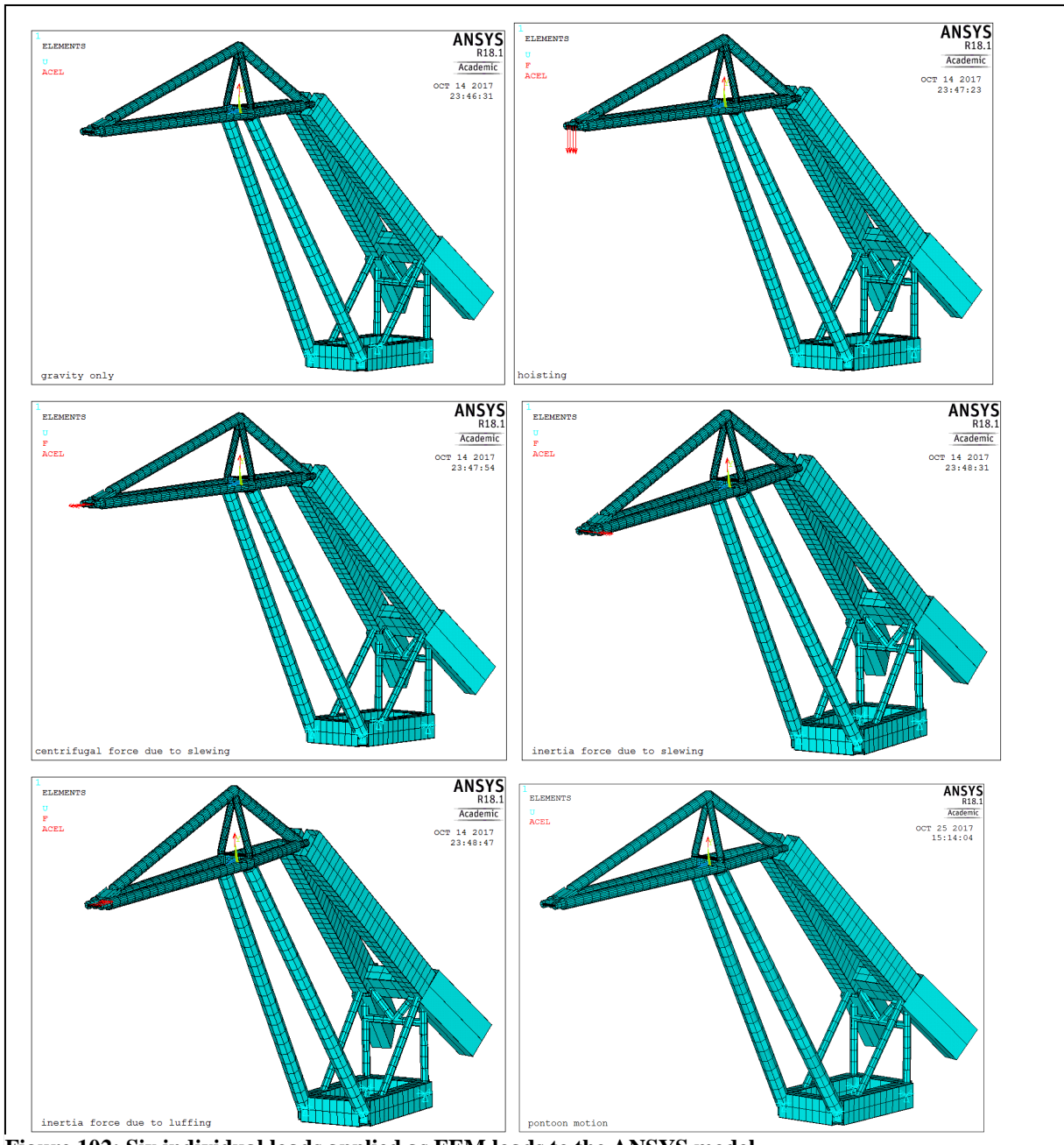


**Figure 102: Six individual loads applied as FEM loads to the ANSYS model**

The next chapter starts with the discussion of the stress analysis in accordance with the NEN crane standard.

### 4.2   Static stress check

The regular occurring loads (fatigue loads) result in stress variations throughout the crane structural members. For this crane type it is assumed that for example when handling scrap metal during grab duty, regularly shock loads occur. This results in overloading of the structure and can result in plastic deformation. To account for this phenomenon the NEN standard demands to check if plasticity occurs for the calculated loads. This is taken into account by dividing the elastic yield stress with a safety factor for of 1.5 for the loading case without wind shown in Figure 103.

| | Case I | Case II | Case III |
|---|---|---|---|
| Values of $v_E$ | 1,5 | 1,33 | 1,1 |
| Permissible stresses $\sigma_a$ | $\sigma_E/1,5$ | $\sigma_E/1,3$ | $\sigma_E/1,1$ |

**Figure 103: Yield stress check NEN2019**

The drawback of this check is that the crane is constructed with different steel qualities with different yield points. For this check S235 or FE360 steel is assumed for the total crane, seen in and Figure 104. With these parameters the equivalent permissible stress is checked for each individual load.

| Table T.3.2.1.1 Values of $\sigma_E$ and $\sigma_a$ for steels A.37 – A.42 – A.52 | | | | |
|---|---|---|---|---|
| | | Maximum permissible stresses: $\sigma_a$ | | |
| Steels | Elastic limit $\sigma_E$ N/mm² | Case I N/mm² | Case II N/mm² | Case III N/mm² |
| E.24 (A.357, Fe 360) | 240 | 160 | 180 | 215 |
| E.26 (A.42) | 260 | 175 | 195 | 240 |
| E.36 (A.52, Fe 510) | 360 | 240 | 270 | 325 |

**Figure 104: Maximum permissible stress check NEN2019**

The allowable stress for all loadings is $\sigma_{allow} = \dfrac{\sigma_{y,S235}}{SF} = \dfrac{240}{1.5} = 160 MPa$ . It must be noticed that the drawback of this check is that only a single material type is assumed for the total crane while in the real case the crane is constructed using material with different yield stresses.

For all six loading cases, a stress check was done using the Von Mises stress criterion. This criterion always gives the highest stress developed, but doesn't provide a direction in which the stress is working. The Von misses stress is calculated with the following equation:

$$\sigma_{VonMises} = \frac{1}{\sqrt{2}}\sqrt{(\sigma_{xx} - \sigma_{yy})^2 + (\sigma_{yy} - \sigma_{zz})^2 + (\sigma_{zz} - \sigma_{xx})^2 + 6(\tau_{xy} + \tau_{yz} + \tau_{zx})^2}$$

The hoisting loading showed to have the most extreme effect on the crane structure. Figure 105 shows potential fatigue critical spots on the upper arm. Of course the total crane must be checked, but this is not part of the research.
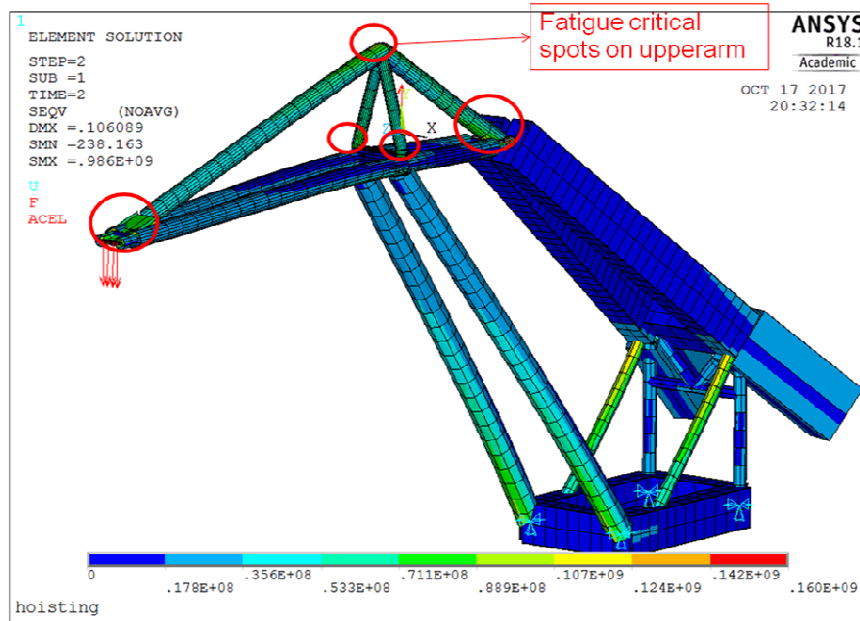


**Figure 105: Fatigue critical spots on upper arm**

The stress checks and reaction force tables for all the other individual loads can be found in Appendix C in Figure 129 to Figure 140.  In the next section the stress analyses is described.

## 4.3   Fatigue stress calculation example

This section illustrates an example calculation of the fatigue stress for the tubular welded joint interface of the forestay member.

First the stress components are determined for each individual load using the FEM model, see Table 27.

| | | Pa | | | | | |
|---|---|---|---|---|---|---|---|
| | | gravity | hoisting load(y) | inertia load(x) | centrifugal load(z) | inertia load (z) | pontoon (y) |
| **stress components** | **Sax** | 8,50E+06 | 4,81E+07 | 8,42E+06 | 8,50E+06 | 8,52E+06 | 9,77E+06 |
| | **Sbny** | 1,35E+05 | 1,33E+05 | 1,50E+05 | -1,28E+07 | 1,31E+05 | 1,55E+05 |
| | **Sbnz** | 2,97E+07 | 4,57E+07 | 3,00E+07 | 2,97E+07 | 2,96E+07 | 3,41E+07 |

**Table 27: Calculation example stress components at forestay due to the individual loads**

Then these stress components are combined to determine the nominal stresses, see Table 28.

$$\sigma_{nom, point1} = \sigma_{axial} + \sigma_{bend_{z-axis}} = 8.5e6 + 2.97e7 = 3.82e7\,Pa$$

$$\sigma_{nom, point2} = \sigma_{axial} - \sigma_{bend_{z-axis}} = 8.5e6 - 2.97e7 = -2.12e7\,Pa$$

$$\sigma_{nom, point3} = \sigma_{axial} + \sigma_{bend_{y-axis}} = 8.5e6 + 1.35e5 = 8.63e6\,Pa$$

$$\sigma_{nom, point4} = \sigma_{axial} - \sigma_{bend_{y-axis}} = 8.5e6 - 1.35e5 = 8.36e6\,Pa$$

|  |  | Pa |  |  |  |  |  |
|---|---|---|---|---|---|---|---|
| **nominal stress = combined stress components** | **point 1** | 3,82E+07 | 9,38E+07 | 3,84E+07 | 3,82E+07 | 3,81E+07 | 4,39E+07 |
|  | **point 2** | -2,12E+07 | 2,40E+06 | -2,15E+07 | -2,12E+07 | -2,11E+07 | -2,43E+07 |
|  | **point 3** | 8,63E+06 | 4,82E+07 | 8,57E+06 | -4,31E+06 | 8,65E+06 | 9,93E+06 |
|  | **point 4** | 8,36E+06 | 4,79E+07 | 8,27E+06 | 2,13E+07 | 8,38E+06 | 9,62E+06 |

**Table 28: Calculation example nominal stresses at forestay due to the individual loads**

The remaining calculation sheets and results of this part of the calculation can be found in Appendix C in Table 60, Table 61 and Table 62.

Subsequently the nominal stress at each point for each load case is determined. This is done by multiplying each nominal stress with a factor defined for each load case defined in Table 26. For example: determine the nominal stress for load case 1, at point 1 (top fiber) for the forestay. A sample by means of load case 1 from Table 26 is chosen see Table 29.

|  | **IL1** | **IL2** | **IL3** | **IL4** | **IL5** | **IL6** |  |
|---|---|---|---|---|---|---|---|
|  | **gravity** | **hoisting load** | **slewing inertia load** | **centrifugal load** | **luffing inertia load** | **pontoon motion** | **Load set Description** |
| LS 1 | 1 |  |  |  |  |  | gravity only |

**Table 29: Load case 1 taken as example from Table 26**

Each load case is assigned with factors:

| Load Set 1 | 1 | 0 | 0 | 0 | 0 | 0 |
|---|---|---|---|---|---|---|

Then calculate the nominal stresses for point 1 as a result of each individual load.

| **point 1** | 3,82E+07 | 9,38E+07 | 3,84E+07 | 3,82E+07 | 3,81E+07 | 4,39E+07 |
|---|---|---|---|---|---|---|

Then calculate the nominal stress at point 1 as a result of load set 1:

$$\sigma_{loadcase1_{point1}} = 3.82e7*1 + 9.38e7*0 + 3.84e7*0 + 3.82e7*0 + 3.81e7*0 + 4.39e7*0 = 3.82e7\,Pa$$

The following Table 30 illustrates the calculation of all nominal stresses which could be expected for all load sets.

| | point 1 | point 2 | point 3 | point 4 |
|---|---|---|---|---|
| **stresses for each load case** | 3,82E+07 | -2,12E+07 | 8,63E+06 | 8,36E+06 |
| | 1,76E+08 | -4,31E+07 | 6,68E+07 | 6,59E+07 |
| | 7,65E+07 | -4,27E+07 | 1,72E+07 | 1,66E+07 |
| | 7,63E+07 | -4,23E+07 | 4,32E+06 | 2,97E+07 |
| | 7,63E+07 | -4,23E+07 | 1,73E+07 | 1,67E+07 |
| | 2,14E+08 | -6,47E+07 | 7,53E+07 | 7,42E+07 |
| | 2,52E+08 | -8,58E+07 | 7,10E+07 | 9,55E+07 |
| | 1,37E+08 | -2,16E+07 | 5,82E+07 | 5,77E+07 |
| | 1,76E+08 | -4,28E+07 | 5,39E+07 | 7,90E+07 |
| | 2,14E+08 | -6,42E+07 | 7,54E+07 | 7,43E+07 |
| | 2,52E+08 | -8,57E+07 | 8,40E+07 | 8,26E+07 |
| | 2,90E+08 | -1,07E+08 | 7,97E+07 | 1,04E+08 |
| | 1,38E+08 | -2,20E+07 | 5,81E+07 | 5,75E+07 |
| | 9,93E+07 | -5,05E+05 | 4,96E+07 | 4,93E+07 |
| | 1,37E+08 | -2,17E+07 | 4,52E+07 | 7,06E+07 |

**Table 30: Calculation example nominal stresses at weld interface forestay for all identified load sets**

The remaining calculation sheets and results of this part of the calculation can be found in Appendix C in Table 63, Table 64, Table 65and Table 66.

Because the NEN2019 crane standard demands to calculate fatigue using minimum and maximum stresses, the last step is to select these for each point, see the red and green highlighted cells. For the used example the stress range and the stress ratio $\kappa = \dfrac{\sigma_{min}}{\sigma_{max}}$ is calculated in Table 31.

| | point 1 | point 2 | point 3 | point 4 |
|---|---|---|---|---|
| **Max stress** | 290,46 | -106,91 | 83,98 | 103,88 |
| **Min stress** | 38,16 | -0,50 | 4,32 | 8,36 |
| **Stress range** | 252,29 | 106,40 | 79,66 | 95,52 |
| **Kappa** | 0,1 | 0,0 | 0,1 | 0,1 |

**Table 31: Calculation example stress range at weld interface points of forestay**

For this stress range, the standard assumes a cyclic stress with constant amplitude, plotted in Figure 106.
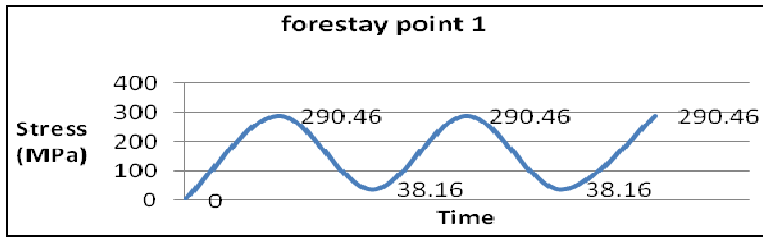
**Figure 106: Cyclic stress with constant amplitude at point 1 of weld interface of forestay**

The remaining final calculation sheets and results of this part of the calculation can be found in Appendix C  "Stress plots".

In the next section the fatigue damage is calculated for the entire tubular welded joint.

### 4.4    Fatigue results according to the NEN crane standard

This chapter discusses the calculation of the fatigue damage at the weld interface connecting the four structural members for the upper arm assuming a constant amplitude nominal stress loading encountered by the weld.

First a weld class is chosen for the point of interest the upper arm. Here one weld type is available. This is fully penetrated square single V-butt/groove weld. Here tubes are welded together which can be seen in Figure 80. Comparing this real weld information with the weld qualities form the weld atlas in the NEN2019 standard, a K3 weld quality is chosen, see Figure 107.



**Figure 107:  K3 notch group for tubular weld detail NEN2019**

Based on the calculated stress ratio values an allowable fatigue stress for the welded joint is chosen from the NEN fatigue criteria spreadsheet developed by Van den Bos, (2010). The allowable stresses calculated by the standard depends on the crane group which is chosen to

be 5 for this specific weld type, the yield stress of the members which is API 5L grade B material, $\sigma_{yield} = 241 MPa$ and the stress ratio, which is chosen on basis if the maximum stress is tension or compression. The allowable stress curves are seen in Figure 108 and Figure 109.
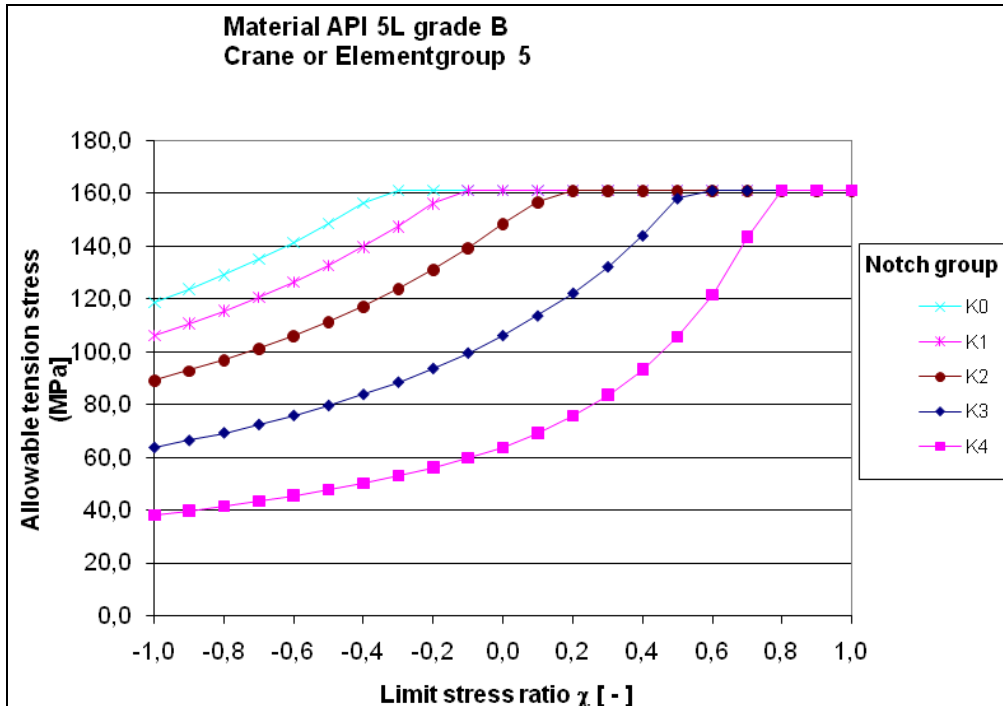


**Figure 108: Allowable fatigue stress-tensile criterion (Van den Bos, 2010)**
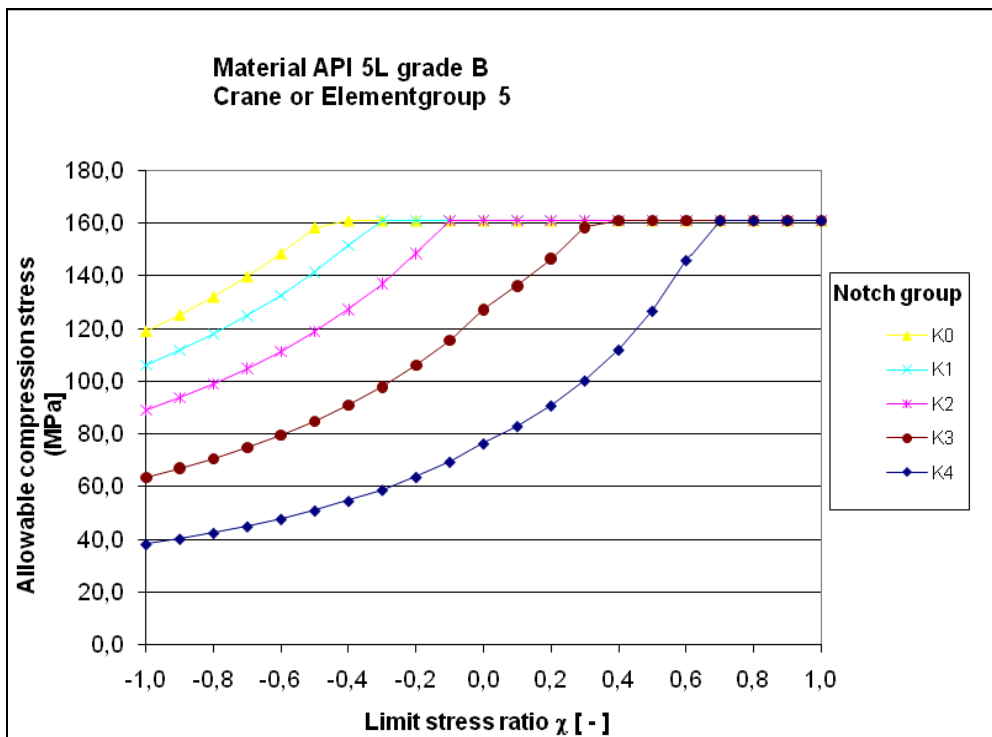


**Figure 109: Allowable fatigue stress-compression criterion (Van den Bos, 2010)**

All values from this graph can be found in Appendix C in Table 70 and Table 71.

The allowable fatigue stresses and allowable stress range results are presented in the following Table 32 and Table 33 for each structural member.

|          | forestay | backstay | pyloon left | pyloon right |
|----------|----------|----------|-------------|--------------|
| **point 1** | 113,5 | 115,7 | 115,7 | 115,71 |
| **point 2** | 115,7 | 115,7 | 115,7 | 115,7 |
| **point 3** | 113,5 | 115,7 | 115,7 | 115,7 |
| **point 4** | 113,5 | 127,3 | 127,3 | 127,3 |

**Table 32: Allowable fatigue stress for notch group K3 based on stress ratio**

|          | forestay | backstay | pyloon left | pyloon right |
|----------|----------|----------|-------------|--------------|
| **point 1** | 227,1 | 231,4 | 231,4 | 231,4 |
| **point 2** | 231,4 | 231,4 | 231,4 | 231,4 |
| **point 3** | 227,1 | 231,4 | 231,4 | 231,4 |
| **point 4** | 227,1 | 254,6 | 254,6 | 254,6 |

**Table 33: Allowable stress range for notch group K3**

In chapter 2.4, the total number of moves have been calculated to be n= 1.31 million moves. The reference number of cycles to fracture is N=2e6. The fatigue damage values are calculated using the equation: $D = \sum \left( \dfrac{\Delta\sigma_{range}}{\Delta\sigma_{FAT}} \right)^m * \dfrac{n}{N}$ , for all measurement points.

On the basis of the calculation example in section 4.3 and the allowable stresses for the forestay weld interface a calculation is illustrated in Table 34.

|                          | point 1  | point 2  | point 3 | point 4 |
|--------------------------|----------|----------|---------|---------|
| **Max_stress**           | 290,46   | -106,91  | 83,98   | 103,88  |
| **Min stress**           | 38,16    | -0,50    | 4,32    | 8,36    |
| **Stress range**         | 252,29   | 106,40   | 79,66   | 95,52   |
| **Kappa**                | 0,1      | 0,0      | 0,1     | 0,1     |
|                          |          |          |         |         |
| **Notchgroup K3**        | 113,5    | 127,3    | 113,5   | 113,5   |
| **current # of cycles**  | 1,31E+06 |          |         |         |
| **# of cycles till fracture** | 2,00E+06 |     |         |         |
| **slope SN-curve**       | 3        |          |         |         |
|                          |          |          |         |         |
| **FAT damage**           | **0,90** | **0,05** | **0,03** | **0,05** |

**Table 34: Fatigue damage- forestay weld interface**

This calculation is performed for all the remaining points of the structural members and is shown in the following  Table 35, Table 36 and Table 37

|  | point 1 | point 2 | point 3 | point 4 |
|---|---|---|---|---|
| **Max stress** | 324,43 | -112,64 | 97,81 | 113,98 |
| **Min stress** | 43,39 | 7,64 | 10,02 | 9,86 |
| **Stress range** | 281,03 | 120,27 | 87,79 | 104,13 |
| **Kappa** | 0,1 | -0,1 | 0,1 | 0,1 |
|  |  |  |  |  |
| **Notchgroup K3** | 113,5 | 115,7 | 113,5 | 113,5 |
| **current # of cycles** | 1,31E+06 |  |  |  |
| **# of cycles till fracture** | 2,00E+06 |  |  |  |
| **slope SN-curve** | 3 |  |  |  |
|  |  |  |  |  |
| **FAT damage** | **1,24** | **0,09** | **0,04** | **0,06** |

**Table 35: Fatigue damage- backstay weld interface**

|  | point 1 | point 2 | point 3 | point 4 |
|---|---|---|---|---|
| **Max stress** | -96,66 | -139,82 | -176,03 | -60,45 |
| **Min stress** | -10,33 | -14,85 | -23,09 | -1,52 |
| **Stress range** | 86,33 | 124,97 | 152,94 | 58,94 |
| **Kappa** | 0,1 | 0,1 | 0,1 | 0,0 |
|  |  |  |  |  |
| **Notchgroup K3** | 115,7 | 115,7 | 115,7 | 127,3 |
| **current # of cycles** | 1,31E+06 |  |  |  |
| **# of cycles till fracture** | 2,00E+06 |  |  |  |
| **slope SN-curve** | 3 |  |  |  |
|  |  |  |  |  |
| **FAT damage** | **0,03** | **0,10** | **0,19** | **0,01** |

**Table 36: Fatigue damage- left pylon weld interface**

|  | point 1 | point 2 | point 3 | point 4 |
|---|---|---|---|---|
| **Max stress** | -135,17 | -89,58 | -169,92 | -56,12 |
| **Min stress** | -14,85 | -10,33 | -23,09 | -1,37 |
| **Stress range** | 120,32 | 79,24 | 146,83 | 54,76 |
| **Kappa** | 0,1 | 0,1 | 0,1 | 0,0 |
|  |  |  |  |  |
| **Notchgroup K3** | 115,7 | 115,7 | 115,7 | 127,3 |
| **current # of cycles** | 1,31E+06 |  |  |  |
| **# of cycles till fracture** | 2,00E+06 |  |  |  |
| **slope SN-curve** | 3 |  |  |  |
|  |  |  |  |  |
| **FAT damage** | **0,09** | **0,03** | **0,17** | **0,01** |

**Table 37: Fatigue damage- right pylon weld interface**

The next chapter discusses the comparison of both fatigue assessment based on the dynamic method and based on the static method.

## 5    Comparison fatigue assessment methods

### 5.1    Results dynamic method

The fatigue assessment based on the dynamic method was performed using simulation software ADAMS and Ansys APDL. ADAMS was used to simulate a representative working cycle of the crane and calculate the dynamic loads. These loads were used in a beam model developed in ANSYS to determine the stress history for one critical identified tubular welded joint. Next the fatigue damage of the past 21 years was calculated for this joint using the following main input parameters:

1. average number of transshipment moves of 1.31 million
2. number of additional counted stress cycles
3. allowable stress range of 36MPa
4. the reference weld life of 2 million cycles

According to the calculation of this method it is concluded that the dynamic loads for 1.31 million transshipment moves resulted in fatigue damage at the tubular welded joint at four points shown in Figure 110. This damage occurs in the corners between the pylons and forestay/backstay weld interface at:

a) the left side for point 3 is 1.2 and for point 4 is 1.6
b) the right side for point 3 is 1.1 and for point 4 is 1.3



| | forestay/backstay |
|---|---|
| point 1 | 0,91 |
| point 2 | 0,06 |
| point 3 | 0,38 |
| point 4 | 0,53 |

| | pylon left | | pylon right |
|---|---|---|---|
| point 1 | 0,129 | point 1 | 0,421 |
| point 2 | 0,424 | point 2 | 0,092 |
| point 3 | 1,299 | point 3 | 1,171 |
| point 4 | 1,644 | point 4 | 1,348 |
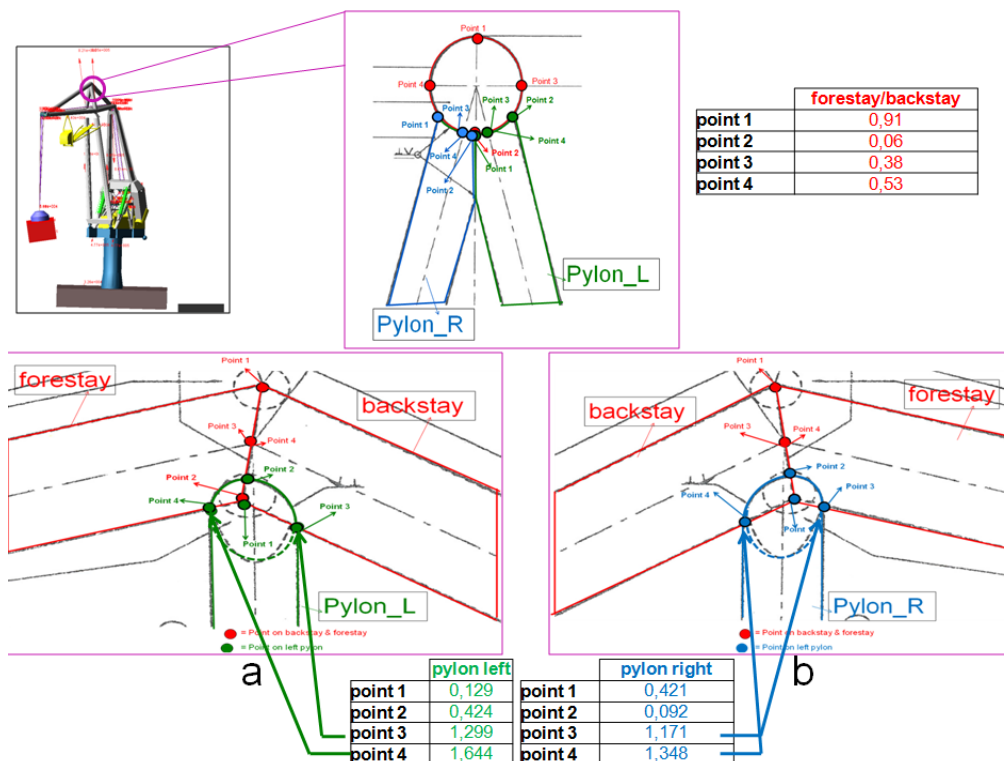
**Figure 110: Illustration fatigue damage at tubular welded joint using MBD-FEM simulation method**

## 5.2    Results of static method

The fatigue assessment based on the static method was performed using the NEN2018/2019 crane standard. The main input parameters for this calculations are:

5.  number of individual loads = 6

6.  number of load sets identified = 15

7.  crane group = 5B

8.  load factor =1.6

9.  material = API 5L grade B

10. notch effect at the point being considered = K3 weld

11. the stress ratio = calculated based on maximum and minimum expected stress

12. allowable stresses dependent upon stress ratio and the tension or compression criterion used

13. assumes that all crane components experience 1.31 million number of load cycles

14. the reference weld life of 2 million cycles

According to the calculations using the static method it is concluded that for 1.31 million transshipment moves, fatigue damage is predicted at one point of the tubular welded joint shown in Figure 111.  This point corresponds to the top part (point 1) with a fatigue damage of 1.07.
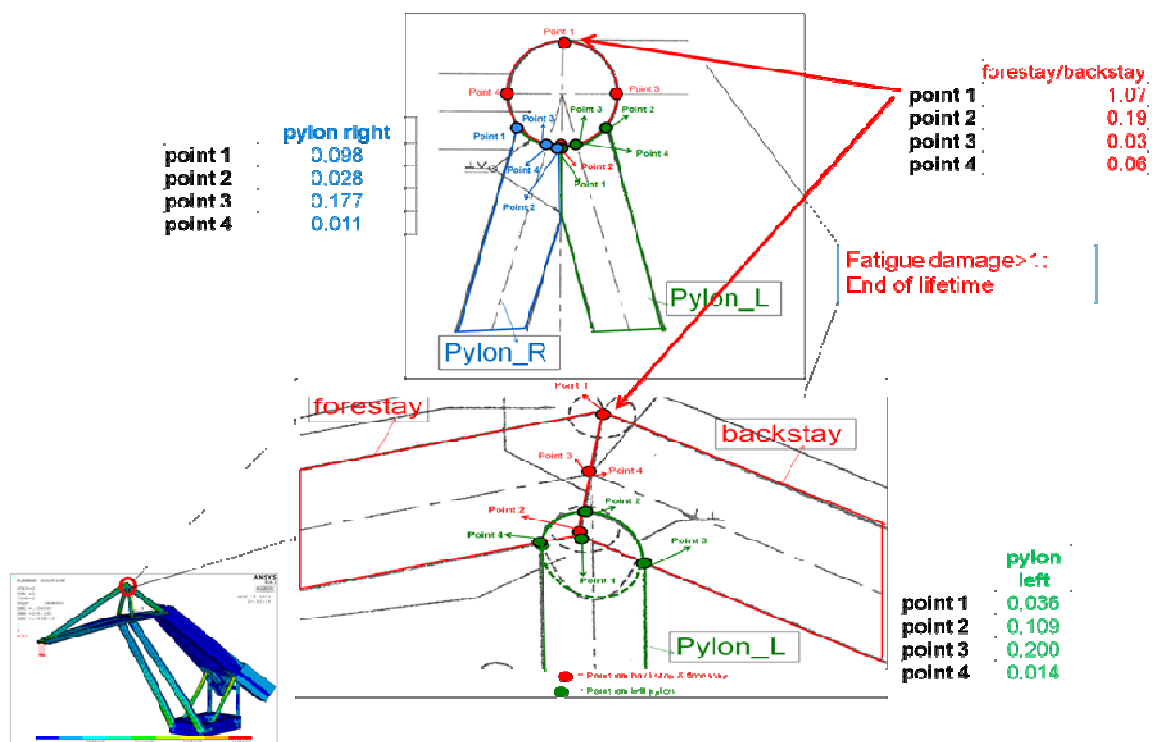


**Figure 111:  Illustration fatigue damage at tubular welded joint according to the NEN crane standard**

## 5.3   Performance of both methods

A comparison shown in Table 38 between the loads calculated by ADAMS at the front end pulleys and the individual loads calculated using the NEN standards shows that the:

1.  ADAMS lateral load is 81% higher than the NEN load
2.  ADAMS vertical load is 17% lower than the NEN load
3.  ADAMS longitudinal load is 80% higher than the NEN load.

| | Max load [kN] | | |
|---|---|---|---|
| | **NEN load** | **ADAMS load** | **Deviation** |
| Fx | 52,05 | 271,35 | *81%* |
| Fy | 392,40 | 325,18 | *17%* |
| Fz | 49,00 | 244,56 | *80%* |

**Table 38: Comparison maximum loads calculated by ADAMS & NEN**

The deviations of the ADAMS lateral and longitudinal loads are quite large compared to the values calculated with the standard. The maximum longitudinal load occurs at t=30s which is during the acceleration phase of luffing-out and at the braking phase of slewing CCW with a full grab of 25t. The maximum lateral load occurs at t=4s which is during the acceleration phase of hoisting a full 25t grab. The reason for this large deviation is assigned to the method used to model the cables with the ADAMS cable module and can be seen as an advantage for a safe structural design at this stadium of the research.

The vertical loads however show a deviation of 17%. The maximum ADAMS vertical load occurs at the instance when the grab is opened at t=64s at maximum flight of 40m. This sudden release of the load induces a impact effects to the structure.

In the fatigue assessment according to the crane standard, a load factor of 1.6 was chosen in section 4.1, see Figure 99. This value is 18.75% higher than the calculated ADAMS load factor of 1.3 from section 3.3, seen in Figure 63. The NEN2018 would suggest based on the calculated value, a hoisting class A for the hoisting mechanism of the crane. This class describes a relatively slack crane during the loading condition with an uneven hoisting acceleration course characteristic during a hoisting movement.

However the ADAMS load factor does show an exact match with the load factor according to NEN it does show a relation with the research results of Vermeer et al., (2013). This study showed that a substantial increased payload of more than 30% on top of the nominal crane load occurs during the unloading stage. Based on this result it is concluded that the ADAMS load factor is found reasonable.

The main difference between the two methods is the choice of the allowable stress for the weld. The NEN standard explicitly demands to choose this value based on the calculated stress ratio, the sign of the maximum stress and the crane group. While for the simulation, this value is chosen based on the weld configuration from the weld atlas seen in Figure 88.

Table 39 shows the fatigue damage results of both methods for the tubular welded joint on the upper arm structure of the crane. This was considered in section 1.5 as the research boundary for the fatigue assessment. For this specific joint, the dynamic simulation method predicted fatigue damage at four points of the weld interface while the NEN predicted fatigue damage at only one point.

On the basis of the calculated fatigue damage for the tubular welded joint it is concluded that the dynamic contribution compared to the static method seen in Table 39 is:

| | forestay/backstay | | | pylon left | | | pylon right | | |
|---|---|---|---|---|---|---|---|---|---|
| | **Damage** | | Contribution dynamic effects | **Damage** | | Contribution dynamic effects | **Damage** | | Contribution dynamic effects |
| | static method | dynamic method | | static method | dynamic method | | static method | dynamic method | |
| **point 1** | 1,07 | 0,91 | 15,0% lower | 0,04 | 0,13 | 71,9% higher | 0,10 | 0,42 | 76,8% higher |
| **point 2** | 0,19 | 0,27 | 30,8% higher | 0,11 | 0,42 | 74,2% higher | 0,03 | 0,09 | 69,5% higher |
| **point 3** | 0,03 | 0,38 | 91,2% higher | 0,20 | 1,30 | 84,6% higher | 0,18 | 1,17 | 84,8% higher |
| **point 4** | 0,06 | 0,53 | 89,5% higher | 0,01 | 1,64 | 99,1% higher | 0,01 | 1,35 | 99,2% higher |

**Table 39: Comparison fatigue damage results dynamic and static method**

From the simulated stress spectrum discussed in section 3.5 and Table 39 it is concluded that:

1. the largest dynamic effects occur at the moment of loading and unloading of the crane. During these moments the weld encounters the largest stress difference and therefore this phase of the working cycle contributes to the largest fatigue damage at the top tubular weld of the upper arm.

2. the left point 3 and right point 4 at fore- and backstay interface encounter a impact loading during the starting phase of luffing-in motion with an empty grab at the moment the crane is slewing CW at maximum velocity. This is the result of both centrifugal and inertia loads occurring simultaneously at this instantaneous moment.

3. The weld interface at both pylons encounter most of the vibration plus impact loading and thus induces fatigue to the crane structure. Therefore this dynamic loading resulted in fatigue damage in the corners between the pylons and the fore- and backstay.

From the simulated crane configuration using the static calculation it is concluded that the largest stress induced is for load case 12. This event simulates the operational conditions of the crane for hoisting the load at maximum flight , slewing CW and luffing-in simultaneously. Logically the minimum stress in the structure occurs with only the gravity effect. Because the NEN standard only uses the maximum and minimum calculated stresses, load case 12 results in fatigue damage at the top fiber (point 1) of the weld.

It is concluded that the dominant influential parameters which determine the outcome of both fatigue assessment methods in this study are:
1. the difference in loading encountered in both methods
2. the difference in the value of the characteristic fatigue strength
3. the difference in number of cycles encountered by the crane component

### 5.4    Case study

At the moment the research was in progress, a longitudinal crack was discovered at the left side (point 3) on the tubular weld of the upper arm of the crane used in this study, seen in Figure 112. Here the fatigue crack possibly initiated from the weld root trough the butt weld. This case indeed shows the relationship with one of the two locations found with simulation model where the dynamic contribution are the largest, see Table 39.
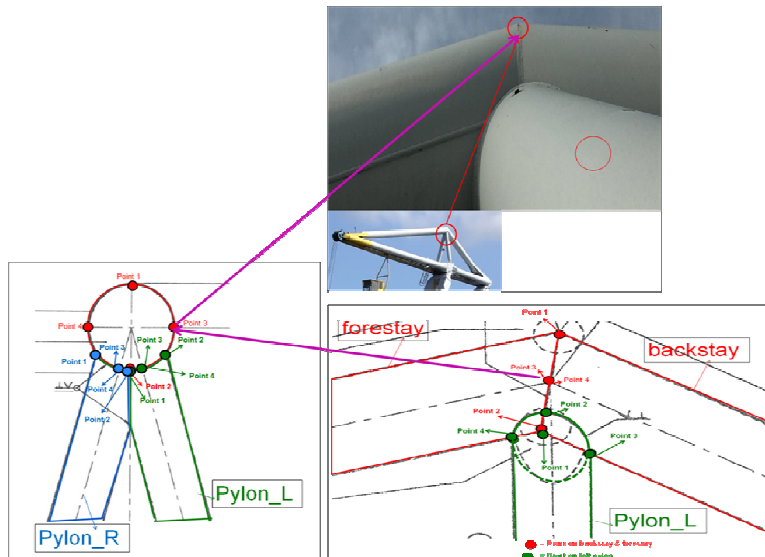


**Figure 112: Discovered cracks at upper arm Cornelis Tromp 25t lemniscate crane (Maja, 2017)**

In the same period the research was in progress, a visible large longitudinal crack was found on the top welded joint of the upper arm for another similar 25t grab crane, seen in Figure 113. Here the crack initiated from toe into the base material. From this second crack discovery it is concluded that this weld area is indeed a very critical fatigue area.
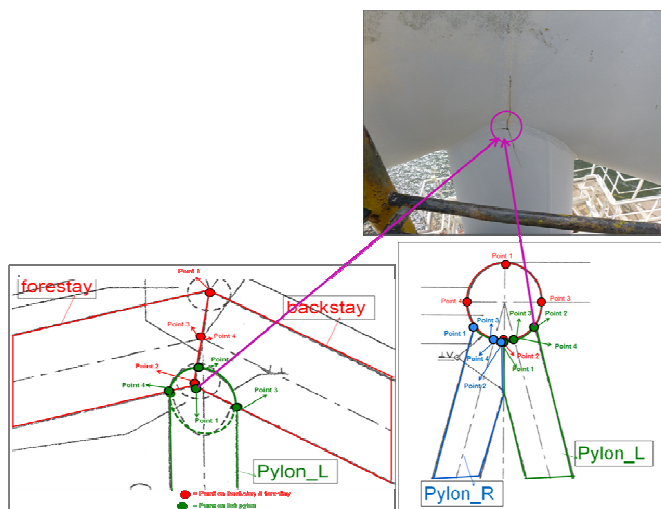


**Figure 113: Cracks at tubular weld on upper arm Skyline 25t lemniscate crane (Maja 2017)**

Both found longitudinal cracks at the tubular weld indeed show a similarity with the cracks found in the past, which was illustrated in Figure 2 of section 1.2.

## 6    Conclusion

The proposed method to perform a crane fatigue assessment using multibody dynamics and finite element method is proven to be feasible and can thus also be applied to a wide range of transport systems in fatigue design methodology.

The research question can only be answered to a certain extent, because each system has a different dynamic behaviour and also the fatigue behaviour for each welded joint is different. That is why the method is used to assess one specific tubular welded joint on the upper arm structure of an aged 25t floating lemniscate crane. For this complex joint the contribution of the dynamic effects during the operational life on the structural fatigue damage using a multibody dynamics and finite element simulation method is about 49%-82% higher compared to a conventional fatigue assessment using the NEN2018/2019 crane standard. The longitudinal fatigue crack found in reality during the moment that this research was conducted show similarities with past found cracks and thus reveals that this tubular joint is indeed a fatigue critical hotspot.

The use of multibody dynamics simulation software ADAMS in the fatigue assessment allows to directly visualize the dynamic loading characteristics of the crane for the simulated load cycle. It provides insight in the dynamic effects which occur during operation and allows to understand when these dynamic load influences occur. Although much higher load values were calculated with ADAMS for the lateral and longitudinal loads compared with the crane standard, it is concluded that in terms of structural safety the use of MBD and FEM is advantageous. However a main disadvantage is that the method requires a large amount of effort to simulate a working cycle close to reality. Finally the added value of the method is, that it can be used as a tool during the design phase of new crane designs, whereby improvements can directly be made for critical points that are under- or over-dimensioned.

### *6.1    Recommendation and future work*

The simulation method showed that the dynamics indeed contributes to the fatigue damage where the crane standard does not predict fatigue failure. The development of a computational representation of contacts and bodies using ADAMS for the crane provided a complete visualization to understand its dynamic loads during operation. Using the ADAMS model with ANSYS resulted in the prediction of the damage at the critical weld for the 25t

lemniscate crane. The results of this method show that this weld needs to be examined using available NDT and additionally repaired.

The recommendations for further future work are:

1.  Incorporate flexibility for cable mechanism and joints connecting the various structural components in the ADAMS crane model. This will result in a more accurate representation of service loads, because current model is a fully rigid model.

2.  Use control theory to develop control systems for the various mechanism instead of using general step functions. This can extend the simulation possibilities for applying the model to study the influence of the dynamic load effects for other transshipment configurations.

3.  Use combination of beam for global modeling and plate elements for detail welded joints modeling. This provides possibilities to model possible initial cracks in the FEM model and use other fatigue life analysis methods like fracture mechanics or strain life method.

# References

1. (n.d.). Retrieved November 13, 2016, from https://www.youngpowertech.com/slewing-drives/

2. ANSYS, (2017). 2.7 Node and Element Loads (UP19980821). [online] Available at: http://www.ANSYS.stuba.sk/html/elem_55/chapter2/ES2-7.htm [Accessed 21 May 2017].

3. ANSYS. (2011, October 07). Transferring Loads from ADAMS to ANSYS. Retrieved May 19, 2017, from https://www.sharcnet.ca/Software/Ansys/14.0/en-us/help/ans_adv/Hlp_G_ADVtrans.html

4. Cae-sim-sol.com. (2016, June 05). Finite Life Fatigue Strength. Retrieved May 30, 2017, from http://www.cae-sim-sol.com/en/limit-stress-evaluation/finite-life-fatigue-strength

5. Cai, F., Wang, X., Liu, J., & Zhao, F. (2014). Fatigue Life Analysis of Crane K-Type Welded Joints Based on Non-Linear Cumulative Damage Theory. Strojniški vestnik-Journal of Mechanical Engineering, 60(2), 135-144.

6. Croese Engineering Consultants mechanical handling & storage systems (1996). Algemeen plan - 25t Drijvende grijper kraan [technical drawing]

7. F. (1970, January 01). About Equipment. Retrieved November 13, 2016, from http://equipmentspecsandcharts.blogspot.nl/2015/02/tower-crane.html

8. Floatingtransshipment.com. (2017). Damen Bulk Solutions offers a total solution for dry bulk transshipment. [online] Available at: http://www.floatingtransshipment.com/ [Accessed 24 Aug. 2016].

9. Fricke, W., 2007. Round-robin study on stress analysis for the effective notch stress approach. *Welding in the world,* 51(3/4), pp. 68-79.

10. He, Bin. (2014). Virtual prototyping-based multibody systems dynamics analysis of offshore crane. International Journal of Advanced Manufacturing Technology. 75. 161-180.

11. Hobbacher, A. F. (2016). Recommendations for fatigue design of welded joints and components.

12. Holleman, M. (2017). Cornelis Tromp crane operational conditions.

13. IV-Groep,(2006). Balancerende kraan. De Ingenieur.

14. Jansen, F. (1996). Kraanboek voor vast opgestelde kraan, op rails rijdende kraan, drijvende kraan. Amsterdam: HTJ international BV. Grijperdraaikraan op ponton (model Lemniscaat)

15. Jesmond Engineering. (2013, October 09). J-Rain (Version 2.0) [Computer software]. Retrieved from https://jesmondengineering.com/engineering-software/j-rain-free-rainflow-counting-software/

16. Jesmondengineering. (n.d.). J-Rain-Rainflow Counting Software (Version 2.0) [Computer software]. Retrieved August 2, 2017, from https://jesmondengineering.com/engineering-software/j-rain-free-rainflow-counting-software/

17. Kaenders, R. (2007). Lemniscaten en kranen. NIEUW ARCHIEF VOOR WISKUNDE, 8(2), 112.

18. Kaenders, R. H. (2005). Kranen en lemniscaten. De schijf van vijf, Syllabus CWI vakantiecursus, 136.

19. Karssen, R. (2014). Searching for an improvement in fatigue assessment to increase lifetime expecancy (published master's thesis). Delft University of Technology.

20. Krabbendam, R. (2013, November 4). Heavy lift news. Retrieved March 1, 2017, from http://www.heavyliftnews.com/cranes/designing-floating-crane-installation.

21. Li, Ying & Liu, Wenyuan. (2013). Dynamic dragline modeling for operation performance simulation and fatigue life prediction. Engineering Failure Analysis. 34. 93-101.

22. Lu, Y. (n.d.). Survey of Multibody Dynamics Software. Retrieved May 14, 2015, from http://www.cs.rpi.edu/~trink/sim_packages.html

23. Maja Stuwadoors BV (2016). Archief Geraadpleegd 15 november 2016

24. Maja Stuwadoors BV (2017). Archief Geraadpleegd 23 augustus 2017

25. McConville, J. B. (2015). Introduction to mechanical system simulation using ADAMS. Mission: SDC Publications

26. McDermoth. (2005, December 2). McDermoth. Retrieved November 30, 2016, from https://www.flickr.com/photos/mcdermoth/

27. Mel, P. V. (2009). *Consequences of the introduction of EN13001 on the design of ship-to-shore cranes* (Master's thesis, Delft University of Technology, 2009). Delft: Delft University of Technology.

28. Mscsoftware. (2014, November 11). ADAMS/View help - ADAMS 2013 [PDF]. Msc software.

29. Nelson, T., & Wang, E. (2004). Fundamentals of Ansys. The Finite Element Method and Applications in Engineering Using Ansys®, 15-35. doi:10.1007/978-0-387-28290-9_2 Zhang J., Zhong J., Gao R. and He L. (2010). "The application of co-simulation technology of ANSYS and MSC.ADAMS in structural engineering," *2010 International Conference on Mechanic Automation and Control Engineering*, Wuhan, 2010, pp. 1033-1036.

30. Netherlands Standards Institution (1983). NEN 2018 - Cranes Loads and combination of loads. Nederlands Normalisatie-instituut.

31. Netherlands Standards Institution (1984). NEN 2019 - Cranes The metal structure. Nederlands Normalisatie-instituut.

32. Nieuwenhuis, G. (2006). De lemniscaatkraan. Nieuw Archief voor Wiskunde, 7(3), 162

33. Nista kraan Vlissingen -. (n.d.). Retrieved October 17, 2016, from http://www.figeeforum.nl/viewtopic.php?t=23

34. Nyström, M., & Tomaz, T. P. (2015). Fatigue analysis of welded joints in a forestry machine- Utilizing the notch stress concept (Unpublished master's thesis). Linnaeus University, Faculty of Technology.

35. P.P. Schipper (1992). De lemniscaatkraan; een voorontwerpstudie, rapport nr. 92.3.TT.2940

36. Pulle,W. (2017). Aantal draaiuren 1996-2017, 25t CT Kraan [Personal interview] (2017, May 11).

37. Qiang, Haiyan & Li, Wanli & Sun, You & Chen, Chen. (2016). Modeling and Dynamic Behavior Simulation Study on Offshore Container Crane Based on ADAMS.

38. Rupar, D & Hladnik, Jurij & Jerman, Boris. (2016). Loader crane inertial forces. 44. 291-297.

39. Si Li Fan, Yu Feng Shu, Hai Ying Zhang, Shuo Ouyang (2016). Kinetic Analysis of Four-link Gantry Crane Hoisting System.

40. Smith, S., & Forbes, B. (2015, August 19). DETAILED CRANE ANALYSIS CRITICAL TO PLATFORM LIFE EXTENSION, DECOMMISSIONING. Offshore-mag. Retrieved November 30, 2015, from http://www.offshore-mag.com/articles/print/volume-75/issue-8/engineering-construction-installation/detailed-crane-analysis-critical-to-platform-life-extension-decommissioning.html

41. Sohoni, V. (1995). A New Smooth Step Function For ADAMS . MSC Conference Papers, 1-3. doi:10.18411/a-2017-023

42. Song, F., He, Y., & Liu, H. (2017). Research on Goods and the Ship Interaction Based on ADAMS. MATEC Web of Conferences, 95, 11002. doi:10.1051/matecconf/20179511002

43. Spyros A. Karamanos, Arie Romeijn, Jaap Wardenier, Stress concentrations in tubular gap K-joints: mechanics and fatigue design, In Engineering Structures, Volume 22, Issue 1, 2000, Pages 4-14, ISSN 0141-0296

44. Starrenburg, H. (2017). Lemniscate crane operational conditions.

45. Tawjoeram, C. (2015). Fatigue reliability for cranes accounting for Bayesian updating (Rep. No. 2015.TEL.7975). TU Delft.

46. Van den Bos, W. (2017, September 19). Plaatje met voorbeeld [E-mail to the author].

47. Van den Bos, W. (2017, September 23). Wb3416-3 Design with Finite Elements (FEM). Lecture presented at NEN_fatigue , Delft.

48. Van Vianen, T. A. (2015). Simulation-integrated Design of Dry Bulk Terminals (Doctoral dissertation, TRAIL Research School).

49. Verheul, C. (2017, February 02). Gebruik van ADAMS [Telephone interview]

50. Vermeer, B., Schuurmans, R., Schott, D., & Lodewijks, G. (2013). Reducing Increased Maximum Load Occurrences of Bulk Cranes. Bulk Solids Handling, 4, 52-56.

51. Verschoof, J. (1999). Cranes: design, practice, and maintenance. Wiley.

52. Verstegen Grabs. (2017). Scrap handling with orange peel grabs - Verstegen Grabs. [online] Available at: https://www.verstegen.net/news/scrap-handling-verstegen-orange-peel-grabs/ [Accessed 10 Feb. 2016].

53. Vorthoren, D. (2017, February 5). Cornelis Tromp acceleration & braking times during a free digging transshipment [Personal interview].

54. Wardeh, M. & Frimpong, S. (2016). VIRTUAL PROTOTYPING AND SIMULATION OF P&H ELECTRIC ROPE SHOVEL -4800 XPC.

55. Wiethorn, J., Gardiner, M., Bond, A., Cox, E., & King, R. (2015, January 5). Tower-crane-life-expectancy (Tech.). Retrieved May 23, 2016, from Haag engineering website: http://haagglobal.com/am-site/media/tower-crane-life-expectancy.pdf

56. Wikipedia. (2009, May 25). OBA Bulk Terminal Amsterdam. Retrieved July 5, 2016, from https://nl.wikipedia.org/wiki/OBA_Bulk_Terminal_Amsterdam#/media/File:CSK_Glory_-_IMO_9224776_-_Callsign_VRXL4_p1.JPG

57. Wu, F. Q. (2014, August). The Dynamic Strength Calculation on the Reel Fulcrum of Crane Based on ADAMS and FEA. In Applied Mechanics and Materials (Vol. 599, pp. 551-554). Trans Tech Publications.

# Appendix A: Scientific Research Paper

# Crane fatigue assessment using Multibody Dynamics and Finite Element Method

C.J. Tawjoeram[1], M. Holleman[2], Dr. ir. X. Jiang[1], Dr. ir. J.H. den Besten[1], Dr. ir. D.L. Schott[1]

[1]Delft University of Technology, Department of Transport Engineering and Logistics, The Netherlands
[2]Maja Stuwadoors BV, Amsterdam,  The Netherlands

**Abstract:** For decades crane standards are used to assess crane fatigue making use of a static method  in combination with factors to take dynamic load effects into account. This is not sufficient to make more accurate predictions. The proposed method benefits from state of the art Multibody Dynamics simulation tool Msc ADAMS and Finite Element software ANSYS to quantify the contribution of the dynamic load influence during operation on the structural fatigue damage.  With a study case, the application of this method is proven feasible and reveals that the contribution of the dynamic effects are higher compared to the NEN2018/2019 crane standard used in this research.

## 1.      Introduction

Cranes fulfill an important role in society and their application are found in many fields. In operation many dynamic load effects like inertia- and centrifugal forces and the pendulum effect are induced to the structure during the acceleration and braking phase of the vertical, horizontal and rotational movements. All these operational effects result that cranes are in general fatigue loaded structures, which is a common problem in practice. Although crane standards have been used for decades to assess this phenomenon, in reality it still occurs with large impact and financial consequences.

In general, standards make use of a static design method to do fatigue calculations, where loads are multiplied using safety, amplification and risk factors. It is a simple and practical approach, but requires a certain expertise to choose the correct values, because these directly affect the reliability of the results and can result in over- or under-dimensioned structures or neglecting certain dynamic effects. Therefore it is of great importance to study, utilize and explore other state of the art alternatives which could be incorporated in crane fatigue assessments.

A method using multibody dynamics (ADAMS) and finite element simulation method (ANSYS) for cranes has not been identified [1]. Therefore this research aims to propose a uniform method to quantify the dynamic load influence during operation on the fatigue damage for one crane type. This method is applied to an aged  25t floating lemniscate transshipment crane which is used as study case, because no ADAMS model is identified for this crane type. The fatigue calculation is performed for one specific multi-planar tubular connection where four tubular members are welded together, indicated in Figure 1.   Past accidents revealed that if this joint fails the consequences are

enormous for machine and human. The final results of the proposed method are compared with a fatigue calculation using the NEN2018/2019 crane standard [2] and [3].



Figure 1. Fatigue critical tubular connection
on upperarm of lemniscate crane

In general the following method is proposed, illustrated with figure 2.
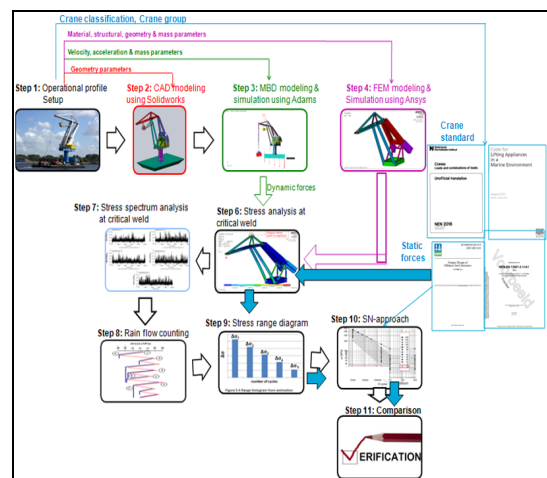


Figure 2: MBD-FEM crane fatigue assessment method

93

## 2.      Working cycle analysis

Typically the following movements occur during a working cycle for the lemniscate crane, illustrated in Figure 3. The crane that is used in this study is in operation for 21 years now and using a cycle time analysis based on a representative crane profile and input from the crane owner and literature [4], the total average number of transshipment moves is estimated to be 1.31 million.
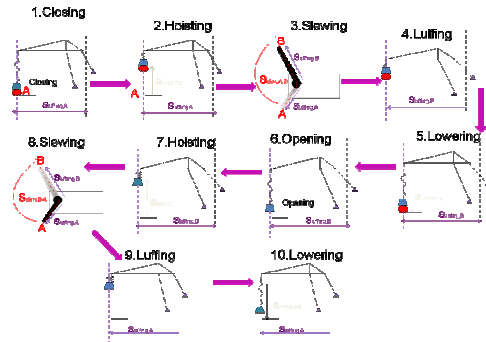


Figure 3. Typical movement sequence of the lemniscate crane

## 3.      Fatigue assessment using MBD-FEM simulation

A dynamic representation of bodies and contacts is developed using multibody dynamics software Msc ADAMS for the crane, seen in Figure 4. To sufficiently formulate an accurate dynamic representation, the main geometric, mass and velocity-time parameters are incorporated in the model according to the real crane specification.
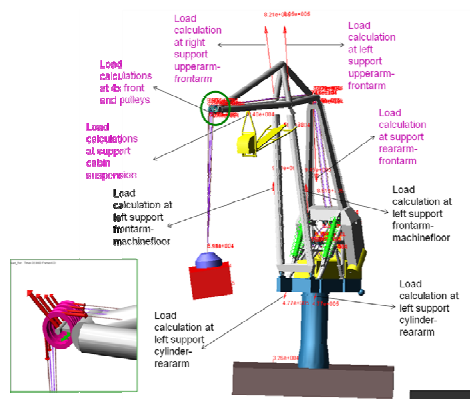


Figure 4. Adams crane simulation model

Subsequently a transshipment cycle is simulated on the basis of the working cycle analysis, indicated in figure 5 and ADAMS automatically calculates the force time history for the entire simulation time of 125s.
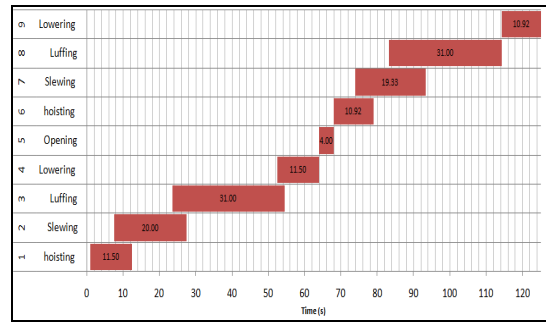


Figure 5. Adams simulated working cycle-time diagram

Then the load history for the rigid body model is exported as FEA loads and imported in ANSYS APDL to use as load boundary condition for a beam model illustrated with Figure 6. Because the cross sectional and moment of inertia is known, it is possible to calculate the elastic axial, in- and out of plane bending stresses at defined extreme fiber points at the outer circumference of each element. This results in the possibility to determine the corresponding nominal stress-time history for each of these points at the node where the four beam elements come together. Due to the complexity of the stress spectrum, a Rainflow counting method using JRain [5] is applied to transform this spectrum into a set of representative stress reversals to calculate the stress ranges. The fatigue damage is then determined  by combining the formula of Haibach [6] and Palgren-Miner's linear damage hypothesis into the following equation:

$$D = \sum \left( \frac{\Delta\sigma_{range}}{\Delta\sigma_{FAT}} \right)^m * \frac{n * \tilde{n}}{N}$$

$m = 3$

$n = current\_transshipment\_moves = 1.31e6$

$\tilde{n} = number\_of\_counted\_cycles$

$N = 2 * 10^6$
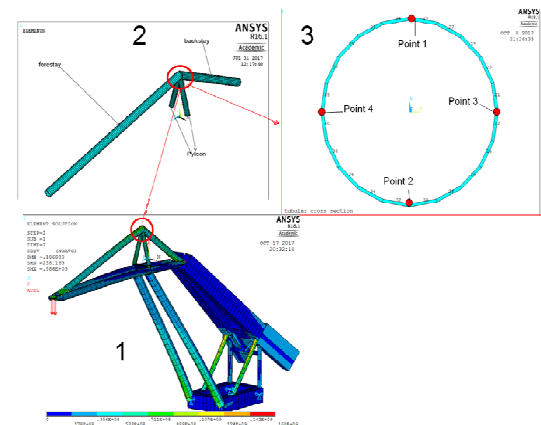


Figure 6. Ansys beam model

## 4.      Fatigue assessment using crane standard

Currently a number of crane standards are available to perform a fatigue assessment like the  NEN2063, NEN2019/FEM1.001, DIN15018, NEN-EN13001, Eurocode 3, the Lloyds crane code and the state of

94

the art DNVGL-RP-C203 issued in may 2016. However this standard is the latest, it reports that a fatigue check may be based on the allowable stresses method used in the NEN2019/FEM1.001 or the limit state method used in the EN13001. In this research the NEN2018/2019 is used. The main input parameters for this calculation are:

1. individual loads; gravity, hoisting weight, centrifugal force, inertia effect and the pontoon motion
2. 15 load sets identified
3. crane group 5B which follows from the crane specification
4. load factor =1.6
5. group factor =1.15
6. material = API 5L grade B
7. K3 notch effect is assumed at the point being considered
8. the calculated stress ratio
9. allowable stresses are chosen based upon the stress ratio and the tension or compression criterion
10. all crane components experience 1.31 million load cycles according to this standard
11. reference weld life is 2 million cycles

The 6 individual static loads are multiplied with the chosen factors and used as FEM loads as boundary conditions in the beam model, the calculation procedure is then repeated and the remaining 10 parameters are used to determine the fatigue damage.

## 6        Comparison fatigue damage results

According to the MBD-FEM simulation method it is concluded that the dynamic loads for 1.31 million transshipment moves resulted in fatigue damage at four points of the tubular welded joint, indicated in figure 7 and table 1.
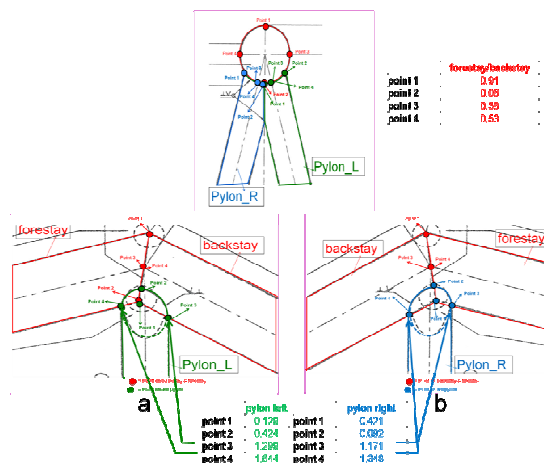


Figure 7. Illustration fatigue damage according to MBD-FEM simulation method

|         | forestay/ backstay | pylon left | pylon right |
|---------|--------------------|------------|-------------|
| point 1 | 0.91               | 0.129      | 0.421       |
| point 2 | 0.27               | 0.424      | 0.092       |
| point 3 | 0.38               | 1.299      | 1.171       |
| point 4 | 0.53               | 1.644      | 1.348       |

Table 1. Results MBD-FEM simulation method

According to the calculations of the NEN2018/2019 crane standard it is concluded that for 1.31 million transshipment moves, fatigue damage is predicted at one point, indicated in figure 8 and table 2.
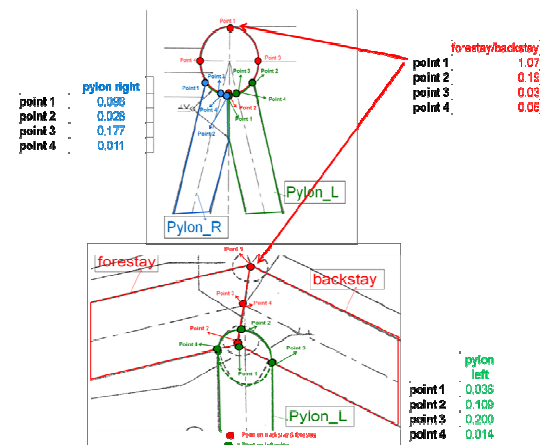


Figure 8. Illustration fatigue damage according to NEN2018/2019 crane standard

|         | forestay/ backstay | pylon left | pylon right |
|---------|--------------------|------------|-------------|
| point 1 | 1,07               | 0,04       | 0,10        |
| point 2 | 0,19               | 0,11       | 0,03        |
| point 3 | 0,03               | 0,20       | 0,18        |
| point 4 | 0,06               | 0,01       | 0,01        |

Table 2. Results NEN2018/2019 crane standard

## 7.       Comparison performance of assessment methods

The MBD-FEM simulation method allows to quantify the fatigue damage. From the calculated force-time history in ADAMS, indicated in figure 9 and the simulated stress spectrum using ANSYS, seen in figure 10 it is concluded that the largest dynamic effects occur at the moment of loading at t=2s and unloading at maximum reach at t=64s. During these two moment in time, the tubular joint encounters the largest stress difference and therefore this phase of the working cycle contributes to the largest fatigue damage. The finding shows a similarity with a research about the maximum load occurrences during the unloading phase for 40t bulk cranes [7]. Measurement data reveals a substantial increased payload of more than 30% on top of the nominal crane load.
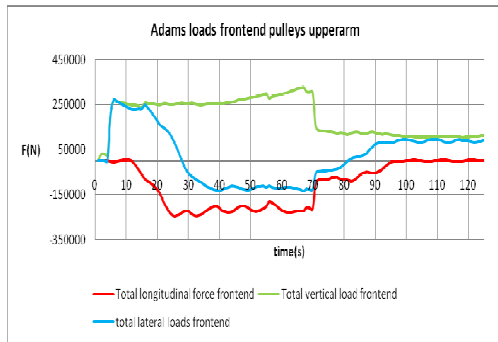
Figure 9. Adams force-time history
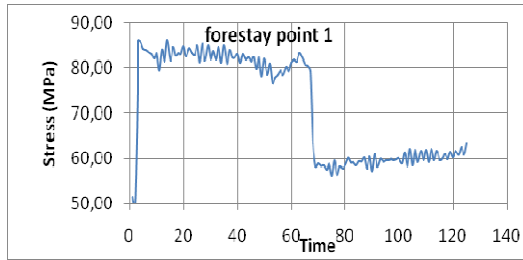

Figure 10. Sample 1 of nominal stress-time history

The left point 3 and right point 4 at forestay and backstay interface encounter a impact loading at t=84s when the luffing-in motion with an empty grab starts and at the moment the crane is slewing CW at maximum velocity. This is the result of both centrifugal and inertia loads occurring simultaneously at this instantaneous moment and thus resulting in this large instantaneous stress fluctuation which is induced to the structure. This is indicated in figure 11.
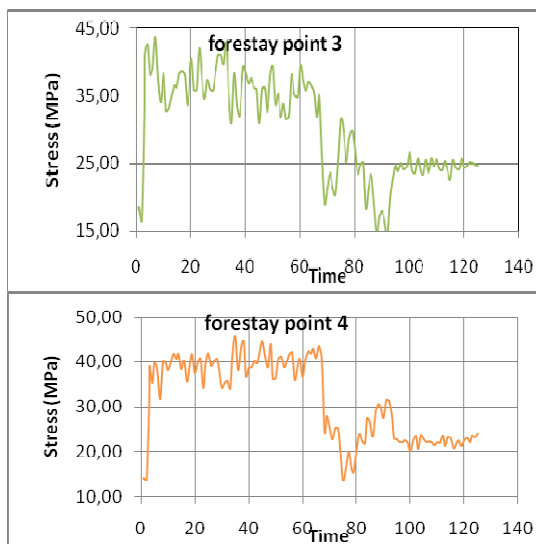

Figure 11. Sample 2 of nominal stress-time history

The weld interface at both pylons encounter most of the vibration plus impact loading as seen in figure 12 and therefore this dynamic loading results in fatigue damage in the corners between the pylons and the fore- and backstay as indicated in table 1.
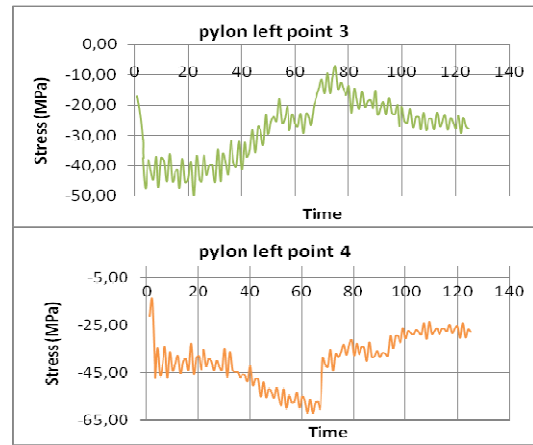

Figure 12. Sample 3 of nominal stress-time history

The NEN2018/2019 crane standard only uses the maximum and minimum calculated stresses in the fatigue damage. The crane operational configurations are simulated using load sets. From these sets is found that the largest possible stress which could be expected occurs for the load case which simulates the hoisting of the load at a maximum reach , slewing CW and luffing-in simultaneously. Logically the minimum stress in the structure occurs with only the gravity effect present. As a results of the assumption made by the standard the fatigue damage for this largest stress difference seen in figure 13 is predicted at the top fiber (point 1) of the forestay weld interface, indicated in figure 8.
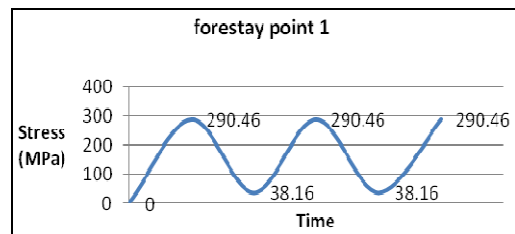

Figure 13. Sample Cyclic stress at point 1 of weld interface of forestay

## 8. Comparison differences of assessment methods

On the basis of the calculated fatigue damage for the tubular welded joint it is concluded that the dynamic contribution compared to the static method at the forestay/backstay weld interface, seen in table 3 is at:

| | forestay/backstay | | |
|---|---|---|---|
| | Damage | | Contribution dynamic effects |
| | static method | dynamic method | |
| point 1 | 1,07 | 0,91 | 15,0% lower |
| point 2 | 0,19 | 0,27 | 30,8% higher |
| point 3 | 0,03 | 0,38 | 91,2% higher |
| point 4 | 0,06 | 0,53 | 89,5% higher |

Table 3. Contribution dynamic effects at forestay/backstay

96

The dynamic contribution compared to the static method at the right pylon weld interface, seen in table 4 is at:

| pylon right | | |
|---|---|---|
| Damage | | Contribution dynamic effects |
| static method | dynamic method | |
| point 1 | 0,10 | 0,42 | 76,8% higher |
| point 2 | 0,03 | 0,09 | 69,5% higher |
| point 3 | 0,18 | 1,17 | 84,8% higher |
| point 4 | 0,01 | 1,35 | 99,2% higher |

Table 4. Contribution dynamic effects at right pylon

And the dynamic contribution compared to the static method at the left pylon weld interface, seen in table 5 is:

| pylon left | | |
|---|---|---|
| Damage | | Contribution dynamic effects |
| static method | dynamic method | |
| point 1 | 0,04 | 0,13 | 71,9% higher |
| point 2 | 0,11 | 0,42 | 74,2% higher |
| point 3 | 0,20 | 1,30 | 84,6% higher |
| point 4 | 0,01 | 1,64 | 99,1% higher |

Table 5. Contribution dynamic effects at left pylon

It is concluded that the dominant influential parameters which determine the outcome of both fatigue assessment methods in this study are:
1. the difference in loading encountered in both methods; the MBD-FEM simulation generates a transient stress spectrum while the crane standards assumes a cyclic stress with constant amplitude
2. the difference in the value of the characteristic fatigue strength; the MBD-FEM method uses a value from the weld atlas based on the weld configuration at the point o interest while the standard uses the stress ratio, sign of the maximum stress, crane group and yield stress of the material to determine the allowable stress
3. the difference in number of cycles encountered by the crane component; the standards assumes that each component undergoes the same amount of stress cycles, while in the MBD-FEM simulation additional counted cycles are also taken into account for the total number of cycles.

## 9.    Conclusion

The proposed method to perform a crane fatigue assessment using multibody dynamics and finite element method is proven to be feasible and can thus also be applied to a wide range of transport systems in fatigue design methodology. The contribution of the dynamic effects during the operational life using a multibody dynamics and finite element simulation method is in average

about 47%-82% higher compared to the NEN2018/2019 crane standard for the tubular welded joint of the crane which is used as a study case in this research. The longitudinal fatigue crack found in reality during the moment that this research was conducted show similarities with past found cracks and thus reveals that this tubular joint is a fatigue critical hotspot, indicated in figure 14 [8] and figure 15 [9].


Figure 14: Past found cracks
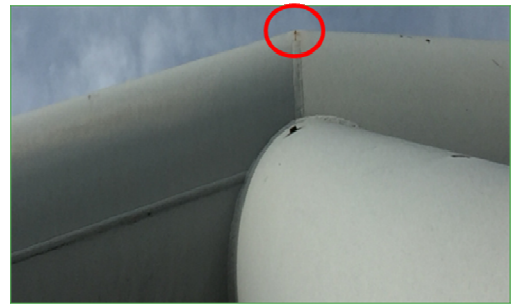



Figure 15: Present found cracks

The use of multibody dynamics simulation software ADAMS in the fatigue assessment allows to directly visualize the dynamic loading characteristics of the crane for the simulated load cycle. It provides insight in the dynamic effects which occur during operation and allows to understand when these dynamic load influences occur. Although much higher load values were calculated with ADAMS for the lateral and longitudinal loads compared with the crane standard, it is concluded that in terms of structural safety the use of MBD and FEM is advantageous. However a main disadvantage is that the method requires a large amount of effort to simulate a working cycle close to reality. Finally the added value of the method is, that it can be used as a tool during the design phase of new crane designs,

97

whereby improvements can directly be made for critical points that are under- or over-dimensioned.

## 10.        Recommendations and future work

In order to increase the accuracy of the service loads, it is recommended to incorporate flexibility for cable mechanism and joints connecting the various structural components in the current fully rigid ADAMS crane model. To extend the simulation possibilities to study the influence of the dynamic load effects for other transshipment configurations the use of control theory to develop control systems for the various mechanism will lower the amount time required for cycle-time programming. It is highly recommended to use a combination of beam for global modeling and plate elements to model present cracks at the complex tubular welded joints in the FEM model and use methods like fracture mechanics or strain life method to obtain direct results.

### References

[1]        Tawjoeram, C. (2015). Fatigue reliability for cranes accounting for Bayesian updating (Rep. No. 2015.TEL.7975). TU Delft.
[2]        Netherlands Standards Institution (1983). NEN 2018 - Cranes Loads and combination of loads. Nederlands Normalisatie-instituut.
[3]        Netherlands Standards Institution (1984). NEN 2019 - Cranes The metal structure. Nederlands Normalisatie-instituut.
[4]        Verschoof, J. (1999). Cranes: design, practice, and maintenance. Wiley.
[5]        Jesmond Engineering. (2013, October 09). J-Rain (Version 2.0) [Computer software]. Retrieved from https://jesmondengineering.com/engineering-software/j-rain-free-rainflow-counting-software/
[6]        Karssen, R. (2014). Searching for an improvement in fatigue assessment to increase lifetime expecancy (published master's thesis). Delft University of Technology.
[7]        Vermeer, B., Schuurmans, R., Schott, D., & Lodewijks, G. (2013). Reducing Increased Maximum Load Occurrences of Bulk Cranes. Bulk Solids Handling, 4, 52-56.
[8]        Nista kraan Vlissingen -. (n.d.). Retrieved October 17, 2016, from http://www.figeeforum.nl/viewtopic.php?t=23[
[9]        Maja Stuwadoors BV (2017). Archief Geraadpleegd 23 augustus 2017

# Appendix B: Multibody dynamics analysis

## Kinematic cycle time calculations

The following table shows the kinematic calculations for the slewing crane movement.

| | Slewing full grab | | | Slewing empty grab | | |
|---|---|---|---|---|---|---|
| | | | | | | |
| Total displacement(m) | 120 | ° | | 120 | ° | |
| velocity(m/min) | 1 | rpm | | 1.5 | rpm | |
| acceleration time (s) | 6 | | | 6 | | |
| deceleration time (s) | 6 | | | 6 | | |
| acceleration | 0.017 | (rad/s^2) | | 0.026 | (rad/s^2) | |
| deceleration | 0.017 | (rad/s^2) | | 0.026 | (rad/s^2) | |
| velocity | 0.104 | (rad/s) | | 0.157 | (rad/s) | |
| **time-displacement** | **t(s)** | | **S(°)** | **t(s)** | | **S(°)** |
| accelerating | 6.0 | | 18.0 | 6.0 | | 27.0 |
| cruising | 14.0 | | 84.0 | 7.3 | | 66.0 |
| braking | 6.0 | | 18.0 | 6.0 | | 27.0 |
| **TOTAL** | **26.0** | | 120.0 | **19.3** | | 120.0 |

**Table 40: Cycle time calculation for slewing movement**

The following table shows the kinematic calculations for the luffing crane movement.

| | Luffing empty & full grab | |
|---|---|---|
| | | |
| Total displacement (m) | 19 | |
| Velocity (m/min) | 60 | |
| acceleration time (s) | 4 | |
| deceleration time (s) | 4 | |
| Acceleration (m/s^2) | 0.25 | |
| Deceleration (m/s^2) | 0.25 | |
| Velocity (m/s) | 1 | |
| **time-displacement** | **t(s)** | **S(m)** |
| | | |
| accelerating | 4.0 | 2.0 |
| cruising | 15.0 | 15.0 |
| braking | 4.0 | 2.0 |
| **TOTAL** | **23.0** | 19.0 |

**Table 41: Cycle time calculation for luffing movement**

The following table presents the load cycle time calculation. The yellow marked fields show the input from the Maja Stuwadoors BV (2016), which was a cycle time calculation for their 32t Skyline lemniscate crane. These yellow marked values were used as a reference in order to combine all the calculated times for each movement of the 25t crane.

**Transshipment load cycle calculation**

Slewing angle: **120** deg

| Motion | Motion phase | Start time | End time | Duration (s) | Time simultaneous movements | Operational parameters | |
|---|---|---|---|---|---|---|---|
| closing | closing grab acc. | 0.00 | 4.00 | 4.00 | | | |
| | closing grab at constant speed | 4.00 | 6.00 | 2.00 | | | |
| | closing dec. | 6.00 | 10.00 | 4.00 | | | |
| hoisting | hoisting acc | 10.00 | 14.00 | 4.00 | | 15 | m |
| | hoisting at constant velocity | 14.00 | 17.50 | 3.50 | | 120 | m/min |
| | hoisting dec. | 18 | 22 | 4.00 | | | |
| Slewing | Slewing acc. | 17 | 23 | 6.00 | 5 | 120 | deg |
| | Slewing at constant speed | 23 | 37 | 14.00 | | 1 | rpm |
| | Slewing dec. | 37 | 43 | 6.00 | | | |
| Luffing | Luffing acc. | 33 | 37 | 4.00 | 10 | 60 | m |
| | Luffing at constant speed | 37 | 52 | 15.00 | | 60 | m/min |
| | Luffing dec. | 52 | 56 | 4.00 | | | |
| Lowering | Lowering acc. | 54 | 58 | 4.00 | 2 | 15 | m |
| | Lowering at constant speed | 58 | 61 | 3.50 | | 120 | m/min |
| | Lowering dec. | 61 | 65 | 4.00 | | | |
| Opening | Opening grab acc. | 65 | 66 | 1.00 | | | |
| | Opening grab | 66 | 68 | 2.00 | | | |
| | Opening grab dec. | 68 | 69 | 1.00 | | | |
| hoisting | hoisting acc | 69 | 73 | 4.00 | | 15 | m |
| | hoisting at constant velocity | 73 | 76 | 2.92 | | 130 | m/min |
| | hoisting dec. | 76 | 80 | 4.00 | | | |
| Slewing | Slewing acc. | 75 | 81 | 6.00 | 5 | 120 | deg |
| | Slewing at constant speed | 81 | 88 | 7.33 | | 1.5 | rpm |
| | Slewing dec. | 88 | 94 | 6.00 | | | |
| Luffing | Luffing acc. | 84 | 88 | 4.00 | 10 | 60 | m |
| | Luffing at constant speed | 88 | 103 | 15.00 | | 60 | m/min |
| | Luffing dec. | 103 | 107 | 4.00 | | | |
| Lowering | Lowering acc. | 107 | 111 | 4.00 | 0 | 15 | m |
| | Lowering at constant speed | 111 | 114 | 2.92 | | 130 | m/min |
| | Lowering dec. | 114 | 118.18 | 4.00 | | | |
| **Total cycle time** | | | **118.18** | **s** | | | |
| **Number of cycles per hour** | | | **30.5** | | | | |

(full grab: closing through first Lowering; empty grab: Opening through last Lowering)

**Table 42: Calculation sheet for cycle time diagram**
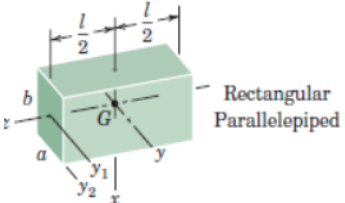
## ADAMS mass, mass inertia & CoM input

The following mass inertia properties were added to each individual component based on calculation input from Solidworks and hand calculations based on rigid body dynamics.

| Part | [kg*m^2] | | |
|------|------|------|------|
|      | Ixx | Iyy | Izz |
| Upper arm | 3516629.93 | 3483061.98 | 110444.36 |
| Front arm | 1735369 | 1629961 | 110712 |
| Rear arm | 2358429.3 | 2031123.07 | 408107.31 |
| Tower | 278136.5 | 377650.69 | 217277.42 |
| Machinefloor | 1507920 | 1768204 | 314124 |
| Cranehouse | 87458 | 100344 | 22427 |
| Foot | 214968 | 43374 | 214968 |
| Grab | 21937 | 35152 | 37264 |
| cab bridge | 80111 | 79656 | 8338 |
| Pontoon | 114544135 | 149774822 | 37847487 |
| Ballast bak | 226837.8333 | 17290.39583 | 8906.25 |
| grabbed material | 25600 | 25600 | 25600 |

**Table 43: mass moment inertia properties relative to the CoM**



Ballast bak

| | | |
|---|---|---|
| m | 47500 | kg |
| a | 1.5 | m |
| b | 2.09 | m |
| L | 7.42 | m |

$$I_{xx} = \tfrac{1}{12}m(a^2 + l^2)$$
$$I_{yy} = \tfrac{1}{12}m(b^2 + l^2)$$
$$I_{zz} = \tfrac{1}{12}m(a^2 + b^2)$$
$$I_{y_1 y_1} = \tfrac{1}{12}mb^2 + \tfrac{1}{3}ml^2$$
$$I_{y_2 y_2} = \tfrac{1}{3}m(b^2 + l^2)$$

**Table 44: mass inertia counterweight at rear arm**

grabbed material

| | | |
|---|---|---|
| m | 16 | t |
| radius | 2 | m |
| mass inertia | 25600 | kg*m^2 |

Solid sphere

$$I = \frac{2}{5} MR^2$$

**Table 45: mass inertia grabbed material**

The following figure shows the centre of Mass for each component of the crane. This has a large influence on the output results and is part of the verification process.
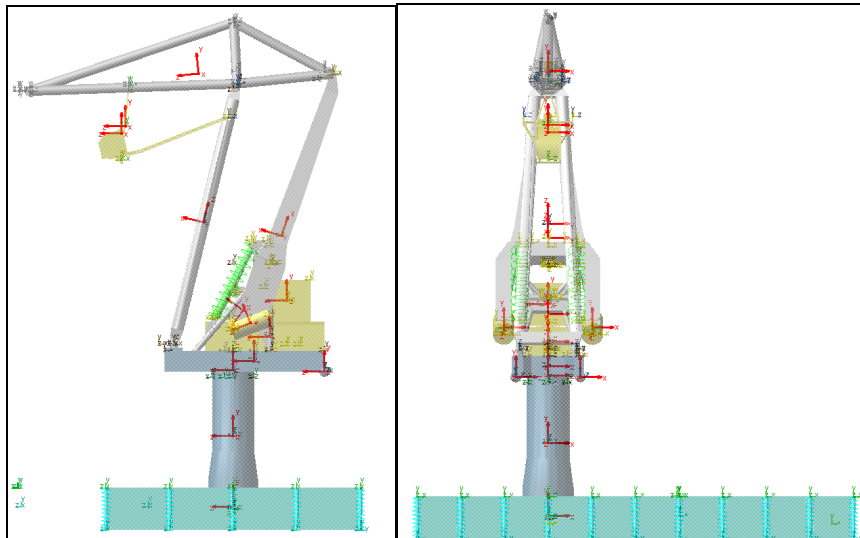


**Figure 114: CoM ADAMS model**

## ADAMS constraints input

Next step was to assign constraints to the different parts. ADAMS uses the Gruebler expression: $m=6*(n_{bodies}-1)-n_{constraints}$, to determine the degrees of freedom of the model. The following table provides explanation why certain joints have been used and the calculation according to Gruebler's equation.
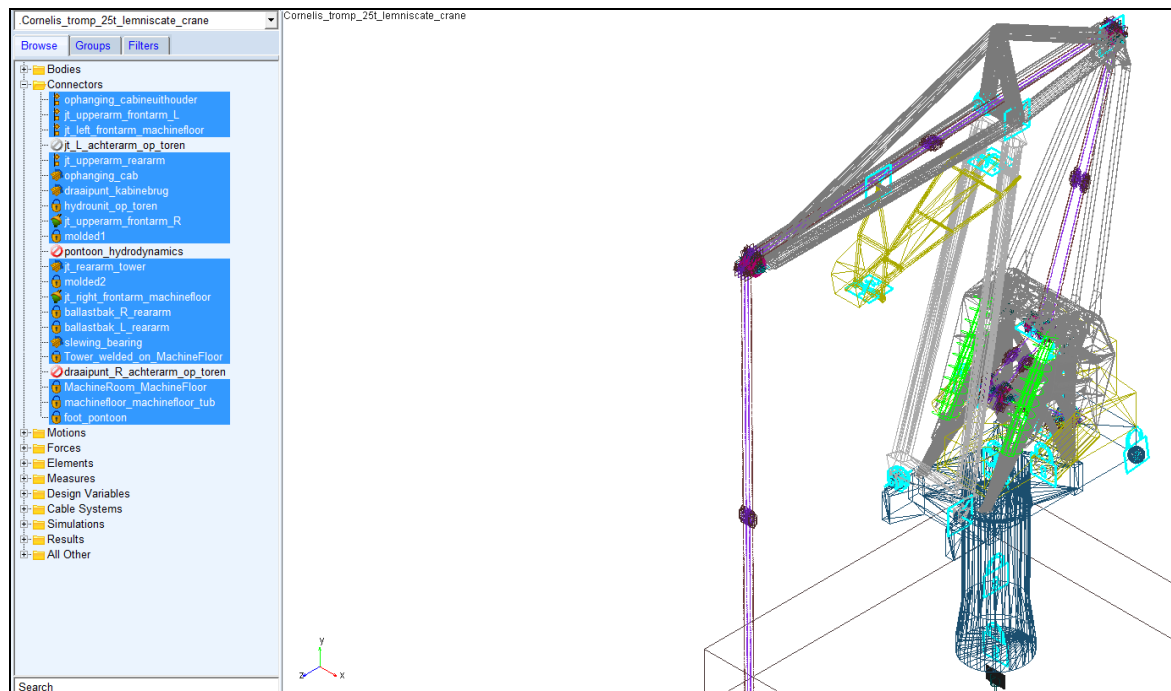


**Figure 115: ADAMS model DOF constraints (joints)**

| I_part | J_part | Constraint | DOFs | Remarks |
|---|---|---|---|---|
| machinefloor_tub | ground | REVOLUTE joint | -5 | rotation of the upper structure relative to the lower structure |

Crane fatigue assessment using Multibody Dynamics and Finite Element Method

| | | ROTATIONAL joint MOTION | -1 | slewing motion,makes rotation possible about the y-axis |
|---|---|---|---|---|
| machinefloor_tub | machine_floor | FIXED joint | -6 | welded in machinefloor |
| machine_house | machine_floor | FIXED joint | -6 | welded on machine floor |
| Tower | machine_floor | FIXED joint | -6 | welded on machine floor |
| Front_arm | machine_floor | SPHERICAL joint | -3 | PIVOT rotation about the machinefloor and reactions on pivot pin |
| | | INLINE Jprim | -2 | PIVOT rotation about the machinefloor |
| upper_arm | Front_arm | INLINE Jprim | -2 | the pivot joints on the real crane are build using bearings allowing axial movement on pivot end and on the other end no axial movement |
| upper_arm | Front_arm | SPHERICAL joint | -3 | |
| upper_arm | rear_arm | INLINE Jprim | -2 | the pivot joints on the real crane are build using bearings allowing axial movement on pivot end and on the other end no axial movement |
| rear_arm | Tower | REVOLUTE joint | -5 | rear arm rotates about the tower and reactions at the pin |
| | | ROTATIONAL joint MOTION | -1 | |
| Hydr_cylinder_barrel R | tower | REVOLUTE joint | -5 | hydraulic cylinder rotates about the tower |
| Hydr_cylinder_barrel L | tower | REVOLUTE joint | -5 | hydraulic cylinder rotates about the tower |
| Hydr_cylinder_rod R | Hydr_cylinder_barrel R | TRANSLATIONAL joint | -5 | cylinder rod slides about the cylinder barrel |
| Hydr_cylinder_rod L | Hydr_cylinder_barrel L | TRANSLATION joint | -5 | cylinder rod slides about the cylinder barrel |
| Rearboom | Hydr_cylinder_rod R | INLINE Jprim | -2 | rearboom is pushed by the rod, while rotating about the rod |
| Rearboom | Hydr_cylinder_rod L | INLINE Jprim | -2 | rearboom is pushed by the rod,while rotating about the rod |
| cab_suspension | upper_arm | INLINE Jprim | -2 | suspension triangular structure rotates about the upper arm |
| cab_bridge | cab_suspension | REVOLUTE joint | -5 | suspension triangular structure is pivoted at the cabine and rotates about the cabine bridge |
| cab_bridge | Front_arm | REVOLUTE joint | -5 | the bridge with cab is pivoted at the front arm |
| counterweight_left | rear_arm | FIXED joint | -6 | Moving counterweight is integrated into rear arm |
| counterweight_right | rear_arm | FIXED joint | -6 | Moving counterweight is integrated into rear arm |
| hydraulic unit | tower | FIXED joint | -6 | Hydraulic unit is welded to tower |
| counterweight | machinefloor | FIXED joint | -6 | extra counterweight in floor |
| counterweight | machinefloor | FIXED joint | -6 | |
| **The # of DOF removed** | | | **-108** | |
| **# of rigid bodies** | **18** | | | |
| **DOF for each rigid body** | 6 | | | |

Crane fatigue assessment using Multibody Dynamics and Finite Element Method

| total # of DOF rigid bodies | | | 108 | |
|---|---|---|---|---|
| **DOF for the crane** | | | **0** | number of DOF must be equal to zero and there must be no redundant constraints |

**Table 46: ADAMS joints for slewing crane upper structure**

## ADAMS cable input

The hoisting mechanism was modeled based on the pulley and cable geometric specification of the crane owner. Material Friction, stiffness, damping and contact properties were defined according to [23]. The following Table 47 provides the parameters used for the pulleys in the ADAMS cable module. Further details on contact mechanics are not discussed and the reader is referred to [21].

| **Material** | steel | | | |
|---|---|---|---|---|
| | **Contact properties** | | | |
| **Hertz_K (stiffness coefficient)** | 1.31e5 (N/mm) | | | |
| **Hertz_E (stiffness exponent)** | 1.85 (hard metal) | | | |
| **Hertz_Cm ( max damping coefficient)** | 1%* Hertz_K | | | |
| **Friction Mu (dynamic coefficient of friction, sliding friction)** | 0.8 | | | |
| **Friction Vt (relative velocity between the pulley and cable at which the full Friction Mu, is applied)** | 100(mm/s) | | | |

**Table 47: Pulley parameters**

| cable diameter | 0.03 | m |
|---|---|---|
| cable specific density | 2.76 | kg/m |
| cable density | 3904.601271 | kg/m^3 |
| Cable youngs modulus (F/A)/(deltaL/L0) | 61064568565 | Pa |

**Table 48: cable parameters**

Crane fatigue assessment using Multibody Dynamics and Finite Element Method

## ADAMS motion input

In the following sheet shows the time durations for the different motions in ADAMS.

| | | | ADAMS Transshipment load cycle calculation - operational profile 1 | | | | |
|---|---|---|---|---|---|---|---|
| | | **Slewing angle** | | **120** deg | | | |
| | **Motion** | **Motion phase** | *Start time* | *End time* | *Duration (s)* | *Time simultaneous movements* | *Operational parameters* |
| | hoisting | hoisting acc | 1.0 | 5.0 | 4.00 | | 15 m |
| | | hoisting at constant velocity | 5.0 | 8.5 | 3.50 | | 120 m/min |
| | | hoisting dec. | 8.5 | 12.5 | 4.00 | | |
| | Slewing | Slewing acc. | 7.5 | 13.5 | 6.00 | 5 | 120 deg |
| | | Slewing at constant speed | 13.5 | 27.5 | 14.00 | | 1 rpm |
| | | Slewing dec. | 27.5 | 33.5 | 6.00 | | |
| | Luffing | Luffing acc. | 23.5 | 27.5 | 4.00 | 10 | 60 m |
| | | Luffing at constant speed | 27.5 | 50.5 | 23.00 | | 60 m/min |
| | | Luffing dec. | 50.5 | 54.5 | 4.00 | | |
| | Lowering | Lowering acc. | 52.5 | 56.5 | 4.00 | 2 | 15 m |
| | | Lowering at constant speed | 56.5 | 60.0 | 3.50 | | 120 m/min |
| | | Lowering dec. | 60.0 | 64.0 | 4.00 | | |
| empty grab | Opening | Opening grab acc. | 64.0 | 65.0 | 1.00 | | |
| | | Opening grab | 65.0 | 67.0 | 2.00 | | |
| | | Opening grab dec. | 67.0 | 68.0 | 1.00 | | |
| | hoisting | hoisting acc | 68.0 | 72.0 | 4.00 | | 15 m |
| | | hoisting at constant velocity | 72.0 | 74.9 | 2.92 | | 130 m/min |
| | | hoisting dec. | 74.9 | 78.9 | 4.00 | | |
| | Slewing | Slewing acc. | 73.9 | 79.9 | 6.00 | 5 | 120 deg |
| | | Slewing at constant speed | 79.9 | 87.3 | 7.33 | | 1.5 rpm |
| | | Slewing dec. | 87.3 | 93.3 | 6.00 | | |
| | Luffing | Luffing acc. | 83.3 | 87.3 | 4.00 | 10 | 60 m |
| | | Luffing at constant speed | 87.3 | 110.3 | 23.00 | | 60 m/min |
| | | Luffing dec. | 110.3 | 114.3 | 4.00 | | |
| | Lowering | Lowering acc. | 114.3 | 118.3 | 4.00 | 0 | 15 m |
| | | Lowering at constant speed | 118.3 | 121.2 | 2.92 | | 130 m/min |
| | | Lowering dec. | 121.2 | 125.2 | 4.00 | | |
| **Total cycle time** | | | | 125.18 s | | | |
| **Number of cycles per hour** | | | | 28.8 | | | |

**Table 49: ADAMS simulated load cycle analysis**

ADAMS results – loads at frontend upper arm

The following graphs and tables show the dynamic forces acting at the front end pulleys on the upper arm. The force results are calculated in the local coordinate system of the pulleys. The longitudinal forces are in the local x-direction and the lateral forces are in the local z-direction of the pulleys.

Figure 116 and Figure 117 show the dynamic character of the longitudinal loads at the front end pulleys on the boom tip.
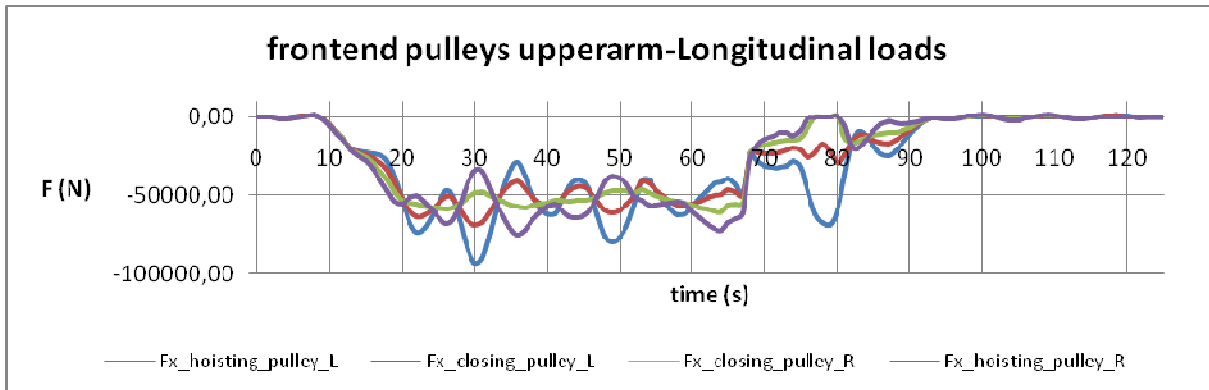


**Figure 116: ADAMS frontend upper arm pulley reaction force -local x direction**

$$F = \sum_{i=4}^{j=3} F_{ij}$$

Due to the load fluctuation, the loads are summed together, $i = 1, 2, 3, 4$ for the four frontend

$$j = x, y, z$$

pulleys longitudinal loads into a single readable load curve, for j=x.
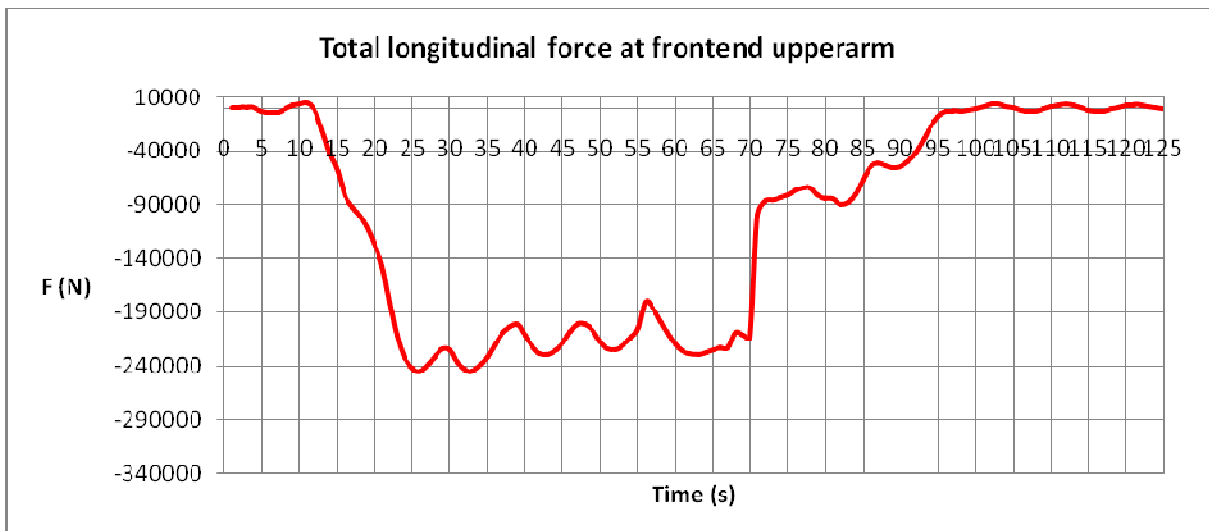


**Figure 117: total longitudinal load at front end pulleys**

The following Figure 118 and Figure 119 show the dynamic character of the longitudinal loads at the front end pulleys on the boom tip.
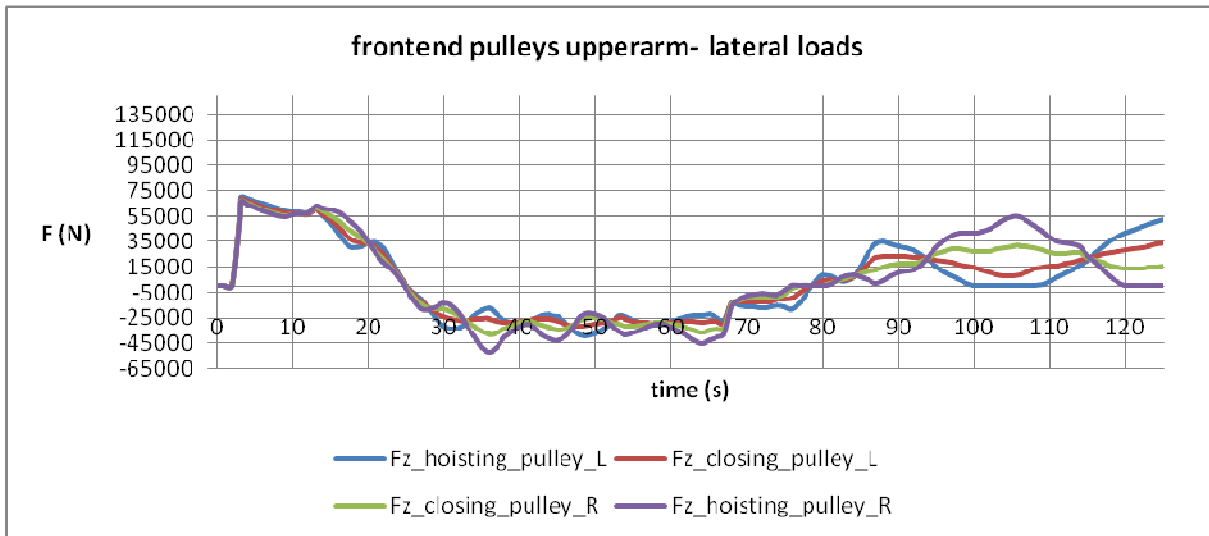
**Figure 118: ADAMS frontend upper arm pulley reaction force -local z direction**
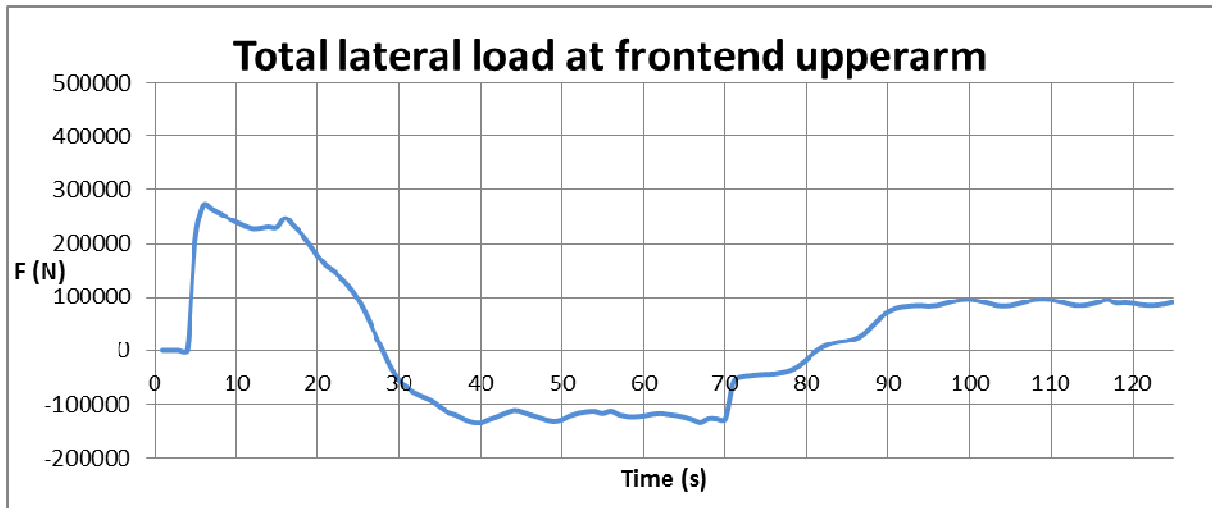


**Figure 119: total lateral load at front end pulleys**

Crane fatigue assessment using Multibody Dynamics and Finite Element Method

**Table 50: Example ADAMS load data - frontend pulleys upper arm**

| Time | Total longitudinal force frontend (x) [N] | Total vertical load frontend(y) [N] | total lateral loads frontend(z) [N] |
|---|---|---|---|
| 0.0 | | | |
| 0.4 | 687 | 28296 | -587 |
| 1.0 | 668 | 28276 | -570 |
| 2.0 | 154 | 27224 | 33 |
| 3.0 | -3467 | 209273 | 206235 |
| 3.2 | -4891 | 267688 | 271349 |
| 4.0 | -3908 | 263761 | 264961 |
| 5.0 | -625 | 260242 | 256739 |
| 6.0 | 1948 | 257010 | 247706 |
| 7.0 | 3832 | 254294 | 239828 |
| 8.0 | 4452 | 251439 | 232757 |
| 9.0 | -2555 | 247509 | 227227 |
| 10.0 | -19942 | 245942 | 228313 |
| 11.0 | -40763 | 242243 | 230534 |
| 12.0 | -59361 | 237640 | 229621 |
| 13.0 | -82069 | 256369 | 247639 |
| 14.0 | -92067 | 253328 | 233315 |
| 15.0 | -100442 | 253552 | 218330 |
| 16.0 | -112189 | 253126 | 199091 |
| 17.0 | -127511 | 251028 | 177353 |
| 18.0 | -147529 | 249420 | 158860 |
| 19.0 | -180608 | 254712 | 147460 |
| 20.0 | -211581 | 254516 | 133732 |
| 21.0 | -231787 | 251393 | 117311 |
| 22.0 | -242544 | 251367 | 95087 |
| 23.0 | -244516 | 253514 | 65519 |
| 24.0 | -239121 | 255320 | 33630 |
| 25.0 | -230815 | 255618 | 786 |
| 26.0 | -223775 | 254252 | -31165 |
| 27.0 | -224563 | 253504 | -55016 |
| 28.0 | -236083 | 256110 | -70437 |
| 29.0 | -243202 | 253072 | -80110 |
| 30.0 | -244558 | 249830 | -87179 |
| 31.0 | -239283 | 248219 | -94102 |
| 32.0 | -230685 | 250931 | -105175 |
| 33.0 | -219032 | 252833 | -114955 |
| 34.0 | -209548 | 253067 | -119982 |
| 35.0 | -203353 | 254204 | -127831 |
| 36.0 | -201485 | 252685 | -133001 |
| 37.0 | -211777 | 255301 | -133929 |
| 38.0 | -222127 | 255255 | -128651 |
| 39.0 | -228415 | 256258 | -123178 |
| 40.0 | -229290 | 257523 | -116749 |
| 41.0 | -225445 | 259910 | -111797 |

Crane fatigue assessment using Multibody Dynamics and Finite Element Method

| | | | |
|---|---|---|---|
| 42.0 | -217870 | 264717 | -113565 |
| 43.0 | -208013 | 268748 | -118908 |
| 44.0 | -201063 | 270748 | -123418 |
| 45.0 | -201562 | 274520 | -128690 |
| 46.0 | -207015 | 277515 | -131392 |
| 47.0 | -217398 | 281619 | -128680 |
| 48.0 | -224050 | 283213 | -121302 |
| 49.0 | -224889 | 286104 | -116423 |
| 50.0 | -220738 | 290081 | -113911 |
| 51.0 | -213447 | 294021 | -112982 |
| 52.0 | -204823 | 298257 | -116896 |
| 53.0 | -180255 | 277283 | -112686 |
| 54.0 | -186053 | 285085 | -119652 |
| 55.0 | -198079 | 291476 | -122886 |
| 56.0 | -209407 | 294746 | -123204 |
| 57.0 | -219277 | 297675 | -121689 |
| 58.0 | -226096 | 300286 | -118541 |
| 59.0 | -228937 | 303728 | -117021 |
| 60.0 | -229362 | 309482 | -118671 |
| 61.0 | -227134 | 314010 | -120765 |
| 62.0 | -224835 | 318398 | -123877 |
| 63.0 | -222745 | 322006 | -128565 |
| 64.0 | -222739 | 325181 | -133518 |
| 65.0 | -208743 | 306254 | -126508 |
| 66.0 | -210837 | 304782 | -126866 |
| 67.0 | -213667 | 302922 | -126715 |
| 68.0 | -99112 | 151907 | -56757 |
| 69.0 | -86577 | 134187 | -48329 |
| 70.0 | -85368 | 132517 | -46407 |
| 71.0 | -83620 | 131035 | -44612 |
| 72.0 | -80450 | 129456 | -43572 |
| 73.0 | -76712 | 127858 | -43257 |
| 74.0 | -74149 | 125273 | -40533 |
| 75.0 | -74247 | 123574 | -36866 |
| 76.0 | -80528 | 125033 | -29074 |
| 77.0 | -84012 | 121297 | -16475 |
| 78.0 | -84774 | 116529 | -3420 |
| 79.0 | -90074 | 121525 | 6510 |
| 80.0 | -87503 | 125791 | 13139 |
| 81.0 | -79567 | 129138 | 16565 |
| 82.0 | -66261 | 125549 | 18498 |
| 83.0 | -54898 | 119773 | 22396 |
| 84.0 | -51058 | 119871 | 31195 |
| 85.0 | -53074 | 124766 | 45482 |
| 86.0 | -55466 | 127155 | 60622 |
| 87.0 | -54381 | 123865 | 71457 |
| 88.0 | -49893 | 120153 | 78489 |

Crane fatigue assessment using Multibody Dynamics and Finite Element Method

| 89.0  | -41017 | 117343 | 81418  |
|-------|--------|--------|--------|
| 90.0  | -29588 | 117450 | 83023  |
| 91.0  | -17341 | 117883 | 83633  |
| 92.0  | -7453  | 115161 | 82127  |
| 93.0  | -3690  | 113757 | 83634  |
| 94.0  | -2704  | 113042 | 87769  |
| 95.0  | -3453  | 111566 | 91895  |
| 96.0  | -2597  | 109866 | 94483  |
| 97.0  | -689   | 108971 | 95065  |
| 98.0  | 1503   | 108446 | 92977  |
| 99.0  | 3043   | 107958 | 89085  |
| 100.0 | 3159   | 107122 | 84939  |
| 101.0 | 1840   | 106383 | 82636  |
| 102.0 | -265   | 106388 | 83615  |
| 103.0 | -2322  | 106624 | 87108  |
| 104.0 | -3425  | 106544 | 91395  |
| 105.0 | -3016  | 106200 | 94651  |
| 106.0 | -1330  | 106154 | 95764  |
| 107.0 | 856    | 106822 | 94588  |
| 108.0 | 2632   | 107522 | 91189  |
| 109.0 | 3186   | 108064 | 87329  |
| 110.0 | 2289   | 107780 | 84031  |
| 111.0 | 400    | 108120 | 83995  |
| 112.0 | -1701  | 108845 | 86981  |
| 113.0 | -3070  | 109047 | 91193  |
| 114.0 | -3030  | 108740 | 94886  |
| 115.0 | -1544  | 102813 | 88655  |
| 116.0 | 409    | 104380 | 89254  |
| 117.0 | 2140   | 106249 | 87837  |
| 118.0 | 2942   | 107552 | 85349  |
| 119.0 | 2681   | 108599 | 83787  |
| 120.0 | 1661   | 109850 | 84251  |
| 121.0 | 345    | 111517 | 86810  |
| 122.0 | -883   | 113263 | 90829  |
| 123.0 | -1760  | 114761 | 95323  |
| 124.0 | -2037  | 115917 | 99476  |
| 125.0 | -1581  | 116794 | 102666 |

ADAMS results – loads at rearend upper arm

Figure 120, Figure 121, Figure 122, Figure 123, Figure 124 and Figure 125 show the dynamic character of the loads at the rear end pulleys of the upper arm.
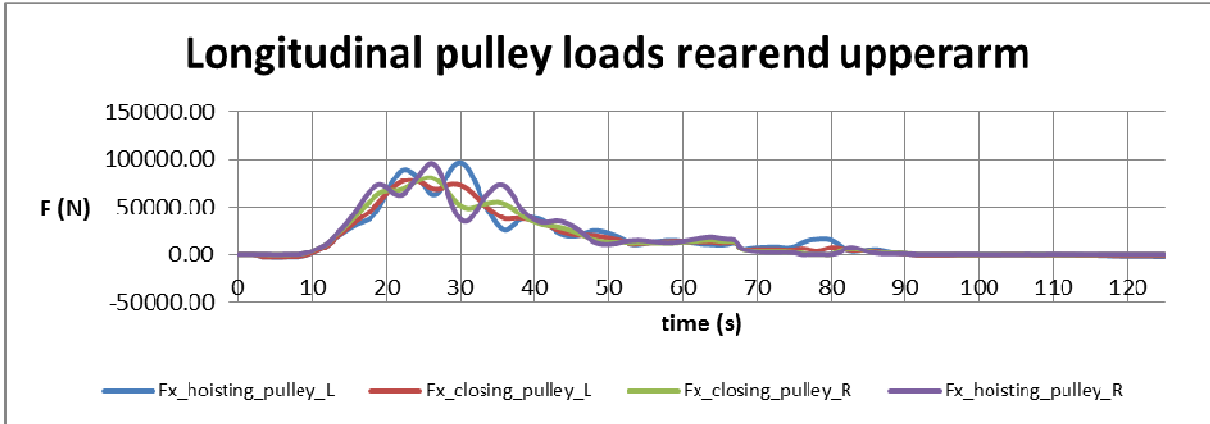


**Figure 120: ADAMS rearend upper arm pulley reaction force -local x direction**
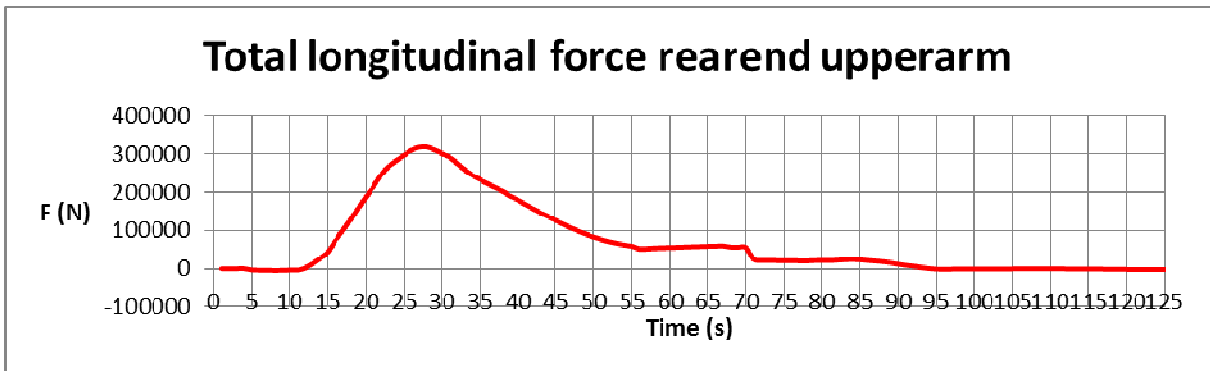


**Figure 121: Total longitudinal load at rear end pulley upper arm/rear arm**
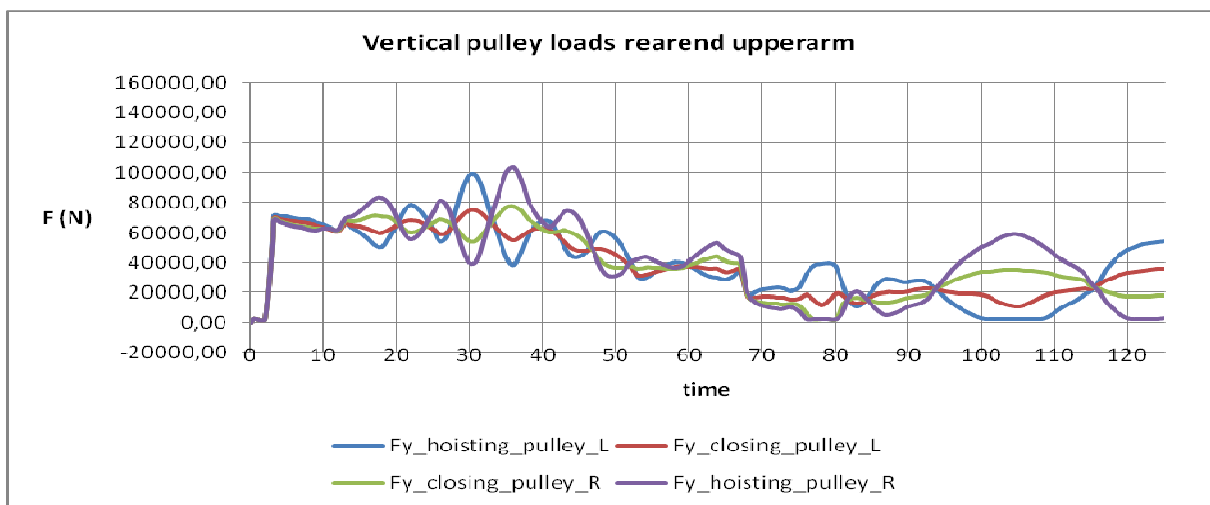


**Figure 122: ADAMS rearend upper arm pulley reaction force -local y direction**
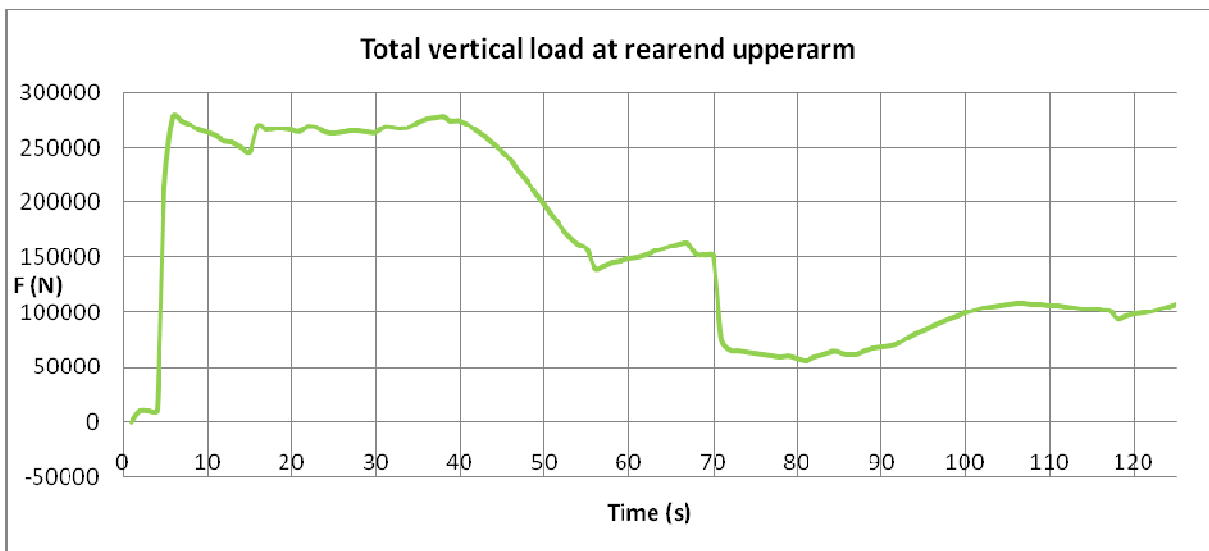
**Figure 123: Total vertical load at rear end pulley upper arm/rear arm**
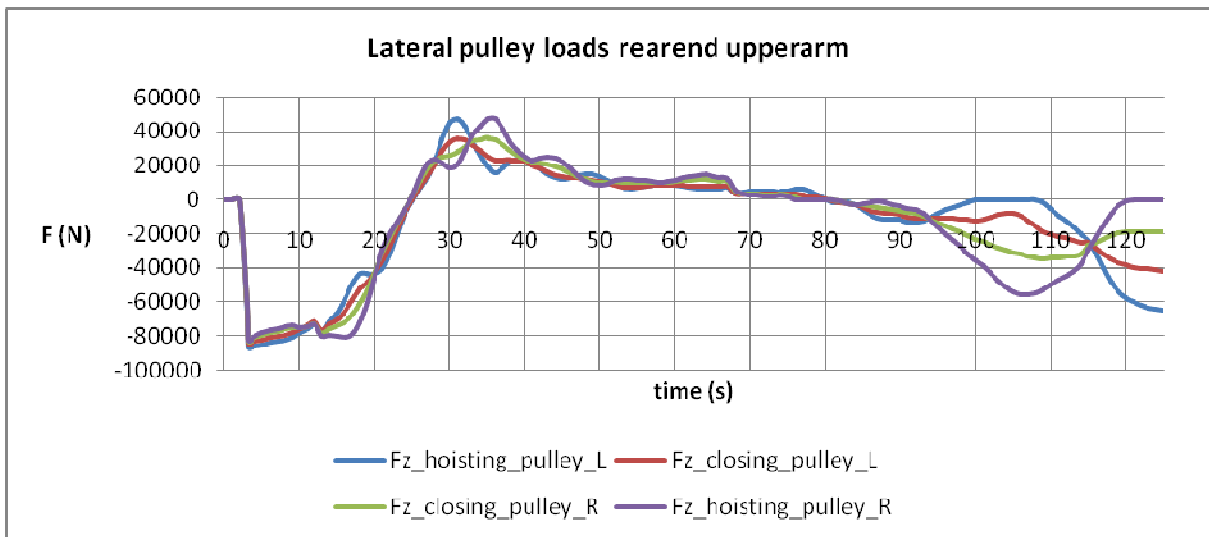


**Figure 124: ADAMS rearend upper arm pulley reaction force -local z direction**
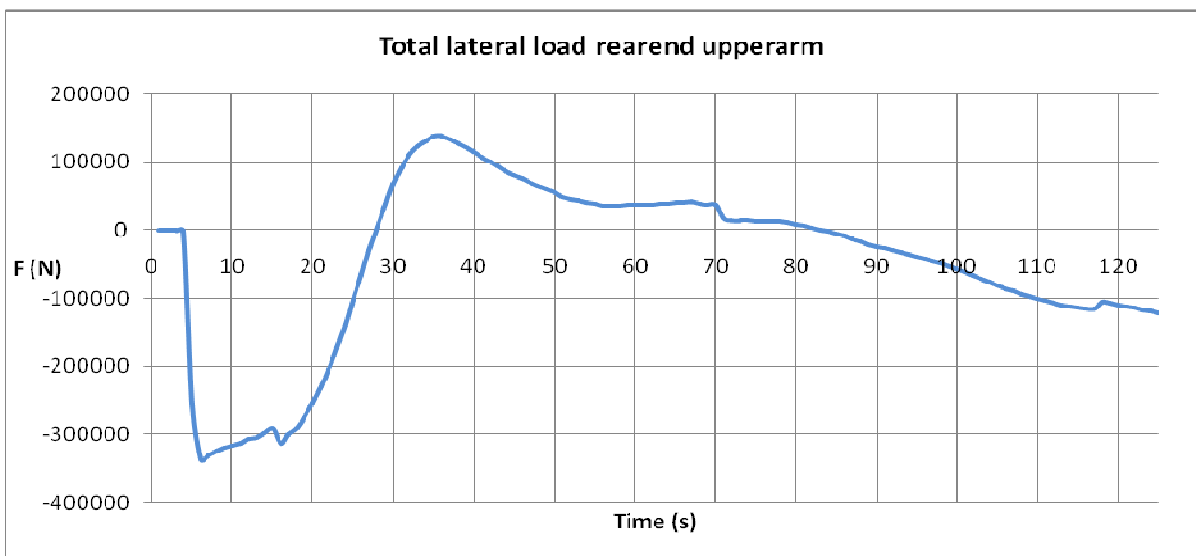


**Figure 125: Total lateral load at rear end pulley upper arm/rear arm**

## ADAMS results – loads at cabin-upper arm support

The following table shows the loads calculated at the cabin suspension support on the upper arm.

**Table 51: Support reactions forces cabin suspension at upper arm**

| Time | cab_suspension.Force.X | cab_suspension.Force.Y | cab_suspension.Force.Z |
|------|------------------------|------------------------|------------------------|
| 0,0  | 0,00     | 0,00      | 0,00     |
| 1,0  | 1392,46  | -95429,48 | 9139,37  |
| 1,0  | 1402,84  | -95385,55 | 9124,20  |
| 2,0  | 1875,19  | -92601,82 | 8239,54  |
| 3,0  | 2131,28  | -91124,43 | 7815,99  |
| 3,1  | 2792,96  | -91107,23 | 7797,41  |
| 4,0  | 2018,20  | -91942,37 | 7829,02  |
| 5,0  | 1756,99  | -91949,66 | 7984,65  |
| 6,0  | 1910,34  | -91662,57 | 7893,86  |
| 7,0  | 2227,53  | -91096,15 | 7644,25  |
| 8,0  | 1886,75  | -91476,89 | 7649,23  |
| 9,0  | 1481,31  | -91880,63 | 7867,09  |
| 10,0 | 1173,30  | -91717,89 | 7892,24  |
| 11,0 | 909,88   | -91238,28 | 7657,25  |
| 12,0 | 285,22   | -91116,17 | 7423,47  |
| 13,0 | -592,06  | -91699,15 | 7459,06  |
| 14,0 | -1532,74 | -91718,24 | 7322,95  |
| 15,0 | -2271,17 | -91261,61 | 6811,31  |
| 16,0 | -3012,78 | -90864,59 | 6157,88  |
| 17,0 | -4012,93 | -91386,83 | 5637,48  |
| 18,0 | -5066,75 | -91608,31 | 4979,42  |
| 19,0 | -5794,24 | -91361,81 | 4117,13  |
| 20,0 | -6351,76 | -91012,93 | 3069,73  |
| 21,0 | -7018,35 | -91077,11 | 1876,32  |
| 22,0 | -7603,98 | -91502,19 | 916,09   |
| 23,0 | -7977,03 | -91567,56 | 2,24     |
| 24,0 | -8044,34 | -91377,32 | -1333,32 |
| 25,0 | -7731,27 | -91160,88 | -2727,65 |
| 26,0 | -7309,59 | -91625,21 | -3456,07 |
| 27,0 | -6536,62 | -91390,82 | -4012,76 |
| 28,0 | -5260,42 | -90745,94 | -4636,99 |
| 29,0 | -3956,60 | -90337,91 | -4815,02 |
| 30,0 | -2766,28 | -90131,25 | -4553,59 |
| 31,0 | -1475,17 | -89565,72 | -4080,97 |
| 32,0 | -200,72  | -88977,10 | -3301,08 |
| 33,0 | 1169,60  | -88313,30 | -2530,24 |
| 34,0 | 2697,90  | -87378,63 | -2048,47 |
| 35,0 | 4064,73  | -86984,43 | -1335,10 |
| 36,0 | 5151,88  | -86361,54 | -184,96  |
| 37,0 | 6636,06  | -85450,92 | 381,10   |
| 38,0 | 8089,25  | -84521,40 | 799,10   |
| 39,0 | 9058,90  | -84316,82 | 1852,61  |

| | | | |
|---|---|---|---|
| 40,0 | 10010,75 | -83649,29 | 2699,32 |
| 41,0 | 11260,96 | -82942,99 | 3037,80 |
| 42,0 | 12215,81 | -82452,96 | 3616,79 |
| 43,0 | 12942,48 | -82260,78 | 4284,45 |
| 44,0 | 13717,43 | -81852,36 | 4505,32 |
| 45,0 | 14335,75 | -81597,01 | 4840,42 |
| 46,0 | 14687,51 | -81419,68 | 5356,05 |
| 47,0 | 15126,04 | -81225,41 | 5400,90 |
| 48,0 | 15434,75 | -81086,21 | 5314,51 |
| 49,0 | 15341,47 | -81090,97 | 5727,53 |
| 50,0 | 15309,26 | -81030,56 | 5933,35 |
| 51,0 | 15568,78 | -80910,57 | 5537,05 |
| 52,0 | 15559,36 | -80940,89 | 5418,96 |
| 53,0 | 15232,80 | -80944,32 | 5739,56 |
| 54,0 | 15239,71 | -80950,06 | 5689,31 |
| 55,0 | 15423,96 | -80797,40 | 5326,64 |
| 56,0 | 15360,40 | -80916,40 | 5457,07 |
| 57,0 | 15148,89 | -80942,10 | 5706,76 |
| 58,0 | 15224,92 | -80844,70 | 5551,43 |
| 59,0 | 15339,75 | -80820,54 | 5446,58 |
| 60,0 | 15264,77 | -80952,02 | 5657,29 |
| 61,0 | 15236,19 | -80925,55 | 5629,15 |
| 62,0 | 15333,39 | -80881,75 | 5430,35 |
| 63,0 | 15284,85 | -80910,15 | 5567,65 |
| 64,0 | 15249,24 | -80991,11 | 5721,42 |
| 65,0 | 15358,13 | -80879,54 | 5462,36 |
| 66,0 | 15376,43 | -80894,31 | 5364,35 |
| 67,0 | 15180,68 | -80907,77 | 5663,96 |
| 68,0 | 15624,37 | -82953,12 | 5911,82 |
| 69,0 | 15306,21 | -80680,49 | 5315,13 |
| 70,0 | 15258,59 | -80899,66 | 5351,06 |
| 71,0 | 15026,75 | -80932,60 | 5646,00 |
| 72,0 | 15119,73 | -80914,67 | 5557,56 |
| 73,0 | 15324,57 | -80860,62 | 5292,58 |
| 74,0 | 14877,10 | -80860,25 | 6025,29 |
| 75,0 | 14746,43 | -81040,38 | 6241,60 |
| 76,0 | 15255,68 | -80889,70 | 5467,00 |
| 77,0 | 16138,56 | -80762,71 | 3884,03 |
| 78,0 | 16654,37 | -80853,25 | 2654,21 |
| 79,0 | 17041,97 | -80693,57 | 1139,47 |
| 80,0 | 17412,68 | -80520,85 | -1402,01 |
| 81,0 | 17411,70 | -80483,97 | -3958,85 |
| 82,0 | 17092,05 | -80505,60 | -6054,02 |
| 83,0 | 16222,51 | -80402,24 | -8615,99 |
| 84,0 | 14720,91 | -80407,63 | -11343,66 |
| 85,0 | 13149,35 | -80409,60 | -13220,64 |
| 86,0 | 11569,03 | -80361,44 | -14724,88 |
| 87,0 | 9264,15 | -80349,14 | -16289,46 |

| | | | |
|---|---|---|---|
| 88,0 | 6860,44 | -80477,97 | -17253,47 |
| 89,0 | 5219,12 | -80501,93 | -17491,97 |
| 90,0 | 3722,95 | -80524,81 | -17528,51 |
| 91,0 | 2063,80 | -80773,40 | -17388,52 |
| 92,0 | 1190,59 | -81000,85 | -16915,56 |
| 93,0 | 1109,52 | -81201,19 | -16282,65 |
| 94,0 | 1741,85 | -81478,52 | -15555,01 |
| 95,0 | 1771,18 | -81776,75 | -14710,55 |
| 96,0 | 1866,91 | -82152,60 | -13737,70 |
| 97,0 | 1775,15 | -82673,94 | -12636,03 |
| 98,0 | 1712,36 | -83246,31 | -11406,32 |
| 99,0 | 1875,52 | -83823,65 | -10094,97 |
| 100,0 | 1934,17 | -84446,63 | -8726,28 |
| 101,0 | 1787,78 | -85192,88 | -7290,46 |
| 102,0 | 1795,69 | -85964,07 | -5769,55 |
| 103,0 | 1928,75 | -86700,25 | -4213,77 |
| 104,0 | 1925,37 | -87412,77 | -2671,85 |
| 105,0 | 1878,60 | -88139,20 | -1139,69 |
| 106,0 | 1896,68 | -88849,14 | 388,35 |
| 107,0 | 1915,08 | -89504,13 | 1862,36 |
| 108,0 | 1958,17 | -90058,49 | 3223,86 |
| 109,0 | 1993,83 | -90531,18 | 4459,77 |
| 110,0 | 1944,38 | -90965,66 | 5561,23 |
| 111,0 | 1914,29 | -91346,40 | 6508,27 |
| 112,0 | 1989,15 | -91607,28 | 7245,59 |
| 113,0 | 2026,68 | -91738,11 | 7728,55 |
| 114,0 | 1958,73 | -91841,64 | 7952,11 |
| 115,0 | 1919,64 | -91579,41 | 7907,82 |
| 116,0 | 1973,66 | -91578,25 | 7921,59 |
| 117,0 | 2005,18 | -91554,92 | 7908,91 |
| 118,0 | 1978,79 | -91555,67 | 7888,68 |
| 119,0 | 1949,55 | -91568,30 | 7888,74 |
| 120,0 | 1948,00 | -91581,08 | 7896,43 |
| 121,0 | 1985,34 | -91576,70 | 7892,48 |
| 122,0 | 2008,13 | -91560,02 | 7883,77 |
| 123,0 | 1962,34 | -91559,39 | 7879,87 |
| 124,0 | 1923,36 | -91585,19 | 7890,95 |
| 125,0 | 1976,25 | -91591,22 | 7902,60 |

Crane fatigue assessment using Multibody Dynamics and Finite Element Method

# Loads file generated by ADAMS for ANSYS

Prior exporting all ADAMS loads to perform a stress analysis, a FEM model must already be available. Within the ANSYS FEM model, the nodal information is known and the node ID's could be assigned within the FEA loads file. The following figure shows the eight key nodes which form the load data exchange 'interface' between ADAMS and ANSYS.

```
!node IDs as specified in the Load File Created From ADAMS Analysis

N,6,1.25,-0.35,0,,,,     !draaipunt_upper arm_front arm_L
N,7,-1.25,-0.35,0,,,,    !draaipunt_upper arm_front arm_R
N,8,0,0,-9.1,,,,         !scharnier_upper arm_reararm_centre
N,24,-0.4,0,20.6,,,,     !pmrk_hijsschijf_bovenarm_R
N,25,-0.15,0,20.6,,,,    !pmrk_sluitschijf_bovenarm_R
N,26,0.15,0,20.6,,,,     !pmrk_sluitschijf_bovenarm_L
N,27,0.4,0,20.6,,,,      !pmrk_hijsschijf_bovenarm_L
N,30,0,0,10.203,,,,      !jt_ophanging_cabine_uithouder
N,31,0,5.5,0,,,,         !FATIGUE JOINT OF INTEREST
```

**Figure 126: Key nodes for data exchange between ADAMS and Ansys**

The following figure shows the load point information of the ADAMS FEA loads file.

```
!          ********   A N S Y S   ********
!          ****** LOADS DATA SET FRAGMENT ******
!          Load File Created From ADAMS Analysis
!          TO BE MERGED WITH  ANSYS INPUT FILE!
!          Created:  Thu Sep 21 21:58:04 2017
!          Number of Load Cases: 128
!          Units: Mass  = kg
!                 Length = meter
!                 Force  = newton
!                 Time   = sec
!          ************************************
!
! Load Point Information  (Global Reference Frame):
! Node ID  ADAMS ID    X            Y            Z       Marker Label
! -------- -------- ------------ ------------ ------------ ------------
!     7    48264 -1.25000e+000 4.04433e+001 -3.82310e-001 draaipunt_upper arm_front arm_R
!     8    53766 0.00000e+000 4.12839e+001 -9.45016e+000 scharnier_upper arm_reararm_centre
!     6    48266 1.25000e+000 4.04433e+001 -3.82310e-001 draaipunt_upper arm_front arm_L
!    30    54315 0.00000e+000 4.02422e+001 9.82471e+000 jt_ophanging_cabine_uithouder
!    24    46535 -4.00000e-001 3.97809e+001 2.02120e+001 pmrk_hijsschijf_bovenarm_R
!    25    46536 -1.50000e-001 3.97809e+001 2.02120e+001 pmrk_sluitschijf_bovenarm_R
!    26    46537 1.50000e-001 3.97809e+001 2.02120e+001 pmrk_sluitschijf_bovenarm_L
!    27    46538 4.00000e-001 3.97809e+001 2.02120e+001 pmrk_hijsschijf_bovenarm_L
```

**Figure 127: ADAMS-Ansys Nodal load information**

The following figure shows all the loads calculated for the upper arm at time=1s. This present a single ADAMS load case which is equivalent to a single ANSYS load step. ANSYS reads during the import all inertial loads which are added to the elements and the nodal loads (action and reaction forces) which are added to the predefined nodes in the FEM model.

```
! LOAD CASE = 2
TIME,1.00000e+000
FDEL, ALL
ACEL,3.75678e-001,1.03402e+001,-3.54619e-001
OMEGA,9.92375e-003,2.53041e-003,8.01465e-003
DOMEGA,-1.19568e-002,7.24066e-003,-8.78317e-003
F, 7, FX,1.10651e+004
F, 7, FY,4.44551e+005
F, 7, FZ,-9.25111e+004
F, 8, FX,0.00000e+000
F, 8, FY,-3.63971e+005
F, 8, FZ,2.23025e+005
F, 6, FX,0.00000e+000
F, 6, FY,4.38343e+005
F, 6, FZ,-1.56234e+005
F, 30, FX,0.00000e+000
F, 30, FY,-1.05527e+005
F, 30, FZ,1.07204e+004
F, 30, MX,0.00000e+000
F, 30, MY,0.00000e+000
F, 30, MZ,0.00000e+000
F,24, FX,-2.55583e+002
F,24, FY,-7.07137e+003
F,24, FZ,2.39225e+002
F,24, MX,0.00000e+000
F,24, MY,-8.36748e-001
F,24, MZ,1.69729e+000
F,25, FX,-2.55570e+002
F,25, FY,-7.06987e+003
F,25, FZ,2.40438e+002
F,25, MX,0.00000e+000
F,25, MY,-8.34425e-001
F,25, MZ,1.69552e+000
F,26, FX,-2.55555e+002
F,26, FY,-7.06806e+003
F,26, FZ,2.41893e+002
F,26, MX,0.00000e+000
F,26, MY,-8.26020e-001
F,26, MZ,1.69110e+000
F,27, FX,-2.55542e+002
F,27, FY,-7.06656e+003
F,27, FZ,2.43106e+002
F,27, MX,0.00000e+000
F,27, MY,-8.21583e-001
F,27, MZ,1.68623e+000
LSWRITE
```

**Figure 128: ADAMS loads file information**

# Stress history tables

The following tables present the nominal stress spectrum determined at the weld interface for the entire transshipment cycle for each individual member.

**Table 52: Nominal stresses at Forestay weld interface**

| Forestay nominal stress (Mpa) | | | |
|---|---|---|---|
| point 1 | point 2 | point 3 | point 4 |
| 50.52 | -18.51 | 18.11 | 13.90 |
| 51.62 | -18.92 | 18.51 | 14.20 |
| 49.16 | -19.02 | 16.52 | 13.61 |
| 75.30 | -7.78 | 34.38 | 33.14 |
| 86.09 | -5.99 | 41.03 | 39.07 |
| 85.71 | -7.58 | 42.67 | 35.46 |
| 84.31 | -6.46 | 38.02 | 39.84 |
| 83.95 | -6.54 | 39.12 | 38.30 |
| 83.59 | -8.03 | 43.76 | 31.80 |
| 83.14 | -5.84 | 37.29 | 40.01 |
| 82.12 | -8.46 | 33.97 | 39.68 |
| 83.38 | -6.97 | 38.23 | 38.17 |
| 79.58 | -7.02 | 32.79 | 39.77 |
| 84.06 | -9.04 | 33.24 | 41.78 |
| 81.43 | -5.75 | 35.02 | 40.66 |
| 86.24 | -7.95 | 36.59 | 41.70 |
| 81.59 | -6.88 | 36.35 | 38.36 |
| 84.72 | -6.24 | 38.26 | 40.22 |
| 82.63 | -8.35 | 38.56 | 35.72 |
| 83.35 | -5.86 | 37.92 | 39.57 |
| 83.10 | -7.73 | 33.73 | 41.64 |
| 84.83 | -6.89 | 40.39 | 37.55 |
| 82.45 | -6.95 | 35.98 | 39.52 |
| 84.38 | -7.75 | 35.98 | 40.66 |
| 83.32 | -7.27 | 42.00 | 34.05 |
| 83.00 | -6.14 | 37.59 | 39.26 |
| 85.04 | -8.66 | 34.55 | 41.84 |
| 81.29 | -4.91 | 37.28 | 39.10 |
| 85.41 | -9.27 | 36.03 | 40.10 |
| 81.59 | -5.11 | 35.83 | 40.65 |
| 85.01 | -8.20 | 38.36 | 38.45 |
| 81.81 | -6.56 | 40.99 | 34.26 |
| 83.68 | -7.40 | 40.99 | 35.29 |
| 81.87 | -6.25 | 39.79 | 35.83 |
| 84.70 | -7.65 | 42.89 | 34.16 |
| 81.08 | -4.74 | 35.32 | 41.02 |
| 85.03 | -8.30 | 30.81 | 45.93 |
| 80.91 | -4.44 | 38.29 | 38.18 |
| 84.04 | -7.51 | 33.60 | 42.92 |
| 82.24 | -5.44 | 32.23 | 44.56 |
| 82.24 | -6.01 | 39.31 | 36.92 |
| 83.15 | -6.37 | 38.24 | 38.54 |
| 81.15 | -5.39 | 36.92 | 38.84 |
| 83.16 | -5.55 | 37.53 | 40.08 |
| 81.84 | -5.90 | 36.24 | 39.70 |

| | | | |
|---|---|---|---|
| 82.29 | -4.48 | 36.06 | 41.75 |
| 81.31 | -6.04 | 30.88 | 44.39 |
| 82.37 | -4.88 | 36.17 | 41.32 |
| 79.91 | -4.96 | 36.17 | 38.77 |
| 82.44 | -6.05 | 32.57 | 43.82 |
| 78.18 | -4.01 | 37.83 | 36.35 |
| 81.95 | -5.98 | 39.44 | 36.52 |
| 78.57 | -4.14 | 33.70 | 40.73 |
| 80.94 | -4.50 | 35.38 | 41.07 |
| 76.48 | -5.72 | 31.93 | 38.83 |
| 77.81 | -4.51 | 33.74 | 39.56 |
| 78.39 | -5.30 | 31.56 | 41.53 |
| 79.47 | -5.25 | 32.16 | 42.06 |
| 78.46 | -4.24 | 38.14 | 36.08 |
| 80.28 | -5.78 | 35.32 | 39.18 |
| 79.34 | -3.82 | 34.90 | 40.62 |
| 81.13 | -4.86 | 39.52 | 36.75 |
| 81.71 | -4.21 | 37.03 | 40.48 |
| 81.41 | -3.35 | 35.82 | 42.25 |
| 83.29 | -4.30 | 37.11 | 41.89 |
| 82.54 | -3.23 | 36.57 | 42.74 |
| 80.70 | -4.27 | 35.55 | 40.87 |
| 80.54 | -5.09 | 31.99 | 43.46 |
| 79.43 | -3.71 | 35.19 | 40.53 |
| 63.37 | -12.66 | 26.34 | 24.38 |
| 58.21 | -11.24 | 19.00 | 27.98 |
| 58.76 | -11.82 | 21.36 | 25.57 |
| 58.31 | -12.21 | 23.51 | 22.59 |
| 58.40 | -11.58 | 21.44 | 25.38 |
| 57.62 | -11.97 | 20.36 | 25.29 |
| 58.73 | -12.57 | 25.44 | 20.72 |
| 56.28 | -11.11 | 31.62 | 13.55 |
| 59.43 | -13.34 | 29.83 | 16.26 |
| 56.38 | -11.29 | 25.13 | 19.96 |
| 58.15 | -13.31 | 28.72 | 16.12 |
| 57.73 | -12.43 | 29.84 | 15.46 |
| 58.60 | -11.97 | 26.64 | 20.00 |
| 60.04 | -12.57 | 23.46 | 24.01 |
| 58.98 | -11.87 | 24.79 | 22.32 |
| 59.17 | -12.26 | 25.10 | 21.81 |
| 58.48 | -12.74 | 18.28 | 27.46 |
| 59.29 | -11.26 | 21.56 | 26.47 |
| 59.24 | -12.68 | 23.24 | 23.31 |
| 60.10 | -12.13 | 18.99 | 28.97 |
| 57.69 | -12.25 | 14.78 | 30.65 |
| 60.30 | -13.22 | 17.10 | 29.99 |
| 57.20 | -11.72 | 17.94 | 27.54 |
| 60.93 | -13.00 | 16.37 | 31.56 |
| 58.13 | -12.51 | 14.30 | 31.31 |
| 59.86 | -12.19 | 19.79 | 27.88 |
| 59.21 | -13.50 | 22.81 | 22.91 |
| 59.57 | -12.03 | 24.82 | 22.72 |
| 59.43 | -13.51 | 23.85 | 22.08 |

| | | | |
|---|---|---|---|
| 59.83 | -12.83 | 24.94 | 22.06 |
| 59.47 | -12.95 | 24.05 | 22.48 |
| 59.82 | -13.22 | 24.63 | 21.97 |
| 60.04 | -13.23 | 26.66 | 20.16 |
| 58.91 | -12.68 | 23.81 | 22.42 |
| 61.34 | -14.33 | 23.55 | 23.46 |
| 58.26 | -12.00 | 25.72 | 20.54 |
| 62.19 | -14.81 | 23.78 | 23.60 |
| 58.48 | -12.46 | 23.32 | 22.70 |
| 61.92 | -14.32 | 25.54 | 22.06 |
| 59.20 | -13.38 | 23.68 | 22.14 |
| 61.66 | -13.80 | 25.76 | 22.11 |
| 59.49 | -13.55 | 24.61 | 21.32 |
| 61.83 | -14.23 | 25.60 | 22.01 |
| 59.20 | -13.08 | 24.17 | 21.95 |
| 62.19 | -14.75 | 23.86 | 23.57 |
| 59.55 | -13.03 | 25.39 | 21.13 |
| 61.62 | -14.41 | 23.94 | 23.27 |
| 59.60 | -14.22 | 22.56 | 22.83 |
| 59.84 | -13.66 | 25.46 | 20.72 |
| 60.97 | -14.76 | 24.41 | 21.80 |
| 59.78 | -13.20 | 24.18 | 22.41 |
| 61.43 | -14.46 | 25.77 | 21.20 |
| 60.24 | -13.51 | 24.38 | 22.36 |
| 61.71 | -13.88 | 24.77 | 23.06 |
| 60.81 | -13.52 | 25.21 | 22.08 |
| 62.55 | -13.99 | 24.96 | 23.59 |
| 60.78 | -12.84 | 24.83 | 23.11 |
| 63.45 | -14.63 | 24.70 | 24.12 |

**Table 53: Nominal stresses at Backstay weld interface**

| Backstay nominal stress (Mpa) | | | |
|---|---|---|---|
| point 1 | point 2 | point 3 | point 4 |
| 50.40 | -12.04 | 20.39 | 17.97 |
| 51.50 | -12.31 | 20.83 | 18.36 |
| 51.82 | -15.86 | 18.86 | 17.10 |
| 76.02 | 2.48 | 39.68 | 38.82 |
| 87.74 | 5.04 | 46.97 | 45.81 |
| 92.63 | -2.57 | 47.03 | 43.03 |
| 86.18 | 3.97 | 44.73 | 45.42 |
| 87.59 | 1.91 | 45.14 | 44.36 |
| 89.40 | -2.13 | 47.20 | 40.06 |
| 84.38 | 5.21 | 44.35 | 45.25 |
| 88.09 | -3.04 | 41.30 | 43.75 |
| 85.77 | 2.71 | 44.14 | 44.34 |
| 82.90 | 1.10 | 39.92 | 44.08 |
| 90.10 | -3.40 | 40.63 | 46.06 |
| 83.58 | 4.04 | 41.91 | 45.71 |
| 91.53 | -1.11 | 43.57 | 46.85 |
| 86.09 | 0.26 | 42.68 | 43.67 |
| 87.92 | 2.90 | 45.03 | 45.78 |
| 89.65 | -3.93 | 43.66 | 42.06 |

| | | | |
|---|---|---|---|
| 85.40 | 4.31 | 44.46 | 45.25 |
| 88.61 | -1.54 | 41.20 | 45.87 |
| 90.47 | -0.50 | 45.56 | 44.40 |
| 85.15 | 2.31 | 42.67 | 44.80 |
| 91.55 | -3.22 | 42.98 | 45.35 |
| 85.67 | 2.45 | 46.30 | 41.82 |
| 88.01 | 0.69 | 43.84 | 44.87 |
| 90.14 | -1.80 | 42.00 | 46.34 |
| 83.92 | 4.40 | 43.16 | 45.17 |
| 90.35 | -2.28 | 42.43 | 45.63 |
| 85.23 | 3.13 | 42.54 | 45.83 |
| 87.65 | 1.39 | 44.44 | 44.60 |
| 87.57 | -0.74 | 45.45 | 41.38 |
| 84.01 | 4.60 | 46.19 | 42.41 |
| 87.25 | 0.05 | 44.98 | 42.32 |
| 86.50 | 2.90 | 46.96 | 42.44 |
| 83.59 | 4.79 | 42.43 | 45.95 |
| 88.71 | 0.22 | 39.84 | 49.08 |
| 81.78 | 6.91 | 43.80 | 44.89 |
| 86.63 | 2.15 | 41.31 | 47.47 |
| 84.79 | 4.22 | 40.89 | 48.12 |
| 81.93 | 6.73 | 44.91 | 43.75 |
| 86.28 | 2.71 | 44.51 | 44.47 |
| 80.18 | 8.01 | 43.76 | 44.42 |
| 84.17 | 5.98 | 44.37 | 45.79 |
| 82.44 | 5.84 | 42.98 | 45.30 |
| 80.07 | 10.58 | 43.32 | 47.33 |
| 82.08 | 5.45 | 39.59 | 47.94 |
| 79.78 | 10.57 | 43.21 | 47.15 |
| 78.05 | 9.33 | 42.64 | 44.74 |
| 81.10 | 7.93 | 41.35 | 47.69 |
| 73.66 | 13.03 | 43.80 | 42.89 |
| 79.94 | 8.66 | 45.13 | 43.47 |
| 74.57 | 12.40 | 41.50 | 45.48 |
| 76.26 | 13.08 | 42.88 | 46.47 |
| 73.67 | 9.03 | 39.01 | 43.70 |
| 71.65 | 14.20 | 40.82 | 45.03 |
| 75.26 | 10.14 | 39.50 | 45.90 |
| 75.13 | 11.64 | 40.34 | 46.42 |
| 73.07 | 13.78 | 43.82 | 43.03 |
| 77.48 | 9.47 | 42.41 | 44.55 |
| 73.69 | 14.67 | 42.71 | 45.65 |
| 77.48 | 11.58 | 45.26 | 43.80 |
| 77.87 | 12.62 | 44.27 | 46.22 |
| 75.78 | 15.46 | 43.68 | 47.56 |
| 80.56 | 11.54 | 44.49 | 47.62 |
| 77.19 | 15.46 | 44.20 | 48.44 |
| 76.60 | 12.67 | 42.75 | 46.52 |
| 77.00 | 11.13 | 40.54 | 47.58 |
| 73.73 | 14.83 | 42.45 | 46.11 |
| 60.08 | -0.10 | 30.40 | 29.58 |
| 53.43 | 2.26 | 25.23 | 30.45 |
| 53.05 | 2.73 | 26.69 | 29.08 |

| | | | |
|---|---|---|---|
| 55.32 | -0.78 | 27.42 | 27.11 |
| 51.76 | 3.96 | 26.73 | 28.99 |
| 54.30 | -0.24 | 25.55 | 28.51 |
| 53.81 | 1.05 | 28.60 | 26.25 |
| 50.78 | 2.86 | 31.65 | 22.00 |
| 56.21 | -1.54 | 31.13 | 23.54 |
| 51.44 | 2.11 | 28.43 | 25.13 |
| 54.47 | -1.17 | 30.47 | 22.83 |
| 55.06 | -1.41 | 31.14 | 22.51 |
| 53.95 | 1.48 | 29.80 | 25.63 |
| 58.87 | -2.79 | 28.02 | 28.05 |
| 55.16 | 0.76 | 28.48 | 27.43 |
| 56.78 | -1.23 | 28.60 | 26.96 |
| 56.89 | -2.70 | 24.43 | 29.76 |
| 55.17 | 1.81 | 27.11 | 29.86 |
| 58.20 | -3.14 | 27.30 | 27.76 |
| 57.33 | -0.52 | 25.42 | 31.39 |
| 55.10 | -1.24 | 22.23 | 31.63 |
| 58.96 | -3.28 | 23.89 | 31.79 |
| 53.73 | 0.20 | 24.04 | 29.89 |
| 59.72 | -3.10 | 23.99 | 32.63 |
| 56.16 | -2.21 | 22.35 | 31.61 |
| 57.18 | -0.79 | 26.00 | 30.40 |
| 59.25 | -5.32 | 26.94 | 26.98 |
| 57.24 | -1.03 | 28.69 | 27.52 |
| 59.37 | -5.20 | 27.56 | 26.61 |
| 59.82 | -4.42 | 28.55 | 26.84 |
| 58.14 | -3.20 | 27.99 | 26.95 |
| 61.43 | -6.65 | 28.31 | 26.47 |
| 59.19 | -3.96 | 29.51 | 25.73 |
| 59.96 | -5.58 | 27.74 | 26.65 |
| 62.42 | -7.11 | 27.73 | 27.59 |
| 58.25 | -3.80 | 28.66 | 25.79 |
| 64.04 | -8.38 | 27.87 | 27.79 |
| 59.40 | -5.32 | 27.21 | 26.88 |
| 62.55 | -6.56 | 28.99 | 27.00 |
| 61.79 | -8.08 | 27.34 | 26.37 |
| 61.37 | -5.03 | 29.35 | 26.98 |
| 62.16 | -8.34 | 27.95 | 25.88 |
| 62.63 | -6.69 | 29.08 | 26.85 |
| 60.26 | -6.11 | 27.78 | 26.37 |
| 64.43 | -8.82 | 27.91 | 27.71 |
| 59.92 | -5.27 | 28.51 | 26.14 |
| 63.60 | -8.24 | 27.83 | 27.53 |
| 61.13 | -7.82 | 26.67 | 26.65 |
| 60.58 | -6.31 | 28.47 | 25.80 |
| 63.40 | -9.20 | 27.96 | 26.23 |
| 60.57 | -5.86 | 28.01 | 26.70 |
| 63.02 | -7.89 | 28.92 | 26.21 |
| 62.43 | -7.66 | 28.09 | 26.68 |
| 62.01 | -5.79 | 28.62 | 27.60 |
| 63.77 | -8.44 | 28.64 | 26.69 |
| 63.15 | -6.13 | 28.85 | 28.17 |

| 62.80 | -6.66 | 28.62 | 27.52 |
| 65.36 | -8.14 | 28.79 | 28.44 |

**Table 54: Nominal stresses at Left pylon weld interface**

| Pylon left nominal stress (Mpa) | | | |
|---------|---------|---------|---------|
| point 1 | point 2 | point 3 | point 4 |
| -15.43 | -22.44 | -17.01 | -20.86 |
| -15.74 | -22.91 | -17.36 | -21.28 |
| -15.06 | -22.00 | -22.56 | -14.49 |
| -28.37 | -44.01 | -30.96 | -41.42 |
| -33.44 | -51.14 | -37.28 | -47.30 |
| -33.25 | -48.91 | -47.55 | -34.61 |
| -32.60 | -51.95 | -38.22 | -46.32 |
| -32.23 | -51.27 | -41.65 | -41.85 |
| -30.91 | -47.67 | -44.37 | -34.22 |
| -31.65 | -52.75 | -37.15 | -47.25 |
| -31.21 | -52.32 | -47.18 | -36.35 |
| -33.11 | -48.48 | -37.40 | -44.19 |
| -32.28 | -47.55 | -38.50 | -41.34 |
| -34.66 | -48.51 | -45.23 | -37.94 |
| -34.02 | -47.41 | -35.98 | -45.46 |
| -34.89 | -50.85 | -45.17 | -40.57 |
| -32.19 | -49.30 | -42.21 | -39.27 |
| -32.83 | -52.57 | -41.49 | -43.91 |
| -32.07 | -48.34 | -47.51 | -32.90 |
| -32.90 | -50.60 | -37.77 | -45.74 |
| -33.60 | -50.56 | -45.37 | -38.79 |
| -34.24 | -48.22 | -44.41 | -38.04 |
| -32.94 | -49.48 | -38.78 | -43.65 |
| -33.04 | -52.55 | -50.12 | -35.46 |
| -31.91 | -47.39 | -36.89 | -42.41 |
| -33.10 | -50.41 | -44.25 | -39.26 |
| -34.36 | -51.13 | -45.18 | -40.31 |
| -34.48 | -46.06 | -36.50 | -44.04 |
| -35.14 | -47.61 | -42.87 | -39.89 |
| -34.18 | -48.52 | -40.07 | -42.63 |
| -33.25 | -50.18 | -39.57 | -43.86 |
| -31.22 | -49.09 | -45.38 | -34.94 |
| -30.95 | -50.45 | -34.58 | -46.81 |
| -31.21 | -50.34 | -45.21 | -36.34 |
| -32.94 | -46.88 | -36.00 | -43.82 |
| -33.61 | -49.81 | -38.70 | -44.71 |
| -35.88 | -51.49 | -42.58 | -44.80 |
| -34.80 | -44.36 | -31.96 | -47.19 |
| -35.54 | -48.94 | -38.83 | -45.65 |
| -34.62 | -52.01 | -40.38 | -46.26 |
| -32.78 | -48.04 | -32.10 | -48.72 |
| -32.50 | -51.24 | -41.37 | -42.37 |
| -31.74 | -51.03 | -32.37 | -50.40 |
| -33.42 | -51.33 | -37.08 | -47.67 |
| -33.54 | -48.95 | -34.86 | -47.63 |
| -35.13 | -48.29 | -28.26 | -55.16 |

| | | | |
|---|---|---|---|
| -35.05 | -49.50 | -35.51 | -49.05 |
| -35.30 | -47.30 | -27.14 | -55.47 |
| -33.59 | -46.59 | -28.30 | -51.88 |
| -33.69 | -52.72 | -33.16 | -53.25 |
| -31.16 | -47.42 | -22.96 | -55.62 |
| -32.17 | -48.75 | -29.53 | -51.39 |
| -32.20 | -49.89 | -25.75 | -56.33 |
| -33.84 | -49.03 | -23.90 | -58.97 |
| -32.42 | -44.66 | -25.26 | -51.83 |
| -33.32 | -44.72 | -18.01 | -60.03 |
| -33.82 | -46.80 | -25.93 | -54.68 |
| -33.36 | -48.69 | -24.44 | -57.62 |
| -31.96 | -45.64 | -20.33 | -57.28 |
| -32.11 | -49.55 | -28.26 | -53.39 |
| -31.82 | -51.02 | -22.90 | -59.95 |
| -32.41 | -48.29 | -25.80 | -54.90 |
| -33.07 | -50.91 | -26.89 | -57.09 |
| -33.92 | -50.58 | -22.65 | -61.86 |
| -34.93 | -50.33 | -28.99 | -56.28 |
| -35.20 | -49.52 | -22.76 | -61.96 |
| -34.51 | -47.48 | -24.30 | -57.69 |
| -34.31 | -49.44 | -26.55 | -57.20 |
| -33.54 | -47.37 | -20.61 | -60.29 |
| -23.47 | -32.72 | -17.21 | -38.98 |
| -22.18 | -33.68 | -14.26 | -41.60 |
| -21.67 | -32.61 | -11.61 | -42.67 |
| -21.32 | -30.51 | -16.28 | -35.54 |
| -21.34 | -32.37 | -9.44 | -44.27 |
| -21.78 | -31.70 | -16.25 | -37.23 |
| -20.79 | -29.29 | -11.55 | -38.52 |
| -19.37 | -23.95 | -7.01 | -36.30 |
| -19.72 | -28.15 | -14.61 | -33.26 |
| -18.93 | -31.08 | -12.40 | -37.61 |
| -18.32 | -29.95 | -14.71 | -33.56 |
| -18.13 | -29.82 | -16.71 | -31.24 |
| -19.60 | -31.82 | -13.60 | -37.83 |
| -21.38 | -33.81 | -22.29 | -32.89 |
| -21.61 | -30.35 | -14.59 | -37.37 |
| -21.69 | -30.20 | -17.55 | -34.34 |
| -22.22 | -33.48 | -21.18 | -34.52 |
| -22.23 | -33.51 | -15.56 | -40.18 |
| -22.31 | -30.44 | -20.57 | -32.18 |
| -23.54 | -33.59 | -18.54 | -38.59 |
| -23.46 | -32.97 | -18.37 | -38.06 |
| -24.26 | -32.90 | -21.17 | -35.98 |
| -22.59 | -31.19 | -15.24 | -38.54 |
| -23.81 | -35.99 | -23.07 | -36.74 |
| -22.07 | -36.42 | -21.44 | -37.05 |
| -22.29 | -34.73 | -19.06 | -37.96 |
| -21.02 | -31.54 | -23.03 | -29.53 |
| -21.33 | -31.37 | -17.72 | -34.97 |
| -20.94 | -30.97 | -22.41 | -29.50 |
| -21.06 | -31.68 | -22.94 | -29.80 |

| | | | |
|---|---|---|---|
| -20.68 | -31.91 | -20.10 | -32.49 |
| -20.50 | -32.65 | -26.88 | -26.27 |
| -20.43 | -30.77 | -20.47 | -30.72 |
| -20.46 | -32.39 | -25.33 | -27.52 |
| -21.37 | -32.80 | -25.82 | -28.34 |
| -20.63 | -29.79 | -21.40 | -29.01 |
| -21.79 | -32.58 | -27.31 | -27.06 |
| -20.93 | -31.10 | -24.07 | -27.95 |
| -21.41 | -31.78 | -24.14 | -29.05 |
| -20.65 | -31.69 | -28.09 | -24.25 |
| -20.82 | -32.64 | -22.45 | -31.01 |
| -20.34 | -31.73 | -28.26 | -23.81 |
| -21.00 | -32.44 | -24.77 | -28.67 |
| -20.56 | -31.44 | -24.49 | -27.51 |
| -21.66 | -32.73 | -28.00 | -26.38 |
| -20.83 | -30.28 | -22.33 | -28.78 |
| -21.75 | -31.91 | -26.91 | -26.75 |
| -20.63 | -31.81 | -25.77 | -26.67 |
| -20.67 | -30.33 | -23.25 | -27.74 |
| -20.64 | -32.18 | -28.04 | -24.78 |
| -20.46 | -32.36 | -24.43 | -28.39 |
| -20.94 | -31.64 | -25.99 | -26.60 |
| -20.75 | -32.46 | -27.57 | -25.64 |
| -21.46 | -32.36 | -23.50 | -30.32 |
| -21.20 | -32.06 | -29.00 | -24.27 |
| -22.06 | -32.50 | -24.34 | -30.21 |
| -21.57 | -32.40 | -27.08 | -26.89 |
| -22.22 | -33.41 | -27.71 | -27.93 |

**Table 55: Nominal stresses at Right pylon weld interface**

| Pylon right nominal stress (Mpa) | | | |
|---|---|---|---|
| point 1 | point 2 | point 3 | point 4 |
| -24.54 | -16.59 | -18.37 | -22.76 |
| -25.06 | -16.91 | -18.76 | -23.21 |
| -23.37 | -16.04 | -23.77 | -15.64 |
| -43.78 | -29.61 | -31.16 | -42.23 |
| -51.94 | -34.44 | -38.03 | -48.35 |
| -53.24 | -34.25 | -50.02 | -37.47 |
| -48.50 | -33.60 | -36.35 | -45.75 |
| -48.98 | -33.87 | -40.37 | -42.49 |
| -51.28 | -34.57 | -46.62 | -39.24 |
| -46.69 | -33.81 | -34.06 | -46.45 |
| -44.42 | -32.85 | -43.13 | -34.14 |
| -50.42 | -32.05 | -38.56 | -43.90 |
| -46.84 | -30.10 | -38.63 | -38.31 |
| -50.11 | -30.53 | -46.75 | -33.90 |
| -50.21 | -30.33 | -37.89 | -42.65 |
| -51.28 | -32.49 | -45.44 | -38.33 |
| -47.98 | -32.10 | -41.84 | -38.24 |
| -48.91 | -34.01 | -39.55 | -43.37 |
| -49.43 | -32.69 | -48.02 | -34.11 |
| -49.25 | -32.82 | -37.14 | -44.94 |

| | | | |
|---|---|---|---|
| -48.03 | -31.59 | -44.02 | -35.60 |
| -53.26 | -32.71 | -47.14 | -38.83 |
| -48.44 | -31.67 | -38.02 | -42.09 |
| -47.83 | -33.30 | -47.39 | -33.74 |
| -51.20 | -33.14 | -38.79 | -45.55 |
| -49.33 | -32.68 | -43.28 | -38.72 |
| -48.95 | -31.80 | -43.64 | -37.11 |
| -52.25 | -30.23 | -39.67 | -42.82 |
| -52.30 | -30.92 | -45.31 | -37.92 |
| -50.21 | -30.86 | -40.81 | -40.26 |
| -49.81 | -32.74 | -38.69 | -43.86 |
| -49.03 | -33.59 | -44.64 | -37.97 |
| -48.19 | -34.07 | -32.87 | -49.39 |
| -48.17 | -33.86 | -43.57 | -38.45 |
| -53.23 | -33.10 | -38.97 | -47.36 |
| -48.71 | -31.28 | -37.68 | -42.30 |
| -48.96 | -30.47 | -41.03 | -38.39 |
| -54.00 | -29.92 | -37.48 | -46.44 |
| -50.88 | -30.35 | -39.79 | -41.44 |
| -47.56 | -30.99 | -37.56 | -40.99 |
| -50.44 | -32.11 | -33.16 | -49.39 |
| -48.81 | -33.54 | -39.79 | -42.56 |
| -46.67 | -32.63 | -29.70 | -49.60 |
| -49.26 | -32.86 | -35.54 | -46.57 |
| -49.61 | -31.49 | -34.95 | -46.15 |
| -51.68 | -30.59 | -30.10 | -52.16 |
| -48.45 | -29.60 | -34.91 | -43.13 |
| -52.44 | -30.29 | -29.89 | -52.84 |
| -50.19 | -30.18 | -30.11 | -50.25 |
| -46.36 | -31.58 | -29.27 | -48.67 |
| -47.61 | -31.37 | -22.94 | -56.04 |
| -49.71 | -32.72 | -29.84 | -52.59 |
| -45.76 | -30.77 | -23.09 | -53.44 |
| -49.13 | -30.69 | -23.71 | -56.11 |
| -47.17 | -28.18 | -26.62 | -48.72 |
| -49.21 | -28.40 | -20.54 | -57.08 |
| -47.78 | -28.52 | -26.33 | -49.98 |
| -46.98 | -29.59 | -23.19 | -53.38 |
| -49.50 | -30.64 | -22.36 | -57.78 |
| -46.92 | -31.46 | -26.59 | -51.79 |
| -45.58 | -31.69 | -19.55 | -57.72 |
| -49.97 | -32.27 | -26.41 | -55.83 |
| -48.69 | -32.48 | -25.37 | -55.79 |
| -49.07 | -31.51 | -21.63 | -58.95 |
| -51.41 | -32.05 | -29.49 | -53.97 |
| -51.74 | -31.29 | -23.81 | -59.21 |
| -50.75 | -30.11 | -25.96 | -54.90 |
| -47.92 | -29.78 | -25.57 | -52.13 |
| -49.42 | -30.08 | -21.67 | -57.83 |
| -36.01 | -22.37 | -18.93 | -39.45 |
| -29.50 | -19.94 | -11.53 | -37.90 |
| -30.54 | -20.39 | -10.23 | -40.70 |
| -32.22 | -20.62 | -17.05 | -35.79 |

| | | | |
|---|---|---|---|
| -30.36 | -20.42 | -8.12 | -42.65 |
| -30.36 | -19.70 | -15.20 | -34.85 |
| -33.29 | -20.99 | -13.51 | -40.76 |
| -36.73 | -21.14 | -14.02 | -43.85 |
| -34.94 | -22.50 | -18.24 | -39.20 |
| -29.74 | -21.69 | -11.26 | -40.17 |
| -31.51 | -22.82 | -15.21 | -39.12 |
| -32.09 | -23.33 | -17.64 | -37.78 |
| -31.31 | -22.53 | -13.03 | -40.82 |
| -31.28 | -22.19 | -20.73 | -32.75 |
| -33.59 | -21.08 | -16.19 | -38.48 |
| -33.89 | -21.17 | -19.62 | -35.44 |
| -29.51 | -19.96 | -18.75 | -30.72 |
| -31.31 | -20.99 | -14.37 | -37.92 |
| -33.61 | -20.58 | -22.31 | -31.88 |
| -31.65 | -20.01 | -17.58 | -34.09 |
| -29.13 | -18.04 | -16.31 | -30.86 |
| -31.76 | -18.99 | -20.66 | -30.09 |
| -30.50 | -18.58 | -15.02 | -34.06 |
| -29.61 | -20.04 | -19.73 | -29.93 |
| -25.90 | -19.60 | -15.69 | -29.81 |
| -29.88 | -20.84 | -16.44 | -34.27 |
| -31.51 | -21.24 | -23.14 | -29.61 |
| -33.00 | -21.65 | -18.88 | -35.77 |
| -32.23 | -21.40 | -23.25 | -30.38 |
| -32.64 | -22.00 | -23.59 | -31.06 |
| -31.51 | -21.72 | -19.97 | -33.25 |
| -31.54 | -22.55 | -26.40 | -27.69 |
| -33.12 | -22.30 | -21.88 | -33.55 |
| -30.98 | -22.00 | -24.69 | -28.30 |
| -32.00 | -22.05 | -25.45 | -28.60 |
| -33.09 | -21.43 | -23.41 | -31.11 |
| -32.89 | -22.09 | -27.66 | -27.32 |
| -31.73 | -21.14 | -24.62 | -28.25 |
| -33.47 | -22.26 | -25.19 | -30.54 |
| -31.43 | -21.70 | -27.98 | -25.16 |
| -32.53 | -22.73 | -22.63 | -32.63 |
| -31.56 | -22.13 | -28.22 | -25.47 |
| -32.72 | -22.61 | -25.01 | -30.33 |
| -31.56 | -21.63 | -24.68 | -28.50 |
| -32.64 | -22.16 | -28.13 | -26.67 |
| -33.01 | -21.51 | -23.99 | -30.53 |
| -32.99 | -21.74 | -27.70 | -27.03 |
| -30.69 | -21.29 | -25.28 | -26.71 |
| -32.81 | -21.61 | -24.73 | -29.68 |
| -31.71 | -22.23 | -27.89 | -26.05 |
| -31.16 | -22.07 | -23.95 | -29.27 |
| -32.93 | -22.32 | -26.72 | -28.53 |
| -31.64 | -22.21 | -27.24 | -26.61 |
| -32.84 | -22.13 | -23.91 | -31.06 |
| -32.88 | -22.35 | -29.69 | -25.54 |
| -33.69 | -22.19 | -25.02 | -30.86 |
| -32.95 | -22.17 | -27.64 | -27.47 |

| -33.56 | -22.60 | -27.88 | -28.28 |

Crane fatigue assessment using Multibody Dynamics and Finite Element Method

## Fatigue damage calculation sheet

| | | | | Stress range histogram FS point 1 | | |
|---|---|---|---|---|---|---|
| block # | Max (Mpa) | Min (Mpa) | counted cycles | Stress range (Mpa) | current total # cycles | Damage |
| 1 | 51,62 | 50,52 | 1 | **1,1** | 1,31E+06 | 0,0000 |
| 2 | 60,573 | 58,765 | 1 | **1,808** | 1,31E+06 | 0,0001 |
| 3 | 83,391 | 80,934 | 1 | **2,457** | 1,31E+06 | 0,0002 |
| 4 | 86,24 | 49,16 | 1 | **37,08** | 1,31E+06 | 0,7170 |
| **Total damage** | | | | | | **0,7173** |

| | | | | Stress range histogram FS point 2 | | |
|---|---|---|---|---|---|---|
| block # | Max (Mpa) | Min (Mpa) | Cycles | Stress range (Mpa) | current total # cycles | Damage |
| 1 | -12,662 | -13,72 | 20 | **1,058** | 2,62E+07 | 0,0003 |
| 2 | -11,225 | -12,97 | 4 | **1,745** | 5,25E+06 | 0,0003 |
| 3 | -5,891 | -8,282 | 12 | **2,391** | 1,57E+07 | 0,0023 |
| 4 | -4,864 | -6,208 | 12 | **1,344** | 1,57E+07 | 0,0004 |
| 5 | -3,53 | -4,695 | 2 | **1,165** | 2,62E+06 | 0,0000 |
| 6 | -3,23 | -19,02 | 1 | **15,79** | 1,31E+06 | 0,0554 |
| **Total damage** | | | | | | **0,0588** |

| | | | | Stress range histogram FS point 3 | | |
|---|---|---|---|---|---|---|
| block # | Max (Mpa) | Min (Mpa) | Cycles | Stress range (Mpa) | current total # cycles | Damage |
| 1 | 17,94 | 14,78 | 1 | **3,16** | 1,31E+06 | 0,0004 |
| 2 | 24,612 | 22,732 | 14 | **1,88** | 1,84E+07 | 0,0013 |
| 3 | 26,66 | 16,52 | 1 | **10,14** | 1,31E+06 | 0,0147 |
| 4 | 30,73 | 22,065 | 2 | **8,665** | 2,62E+06 | 0,0183 |
| 5 | 33,74 | 31,93 | 1 | **1,81** | 1,31E+06 | 0,0001 |
| 6 | 38,593 | 32,807 | 12 | **5,786** | 1,57E+07 | 0,0327 |
| 7 | 38,937 | 36,959 | 7 | **1,978** | 9,19E+06 | 0,0008 |
| 8 | 43,76 | 14,3 | 1 | **29,46** | 1,31E+06 | 0,3596 |
| **Total damage** | | | | | | **0,4278** |

| | | | | Stress spectrum FS point 4 | | |
|---|---|---|---|---|---|---|
| block # | Max (Mpa) | Min (Mpa) | Cycles | Stress range (Mpa) | current total # cycles | Damage |
| 1 | 14,2 | 13,9 | 1 | **0,3** | 1,31E+06 | 0,0000 |
| 2 | 19,96 | 15,46 | 1 | **4,5** | 1,31E+06 | 0,0013 |
| 3 | 23,611 | 21,717 | 14 | **1,894** | 1,84E+07 | 0,0013 |
| 4 | 29,315 | 25,96 | 2 | **3,355** | 2,62E+06 | 0,0011 |
| 5 | 31,56 | 13,61 | 1 | **17,95** | 1,31E+06 | 0,0813 |
| 6 | 35,83 | 34,26 | 1 | **1,57** | 1,31E+06 | 0,0001 |
| 7 | 41,384 | 34,803 | 7 | **6,581** | 9,19E+06 | 0,0281 |
| 8 | 41,752 | 38,904 | 13 | **2,848** | 1,71E+07 | 0,0042 |
| 9 | 45,93 | 13,55 | 1 | **32,38** | 1,31E+06 | 0,4774 |
| **Total damage** | | | | | | **0,5948** |

**Table 56: Fatigue damage calculation sheet- forestay weld interface**

The following table present the stress range, counted cycles and damage calculation at the backstay.

| block # | Max (Mpa) | Min (Mpa) | Cycles | Stress range (Mpa) | current total # cycles | Damage |
|---|---|---|---|---|---|---|
| | Stress spectrum BS  point 1 | | | | | |
| 1 | 54.893 | 52.92 | 3 | 2 | 3.94E+06 | 0.00 |
| 2 | 59.082 | 53.563 | 6 | 6 | 7.87E+06 | 0.01 |
| 3 | 62.314 | 59.684 | 13 | 3 | 1.71E+07 | 0.00 |
| 4 | 78.31 | 73.018 | 4 | 5 | 5.25E+06 | 0.01 |
| 5 | 86.314 | 82.253 | 20 | 4 | 2.62E+07 | 0.02 |
| 6 | 92.63 | 50.4 | 1 | 42 | 1.31E+06 | 1.06 |
| Total damage | | | | | | **1.1041** |

| block # | Max (Mpa) | Min (Mpa) | Cycles | Stress range (Mpa) | current total # cycles | Damage |
|---|---|---|---|---|---|---|
| | Stress spectrum BS point 2 | | | | | |
| 1 | -5.358 | -8.115 | 10 | 3 | 1.31E+07 | 0.00 |
| 2 | -2.115 | -5.26 | 2 | 3 | 2.62E+06 | 0.00 |
| 3 | 1.616 | -1.984 | 13 | 4 | 1.71E+07 | 0.01 |
| 4 | 4.625 | -3.665 | 2 | 8 | 2.62E+06 | 0.02 |
| 5 | 4.784 | -0.659 | 10 | 5 | 1.31E+07 | 0.02 |
| 6 | 8.01 | 5.84 | 1 | 2 | 1.31E+06 | 0.00 |
| 7 | 11.815 | 7.768 | 4 | 4 | 5.25E+06 | 0.00 |
| 8 | 14.588 | 10.772 | 5 | 4 | 6.56E+06 | 0.00 |
| 9 | 15.46 | -15.86 | 1 | 31 | 1.31E+06 | 0.43 |
| Total damage | | | | | | **0.4909** |

| block # | Max (Mpa) | Min (Mpa) | Cycles | Stress range (Mpa) | current total # cycles | Damage |
|---|---|---|---|---|---|---|
| | Stress spectrum BS point 3 | | | | | |
| 1 | 24.897 | 23.18 | 4 | 2 | 5.25E+06 | 0.00 |
| 2 | 29.064 | 27.058 | 13 | 2 | 1.71E+07 | 0.00 |
| 3 | 29.965 | 28.525 | 2 | 1 | 2.62E+06 | 0.00 |
| 4 | 44.403 | 41.846 | 22 | 3 | 2.89E+07 | 0.01 |
| 5 | 47.2 | 18.86 | 1 | 28 | 1.31E+06 | 0.32 |
| Total damage | | | | | | **0.3271** |

| block # | Max (Mpa) | Min (Mpa) | Cycles | Stress range (Mpa) | current total # cycles | Damage |
|---|---|---|---|---|---|---|
| | Stress spectrum BS point 4 | | | | | |
| 1 | 18.36 | 17.97 | 1 | 0 | 1.31E+06 | 0.00 |
| 2 | 27.438 | 26.222 | 16 | 1 | 2.10E+07 | 0.00 |
| 3 | 31.12 | 29.735 | 2 | 1 | 2.62E+06 | 0.00 |
| 4 | 31.245 | 24.88 | 2 | 6 | 2.62E+06 | 0.01 |
| 5 | 46.085 | 43.659 | 22 | 2 | 2.89E+07 | 0.00 |
| 6 | 49.08 | 17.1 | 1 | 32 | 1.31E+06 | 0.46 |
| Total damage | | | | | | **0.4721** |

**Table 57: Fatigue damage calculation sheet- backstay weld interface**

The following table present the stress range, counted cycles and damage calculation at the left pylon.

| | Stress spectrum Pyl_L point 1 | | | | | |
|---|---|---|---|---|---|---|
| block # | Max (Mpa) | Min (Mpa) | Cycles | Stress range (Mpa) | current total # cycles | Damage |
| 1 | -32,413 | -33,978 | 17 | 2 | 2,23E+07 | 0,0009 |
| 2 | -22,422 | -22,925 | 4 | 1 | 5,25E+06 | 0,0000 |
| 3 | -20,252 | -22,243 | 6 | 2 | 7,87E+06 | 0,0007 |
| 4 | -20,192 | -20,502 | 11 | 0 | 1,44E+07 | 0,0000 |
| 5 | -15,06 | -35,88 | 1 | 21 | 1,31E+06 | 0,1269 |
| | Total damage | | | | | **0,1285** |

| | Stress spectrum Pyl_L point 2 | | | | | |
|---|---|---|---|---|---|---|
| block # | Max (Mpa) | Min (Mpa) | Cycles | Stress range (Mpa) | current total # cycles | Damage |
| 1 | -47,553 | -50,865 | 21 | 3 | 2,76E+07 | 0,0107 |
| 2 | -32,12 | -32,572 | 5 | 0 | 6,56E+06 | 0,0000 |
| 3 | -30,201 | -33,137 | 13 | 3 | 1,71E+07 | 0,0046 |
| 4 | -26,13 | -26,995 | 2 | 1 | 2,62E+06 | 0,0000 |
| 5 | -22 | -52,75 | 1 | 31 | 1,31E+06 | 0,4089 |
| | Total damage | | | | | **0,4243** |

| | Stress spectrum Pyl_L point 3 | | | | | |
|---|---|---|---|---|---|---|
| block # | Max (Mpa) | Min (Mpa) | Cycles | Stress range (Mpa) | current total # cycles | Damage |
| 1 | -41,49 | -45,17 | 1 | 4 | 1,31E+06 | 0,0007 |
| 2 | -36,377 | -44,629 | 13 | 8 | 1,71E+07 | 0,1027 |
| 3 | -32,37 | -37,08 | 1 | 5 | 1,31E+06 | 0,0015 |
| 4 | -27,7 | -34,335 | 2 | 7 | 2,62E+06 | 0,0082 |
| 5 | -22,725 | -27,056 | 17 | 4 | 2,23E+07 | 0,0194 |
| 6 | -16,945 | -23,662 | 8 | 7 | 1,05E+07 | 0,0341 |
| 7 | -12,537 | -15,867 | 3 | 3 | 3,94E+06 | 0,0016 |
| 8 | -9,44 | -16,25 | 1 | 7 | 1,31E+06 | 0,0044 |
| 9 | -7,01 | -50,12 | 1 | 43 | 1,31E+06 | 1,1267 |
| | Total damage | | | | | **1,2994** |

| | Stress spectrum Pyl_L point 4 | | | | | |
|---|---|---|---|---|---|---|
| block # | Max (Mpa) | Min (Mpa) | Cycles | Stress range (Mpa) | current total # cycles | Damage |
| 1 | -53,944 | -58,726 | 8 | 5 | 1,05E+07 | 0,0123 |
| 2 | -48,34 | -52,78 | 2 | 4 | 2,62E+06 | 0,0025 |
| 3 | -39,848 | -43,902 | 9 | 4 | 1,18E+07 | 0,0084 |
| 4 | -34,466 | -42,351 | 15 | 8 | 1,97E+07 | 0,1034 |
| 5 | -27,273 | -29,886 | 9 | 3 | 1,18E+07 | 0,0023 |
| 6 | -24,278 | -30,08 | 4 | 6 | 5,25E+06 | 0,0110 |
| 7 | -20,86 | -21,28 | 1 | 0 | 1,31E+06 | 0,0000 |
| 8 | -14,49 | -61,96 | 1 | 47 | 1,31E+06 | 1,5043 |
| | Total damage | | | | | **1,6442** |

**Table 58: Fatigue damage calculation sheet- left pylon weld interface**

The following table present the stress range, counted cycles and damage calculation at the right pylon.

| block # | Max (Mpa) | Min (Mpa) | Cycles | Stress range (Mpa) | current total # cycles | Damage |
|---|---|---|---|---|---|---|
| | Stress spectrum Pyl_R point 1 | | | | | |
| 1 | -47,398 | -50,994 | 19 | 4 | 2,49E+07 | 0,0124 |
| 2 | -32,95 | -33,56 | 1 | 1 | 1,31E+06 | 0,0000 |
| 3 | -30,653 | -33,374 | 14 | 3 | 1,84E+07 | 0,0040 |
| 4 | -28,828 | -30,283 | 4 | 1 | 5,25E+06 | 0,0002 |
| 5 | -23,37 | -54 | 1 | 31 | 1,31E+06 | 0,4041 |
| Total damage | | | | | | 0,4207 |

| block # | Max (Mpa) | Min (Mpa) | Cycles | Stress range (Mpa) | current total # cycles | Damage |
|---|---|---|---|---|---|---|
| | Stress spectrum Pyl_R point 2 | | | | | |
| 1 | -30,961 | -32,405 | 17 | 1 | 2,23E+07 | 0,0007 |
| 2 | -21,673 | -22,152 | 15 | 0 | 1,97E+07 | 0,0000 |
| 3 | -19,233 | -22,35 | 3 | 3 | 3,94E+06 | 0,0013 |
| 4 | -18,678 | -19,14 | 4 | 0 | 5,25E+06 | 0,0000 |
| 5 | -16,04 | -34,57 | 1 | 19 | 1,31E+06 | 0,0895 |
| Total damage | | | | | | 0,0915 |

| block # | Max (Mpa) | Min (Mpa) | Cycles | Stress range (Mpa) | current total # cycles | Damage |
|---|---|---|---|---|---|---|
| | Stress spectrum Pyl_R point 3 | | | | | |
| 1 | -37,439 | -45,223 | 12 | 8 | 1,57E+07 | 0,0796 |
| 2 | -33,58 | -38,163 | 3 | 5 | 3,94E+06 | 0,0041 |
| 3 | -29,795 | -32,825 | 2 | 3 | 2,62E+06 | 0,0008 |
| 4 | -23,324 | -27,269 | 16 | 4 | 2,10E+07 | 0,0138 |
| 5 | -17,496 | -24,23 | 7 | 7 | 9,19E+06 | 0,0301 |
| 6 | -13,318 | -17,913 | 6 | 5 | 7,87E+06 | 0,0082 |
| 7 | -8,12 | -50,02 | 1 | 42 | 1,31E+06 | 1,0345 |
| Total damage | | | | | | 1,1710 |

| block # | Max (Mpa) | Min (Mpa) | Cycles | Stress range (Mpa) | current total # cycles | Damage |
|---|---|---|---|---|---|---|
| | Stress spectrum Pyl_R point 4 | | | | | |
| 1 | -51,705 | -56,794 | 8 | 5 | 1,05E+07 | 0,0148 |
| 2 | -42,558 | -50,135 | 4 | 8 | 5,25E+06 | 0,0245 |
| 3 | -37,974 | -43,639 | 13 | 6 | 1,71E+07 | 0,0332 |
| 4 | -33,74 | -48,35 | 1 | 15 | 1,31E+06 | 0,0439 |
| 5 | -32,869 | -41,176 | 7 | 8 | 9,19E+06 | 0,0564 |
| 6 | -27,677 | -31,567 | 15 | 4 | 1,97E+07 | 0,0124 |
| 7 | -22,76 | -23,21 | 1 | 0 | 1,31E+06 | 0,0000 |
| 8 | -15,64 | -59,21 | 1 | 44 | 1,31E+06 | 1,1632 |
| Total damage | | | | | | 1,3484 |

**Table 59: Fatigue damage calculation sheet- right pylon weld interface**

# Appendix C Fatigue calculation according to NEN crane standard

This chapter discusses all the fatigue calculation steps according to the NEN2018 crane standard.

### 1.  vertical load due to hoisting

The inertia forces in a vertical direction from the load hoisting movement, including those which occur when taking up and setting down the load, make it necessary to take into account more than the weight of the hoisting load. The type of crane investigated is a floating harbor crane intended for grab operations based on crane group 5 and hoisting class B.

$$m_{hoist} = \text{Capacity at the ropes (grab+load)} = 25t$$
$$F_{static,hoist} = m_{hoist} * g = 245.25kN$$
$$\phi_{load} = 1.6$$
$$m_{hoist} = 25t$$
$$m_{hoist,\phi} = m_{hoist} \times \phi = 40t$$
$$F_{dynamic,hoist} = m_{hoist,\phi} * g = 392.4kN$$

### 2.  Horizontal load resulting from inertia forces from crane slewing

Due to slewing acceleration and deceleration of the crane, a horizontal side load is exerted on the boom. The following method from the standard is used.

```
The inertia force F_hc to be calculated at a construction part
with mass m is supplied by the expression:

     F_hc = 2 m · a,

in which a is the acceleration of the construction part consi-
dered, which corresponds with the acceleration a_h, measured at
the point of suspension of the load.
The calculation is based on the following values of the accelera-
tion a_h, measured at the point of suspension of the load, if the
maximum starting couple is unknown:
-- crane movement          : 0,5 m/s²
-- crab movement           : 0,5 m/s²
-- luffing movement        : 0,6 m/s²
-- slewing movement        : 0,7 m/s²
```

```
Note
In using the alternative method for the calculation of the
inertia forces, as mentioned in appendix A these forces
do not need to be multiplied by the group factor M.
```

$$a_{,\tan gential,slew} = \frac{\omega * R}{t_{,acc}} = \frac{1.5*(2\pi/60)*40}{6} = 1.0472 m/s^2$$
$$F_{x,,\tan gential,slew} = 2*m_{hoist}*a_{,\tan gential,slew} = 2*25*1.0472 = 52.05kN$$

### 3.  Horizontal load resulting from centrifugal forces from crane slewing

$$a_{,normal} = \omega^2 * R = (1.5*(2\pi/60))^2 *40 = 0.98 m/s^2$$
$$F_{z,,centrifugal,slew} = 2*m_{hoist}*a_{,normal,slew} = 2*25*0.98 = 49kN$$

### 4.  Horizontal load resulting from inertia forces from crane luffing

$$a_{,normal,luffing} = 0.25 m/s^2$$
$$F_{z,,inertia,luffing} = 2*m_{hoist}*a_{,normal,luffing} = 2*25*0.25 = 12.5kN$$

**5. Pontoon motion**

$$g^*_{pontoon,motion} = g * M = 9.81 * 1.15 = 11.28 \frac{m}{s^2}$$

## Allowable static stress check for total crane

The following figure and table show the effect of gravity load g=9.81m/s^2 on the structure and the resulting reaction forces at the supports.
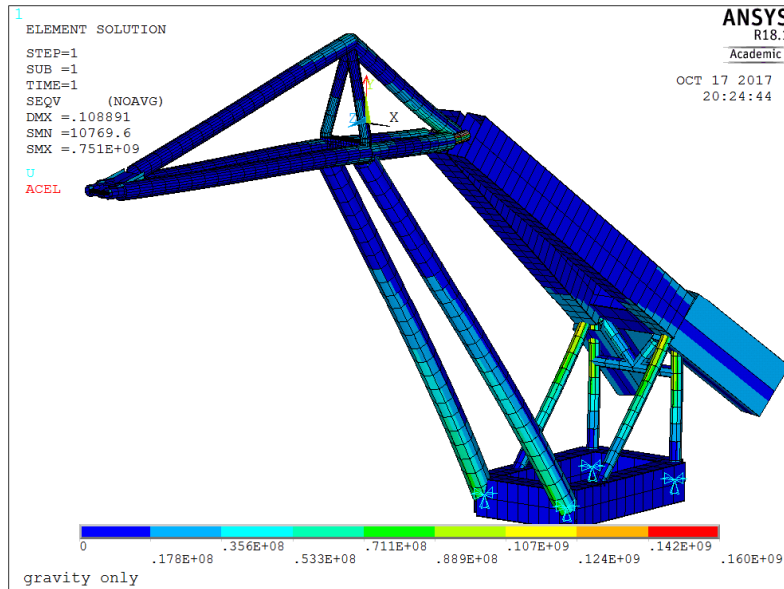


**Figure 129: Equivalent stress check gravity load**

```
 PRINT F    REACTION SOLUTIONS PER NODE

  ***** POST1 TOTAL REACTION SOLUTION LISTING *****

 LOAD STEP=    1  SUBSTEP=    1
  TIME=    1.0000      LOAD CASE=   0

 THE FOLLOWING X,Y,Z SOLUTIONS ARE IN THE GLOBAL COORDINATE SYSTEM

   NODE      FX         FY         FZ
   325   33200.     0.14020E+007 -927.99
   350  -33200.     0.14020E+007 -927.99
   500   658.57     0.63244E+006  927.99
   509  -658.57     0.63244E+006  927.99

 TOTAL VALUES
 VALUE  -0.32843E-006 0.40689E+007 -0.53637E-004
```

**Figure 130: Reaction forces gravity load**

The following figure and table show the effect of hoisting a load on the structure and the resulting reaction forces at the supports.
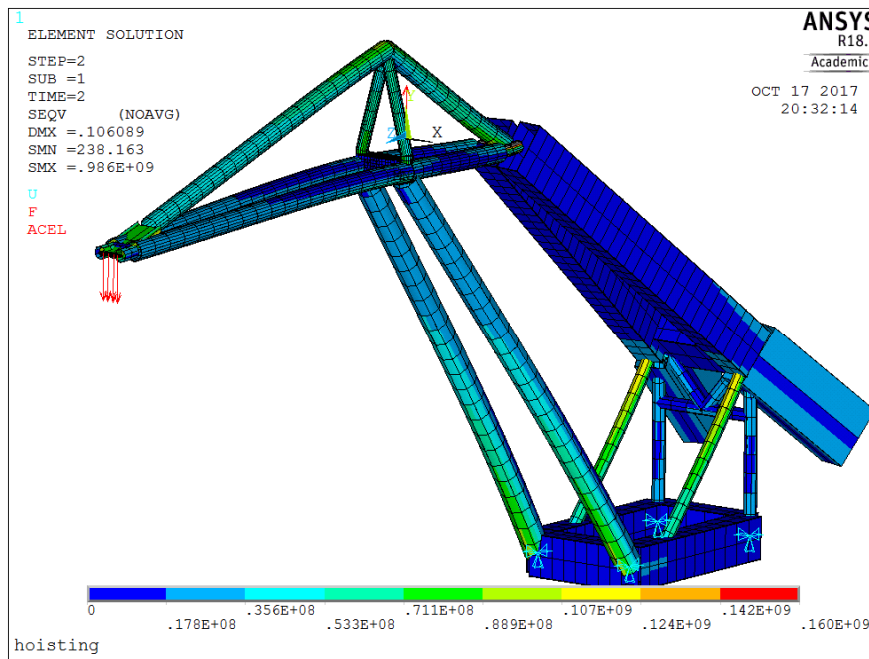


**Figure 131: Equivalent stress check hoisting load**

```
PRINT F    REACTION SOLUTIONS PER NODE

 ***** POST1 TOTAL REACTION SOLUTION LISTING *****

 LOAD STEP=    2  SUBSTEP=     1
  TIME=    2.0000     LOAD CASE=   0

 THE FOLLOWING X,Y,Z SOLUTIONS ARE IN THE GLOBAL COORDINATE SYSTEM

   NODE      FX         FY         FZ
   325   70646.      0.23419E+007 0.10971E+006
   350  -70646.      0.23419E+007 0.10971E+006
   500  -2641.2     -0.11122E+006-0.10971E+006
   509   2641.2     -0.11122E+006-0.10971E+006


 TOTAL VALUES
 VALUE  -0.26049E-006 0.44613E+007 0.44506E-004
```

**Figure 132: Reaction forces hoisting load**

The following figure and table show the effect which the 42kN centrifugal force has on the structure and the resulting reaction forces at the supports.
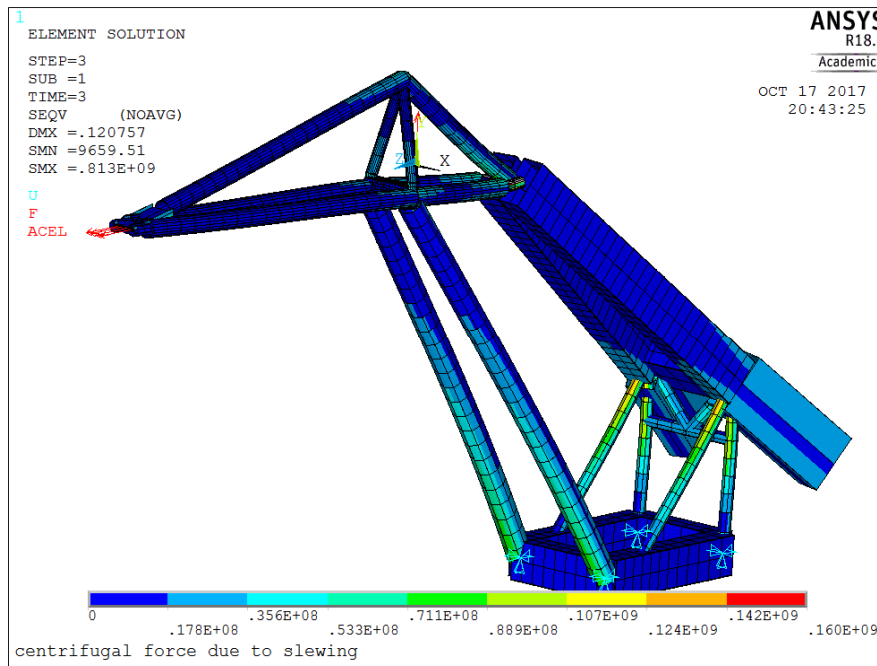


**Figure 133: Equivalent stress check centrifugal load due to slewing**

```
PRINT F    REACTION SOLUTIONS PER NODE

 ***** POST1 TOTAL REACTION SOLUTION LISTING *****

 LOAD STEP=    3  SUBSTEP=    1
  TIME=   3.0000     LOAD CASE=   0

 THE FOLLOWING X,Y,Z SOLUTIONS ARE IN THE GLOBAL COORDINATE SYSTEM

    NODE     FX        FY        FZ
    325   34100.    0.14608E+007 -26207.
    350  -34100.    0.14608E+007 -26207.
    500   178.35    0.57370E+006  1706.6
    509  -178.35    0.57370E+006  1706.6


 TOTAL VALUES
 VALUE  -0.36788E-006 0.40689E+007 -49000.
```

**Figure 134: Reaction forces centrifugal force due to slewing**

The following figure and table show the effect which the lateral inertia load of 52kN on the structure and the resulting reaction forces at the supports.
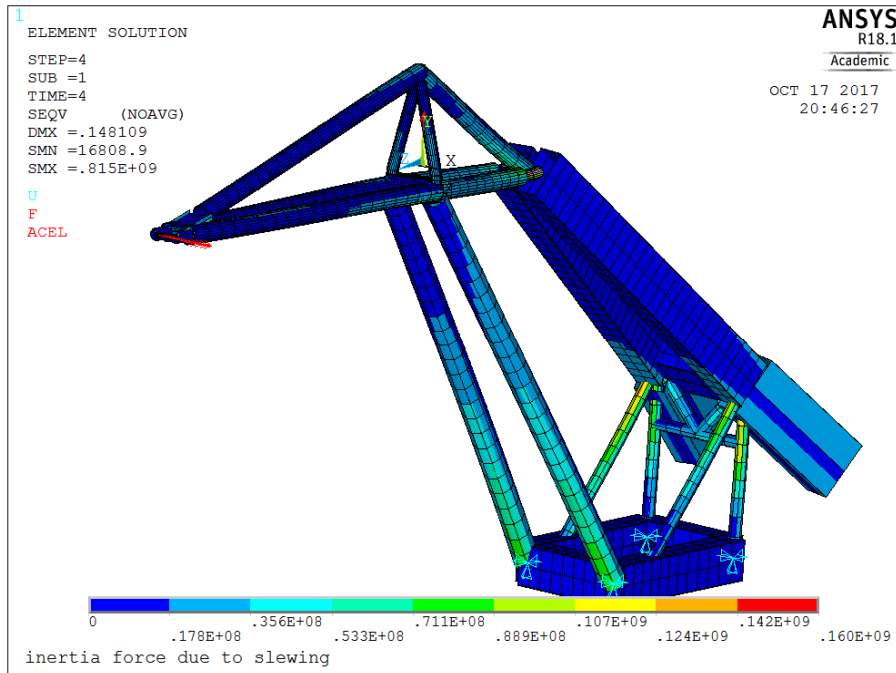


**Figure 135: Equivalent stress check inertia load due to slewing**

```
PRINT F    REACTION SOLUTIONS PER NODE

  ***** POST1 TOTAL REACTION SOLUTION LISTING *****

 LOAD STEP=    4  SUBSTEP=    1
  TIME=    4.0000     LOAD CASE=   0

 THE FOLLOWING X,Y,Z SOLUTIONS ARE IN THE GLOBAL COORDINATE SYSTEM

   NODE     FX        FY         FZ
   325  -862.40    0.13237E+007-0.27122E+006
   350  -67262.    0.14803E+007 0.26936E+006
   500   8696.0    0.49455E+006 -42765.
   509   7378.9    0.77033E+006  44621.


 TOTAL VALUES
 VALUE  -52050.     0.40689E+007-0.53278E-004
```

**Figure 136: Reaction forces inertia load due to slewing**

The following figure and table show the effect which the 12.5kN inertia load effect on the structure and the resulting reaction forces at the supports.
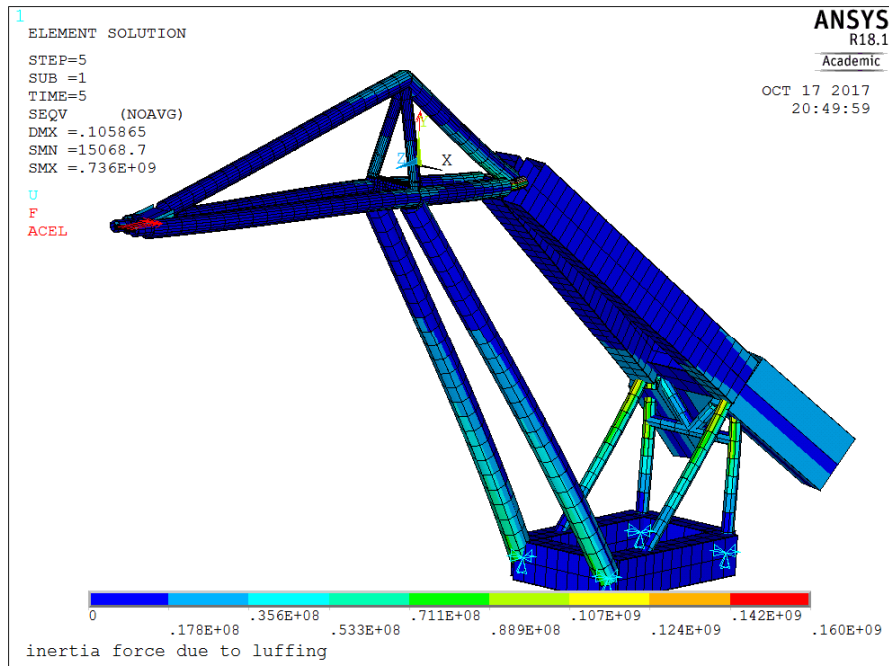


**Figure 137: Equivalent stress check inertia load due to luffing**

```
PRINT F    REACTION SOLUTIONS PER NODE

 ***** POST1 TOTAL REACTION SOLUTION LISTING *****

 LOAD STEP=    5  SUBSTEP=    1
  TIME=   5.0000     LOAD CASE=   0

 THE FOLLOWING X,Y,Z SOLUTIONS ARE IN THE GLOBAL COORDINATE SYSTEM

   NODE      FX        FY         FZ
   325   32970.     0.13870E+007  5520.6
   350  -32970.     0.13870E+007  5520.6
   500   781.08     0.64743E+006  729.37
   509  -781.08     0.64743E+006  729.37

 TOTAL VALUES
 VALUE  -0.31932E-006 0.40689E+007  12500.
```

**Figure 138: Reaction forces inertia load due to luffing**

The pontoon pendulum motion is simulated by multiplying the gravity load in the vertical direction with the group factor, seen in Figure 139 and Figure 140.
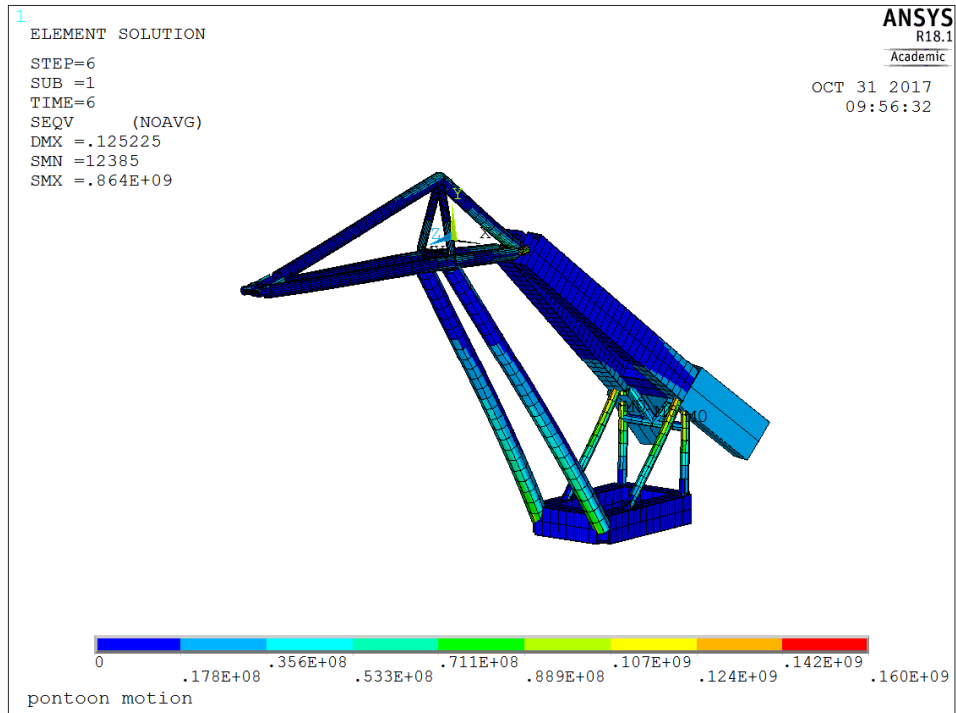


**Figure 139: Pontoon pendulum motion load**
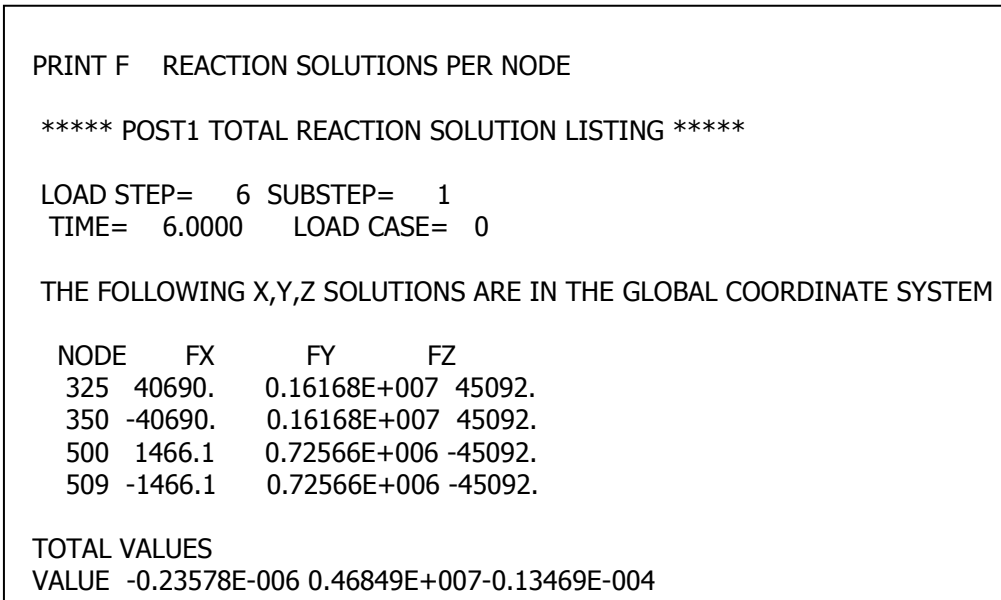


**Figure 140: Reaction forces pontoon motion**

## Stress analysis results

The stress components are the results calculated using the FEM model. Then the nominal stress at each point is calculated. The following table shows the calculated stress components and nominal stresses for the four measurement points of the backstay.

|  |  | gravity | hoisting load(y) | inertia load(x) | centrifugal load(z) | inertia load (z) | pontoon (y) |
|---|---|---|---|---|---|---|---|
| stress components | **Sax** | 9.94E+06 | 5.48E+07 | 9.78E+06 | 9.94E+06 | 9.98E+06 | 1.14E+07 |
|  | **Sbny** | 8.21E+04 | 7.90E+04 | 9.12E+04 | -8.51E+06 | 7.98E+04 | 9.46E+04 |
|  | **Sbnz** | 3.35E+07 | 4.50E+07 | 3.51E+07 | 3.35E+07 | 3.30E+07 | 3.85E+07 |
|  |  |  |  |  |  |  |  |
| nominal stress = combined stress components | **point 1** | 4.34E+07 | 9.98E+07 | 4.49E+07 | 4.34E+07 | 4.30E+07 | 4.99E+07 |
|  | **point 2** | -2.35E+07 | 9.82E+06 | -2.53E+07 | -2.35E+07 | -2.31E+07 | -2.70E+07 |
|  | **point 3** | 1.00E+07 | 5.49E+07 | 9.87E+06 | 1.42E+06 | 1.01E+07 | 1.15E+07 |
|  | **point 4** | 9.86E+06 | 5.47E+07 | 9.69E+06 | 1.85E+07 | 9.90E+06 | 1.13E+07 |

**Table 60: Stress results weld interface backstay**

The following table shows the calculated stress components and nominal stresses for the four measurement points of the left pylon.

|  |  | gravity | hoisting load(y) | inertia load(x) | centrifugal load(z) | inertia load (z) | pontoon (y) |
|---|---|---|---|---|---|---|---|
| stress components | **Sax** | -1.26E+07 | -5.04E+07 | -1.27E+07 | -1.55E+07 | -1.26E+07 | -1.45E+07 |
|  | **Sbny** | -1.05E+07 | -1.54E+06 | -1.32E+07 | -1.06E+07 | -9.80E+06 | -1.21E+07 |
|  | **Sbnz** | 2.26E+06 | 1.06E+07 | 2.26E+06 | 1.65E+06 | 2.26E+06 | 2.60E+06 |
|  |  |  |  |  |  |  |  |
| nominal stress = combined stress components | **point 1** | -1.03E+07 | -3.98E+07 | -1.04E+07 | -1.39E+07 | -1.03E+07 | -1.19E+07 |
|  | **point 2** | -1.48E+07 | -6.10E+07 | -1.49E+07 | -1.72E+07 | -1.48E+07 | -1.71E+07 |
|  | **point 3** | -2.31E+07 | -5.19E+07 | -2.59E+07 | -2.61E+07 | -2.24E+07 | -2.66E+07 |
|  | **point 4** | -2.09E+06 | -4.89E+07 | 5.73E+05 | -4.90E+06 | -2.77E+06 | -2.40E+06 |

**Table 61: Stress results weld interface left pylon**

The following table shows the calculated stress components and nominal stresses for the four measurement points of the right pylon.

|  |  | gravity | hoisting load(y) | inertia load(x) | centrifugal load(z) | inertia load (z) | pontoon (y) |
|---|---|---|---|---|---|---|---|
| stress components | **Sax** | -1.26E+07 | -5.04E+07 | -1.27E+07 | -9.66E+06 | -1.26E+07 | -1.45E+07 |
|  | **Sbny** | -1.05E+07 | -1.54E+06 | -1.32E+07 | -1.04E+07 | -9.80E+06 | -1.21E+07 |
|  | **Sbnz** | -2.26E+06 | -1.06E+07 | -2.26E+06 | -2.87E+06 | -2.26E+06 | -2.60E+06 |
|  |  |  |  |  |  |  |  |
| nominal stress = combined stress components | **point 1** | -1.48E+07 | -6.10E+07 | -1.49E+07 | -1.25E+07 | -1.48E+07 | -1.71E+07 |
|  | **point 2** | -1.03E+07 | -3.98E+07 | -1.04E+07 | -6.79E+06 | -1.03E+07 | -1.19E+07 |
|  | **point 3** | -2.31E+07 | -5.19E+07 | -2.59E+07 | -2.00E+07 | -2.24E+07 | -2.66E+07 |
|  | **point 4** | -2.09E+06 | -4.89E+07 | 5.73E+05 | 7.24E+05 | -2.77E+06 | -2.40E+06 |

**Table 62: Stress results weld interface right pylon**

The calculated stress values for all the 15 defined load cases for each cross sectional point in the forestay is shown in the following table. The highlighted values represent the expected minimum and maximum stress value and are used to calculate the stress range and stress ratio value.

| | point 1 | point 2 | point 3 | point 4 |
|---|---|---|---|---|
| **stresses for each load case** | 3.82E+07 | -2.12E+07 | 8.63E+06 | 8.36E+06 |
| | 1.76E+08 | -4.31E+07 | 6.68E+07 | 6.59E+07 |
| | 7.65E+07 | -4.27E+07 | 1.72E+07 | 1.66E+07 |
| | 7.63E+07 | -4.23E+07 | 4.32E+06 | 2.97E+07 |
| | 7.63E+07 | -4.23E+07 | 1.73E+07 | 1.67E+07 |
| | 2.14E+08 | -6.47E+07 | 7.53E+07 | 7.42E+07 |
| | 2.52E+08 | -8.58E+07 | 7.10E+07 | 9.55E+07 |
| | 1.37E+08 | -2.16E+07 | 5.82E+07 | 5.77E+07 |
| | 1.76E+08 | -4.28E+07 | 5.39E+07 | 7.90E+07 |
| | 2.14E+08 | -6.42E+07 | 7.54E+07 | 7.43E+07 |
| | 2.52E+08 | -8.57E+07 | 8.40E+07 | 8.26E+07 |
| | 2.90E+08 | -1.07E+08 | 7.97E+07 | 1.04E+08 |
| | 1.38E+08 | -2.20E+07 | 5.81E+07 | 5.75E+07 |
| | 9.93E+07 | -5.05E+05 | 4.96E+07 | 4.93E+07 |
| | 1.37E+08 | -2.17E+07 | 4.52E+07 | 7.06E+07 |

**Table 63: stresses for each load case at Forestay**

| | point 1 | point 2 | point 3 | point 4 |
|---|---|---|---|---|
| stresses for each load case | 4.34E+07 | -2.35E+07 | 1.00E+07 | 9.86E+06 |
| | 1.93E+08 | -4.07E+07 | 7.64E+07 | 7.59E+07 |
| | 8.83E+07 | -4.88E+07 | 1.99E+07 | 1.95E+07 |
| | 8.68E+07 | -4.70E+07 | 1.14E+07 | 2.83E+07 |
| | 8.64E+07 | -4.66E+07 | 2.01E+07 | 1.98E+07 |
| | 2.38E+08 | -6.61E+07 | 8.63E+07 | 8.56E+07 |
| | 2.81E+08 | -8.96E+07 | 8.77E+07 | 1.04E+08 |
| | 1.48E+08 | -1.54E+07 | 6.66E+07 | 6.62E+07 |
| | 1.92E+08 | -3.89E+07 | 6.80E+07 | 8.47E+07 |
| | 2.36E+08 | -6.38E+07 | 8.65E+07 | 8.58E+07 |
| | 2.81E+08 | -8.91E+07 | 9.64E+07 | 9.55E+07 |
| | 3.24E+08 | -1.13E+08 | 9.78E+07 | 1.14E+08 |
| | 1.50E+08 | -1.77E+07 | 6.64E+07 | 6.60E+07 |
| | 1.05E+08 | 7.64E+06 | 5.65E+07 | 5.63E+07 |
| | 1.49E+08 | -1.59E+07 | 5.79E+07 | 7.48E+07 |

**Table 64: stresses for each load case at backstay**

|  | point 1 | point 2 | point 3 | point 4 |
|---|---|---|---|---|
| stresses for each load case | -1.03E+07 | -1.48E+07 | -2.31E+07 | -2.09E+06 |
|  | -6.21E+07 | -9.29E+07 | -1.02E+08 | -5.34E+07 |
|  | -2.08E+07 | -2.98E+07 | -4.90E+07 | -1.52E+06 |
|  | -2.42E+07 | -3.20E+07 | -4.92E+07 | -6.99E+06 |
|  | -2.06E+07 | -2.97E+07 | -4.55E+07 | -4.86E+06 |
|  | -7.25E+07 | -1.08E+08 | -1.28E+08 | -5.28E+07 |
|  | -8.64E+07 | -1.25E+08 | -1.54E+08 | -5.77E+07 |
|  | -5.16E+07 | -7.80E+07 | -7.57E+07 | -5.39E+07 |
|  | -6.55E+07 | -9.51E+07 | -1.02E+08 | -5.88E+07 |
|  | -7.24E+07 | -1.08E+08 | -1.24E+08 | -5.61E+07 |
|  | -8.28E+07 | -1.23E+08 | -1.50E+08 | -5.55E+07 |
|  | -9.67E+07 | -1.40E+08 | -1.76E+08 | -6.05E+07 |
|  | -5.17E+07 | -7.81E+07 | -7.92E+07 | -5.06E+07 |
|  | -4.13E+07 | -6.31E+07 | -5.33E+07 | -5.12E+07 |
|  | -5.52E+07 | -8.03E+07 | -7.94E+07 | -5.61E+07 |

**Table 65: stresses for each load case at left pylon**

|  | point 1 | point 2 | point 3 | point 4 |
|---|---|---|---|---|
| stresses for each load case | -1.48E+07 | -1.03E+07 | -2.31E+07 | -2.09E+06 |
|  | -9.29E+07 | -6.21E+07 | -1.02E+08 | -5.34E+07 |
|  | -2.98E+07 | -2.08E+07 | -4.90E+07 | -1.52E+06 |
|  | -2.74E+07 | -1.71E+07 | -4.31E+07 | -1.37E+06 |
|  | -2.97E+07 | -2.06E+07 | -4.55E+07 | -4.86E+06 |
|  | -1.08E+08 | -7.25E+07 | -1.28E+08 | -5.28E+07 |
|  | -1.20E+08 | -7.93E+07 | -1.48E+08 | -5.21E+07 |
|  | -7.80E+07 | -5.16E+07 | -7.57E+07 | -5.39E+07 |
|  | -9.05E+07 | -5.84E+07 | -9.57E+07 | -5.32E+07 |
|  | -1.08E+08 | -7.24E+07 | -1.24E+08 | -5.61E+07 |
|  | -1.23E+08 | -8.28E+07 | -1.50E+08 | -5.55E+07 |
|  | -1.35E+08 | -8.96E+07 | -1.70E+08 | -5.48E+07 |
|  | -7.81E+07 | -5.17E+07 | -7.92E+07 | -5.06E+07 |
|  | -6.31E+07 | -4.13E+07 | -5.33E+07 | -5.12E+07 |
|  | -7.56E+07 | -4.81E+07 | -7.33E+07 | -5.04E+07 |

**Table 66: stresses for each load case at right pylon**

Stress plots

Figure 141 shows the cyclic stress plots at the forestay weld interface. Measurement points 1, 3 and 4 are subjected to a variable tensile stress range condition and at point 2 a compression stress range condition.
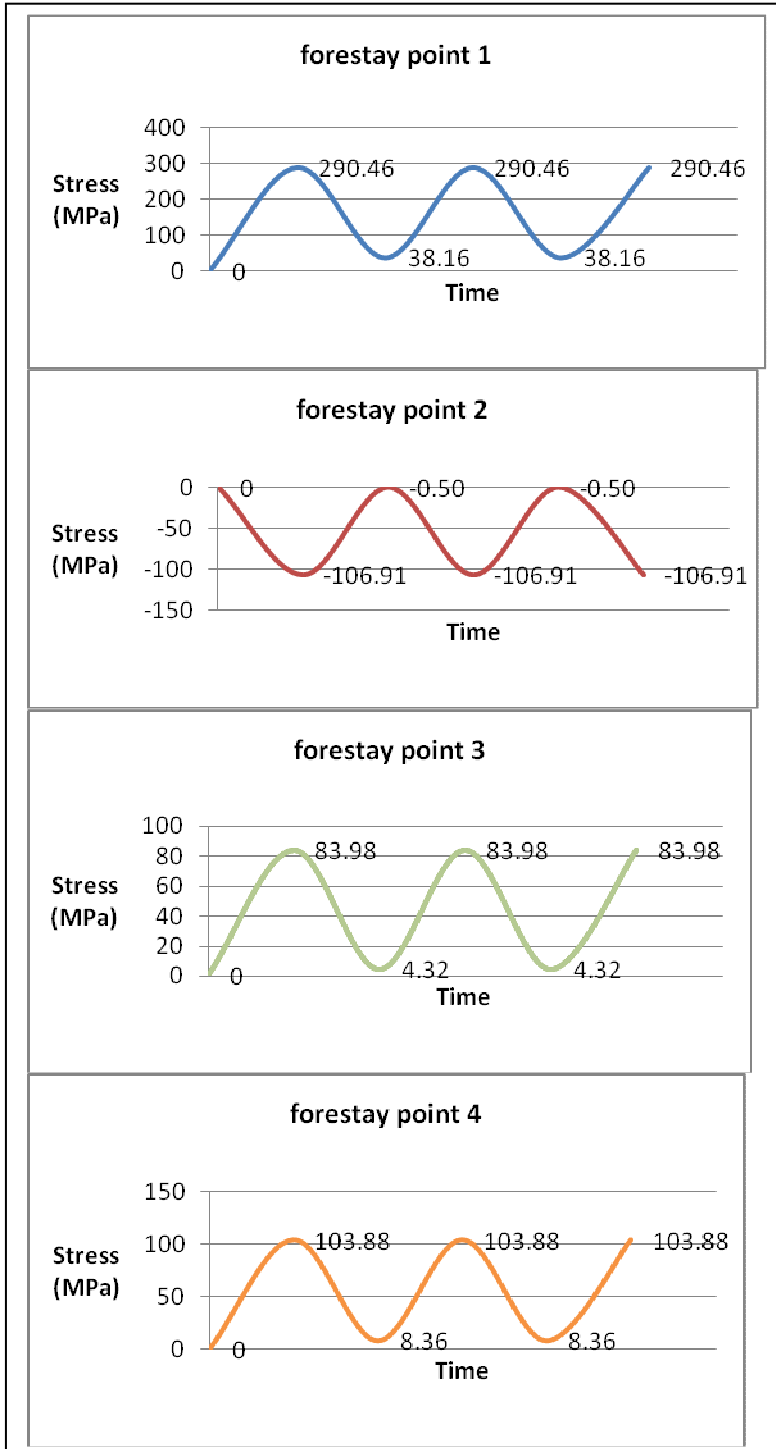


**Figure 141: Illustration cyclic stresses at the forestay weld interface**

Figure 142 shows the cyclic stress plots for Table 67 at the backstay weld interface. Measurement points 1, 3 and 4 are subjected to a variable tensile stress range condition and at point 2 an alternating compression stress range condition.

| | point 1 | point 2 | point 3 | point 4 |
|---|---|---|---|---|
| **Max stress** | 324,43 | -112,64 | 97,81 | 113,98 |
| **Min stress** | 43,39 | 7,64 | 10,02 | 9,86 |
| **Stress range** | 281,03 | 120,27 | 87,79 | 104,13 |
| **Kappa** | 0,1 | -0,1 | 0,1 | 0,1 |

**Table 67: Cyclic stresses-backstay weld interface**
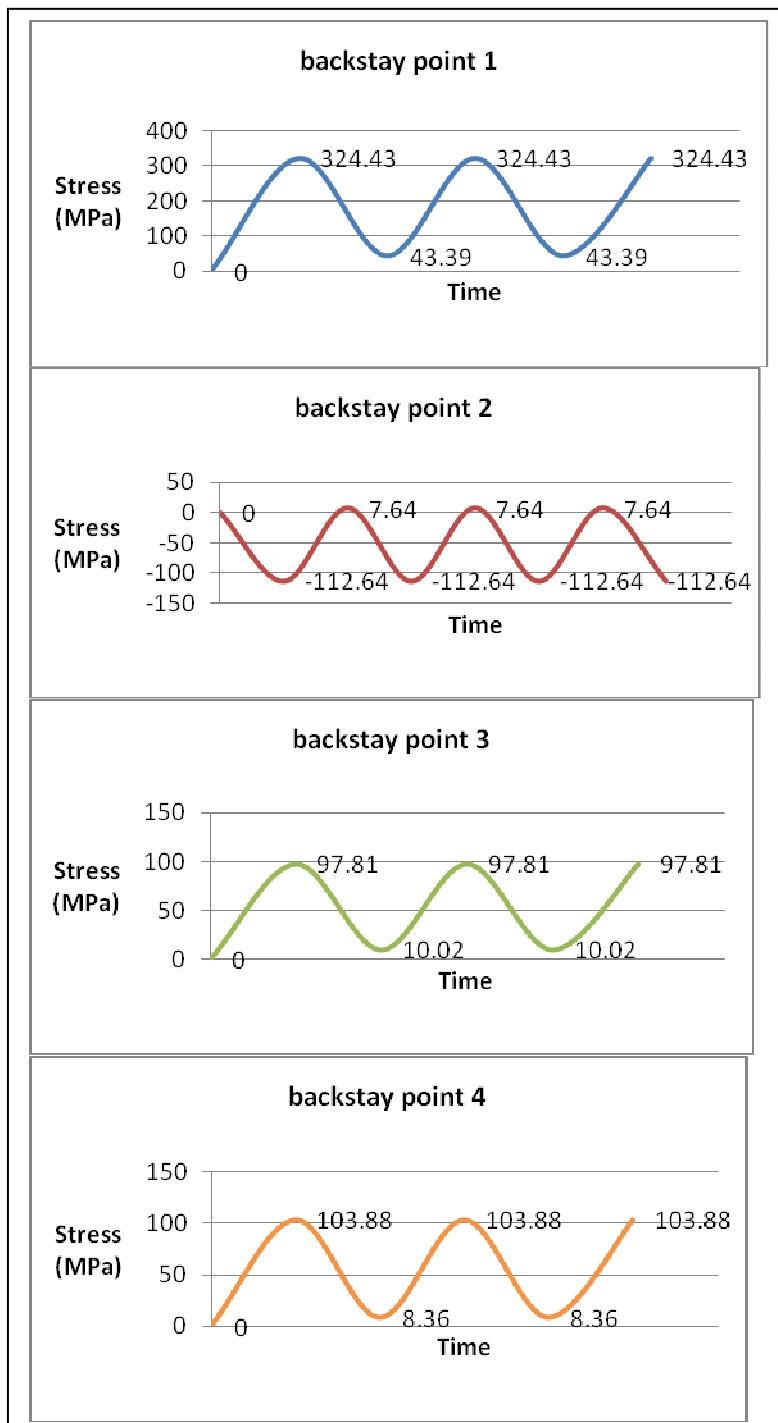


**Figure 142: Illustration cyclic stresses at the backstay weld interface**

Crane fatigue assessment using Multibody Dynamics and Finite Element Method

Figure 143 shows the cyclic stress plots for Table 68 at the left pylon weld interface. All measurement points are subjected to a variable compression stress range condition is calculated.

| | point 1 | point 2 | point 3 | point 4 |
|---|---|---|---|---|
| **Max stress** | -96,66 | -139,82 | -176,03 | -60,45 |
| **Min stress** | -10,33 | -14,85 | -23,09 | -1,52 |
| **Stress range** | 86,33 | 124,97 | 152,94 | 58,94 |
| **Kappa** | 0,1 | 0,1 | 0,1 | 0,0 |

**Table 68:Cyclic stresses-left pylon weld interface**
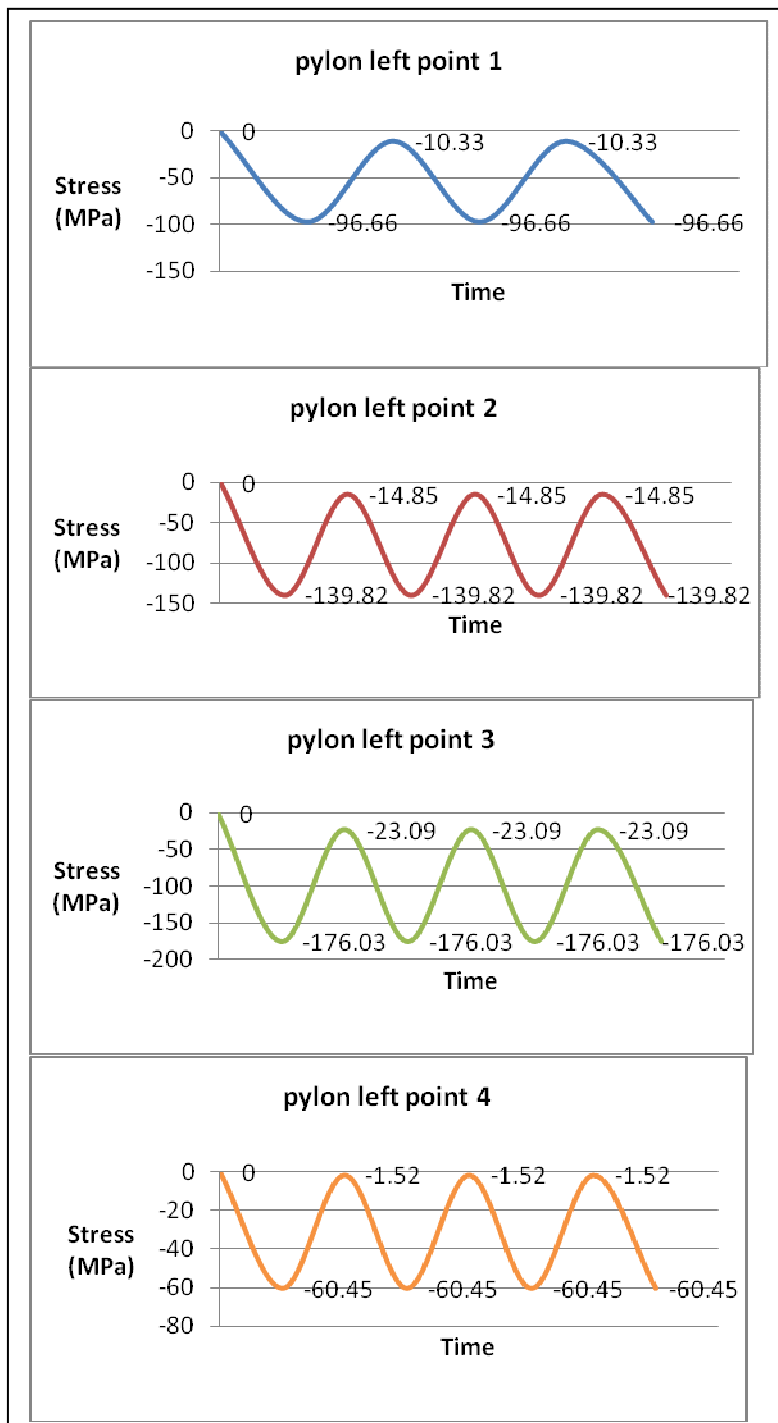


**Figure 143: Illustration cyclic stresses at the left pylon weld interface**

Figure 144 shows the cyclic stress plots for Table 69 at the right pylon weld interface. At all measurement points are subjected to a variable compression stress range condition.

|              | point 1 | point 2 | point 3 | point 4 |
|--------------|---------|---------|---------|---------|
| **Max stress**   | -135,17 | -89,58  | -169,92 | -56,12  |
| **Min stress**   | -14,85  | -10,33  | -23,09  | -1,37   |
| **Stress range** | 120,32  | 79,24   | 146,83  | 54,76   |
| **Kappa**        | 0,1     | 0,1     | 0,1     | 0,0     |

**Table 69: Cyclic stresses-right pylon weld interface**
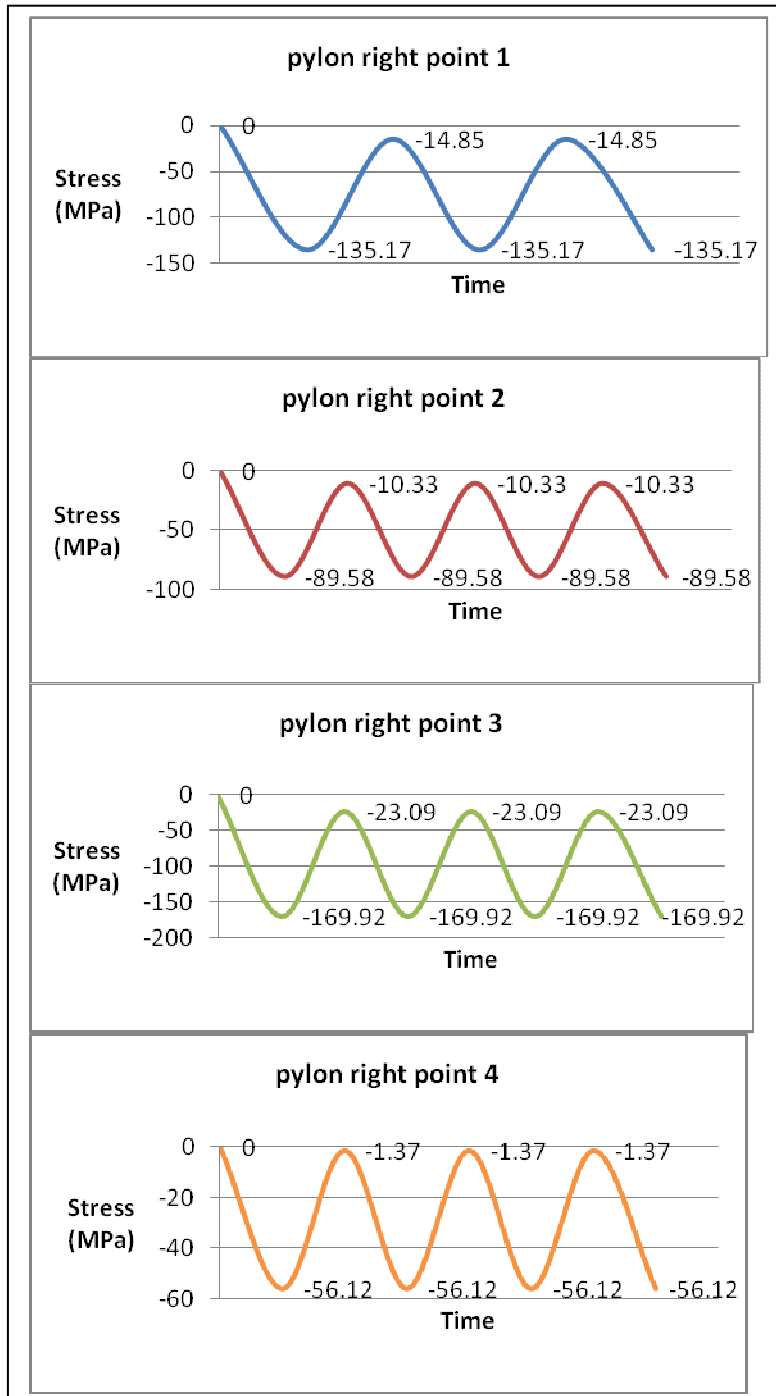


**Figure 144: Illustration cyclic stresses at the right pylon weld interface**

Crane fatigue assessment using Multibody Dynamics and Finite Element Method

## Allowable fatigue stress

| Crane or Element group | Material | Notch group | | | | |
|---|---|---|---|---|---|---|
| **5** | **API 5L grade B** | **K0** | **K1** | **K2** | **K3** | **K4** |
| χ values | -1,0 | 118,8 | 106,1 | 89,1 | 63,6 | 38,2 |
| | -0,9 | 123,7 | 110,5 | 92,8 | 66,3 | 39,8 |
| | -0,8 | 129,1 | 115,3 | 96,8 | 69,2 | 41,5 |
| | -0,7 | 135,0 | 120,5 | 101,2 | 72,3 | 43,4 |
| | -0,6 | 141,4 | 126,3 | 106,1 | 75,8 | 45,5 |
| | -0,5 | 148,5 | 132,6 | 111,4 | 79,5 | 47,7 |
| | -0,4 | 156,3 | 139,6 | 117,2 | 83,7 | 50,2 |
| | -0,3 | 161,0 | 147,3 | 123,7 | 88,4 | 53,0 |
| | -0,2 | 161,0 | 156,0 | 131,0 | 93,6 | 56,2 |
| | -0,1 | 161,0 | 161,0 | 139,2 | 99,4 | 59,7 |
| | 0,0 | 161,0 | 161,0 | 148,5 | 106,1 | 63,6 |
| | 0,1 | 161,0 | 161,0 | 156,6 | 113,5 | 69,1 |
| | 0,2 | 161,0 | 161,0 | 161,0 | 122,1 | 75,7 |
| | 0,3 | 161,0 | 161,0 | 161,0 | 132,1 | 83,6 |
| | 0,4 | 161,0 | 161,0 | 161,0 | 143,9 | 93,3 |
| | 0,5 | 161,0 | 161,0 | 161,0 | 158,0 | 105,6 |
| | 0,6 | 161,0 | 161,0 | 161,0 | 161,0 | 121,6 |
| | 0,7 | 161,0 | 161,0 | 161,0 | 161,0 | 143,4 |
| | 0,8 | 161,0 | 161,0 | 161,0 | 161,0 | 161,0 |
| | 0,9 | 161,0 | 161,0 | 161,0 | 161,0 | 161,0 |
| | 1,0 | 161,0 | 161,0 | 161,0 | 161,0 | 161,0 |

**Table 70: Allowable tensile stress at values for stress ratio (Van den Bos, 2010)**

| Crane or Element group | Material | Notch group | | | | |
|---|---|---|---|---|---|---|
| **5** | **API 5L grade B** | **K0** | **K1** | **K2** | **K3** | **K4** |
| χ values | -1,0 | 118,8 | 106,1 | 89,1 | 63,6 | 38,2 |
| | -0,9 | 125,0 | 111,6 | 93,8 | 67,0 | 40,2 |
| | -0,8 | 132,0 | 117,9 | 99,0 | 70,7 | 42,4 |
| | -0,7 | 139,8 | 124,8 | 104,8 | 74,9 | 44,9 |
| | -0,6 | 148,5 | 132,6 | 111,4 | 79,5 | 47,7 |
| | -0,5 | 158,4 | 141,4 | 118,8 | 84,9 | 50,9 |
| | -0,4 | 161,0 | 151,5 | 127,3 | 90,9 | 54,5 |
| | -0,3 | 161,0 | 161,0 | 137,1 | 97,9 | 58,7 |
| | -0,2 | 161,0 | 161,0 | 148,5 | 106,1 | 63,6 |
| | -0,1 | 161,0 | 161,0 | 161,0 | 115,7 | 69,4 |
| | 0,0 | 161,0 | 161,0 | 161,0 | 127,3 | 76,4 |
| | 0,1 | 161,0 | 161,0 | 161,0 | 136,2 | 83,0 |
| | 0,2 | 161,0 | 161,0 | 161,0 | 146,6 | 90,8 |
| | 0,3 | 161,0 | 161,0 | 161,0 | 158,6 | 100,3 |
| | 0,4 | 161,0 | 161,0 | 161,0 | 161,0 | 111,9 |
| | 0,5 | 161,0 | 161,0 | 161,0 | 161,0 | 126,7 |
| | 0,6 | 161,0 | 161,0 | 161,0 | 161,0 | 145,9 |
| | 0,7 | 161,0 | 161,0 | 161,0 | 161,0 | 161,0 |
| | 0,8 | 161,0 | 161,0 | 161,0 | 161,0 | 161,0 |
| | 0,9 | 161,0 | 161,0 | 161,0 | 161,0 | 161,0 |
| | 1,0 | 161,0 | 161,0 | 161,0 | 161,0 | 161,0 |

**Table 71: Allowable compression stress at values for stress ratio (Van den Bos, 2010)**

# Appendix D: ANSYS APDL code

```
/BATCH
!This FEM code is developed by Clive Tawjoeram
!master thesis: Fatigue assessment using MBD & ANSYS
! an aged 25t lemniscate crane
!using ANSYS MAPDL 17.1 & 18.1
!_____model structural geometry
/TITLE,draw upper arm structure geometry
/REPLOT

KEYW,PR_STRUC,1
/PREP7
!Change background colour to white
/RGB,INDEX,100,100,100, 0
/RGB,INDEX, 80, 80, 80,13
/RGB,INDEX, 60, 60, 60,14
/RGB,INDEX, 0, 0, 0,15
!_____define element types
ET,1,LINK180    !link 180 element, uniaxial tension-compression element
                        !three degrees of freedom at each node
KEYOPT,1,2,0    !Cross-section scaling:cross section is scaled as a function
        !of axial stretch
!_____
ET,2,BEAM188  !beam 188 element, linear, quadratic, or cubic two-node
        !beam element in 3-D
                        !six or seven degrees of freedom at each node
                        !based on Timoshenko beam theory
KEYOPT,2,1,0    !Warping degree of freedom:Six degrees of freedom per node
        !unrestrained warping
KEYOPT,2,3,0    !Shape functions along the length:linear
KEYOPT,2,4,2    !Shear stress output:Output a combined state of torsion-
        !& flexure-related shear stresses

KEYOPT,2,7,2    !Output control at integration points:
        !Maximum and minimum stresses/strains
                        !plus stresses and strains at each section point
KEYOPT,2,9,2    !Output control for values extrapolated to the element
        !and section nodes:Maximum and minimum stresses/strains
                        !plus stresses and strains along the exterior boundary
        !of the cross-section
KEYOPT,2,15,0  !Results file format: Store averaged results at each
        !section corner node
!_____
ET,3,PIPE288     !pipe 288 elements, two-node pipe element in 3-D
                        !six degrees of freedom at each node
KEYOPT,3,3,0    !Shape functions along the length:Cubic
KEYOPT,3,4,2    !Hoop strain treatment:Thick pipe theory, radius
        !to thickness (R/t)ratio of 35.984252.  If the R/t ratio < 50,
        !use the thick pipeformulation
KEYOPT,3,7,3    !Output control for section forces/moments and strains/curvatures:
                        !Output section forces/moments, strains/curvatures, internal and
        !external pressures,
                        !effective tension, and maximum hoop stress extrapolated to the
        !element nodes
KEYOPT,3,8,0    !Shear stress output:combined state of torsion & flexure-related
        !transverse-shear stresses
KEYOPT,3,9,2    !Output control at integration points:Maximum and minimum
        !stresses/strains plus stresses and strains at each section node
KEYOPT,3,11,3 !Maximum and minimum stresses/strains plus stresses and strains
        !at all section nodes
```

148

```
KEYOPT,3,15,0  ! KEYOPT(15) = 0,value is the section node number
!_____
ET,4,MASS21      !MASS21 Structural Mass
                        !point element having up to six degrees of freedom
KEYOPT,4,1,0    !interpret real constants as masses-inertias
KEYOPT,4,2,1    !Element coordinate system is initially parallel to the nodal
        !coordinate system
KEYOPT,4,3,2    !3-D mass without rotary inertia
/output,info_elements,txt    !write output file:used element info
etlist
/output,
SAVE
!_____define material properties

!material profile 1: steel S235
MPTEMP,,,,,,,,
MPTEMP,1,0
MPDATA,EX,1,,2.1e11
MPDATA,PRXY,1,,0.29
MPTEMP,,,,,,,,
MPTEMP,1,0
MPDATA,DENS,1,,7850
!material pipe profile 2: API 5L grade B carbon steel
MPTEMP,,,,,,,,
MPTEMP,1,0
MPDATA,EX,2,,2.1e11    !Young's Modulus
MPDATA,PRXY,2,,0.3    !Poisson ratio
MPTEMP,,,,,,,,
MPTEMP,1,0
MPDATA,DENS,2,,7841.99         !Density
!material pipe profile 3: API 5L grade B carbon steel
MPTEMP,,,,,,,,
MPTEMP,1,0
MPDATA,EX,3,,2.1e11
MPDATA,PRXY,3,,0.3
MPTEMP,,,,,,,,
MPTEMP,1,0
MPDATA,DENS,3,,7865.9
!material profile 4: steel S235
MPTEMP,,,,,,,,
MPTEMP,1,0
MPDATA,EX,4,,2.1e11
MPDATA,PRXY,4,,0.29
MPTEMP,,,,,,,,
MPTEMP,1,0
MPDATA,DENS,4,,7850*1.3
!material profile 5: steel S235
MPTEMP,,,,,,,,
MPTEMP,1,0
MPDATA,EX,5,,2.1e11
MPDATA,PRXY,5,,0.29
MPTEMP,,,,,,,,
MPTEMP,1,0
MPDATA,DENS,5,,7850*1.1
/output,info_material_ properties,txt         !save material properties as txt files
mplis
/output,
SAVE
!_____Define mass points
R,1,(29e3)/4,  !Front arm
R,2,(48e3)/4,  !Rear arm
R,3,(95e3)/2,  !Counterweight at rear arm
```

```
R,4,(32e3)/9,  !Tower
R,5,(81e3)/4,  !Machine floor
R,6,(8e3)/6,   !Crane house
R,7,(42e3),         !weight at machinefloor
!_____define section properties
SECTYPE,1,PIPE, ,pipe1                              !pipe profile 1
SECDATA,0.914,0.0127,20,0,1,0,0,0,          !radial devision =1 cells
SECOFFSET,0,0,
SECCONTROL,95,

SECTYPE,2,PIPE, ,pipe2                              !pipe profile 2
SECDATA,0.559,0.0095,20,0,1,0,0,0,
SECOFFSET,0,0,
SECCONTROL,80,

SECTYPE,   4, BEAM, HREC, koker1, 3        !dwars koker profiel 1
SECOFFSET, CENT
SECDATA,1,1.11,0.02,0.02,0.02,0.02,0,0,0,0,0,0

SECTYPE,   5, BEAM, CSOLID, shaft_frnt,3            !solid shaft at front end pulleys
SECOFFSET, CENT
SECDATA,0.075,20,20,0,0,0,0,0,0,0,0,0        !!radial devision =20 cells

SECTYPE,   6, BEAM, CSOLID, shaft_rear, 0          !solid shaft at rear end pulleys
SECOFFSET, CENT
SECDATA,0.13,0,0,0,0,0,0,0,0,0,0,0

SECTYPE,   7, BEAM, CSOLID, shaft_cab, 0          !solid shaft at cabin suspension
SECOFFSET, CENT
SECDATA,0.05,0,0,0,0,0,0,0,0,0,0,0

SECTYPE,   8, BEAM, RECT, jnt_plate, 0       !joint ear plates
SECOFFSET, CENT
SECDATA,0.030,.200,0,0,0,0,0,0,0,0,0,0

SECTYPE,11,PIPE, ,pipe3_dwars                              !pipe profile 3
SECDATA,0.61,0.0127,10,0,1,0,0,0,
SECOFFSET,0,0,
SECCONTROL,228,

SECTYPE,   13, BEAM, HREC, CW_beam, 0   !counterweight beam
SECOFFSET, CENT
SECDATA,1.5,2.996,0.008,0.008,0.008,0.008,0,0,0,0,0,0

SECTYPE,   14, BEAM, HREC, rear arm_1, 0 !rear arm_beam1
SECOFFSET, CENT
SECDATA,1.28,2.395,0.025,0.025,0.025,0.025,0,0,0,0,0,0

SECTYPE,   15, BEAM, CTUBE, front arm1, 0        !Front arm_pipe
SECOFFSET, CENT
SECDATA,0.5975,0.6095,0,0,0,0,0,0,0,0,0,0

SECTYPE,   16, BEAM, CTUBE, tower_tube1, 0
SECOFFSET, CENT
SECDATA,0.29,0.3,0,0,0,0,0,0,0,0,0,0

SECTYPE,   17, BEAM, HREC, floor_beam1, 0    !machinefloor_beam1
SECOFFSET, CENT
SECDATA,1.28,1.970,0.025,0.025,0.025,0.025,0,0,0,0,0,0

SECTYPE,   18, BEAM, I, insteek_voor, 0
SECOFFSET, CENT
SECDATA,0.35,0.35,1.260,0.010,0.01,0.01,0,0,0,0,0,0
```

```
SECTYPE,   19, BEAM, I, insteek_achter, 0
SECOFFSET, CENT
SECDATA,0.35,0.35,1.720,0.01,0.01,0.01,0,0,0,0,0,0

SECTYPE,   20, BEAM, I, klauw_rear, 0
SECOFFSET, CENT
SECDATA,0.300,0.300,0.916,0.010,0.010,0.010,0,0,0,0,0,0

SAVE
/output,info_element_cross_section,'txt'      !save cross section properties txt file
slist,,,,,
/output,
!_____draw crane geometry
!model keypoints
!hulp hartlijn
!dwarsbalk bij bovenarm-voorarm
K,1 ,1.25,0,0,
K,2 ,-1.25,0,0,
!scharnierpunten bovenarm-voorarm
K,3 ,1.25,-0.35,0,
K,4 ,-1.25,-0.35,0,
!schijvenas achter
K,5 ,0,0,-9.1,
K,6 ,0.75,0,-9.1,
K,7 ,-0.75,0,-9.1,
!aansluitpunt schoorpijp achter met dwarsbalk
K,8 ,0,0,-7.6,
K,9 ,0.75,0,-7.6,
K,10 ,-0.75,0,-7.6,
!schijven op achteras
K,11 ,0.125,0,-9.1,
K,12 ,-0.125,0,-9.1,
K,13 ,0.275,0,-9.1,
K,14 ,-0.275,0,-9.1,
!ophangpunt kabineuithouder
K,15 ,0,0,10.203,
K,16 ,0.749,0,10.203,
K,17 ,-0.749,0,10.203,
K,18 ,0.905,0,10.203,
K,19 ,-0.905,0,10.203,
!aansluitpunt schoorpijp-voor met dwarsbalk
K,20 ,0,0,19.6,
K,21 ,0.5725,0,19.6,
K,22 ,-0.5725,0,19.6,
 !schijvenas voorzijde
K,23 ,0,0,20.6,
K,24 ,0.5725,0,20.6,
K,25 ,-0.5725,0,20.6,
!topschijven op as voor
K,26 ,0.15,0,20.6,
K,27 ,-0.15,0,20.6,
K,28 ,0.4,0,20.6,
K,29 ,-0.4,0,20.6,
!koppelpunt pyloon met plaat&dwarsbalk bij scharnieren met voorarm
K,30 ,1.25,0.76,0,
K,31 ,-1.25,0.76,0,
!aansluitpunt pyloon met voor en achter schoorbuizen
K,32 ,0,5.5,0,
!aansluitpunt insteekplaat met schoorpijp-achterzijde
K,33,0,5.5-2.1/sin(acos(9.1/10.633)),-9.1+2.1/cos(acos(9.1/10.633))
!aansluitpunt insteekplaat met schoorpijp-voorzijde
K,34,0,5.5-18.36*cos(atan(20.6/5.5)),18.36*sin(atan(20.6/5.5))
```

!front arm
K,35 ,-2.6,-21.6016,-13.5507,
K,36 ,2.6,-21.6016,-13.5507,
!rear arm
K,37 ,-2.6,-13.1456,-22.5607,
K,38 ,2.6,-13.1456,-22.5607,
!contragewicht
K,39 ,-4.05,-18.1326,-27.7123,
K,40 ,4.05,-18.1326,-27.7123,
 !Toren
K,41 ,-2.6,-16.1006,-22.5607,
K,42 ,2.6,-16.1006,-22.5607,
K,43 ,0,-16.1006,-22.5607
K,44 ,2.6,-18.6816,-22.5607
K,45 ,-2.6,-18.6816,-22.5607
K,46 ,-2.6,-21.6016,-22.5607,
K,47 ,2.6,-21.6016,-22.5607,
K,48 ,2.6,-18.6816,-19.5807
K,49 ,-2.6,-18.6816,-19.5807
K,50 ,2.6,-21.6016,-15.5607,
K,51 ,-2.6,-21.6016,-15.5607,
!machinefloor
K,52 ,-2.6,-21.6016,-19.1267,
K,53 ,2.6,-21.6016,-19.1267,
K,54 ,0,-21.6016,-19.1267,
K,55 ,0,-21.6016,-13.5507,
K,56 ,0,-21.6016,-22.5607,
!foot
K,57 ,0,-29,-19.1267,
!orientation keypoint
K,80 ,-3,0,-9.1,
K,81 ,-3,0,20.6,
K,83 ,0,-22,-13.5507,
K,90 ,0,6,0,
K,91,0,5.5+1*sin(20.6/5.5),5.5+1*cos(20.6/5.5)
K,92,0,5.5+1*sin(9.1/5.5),-1
K,93 ,-2.6,-22,-22.5607,
K,94 ,-1,6,0,
K,95 ,1,6,0,
K,96 ,-2.6,-22,-13.5507,
K,97 ,2.6,-22,-13.5507,
K,98 ,-2.6,-12,-22.5607,
K,99 ,2.6,-12,-22.5607,
K,100 ,0,0,-9.1,
K,102 ,0,-12,-22.5607,
!draw lines
!dwarsbalk bij bovenarm-voorarm
L,     2,     1
!dwarsbalk schoorpijp achter met rear girders
L,    10,     8,2
L,     8,     9,2
!balk achtereind met as achterschijvenpakket
L,     6,     9,2
L,     7,    10,2
!schijvenas achter
L,     7,    14,2
L,    14,    12
L,    12,     5
L,     5,    11
L,    11,    13
L,    13,     6,2
!as kabineuithouder
L,    19,    17

```
L,    17,    15,2
L,    15,    16,2
L,    16,    18
!dwarsbalk schoorpijp-voor met constructie schijvenpakket-voor
L,    22,    20,2
L,    20,    21,2
!balk vooreind met schijvenas-voor
L,    21,    24,2
L,    22,    25,2
!schijvenas voorzijde
L,    25,    29
L,    29,    27
L,    27,    23
L,    23,    26
L,    26,    28
L,    28,    24
! scharnierbalk pyloon met voorarm
L,    4,    2,2
L,    3,    1,2
! scharnierbalk pyloon met plaat&dwarsbalk bij scharnieren met voorarm
L,    2,    31,4
L,    1,    30,4
!pylons
L,    31,    32,5  !right
L,    30,    32,5  !left
!backstay
L,    5,    33,2 !insteekplaat
L,    33,    32,8 !buis
!forestay
L,    32,    34,21  !buis
L,    34,    23,2  !insteekplaat


!rear girder left
L,    9,    1,10
!rear girder right
L,    10,    2,10
!front girder left
L,    1,    18,11
L,    18,    21,9
!front girder right
L,    2,    19,11
L,    19,    22,9
!front arm
L,    35,    4,25
L,    36,    3,25
!rear arm
L,    37,    7,28
L,    38,    6,28


L,    37,    38,5


!ballast
L,    39,    37,1
L,    40,    38,1
!tower
L, 46,45
L, 45,41
L, 41,37
L, 47,44
L, 44,42
L, 42,38


L, 37,38
```

```
L, 41,43
L, 43,42
L, 43,37
L, 43,38

L, 38,50
L,37,51
!machinefloor
L,    46,    47
L,    35,    36
L,    46,    51
L,    51,    35
L,    47,    50
L,    50,    36
L,    52,    54
L,    54,    53
L,    55,    54
L,    54,    56

!glue all lines together
FLST,2,66,4,ORDE,2
FITEM,2,1
FITEM,2,-66
LGLUE,P51X
SAVE
!_____
/COM,Preferences for GUI filtering have been set to display:
/COM,  Structural
!_____!Define Load Point Information to apply ADAMS loads
!node IDs as specified in the Load File Created From ADAMS Analysis

N,6,1.25,0,0,,,,        !draaipunt_upper arm_front arm_L

N,7,-1.25,0,0,,,,       !draaipunt_upper arm_front arm_R

N,8,0,0,-9.1,,,,        !scharnier_upper arm_rear arm_centre

N,17,0,0,20.6,,,,

N,24,-0.4,0,20.6,,,,        !pmrk_hijsschijf_bovenarm_R

N,25,-0.15,0,20.6,,,,       !pmrk_sluitschijf_bovenarm_R

N,26,0.15,0,20.6,,,,        !pmrk_sluitschijf_bovenarm_L

N,27,0.4,0,20.6,,,,          !pmrk_hijsschijf_bovenarm_L

N,30,0,0,10.203,,,,          !jointt_ophanging_cabine_uithouder

N,31,0,5.5,0,,,,        !FATIGUE POINT OF INTEREST

N,54,-1.25,0.76,0

N,55,1.25,0.76,0

/VIEW,1,1,1,1
/ANG,1
/AUTO,1
/REP,FAST
GPLOT
SAVE
!_____add attributes to the profiles
/NUMBER,1
```

154

/PNUM,SECT,1

!schoorpijp achter =backstay
CM,_Y,LINE
LSEL, , , ,      33
CM,_Y1,LINE
CMSEL,S,_Y
CMSEL,S,_Y1
LATT,2,1,3, ,      92, ,1
CMSEL,S,_Y
CMDELE,_Y
CMDELE,_Y1
LMESH,      33

!insteek plaat backstay
CM,_Y,LINE
LSEL, , , ,      32
CM,_Y1,LINE
CMSEL,S,_Y
!*
!*
CMSEL,S,_Y1
LATT,5,1,3, ,      80, ,1
CMSEL,S,_Y
CMDELE,_Y
CMDELE,_Y1
LMESH,      32

!schoor pijp voor= forestay
CM,_Y,LINE
LSEL, , , ,      34
CM,_Y1,LINE
CMSEL,S,_Y

CMSEL,S,_Y1
LATT,2,1,3, ,      91, ,1
CMSEL,S,_Y
CMDELE,_Y
CMDELE,_Y1
LMESH,      34

!insteekplaat  forestay
CM,_Y,LINE
LSEL, , , ,      35
CM,_Y1,LINE
CMSEL,S,_Y
!*
!*
CMSEL,S,_Y1
LATT,4,1,2, ,      81, ,18
CMSEL,S,_Y
CMDELE,_Y
CMDELE,_Y1
LMESH,      35

!schoor pijp= pyloon rechts
CM,_Y,LINE
LSEL, , , ,      30
CM,_Y1,LINE
CMSEL,S,_Y

CMSEL,S,_Y1
LATT,3,1,3, ,      94, ,2

```
CMSEL,S,_Y
CMDELE,_Y
CMDELE,_Y1
LMESH,    30

CM,_Y,LINE
LSEL, , , ,    31
CM,_Y1,LINE
CMSEL,S,_Y

CMSEL,S,_Y1
LATT,3,1,3, ,    94, ,2
CMSEL,S,_Y
CMDELE,_Y
CMDELE,_Y1
LMESH,    31

!dwarsbalk at joints upper arm & front arm
CM,_Y,LINE
LSEL, , , ,    1
CM,_Y1,LINE
CMSEL,S,_Y
CMSEL,S,_Y1
LATT,4,1,2, ,    90, ,4
CMSEL,S,_Y
CMDELE,_Y
CMDELE,_Y1
LMESH,    1

!front girders
FLST,5,4,4,ORDE,2
FITEM,5,38
FITEM,5,-41
CM,_Y,LINE
LSEL, , , ,P51X
CM,_Y1,LINE
CMSEL,S,_Y
CMSEL,S,_Y1
LATT,2,1,3, , , ,1
CMSEL,S,_Y
CMDELE,_Y
CMDELE,_Y1
FLST,2,4,4,ORDE,2
FITEM,2,38
FITEM,2,-41
LMESH,P51X

!rear girders
FLST,5,2,4,ORDE,2
FITEM,5,36
FITEM,5,-37
CM,_Y,LINE
LSEL, , , ,P51X
CM,_Y1,LINE
CMSEL,S,_Y

CMSEL,S,_Y1
LATT,2,1,3, ,    90, ,1
CMSEL,S,_Y
CMDELE,_Y
CMDELE,_Y1
FLST,2,2,4,ORDE,2
FITEM,2,36
```

```
FITEM,2,-37
LMESH,P51X

!front end pulley shaft
FLST,5,6,4,ORDE,2
FITEM,5,20
FITEM,5,-25
CM,_Y,LINE
LSEL, , , ,P51X
CM,_Y1,LINE
CMSEL,S,_Y

CMSEL,S,_Y1
LATT,1,1,2, , , ,5
CMSEL,S,_Y
CMDELE,_Y
CMDELE,_Y1
FLST,2,6,4,ORDE,2
FITEM,2,20
FITEM,2,-25
LMESH,P51X

!shaft cabine suspension
FLST,5,4,4,ORDE,2
FITEM,5,12
FITEM,5,-15
CM,_Y,LINE
LSEL, , , ,P51X
CM,_Y1,LINE
CMSEL,S,_Y
CMSEL,S,_Y1
LATT,1,1,2, , , ,7
CMSEL,S,_Y
CMDELE,_Y
CMDELE,_Y1
FLST,2,4,4,ORDE,2
FITEM,2,12
FITEM,2,-15
LMESH,P51X

!pulley shaft rear end
FLST,5,6,4,ORDE,2
FITEM,5,6
FITEM,5,-11
CM,_Y,LINE
LSEL, , , ,P51X
CM,_Y1,LINE
CMSEL,S,_Y

CMSEL,S,_Y1
LATT,1,1,2, , , ,6
CMSEL,S,_Y
CMDELE,_Y
CMDELE,_Y1
FLST,2,6,4,ORDE,2
FITEM,2,6
FITEM,2,-11
LMESH,P51X

!jt upper front arm
FLST,5,2,4,ORDE,2
FITEM,5,26
FITEM,5,-27
```

157

```
CM,_Y,LINE
LSEL, , , ,P51X
CM,_Y1,LINE
CMSEL,S,_Y
CMSEL,S,_Y1
LATT,1,1,2, , , ,8
CMSEL,S,_Y
CMDELE,_Y
CMDELE,_Y1

FLST,2,2,4,ORDE,2
FITEM,2,26
FITEM,2,-27
LMESH,P51X

!Pyloon_foot
FLST,5,2,4,ORDE,2
FITEM,5,28
FITEM,5,-29
CM,_Y,LINE
LSEL, , , ,P51X
CM,_Y1,LINE
CMSEL,S,_Y

CMSEL,S,_Y1
LATT,3,1,3, , , ,2
CMSEL,S,_Y
CMDELE,_Y
CMDELE,_Y1
!*
FLST,2,2,4,ORDE,2
FITEM,2,28
FITEM,2,-29
LMESH,P51X

!dwars balk rearend
FLST,5,2,4,ORDE,2
FITEM,5,2
FITEM,5,-3
CM,_Y,LINE
LSEL, , , ,P51X
CM,_Y1,LINE
CMSEL,S,_Y

CMSEL,S,_Y1
LATT,1,1,3, , , ,11
CMSEL,S,_Y
CMDELE,_Y
CMDELE,_Y1
!*
FLST,2,2,4,ORDE,2
FITEM,2,2
FITEM,2,-3
LMESH,P51X

!klauw jnt upper arm rear arm
CMSEL,S,_Y1
LATT,1,1,3, ,    90, ,1
CMSEL,S,_Y
CMDELE,_Y
CMDELE,_Y1
FLST,2,2,4,ORDE,2
FITEM,2,4
```

158

```
FITEM,2,-5
LMESH,P51X

!dwarsbalk frontend
FLST,5,2,4,ORDE,2
FITEM,5,16
FITEM,5,-17
CM,_Y,LINE
LSEL, , , ,P51X
CM,_Y1,LINE
CMSEL,S,_Y

CMSEL,S,_Y1
LATT,1,1,3, , , ,11
CMSEL,S,_Y
CMDELE,_Y
CMDELE,_Y1

FLST,2,2,4,ORDE,2
FITEM,2,16
FITEM,2,-17
LMESH,P51X

!frontend klauw
FLST,5,2,4,ORDE,2
FITEM,5,18
FITEM,5,-19
CM,_Y,LINE
LSEL, , , ,P51X
CM,_Y1,LINE
CMSEL,S,_Y

CMSEL,S,_Y1
LATT,1,1,3, , , ,11
CMSEL,S,_Y
CMDELE,_Y
CMDELE,_Y1
!*
FLST,2,2,4,ORDE,2
FITEM,2,18
FITEM,2,-19
LMESH,P51X

 !front arm
FLST,5,2,4,ORDE,2
FITEM,5,42
FITEM,5,-43
CM,_Y,LINE
LSEL, , , ,P51X
CM,_Y1,LINE
CMSEL,S,_Y

CMSEL,S,_Y1
LATT,5,1,2, , , ,15
CMSEL,S,_Y
CMDELE,_Y
CMDELE,_Y1
FLST,2,2,4,ORDE,2
FITEM,2,42
FITEM,2,-43

FLST,2,2,4,ORDE,2
FITEM,2,42
```

159

```
FITEM,2,-43
LMESH,P51X

!rear arm

CM,_Y,LINE
LSEL, , , ,     44
CM,_Y1,LINE
CMSEL,S,_Y

CMSEL,S,_Y1
LATT,5,1,2, ,     98, ,14
CMSEL,S,_Y
CMDELE,_Y
CMDELE,_Y1

LMESH,    44

CM,_Y,LINE
LSEL, , , ,     45
CM,_Y1,LINE
CMSEL,S,_Y

CMSEL,S,_Y1
LATT,5,1,2, ,     99, ,14
CMSEL,S,_Y
CMDELE,_Y
CMDELE,_Y1

LMESH,    45

CM,_Y,LINE
LSEL, , , ,     46
CM,_Y1,LINE
CMSEL,S,_Y

CMSEL,S,_Y1
LATT,5,1,2, ,    100, ,14
CMSEL,S,_Y
CMDELE,_Y
CMDELE,_Y1

LMESH,    46

!CW_beam
CM,_Y,LINE
LSEL, , , ,     47
CM,_Y1,LINE
CMSEL,S,_Y

CMSEL,S,_Y1
LATT,4,1,2, ,     98, ,13
CMSEL,S,_Y
CMDELE,_Y
CMDELE,_Y1

LMESH,    47

CM,_Y,LINE
LSEL, , , ,     48
CM,_Y1,LINE
CMSEL,S,_Y
```

```
CMSEL,S,_Y1
LATT,4,1,2, ,    99, ,13
CMSEL,S,_Y
CMDELE,_Y
CMDELE,_Y1

LMESH,    48

!tower
FLST,5,12,4,ORDE,2
FITEM,5,49
FITEM,5,-60
CM,_Y,LINE
LSEL, , , ,P51X
CM,_Y1,LINE
CMSEL,S,_Y

CMSEL,S,_Y1
LATT,1,1,2, , , ,16
CMSEL,S,_Y
CMDELE,_Y
CMDELE,_Y1

FLST,2,12,4,ORDE,2
FITEM,2,49
FITEM,2,-60
LMESH,P51X

!floor
FLST,5,2,4,ORDE,2
FITEM,5,63
FITEM,5,-64
CM,_Y,LINE
LSEL, , , ,P51X !right beam
CM,_Y1,LINE
CMSEL,S,_Y

CMSEL,S,_Y1
LATT,4,1,2, ,    96, ,17
CMSEL,S,_Y
CMDELE,_Y
CMDELE,_Y1

FLST,2,2,4,ORDE,2
FITEM,2,63
FITEM,2,-64
LMESH,P51X

!_____

FLST,5,2,4,ORDE,2
FITEM,5,65
FITEM,5,-66
CM,_Y,LINE
LSEL, , , ,P51X
CM,_Y1,LINE
CMSEL,S,_Y
CMSEL,S,_Y1
LATT,4,1,2, ,    97, ,17
CMSEL,S,_Y
CMDELE,_Y
CMDELE,_Y1
```

```
FLST,2,2,4,ORDE,2
FITEM,2,65
FITEM,2,-66
LMESH,P51X
!_____
CM,_Y,LINE
LSEL, , , ,      62
CM,_Y1,LINE
CMSEL,S,_Y

CMSEL,S,_Y1
LATT,4,1,2, ,      96, ,17
CMSEL,S,_Y
CMDELE,_Y
CMDELE,_Y1

LMESH,      62
!_____
CM,_Y,LINE
LSEL, , , ,      61
CM,_Y1,LINE
CMSEL,S,_Y

CMSEL,S,_Y1
LATT,4,1,2, ,      93, ,17
CMSEL,S,_Y
CMDELE,_Y
CMDELE,_Y1

LMESH,      61

/ESHAPE,1.0
/EFACET,1
/RATIO,1,1,1
/CFORMAT,32,0
/REPLOT


!rear arm mass distribution
FLST,5,4,3,ORDE,4
FITEM,5,6
FITEM,5,-7
FITEM,5,37
FITEM,5,-38
CM,_Y,KP
KSEL, , , ,P51X
CM,_Y1,KP
CMSEL,S,_Y

CMSEL,S,_Y1
KATT,     1,    2,   4,     0
CMSEL,S,_Y
CMDELE,_Y
CMDELE,_Y1
FLST,2,3,3,ORDE,3
FITEM,2,7
FITEM,2,37
FITEM,2,-38
KMESH,P51X

CM,_Y,KP
KSEL, , , ,      6
CM,_Y1,KP
```

162

```
CMSEL,S,_Y

CMSEL,S,_Y1
KATT,    1,    2,   4,    0
CMSEL,S,_Y
CMDELE,_Y
CMDELE,_Y1

KMESH,    6

!mass distribution Counterweight
FLST,5,2,3,ORDE,2
FITEM,5,39
FITEM,5,-40
CM,_Y,KP
KSEL, , , ,P51X
CM,_Y1,KP
CMSEL,S,_Y

CMSEL,S,_Y1
KATT,    1,    3,   4,    0
CMSEL,S,_Y
CMDELE,_Y
CMDELE,_Y1

FLST,2,2,3,ORDE,2
FITEM,2,39
FITEM,2,-40
KMESH,P51X

!mass dsitribution tower
FLST,5,9,3,ORDE,8
FITEM,5,37
FITEM,5,-38
FITEM,5,41
FITEM,5,-43
FITEM,5,46
FITEM,5,-47
FITEM,5,50
FITEM,5,-51
CM,_Y,KP
KSEL, , , ,P51X
CM,_Y1,KP
CMSEL,S,_Y

CMSEL,S,_Y1
KATT,    1,    4,   4,    0
CMSEL,S,_Y
CMDELE,_Y
CMDELE,_Y1

FLST,2,9,3,ORDE,8
FITEM,2,37
FITEM,2,-38
FITEM,2,41
FITEM,2,-43
FITEM,2,46
FITEM,2,-47
FITEM,2,50
FITEM,2,-51
KMESH,P51X

!mass distribution machinefloor
```

163

```
FLST,5,4,3,ORDE,4
FITEM,5,35
FITEM,5,-36
FITEM,5,46
FITEM,5,-47
CM,_Y,KP
KSEL, , , ,P51X
CM,_Y1,KP
CMSEL,S,_Y

CMSEL,S,_Y1
KATT,     1,     5,   4,     0
CMSEL,S,_Y
CMDELE,_Y
CMDELE,_Y1

FLST,2,4,3,ORDE,4
FITEM,2,35
FITEM,2,-36
FITEM,2,46
FITEM,2,-47
KMESH,P51X

!mass distribution front arm
FLST,5,2,3,ORDE,2
FITEM,5,3
FITEM,5,-4
CM,_Y,KP
KSEL, , , ,P51X
CM,_Y1,KP
CMSEL,S,_Y

CMSEL,S,_Y1
KATT,     1,     1,   4,     0
CMSEL,S,_Y
CMDELE,_Y
CMDELE,_Y1

FLST,2,2,3,ORDE,2
FITEM,2,3
FITEM,2,-4
KMESH,P51X

NUMMRG,NODE, , , ,LOW         !Merge coincident or equivalently defined Nodes
                             !the higher numbered node will be deleted and will be replaced with the
                             !lower numbered coincident node
EPLOT
/REPLOT

FINISH
SAVE
!_____Enter solution phase:dynamic structural analysis
!crane system = mechanism in ADAMS, so inertial effect is not neglected
!transient analysis, time varying loads can be applied to get responses of the component over time
!to study the response of the component in different loading conditions or combination of loads

/SOL

ANTYPE,4        !Specifies the analysis type and restart status = perform a transient analysis,Valid for all
degrees of freedom.
TRNOPT,FULL !Specifies transient analysis options = Full method
LUMPM,0                 !Specifies a lumped mass matrix formulation = OFF
OUTRES,ALL    !Controls the solution data written to the database =
```

```
                        !All solution items except LOCI(Integration point locations) and SVAR(State variables)
RESCONTROL,NORESTART,all  !RESCONTROL, Action, Ldstep, Frequency, MAXFILES
                                !Controls file writing for multiframe restarts
                                !NORESTART = cleans up some of the restart files after a Distributed
ANSYS solution.
OUTRES, all,,,,,  !OUTRES, Item, Freq, Cname, -- , NSVAR, DSUBres
                        !Controls the solution data written to the database
                        !All solution items except LOCI and SVAR
!_____add boundary conditions to model
/REPLOT
FLST,2,4,1,ORDE,4
FITEM,2,325
FITEM,2,350
FITEM,2,500
FITEM,2,509
/GO
D,P51X, ,0, , , ,UX,UY,UZ, , ,

!Total number of constrains = 6,OK
/output,info_DOF_crane,txt            !WRITE .TXT OUTPUT FILE
DLIST, ALL
/output,

/SHRINK,0
/ESHAPE,1.0
/EFACET,1
/RATIO,1,1,1
/CFORMAT,32,0

/USER,  1
/VIEW, 1, 0.590299717212   , 0.197062320347   , 0.782759660279
/ANG,   1, -0.331623260411
/ZOOM,1,SCRN,0.458136,0.077586,0.582305,-0.602586
/DIST,1,0.729,1
/REP,FAST
/REPLOT

/NUMBER,1
/PNUM,SECT,1
/REPLOT
/TITLE,Initial design 25t lemniscate crane
/REPLOT

/AUTO,1
/REP,FAST
SAVE
!*****************COSIMULATION ADAMS ANSYS*********************************
!_____Importing simulated dutycycle ADAMS UPPER ARM loads
/TITLE,Importing ADAMS loads
/REPLOT
!import loads only
!loads are applied to the nodes defined based on the ADAMS loads file

/INPUT,'ADAMS_loads_upper arm_for_ANSYS','txt','.'
!_____!Solve all load steps
/TITLE,Solve ADAMS loads
/REPLOT

LSSOLVE,2,128,1,!LSSOLVE, LSMIN, LSMAX, LSINC: Reads and solves multiple load steps
                !solve using LS files 0 to 128
FINISH            !EXIT SOLUTION PHASE
SAVE
/TITLE,fatigue assessment upper arm 25t lemniscate crane
```

165

```
/REPLOT

/NUMBER,0
/PNUM,SECT,0
/REPLOT
!_____!!write all ADAMS loads at boomtip to a .txt file
/POST1

/delete,Info_ADAMS_loads_import_verification,txt
/output,Info_ADAMS_loads_import_verification,txt,,append
*SET,i
*do,i,1,127          !*DO, Par, IVAL, FVAL, INC
                     !Defines the beginning of a do-loop
                     !Defines the data set to be read from the results file: Read load step i
SET,i
FLST,2,5,1,ORDE,3          !print all loads at boomtip for hoisting & closing pulleys
FITEM,2,17
FITEM,2,24
FITEM,2,-27
FLIST,P51X
/gopr
*enddo                     !Ends a do-loop and starts the looping action
/output,            !Go back to the standard output
FINISH
!_____
!****************Post Processing over Multiple Time/Load Steps
!TimeHist PostProcessor: Define time-history variables
!To view the response of the nodes of interest with time,use the TimeHist PostProcessor

/POST26
!POST26 is used to review results at specific points in the model as functions of time
!Time-history processor looks for the results files

FILE,,'rst','.'                   !Specifies the data file where results are to be found
/UI,COLL,1                        !Activates specified GUI dialog boxes
NUMVAR,200                        !Specifies the number of variables allowed in POST26
SOLU,191,NCMIT                    !Specifies solution summary data per substep to be stored
STORE,MERGE                       !Stores data in the database for the defined variables
FILLDATA,191,,,,1,1              !Fills a variable by a ramp function
REALVAR,191,191                   !Forms a variable using only the real part of a complex variable

XVAR,1!Specifies the X variable to be displayed = time (s)!TIME (time) or FREQ (frequency) is always
variable 1
!_____
!forestay
ESOL,3,11,31 ,SMISC,31,fs_axialstress_i          !Axial stress at node 31 = i-node of element 11
STORE,MERGE
FORCE,TOTAL

ESOL,4,11,31 ,SMISC,32,fs_SByT_i                 !bending stress about the + y-axis
STORE,MERGE

ESOL,5,11,31 ,SMISC,34,fs_SBzT_i                 !bending stress about the + z-axis
STORE,MERGE
!_____
!backstay
ESOL,7,8,31 ,SMISC,36,bs_axialstress_j           !Axial stress at node 31 = j-node of element 8
STORE,MERGE
FORCE,TOTAL

ESOL,8,8,31 ,SMISC,37,bs_SByT_j                  !bending stress about the + y-axis
STORE,MERGE
```

```
ESOL,9,8,31 ,SMISC,39,bs_SBzT_j                  !bending stress about the + z-axis
STORE,MERGE
!_____
!pyloon left

ESOL,11,43,31 ,SMISC,36,pyl_L_axialstress_j      !Axial stress at node 31 = j-node of element 43
STORE,MERGE
FORCE,TOTAL

ESOL,12,43,31 ,SMISC,37,pyl_LSByT_j              !bending stress about the + y-axis
STORE,MERGE

ESOL,13,43,31 ,SMISC,39,pyl_LSBzT_j              !bending stress about the +z-axis
STORE,MERGE
!_____
!pyloon right

ESOL,14,38,31 ,SMISC,36,pyl_R_axialstress_j      !Axial stress at node 31 = j-node of element 38
STORE,MERGE
FORCE,TOTAL

ESOL,15,38,31 ,SMISC,37,pyl_R_SByT_j             !bending stress about the + y-axis
STORE,MERGE

ESOL,16,38,31 ,SMISC,39,pyl_R_SBzT_j             !bending stress about the + z-axis
STORE,MERGE
!_____
!vertical displacement IN Y-DIRECTION at the frontend pulley locations
NSOL,17,24,U,Y, UY_pulley_hoisting_R,
STORE,MERGE
NSOL,18,25,U,Y, UY_pulley_closing_R,
STORE,MERGE
NSOL,19,26,U,Y, UY_pulley_closing_L,
STORE,MERGE
NSOL,20,27,U,Y, UY_pulley_hoisting_L,
STORE,MERGE

!horizontal displacement IN X-DIRECTION at the frontend pulley locations
NSOL,21,24,U,X, UX_pulley_hoisting_R,
STORE,MERGE
NSOL,22,25,U,X, UX_pulley_closing_R,
STORE,MERGE
NSOL,23,26,U,X, UX_pulley_closing_L,
STORE,MERGE
NSOL,24,27,U,X, UX_pulley_hoisting_L,
STORE,MERGE

!horizontal displacement IN Z-DIRECTION at the frontend pulley locations
NSOL,25,24,U,Z, UZ_pulley_hoisting_R,
STORE,MERGE
NSOL,26,25,U,Z, UZ_pulley_closing_R,
STORE,MERGE
NSOL,27,26,U,Z, UZ_pulley_closing_L,
STORE,MERGE
NSOL,28,27,U,Z, UZ_pulley_hoisting_L,
STORE,MERGE

/REPLOT
/TITLE,FAT assessment CoSim MBD/FEM: remaining life 25t lemniscate crane C.Tawjoeram
/REPLOT
!_____export stress results
! Save time history variables to file stress_forestay.csv
*CREATE,scratch,gui
```

167

```
*DEL,_P26_EXPORT
*DIM,_P26_EXPORT,TABLE,127,3
VGET,_P26_EXPORT(1,0),1
VGET,_P26_EXPORT(1,1),3
VGET,_P26_EXPORT(1,2),4
VGET,_P26_EXPORT(1,3),5
/OUTPUT,'stress_forestay','csv','.'
*VWRITE,'TIME','fs_axialstress_i','fs_SByT_i','fs_SBzT_i'
%C, %C, %C, %C
*VWRITE,_P26_EXPORT(1,0),_P26_EXPORT(1,1),_P26_EXPORT(1,2),_P26_EXPORT(1,3)
%G, %G, %G, %G
/OUTPUT,TERM
*END
/INPUT,scratch,gui
! End of time history save

! Save time history variables to file stress_Backstay.csv
*CREATE,scratch,gui
*DEL,_P26_EXPORT
*DIM,_P26_EXPORT,TABLE,127,3
VGET,_P26_EXPORT(1,0),1
VGET,_P26_EXPORT(1,1),7
VGET,_P26_EXPORT(1,2),8
VGET,_P26_EXPORT(1,3),9
/OUTPUT,'stress_Backstay','csv','.'
*VWRITE,'TIME','bs_axialstress_j','bs_SByT_j','bs_SBzT_j'
%C, %C, %C, %C
*VWRITE,_P26_EXPORT(1,0),_P26_EXPORT(1,1),_P26_EXPORT(1,2),_P26_EXPORT(1,3)
%G, %G, %G, %G
/OUTPUT,TERM
*END
/INPUT,scratch,gui
! End of time history save

! Save time history variables to file stress_Pyl_L.csv
*CREATE,scratch,gui
*DEL,_P26_EXPORT
*DIM,_P26_EXPORT,TABLE,127,3
VGET,_P26_EXPORT(1,0),1
VGET,_P26_EXPORT(1,1),11
VGET,_P26_EXPORT(1,2),12
VGET,_P26_EXPORT(1,3),13
/OUTPUT,'stress_Pyl_L','csv','.'
*VWRITE,'TIME','pyl_L_axialstress_j','pyl_LSByT_j','pyl_LSBzT_j'
%C, %C, %C, %C
*VWRITE,_P26_EXPORT(1,0),_P26_EXPORT(1,1),_P26_EXPORT(1,2),_P26_EXPORT(1,3)
%G, %G, %G, %G
/OUTPUT,TERM
*END
/INPUT,scratch,gui
! End of time history save

! Save time history variables to file stress_Pyl_R.csv
*CREATE,scratch,gui
*DEL,_P26_EXPORT
*DIM,_P26_EXPORT,TABLE,127,4
VGET,_P26_EXPORT(1,0),1
VGET,_P26_EXPORT(1,1),4
VGET,_P26_EXPORT(1,2),14
VGET,_P26_EXPORT(1,3),15
VGET,_P26_EXPORT(1,4),16
/OUTPUT,'stress_Pyl_R','csv','.'
*VWRITE,'TIME','fs_SByT_i','pyl_R_axialstress_j','pyl_R_SByT_j','pyl_R_SBzT_j'
```

```
%C, %C, %C, %C, %C
*VWRITE,_P26_EXPORT(1,0),_P26_EXPORT(1,1),_P26_EXPORT(1,2),_P26_EXPORT(1,3),_P26_EXPOR
T(1,4)
%G, %G, %G, %G, %G
/OUTPUT,TERM
*END
/INPUT,scratch,gui
! End of time history save


!_____
! Save time history variables to file Ux_upper arm_tip.csv
*CREATE,scratch,gui
*DEL,_P26_EXPORT
*DIM,_P26_EXPORT,TABLE,127,4
VGET,_P26_EXPORT(1,0),1
VGET,_P26_EXPORT(1,1),21
VGET,_P26_EXPORT(1,2),22
VGET,_P26_EXPORT(1,3),23
VGET,_P26_EXPORT(1,4),24
/OUTPUT,'Ux_upper arm_tip','csv','.'
*VWRITE,'TIME','UX_pulley_hoisting_R','UX_pulley_closing_R','UX_pulley_closing_L','UX_pulley_hoisting
_L'
%C, %C, %C, %C, %C
*VWRITE,_P26_EXPORT(1,0),_P26_EXPORT(1,1),_P26_EXPORT(1,2),_P26_EXPORT(1,3),_P26_EXPOR
T(1,4)
%G, %G, %G, %G, %G
/OUTPUT,TERM
*END
/INPUT,scratch,gui
! End of time history save



! Save time history variables to file Uy_upper arm_tip.csv
*CREATE,scratch,gui
*DEL,_P26_EXPORT
*DIM,_P26_EXPORT,TABLE,127,4
VGET,_P26_EXPORT(1,0),1
VGET,_P26_EXPORT(1,1),17
VGET,_P26_EXPORT(1,2),18
VGET,_P26_EXPORT(1,3),19
VGET,_P26_EXPORT(1,4),20
/OUTPUT,'Uy_upper arm_tip','csv','.'
*VWRITE,'TIME','UY_pulley_hoisting_R','UY_pulley_closing_R','UY_pulley_closing_L','UY_pulley_hoisting
_L'
%C, %C, %C, %C, %C
*VWRITE,_P26_EXPORT(1,0),_P26_EXPORT(1,1),_P26_EXPORT(1,2),_P26_EXPORT(1,3),_P26_EXPOR
T(1,4)
%G, %G, %G, %G, %G
/OUTPUT,TERM
*END
/INPUT,scratch,gui
! End of time history save

! Save time history variables to file Uz_upper arm_tip.csv
*CREATE,scratch,gui
*DEL,_P26_EXPORT
*DIM,_P26_EXPORT,TABLE,127,4
VGET,_P26_EXPORT(1,0),1
VGET,_P26_EXPORT(1,1),25
VGET,_P26_EXPORT(1,2),26
VGET,_P26_EXPORT(1,3),27
VGET,_P26_EXPORT(1,4),28
```

```
/OUTPUT,'Uz_upper arm_tip','csv','.'
*VWRITE,'TIME','UZ_pulley_hoisting_R','UZ_pulley_closing_R','UZ_pulley_closing_L','UZ_pulley_hoisting_L'
%C, %C, %C, %C, %C
*VWRITE,_P26_EXPORT(1,0),_P26_EXPORT(1,1),_P26_EXPORT(1,2),_P26_EXPORT(1,3),_P26_EXPORT(1,4)
%G, %G, %G, %G, %G
/OUTPUT,TERM
*END
/INPUT,scratch,gui
! End of time history save


SAVE
FINISH
!_____!Postprocessing:
/POST1


!_____Allowable Stress analysis: Sigma_allow=240MPa/1.5=160MPa
/contour,,9,0,,160e6  !stress contour plot based on K3 notch behaviour group
/REPLOT


*SET,i
*do,i,1,127        !*DO, Par, IVAL, FVAL, INC
                   !Defines the beginning of a do-loop
                   !Defines the data set to be read from the results file: Read load step i
SET,i
PLESOL, S,EQV, 0,1.0


*enddo

/contour,,9,0,,
EPLOT
/REPLOT
/TITLE,FAT assessment CoSim MBD/FEM: remaining life 25t lemniscate crane C.Tawjoeram
/REPLOT
SAVE
FINISH


/eof ***********September 2017************
```